Amyloid Fibrils in Bionanomaterials

A thesis submitted in partial
fulfilment of the requirements for the degree of

Doctor of Philosophy in Biochemistry

at the

University of Canterbury

by

Shiva Priya Rao

2008

In memory of my dad, Mr. Bhujang Rao, who taught me the value of education.

Acknowledgements

This thesis would not have been successful without the guidance from Prof. Juliet Gerrard. Thank you heaps Juliet, for your excellent supervision and enthusiasm at all times during my research.

Thanks also to my co-supervisor Dr. Kevin Sutton, for your encouragement and support through out this project and for proof reading my thesis.

Dr. Susie Meade, your advice and enthusiasm has been great. Thank you for the suggestions and proof reading, it has been exceptional.

I am grateful to the Foundation for Research, Science and Technology for funding my research and NZ Institute of Crop and Food Research, for supporting my study leave.

Thank you to everyone in Juliet's lab group who have been of help over the years: Grant, Genevieve, Chris, Tatiana, Sean, Sophie, Ren, Andrew, Sarah, Jared and Laura.

Jackie Healy for your help with all the technical aspects of my experiments.

Manfred Ignerfeld for your excellent microscopy techniques (TEM) and help with redrawing of diagrams.

Nigel Joyce for your help and patience with all of my mass spectrometry work.

Dr. Mark Staiger for your suggestions and help with the mechanical aspect of this project.

To the FBI team at Crop and Food Research, for your input in various aspects of my research especially Sarah Roberts, Nigel Larsen, Lidia Motoi, Hassam Razzaq, Nick Tucker.

Many thanks to my mum, Mrs L. K. Rao and sisters, Vibha and Jaya for their continual encouragement during my studies.

Finally a big thank you to my husband Kamlesh Mani for his understanding and patience, over the years. Kamal, your sense of belief and pride in my studies is appreciated.

Table of Contents

Abbreviations

AFM	atomic force microscopy
amu	atomic mass unit
ASTM	American standard testing method
A.U.	absorption units
BSA	bovine serum albumin
cm	centimetre
CNT	carbon nanotube
CR	Congo red
Da	Daltons
^{o}C	degrees centigrade
dH_2O	distilled water
DMA	dynamic mechanical analyser
DSC	differential scanning calorimetry
DSC-TGA	differential scanning calorimetry - thermogravimetric analyser
DTE	dithioerythritol
E′	storage modulus
E″	loss modulus
EDTA	ethylenediaminetetraacetic acid
EM	electron microscopy
ESI	electrospray ionisation
ESI-MS	electrospray ionisation-mass spectrometry
FA	formic acid
FE-SEM	field emission-scanning microscope
FPLC	fast performance liquid chromatography
g	grams
GPa	gigaPascal
HCl	hydrochloric acid

HMW	high molecular weight
H_2O	water
hr	hour
Hz	Hertz
IAA	iodoacetic acid
kDa	kiloDaltons
l	litre
LC	liquid chromatography
LC-ESI-MS	liquid chromatography electrospray ionisation-mass spectrometry
LC-MS	liquid chromatography mass spectrometry
LDS	lithium salt of sodium dodecyl sulphate
LMW	low molecular weight
M	molar
mA	milliAmperes
mbar	millibar
MES	2-(N-morpholino)ethanesulfonic acid
µg	micrograms
mg	milligrams
min	minute
µl	microlitres
ml	millilitres
µm	micrometres
mm	millimetres
mM	millimolar
MOPS	3-morpholinopropanesulfonic acid
MPa	megaPascal
mPEG	monomethyloxypoly(ethylene glycol)
MS	mass spectrometry
msec	milliseconds
MS/MS	mass spectrometry mass spectrometry
mV	milliVolts
MW	molecular weight
MWCO	molecular weight cut off

m/z	mass to charge ratio
NaCl	sodium chloride
NaOH	sodium hydroxide
nm	nanometres
NMR	nuclear magnetic resonance spectrometry
ns	nanoseconds
NuPAGE	Novex polyacrylamide gel electrophoresis
Pa	pascal
%	percent
PDA	photodiode array detector
PMSF	phenylmethylsulfonyl fluoride
PVOH	polyvinyl alcohol
RCM	reduced carboxymethylated
RH	relative humidity
RPE	reduced pyridylethylated
rpm	revolutions per minute
RT	retention time
SAXS	small-angle X-ray scattering
SDS	sodium dodecyl sulfate
sec	second
SEM	scanning electron microscope
ssNMR	solid-state nuclear magnetic resonance spectroscopy
Tan δ	loss factor
TEM	transmission electron microscopy
TFE	2,2,2-trifluoroethanol
T_g	glass transition temperature
TGA	thermogravimetric analyser
ThT	thioflavin T
TIC	total ion count
TPCK	L-1-tosylamide-2-phenylethyl chloromethyl ketone
Tris	tris(hydroxymethyl)aminomethane
TTR	transthyretin
UTM	universal testing machine
UV	ultraviolet

4-VP	4-vinylpyridine
v/v	unit volume per unit volume
W	Watt
wt	weight
w/v	unit weight per unit volume
w/w	unit weight per unit weight
XRD	x-ray diffractometer

Abstract

Amyloid fibrils are a type of protein nanofibres that form when a normally soluble protein aggregates in a regular fashion *via* self-association. Their organised and repetitive β-sheet structure is thought to be a generic property of all proteins, depending on the environmental conditions. The nanometre size and high stability of these protein nanofibres are attractive features to exploit in bionanomaterials.

This thesis aimed to manipulate insulin amyloid fibrils, as a model protein nanofibre system, through investigating the effect of chemical modification on insulin fibril formation in heterogeneous mixtures. Using acetylation, reduction carboxymethylation, reduction pyridylethylation, trypsin digestion and chymotrypsin digestion, it was shown that nanofibres can form in heterogeneous mixtures of modified insulin at variable rates to produce fibrils of distinct morphologies. Distinctively well defined, long, unbranched nanofibres were observed in the crude reduced carboxymethylated insulin mixture after incubation at 60°C (pH 7.4), which formed at a faster rate than native insulin. The crude reduced pyridylethylated insulin revealed the formation of “wavy” fibrils when exposed to 60°C and pH 1.6, compared to the straight native insulin amyloid fibrils. Although, the trypsin digestion inhibited nanofibre formation at 60°C and pH 1.6, chymotrypsin digestion of insulin produced a mixture of long and short nanofibres under the same conditons. Thus chemical modification provides a simple means of manipulating protein nanofibre assembly for use in bionanotechnology.

Protein nanofibres were incorporated into a model polymer polyvinylalcohol (PVOH) film in order to assess the impact on material properties. A systematic study involving both insulin and a crude source of crystallin proteins derived from bovine eye lens was undertaken. A protein nanofibre-PVOH nanocomposite was successfully fabricated by a procedure of solution mixing and casting. Dynamic mechanical analysis showed that the addition of insulin fibrils did not change the stiffness of the PVOH. However, an increase in the stiffness of the PVOH-crude bovine eye lens composites was found. Both insulin and bovine eye lens nanofibres reduced the damping properties of the polymer, which suggested a reduction in molecular mobility/slipping.

The results revealed that protein nanofibre formation can be controlled through the modification of the protein and that nanofibres may alter polymer properties in a protein specific manner. Employing these findings in the development of novel bionanomaterials that use the protein nanofibres as a form of natural scaffolding offers a fruitful avenue of future research.

Introduction

This thesis aims to explore the self-assembly of amyloid fibrils from a model protein (bovine insulin) with the long term aim of using amyloid fibrils made from cheap, readily available proteins. The nanosized structure of fibrils, together with their strength and chemical functionality, inspired this study for their potential use in bionanomaterials.

Amyloid fibrils are formed when a normally soluble protein self associates into an insoluble β-sheet aggregate. Studies have shown that these structures are highly ordered and generic to most, if not all, proteins. Although amyloid fibrils have been of wide interest from the medical perspective, their potential as bionanomaterials is less well explored. This chapter will provide a background on the ability of proteins to form amyloid fibrils and the factors affecting their formation. It will also highlight the current prospects of fibrils in the development of bionanomaterials.

1.1 What are Amyloid Fibrils?

Amyloid fibrils are highly ordered, insoluble aggregates of proteins or polypeptides that arise when the proteins' or polypeptides' normally soluble, native structures are partially denatured and the denatured species self-assemble into structured nanofibres (Chiti and Dobson 2006). They have been reviewed in detail in a number of papers due to their association with a growing number of human diseases, including Alzheimer's disease, Parkinson's disease, Huntington's disease, prion diseases, and numerous others (Chiti and Dobson 2006, Pedersen and Otzen 2008, Sipe and Cohen 2000). However, in the early days, the term "amyloid" was used to describe histological deposits, as it was thought that they were composed of starch (Cohen and Calkins 1959, Sipe and Cohen 2000). Today, it is known that protein constitutes the main component of

amyloid deposits. The term amyloid is now assigned to aggregates that have a highly ordered molecular assembly and satisfy other criteria, including the ability to bind and shift the spectral properties of certain hydrophobic dyes (Eisert *et al.* 2006, Krebs *et al.* 2005, Nilsson 2004) and a strong scattering of X-rays at an angle corresponding to a 4.7 Å molecular spacing along the same direction as the fibre and a more diffuse reflection at 10 Å perpendicular to the fibre direction (Sunde *et al.* 1997), being diagnostic for ordered β-sheet structure (Makin and Serpell 2005, Nelson and Eisenberg 2006). The X-ray diffraction patterns for amyloid fibrils can be visualised by clear arcs at the two different angles. A model of amyloid fibril structure, as a protein or peptide cross-β core with β-strands stacked in β-sheets along the fibril axis and adjacent β-sheets stacked perpendicular to the fibril axis was first proposed in the 1950s (Cohen and Calkins 1959).

Other than the cross β-sheet structure, amyloid fibrils have been proposed to have structures including β-helices and concentric cylinders (Perutz *et al.* 2002, Wille *et al.* 2002), which are water filled. In contrast, a recent review has suggested that there is no difference in the hydrated and dried fibril structures from transthyretin (TTR) and lysozyme (Squires *et al.* 2006). This suggests that hydrated fibril structures do not contain water within the fibril core and are unlikely to be hollow nanotubes, hence being referred to as nanofibres (Gras 2007a). A review by Makin and Serpell (2005) discussed amyloid structure in detail adding further support for the cross-β fibril structure (section 1.4).

In addition to over 25 different proteins associated with different amyloid pathologies (Krishnan and Lindquist 2005) many other nonpathogenic proteins can be induced to form the amyloid structure *in vitro* (Stefani and Dobson 2003). These attributes make the amyloid structure broadly interesting, not only from the point of view of human disease but also in terms of fundamental aspects of protein folding and function. The formation of these “non-native” protein structures has long been the subject of much research in the biomedical arena, given the manifestation of amyloid fibrils with the diseases of protein misfolding (Krishnan and Lindquist 2005, Westermark *et al.* 2005). Thus there is considerable literature on protein fibril formation *in vivo*, and some well

characterised examples of proteins from which fibrils can be formed. Other than their association with disease, amyloid fibrils have been found to play useful biological roles in spider silk (Kenney *et al.* 2002), moth silk (Iconomidou *et al.* 2000), curli protein in bacteria (Chapman *et al.* 2002), SUP35 protein in yeast (King *et al.* 1997), bacterial inclusion bodies (Carrio *et al.* 2005) and recently in melanosomes of humans (Dantzker 2005, Fowler *et al.* 2006) and fungal spores (Kwan *et al.* 2006).

Among the proteins that form well defined fibrils is the 84-residue SH3 domain of the p85a subunit of bovine phosphatidylinositol-3′-kinase, which forms amyloid fibrils at low pHs (Chiti *et al.* 1999, Guijarro *et al.* 1998). An example of a molecular model of an amyloid fibril derived from cryo-EM analysis of fibrils grown from a SH3 domain is shown in Figure 1.1. The fibril consists of four 'protofilaments' that twist around one another to form a hollow fibre with a diameter of approximately 60 Å (Jiménez *et al.* 1999). This particular model represents one way in which regions of the polypeptide chain involved in β-sheet structure could be assembled within the fibrils (Dobson 1999). Cryoelectron microscopy characterisation of insulin fibrils on the other hand have revealed two, four, or six protofilaments per insulin fibril, with the cross β-sheet structure composed of relatively flat β-sheets (Jiménez *et al.* 2002). The structural features of amyloid fibril are further described in section 1.4.

Other proteins that are not known to form fibrils in disease or nature but can be induced to form fibrils *in vitro*, include bovine insulin (Nielsen *et al.* 2001c), bovine crystallins (Garvey *et al.* 2008), wheat proteins (Mackintosh *et al.* 2008), hen egg lysozyme (Krebs *et al.* 2000), α-lactoglobulin (Graveland-Bikker and de Kruif 2006), milk proteins (Thorn *et al.* 2005), ovalbumin and bovine serum albumin (Pearce *et al.* 2007). Of the several proteins available, bovine insulin was selected to be the model protein in this thesis because it has been well characterised from the fibril forming perspective (Brange *et al.* 1997a, Brange *et al.* 1997b, Jiménez *et al.* 2002, Nielsen *et al.* 1999, Nielsen *et al.* 2001a, Nielsen *et al.* 2001b, Nielsen *et al.* 2001c) and was available at reasonable cost.

In most cases, fibrils are obtained by altering conditions such as pH or temperature, or by altering salt or metal ion concentrations, or by using solvents and chaotropic agents, which suggests fibril formation *in vitro* is dependent on conformational stability of the protein (Aggeli *et al.* 2001, Calamai *et al.* 2005, Chiti *et al.* 1999, Ramirez-Alvarado *et al.* 2000, Smith *et al.* 2003). Thus it is becoming apparent that the formation of amyloid fibrils may be a generic feature of proteins that can be induced given the appropriate physical and chemical conditions (Dobson and Karplus 1999, Fändrich *et al.* 2001, Fändrich *et al.* 2003, Guijarro *et al.* 1998).

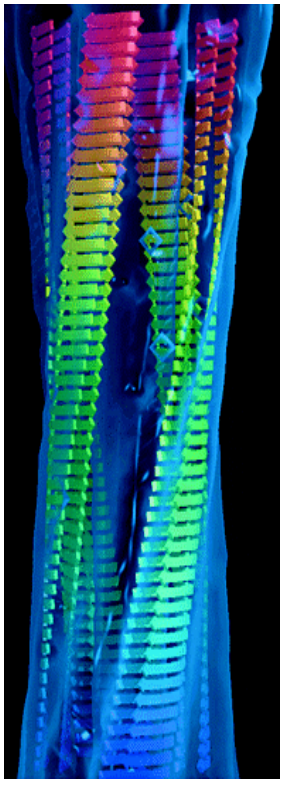

Figure 1.1 *Molecular model of an amyloid fibril derived from cryo-EM analysis of fibrils grown from an SH3 domain showing one way in which regions of the polypeptide chain involved in β-sheet structure is assembled within the fibrils, from (Dobson 1999).*

Although amyloid fibrils can be formed from a diverse group of proteins either as complete peptides or cleaved peptide fragments, the final conformation of the amyloid structure remains morphologically very similar, regardless of the protein source (Makin and Serpell 2002, Sunde *et al.* 1997). The ability to form amyloid is dependent on the common feature among all proteins, the

polypeptide chain backbone, but the propensity to form amyloid fibrils depends on sequence (Esteras-Chopo *et al.* 2005, Fändrich and Dobson 2002, Lopez de la Paz and Serrano 2004) which has allowed the design of *de novo* sequences which readily form fibrils (Lopez de la Paz *et al.* 2002, Lopez de la Paz and Serrano 2004). Prediction algorithms have been published attempting to predict amyloidogenic regions in protein sequences (Galzitskaya *et al.* 2006, Pawar *et al.* 2005, Thompson *et al.* 2006); these will be discussed further in section 1.5.

1.2 Protein Folding and Misfolding

Proteins have to leave a disorganised state and enter a highly organised state to be able to function (Dobson 2003). This process, known as protein folding, is of vital importance because proteins enable or control essentially every chemical process that takes place in all living organisms. Given that the amyloid state may represent a primitive ground state of protein folding and assembly reactions, research into the specific features of polypeptides that ensure folding to the correct, functional native state has increased tremendously (Chen *et al.* 2008, Dobson 2003, Dobson 2004b, Harrison *et al.* 2007, Jahn and Radford 2008).

Figure 1.2 illustrates the various states that can be attained by a protein once it is synthesised on the ribosome. Depending on the details of the external conditions (temperature, pH, solution composition) different conformational changes may lead to different aggregation pathways, resulting in structurally different supramolecular aggregates, such as amorphous aggregates or amyloid fibrils (Hamada and Dobson 2002).

In living systems, transitions between the different states are highly regulated by the environment and by the presence of molecular chaperones, proteolytic enzymes and other factors (Dobson 2003). *In vitro*, these constraints are relaxed, and the potential to increase the yield of the amyloid form is released. Amyloid fibrils are just one of the types of aggregate that can be formed by proteins, although a significant feature of amyloid is that its highly organised

hydrogen-bonded structure is likely to give it unique kinetic and/or thermodynamic stability. Thus, once formed, such aggregates can persist for long periods. Henceforth, in this thesis, all aggregates other than amyloid will be referred to as amorphous aggregates.

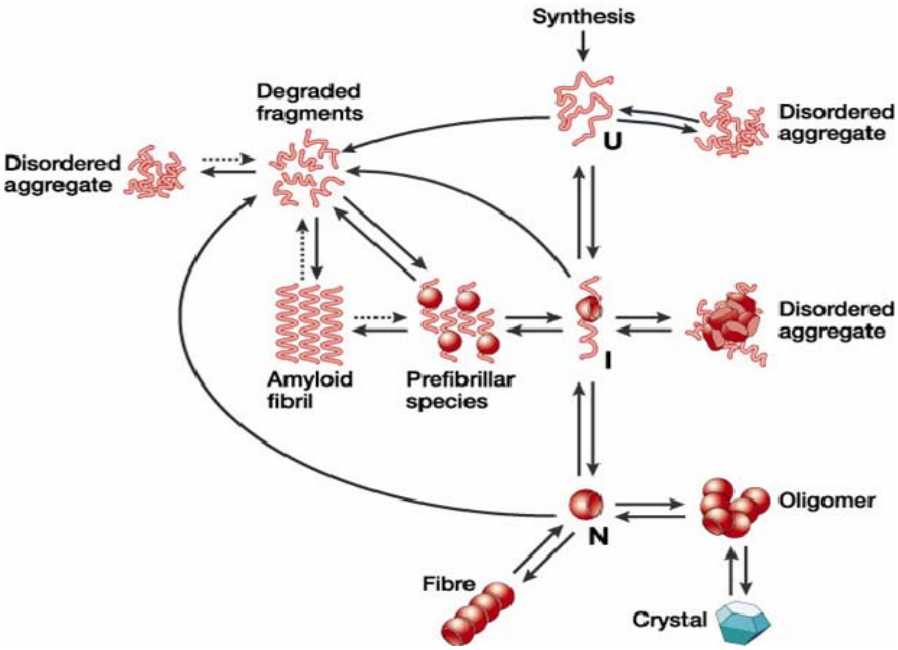

Figure 1.2 *Schematic mechanism showing states a protein molecule can access. I, intermediate; N, native; U, unfolded, from (Dobson 2003).*

The folding process provides proteins with access to several conformational states under given conditions. To illustrate this, energy landscapes have been proposed that describe protein folding as an entropically driven process (Jahn and Radford 2005, Radford 2000). They show the advancement of the unfolded polypeptide chains along an energy landscape towards the folded native structure. The simple sloping funnel-like nature of the energy landscape directs the folding polypeptide towards the energetically stable native state *via* a rough surface, while the intermolecular associations lead to aggregation *via* a more rugged energy landscape (as depicted in Figure 1.3). The landscape may be funnel-like for small proteins to fold rapidly and reliably towards a native state (Watters *et al.* 2007). Larger polypeptide sequences may have a rougher

energy landscapes, allowing partially folded species that may be on- or off-pathway to the native state (Brockwell and Radford 2007, Vendruscolo *et al.* 2003). However, the ruggedness of the energy surface is affected by factors like protein sequence and conditions under which protein folding or misfolding occurs.

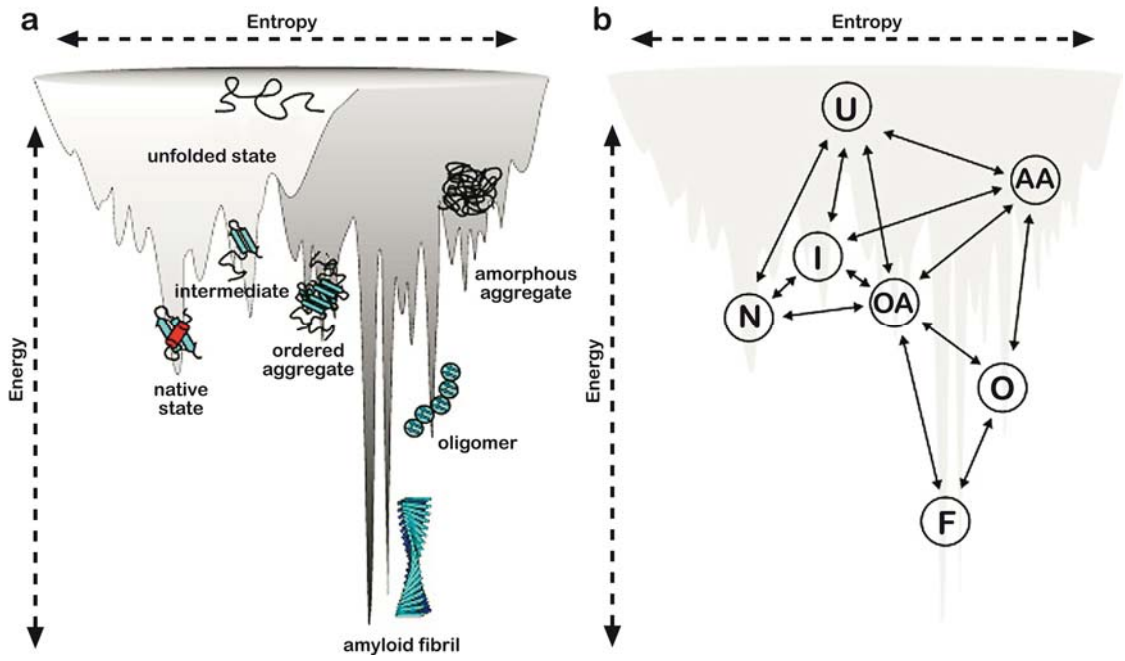

Figure 1.3 *"Illustration of a combined energy landscape for protein folding and aggregation. (a) The surface illustrates the roughness of the protein energy landscape, showing the multitude of conformational states available to a polypeptide chain. While rather simple folding funnels (light grey) can describe the conformational search of a single polypeptide chain to a functional monomer, intermolecular protein association dramatically increases ruggedness (dark grey). (b) Proposed pathways linking the conformational states shown in (a) populated on the combined folding and aggregation energy landscape. N, native; I, intermediate; U, unfolded; OA, ordered aggregate; AA, amorphous aggregate; F, fibril " from (Jahn and Radford 2008).*

Modifying the conditions under which a protein folds *in vivo or in vitro* alters the nature of the folding landscape. Different routes might be populated and/or different intermediates and transition states are observed as a consequence of

small alterations in the energy profile. Changes may result in local energy minima, which may become populated with partially folded intermediate protein structures. Under normal protein folding conditions, these minima are populated by transient intermediate structures. However, if an intermediate structure is stable enough, an energy barrier will be created which delays native folding. The increasing population of the long lived stable intermediate structures may lead to their self association. Such protein misfolding results in protein aggregation, including amyloid formation (Jahn and Radford 2008).

1.3 Mechanism for Amyloid Formation

1.3.1 Amyloid fibril formation *in vitro*

The generic nature of the aggregation process has enabled extensive studies of the transition between soluble precursor states and insoluble amyloid fibrils *in vitro* (Uversky and Fink 2004). The native conformation of globular proteins must usually be destabilised to allow protein amyloid aggregation to occur on a viable timescale (McParland *et al.* 2000). Specific protein destabilisation results in an increased population of partially folded conformations, with exposed aggregation-prone regions that enhance the probability of intermolecular interactions (Figure 1.4). In the case of lysozyme, the aggregation of which is involved in hereditary systemic amyloidosis, a single point mutation in the lysozyme gene is associated with fibril deposition in several tissues (Selkoe 2003). Partially structured folding intermediates are believed to play a key role in fibril formation by many amyloidogenic proteins (Wiseman *et al.* 2005). However, other assembly mechanisms have been suggested, including aggregation from a fully denatured state (Ferguson *et al.* 2006) or from the partially destabilised and predominantly native state (Plakoutsi *et al.* 2005) (Figure 1.4). In the absence of strong denaturants, the non-native oligomeric forms of the native proteins may play the role of promoting amyloid formation.

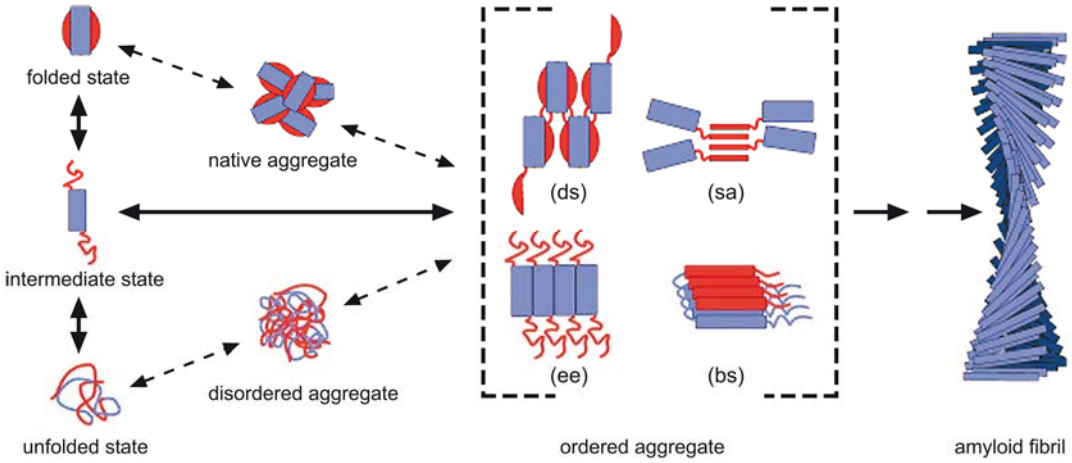

Figure 1.4 *"Proposed mechanisms of protein aggregation. Amyloid fibril formation for many proteins proceeds from intermediate partially folded states that are formed via partial unfolding of the native structure or via the partial structuring of unfolded polypeptides. Ordered aggregates associate via mechanisms such as domain swapping (ds), strand association (sa), edge-edge-association (ee) or β-strand stacking (bs). Self-association of these early oligomeric species, possibly involving further conformational changes, then leads to the formation of amyloid fibrils. The generic principles that govern this self-association process and the structure of the final amyloid fibril may depend critically on the polypeptide sequence and the solution conditions. In some proteins, association of native-like monomers or non-specific self-association into disordered aggregates has been observed as the initial step in amyloid assembly, in the latter route the polypeptide adopts an ordered β-sheet structure within the initially disordered aggregate before amyloid fibril formation proceeds" from (Jahn and Radford 2008).*

1.3.2 Intermolecular association pathways

Although several models for amyloid fibril formation have been suggested based on monitoring fibrillogenesis via microscopy, spectroscopic techniques and/or the binding of amyloid-specific dyes (Scheibel *et al.* 2004), it is generally agreed that amyloid fibrils are formed in a nucleation-dependent manner, in which the protein monomer is converted into a fibril structure via a transiently populated aggregation nucleus (Chiti and Dobson 2006, Dobson 2004a, Harper and Lansbury 1997). After the rate-limiting step of nucleus formation, aggregate growth proceeds rapidly by further addition of monomers or other assembly-

competent species. Even though the formation of the nucleus is thermodynamically unfavourable, its subsequent elongation is highly favourable and proceeds rapidly to the ultimate fibril structure (O'Nuallain *et al.* 2005).

In the initial lag phase of growth, the partially unfolded intermediate structures accumulate and form pre-fibrillar aggregates (Chiti and Dobson 2006). The association of the intermediate structures continues until a critical number associate to form an oligomeric structure known as the fibril nucleus (labelled 'prefibrillar species' in Figure 1.2). At this point, the slow lag phase ends and an exponential amyloid growth phase commences. In the growth phase, the oligomeric nucleating species and additional intermediates are thought to associate further into structures known as protofibrils. The protofibrils then associate to form longer filaments and growth continues with the addition of subsequent intermediate structural units, until the mature amyloid fibril is formed (Pedersen and Otzen 2008).

The fibril formation mechanism has been likened to the crystallisation process (Sawaya *et al.* 2007). There is a wealth of evidence in support of a nucleation-polymerisation mechanism, with aggregation being dependent on both protein concentration and time (Ahmad *et al.* 2005, Powers and Powers 2008). Nucleation is dependent on the monomer (or equivalent intermediate species) concentration exceeding a threshold value, known as the critical concentration, with the formation of the nucleus considered the rate-limiting step (Jarrett and Lansbury 1993, Powers and Powers 2008). High protein concentrations can therefore often accelerate nucleation, but may also result in formation of both on- and off-pathway oligomeric intermediates (Ahmad *et al.* 2005). The seeding of a supersaturated protein solution results in a greatly reduced lag time, supporting the formation of the nucleus as a limiting step (Powers and Powers 2008). The existence of the rate limiting step suggests that the formation of amyloid nuclei may be a heavily regulated step in biological systems, as a means of avoiding amyloid growth. Knowledge of the rate limiting step also provides a potential means to accelerate the process *in vitro*. Pathways of fibril formation, fibril morphologies and stability of protofibrillar intermediates are influenced strongly by experimental conditions (e.g. protein concentration, pH

and ionic strength) (Jahn *et al.* 2006), and elongation rates can depend on the stability of aggregation prone folding intermediates (Gosal *et al.* 2005).

As studies involving amyloidogenic proteins have advanced, it has been discovered that not all proteins conform to this model, but may instead involve pathways with additional or alternative rate-limiting steps. The assembly of spherical oligomers and other prefibrillar forms occurs with nucleation-independent kinetics, and results in the formation of spherical particles or "worm-like" fibrils (Smith *et al.* 2006a). Such routes towards fibrillation do not have a lag phase (Jahn and Radford 2008). In some cases, oligomeric species have been suggested to be the direct precursors of long-straight amyloid fibrils, whilst in other cases, an off-pathway role has been proposed (Necula *et al.* 2007) where the changes in intrinsic β-aggregation propensity affect the accessibility of parallel routes of aggregation (Pellarin *et al.* 2007). However, the primary protein used in this study, bovine insulin, conforms to the nucleation-polymerisation model, which will be described in more detail in chapter 2.

1.4 Fibril Structure

An enormous amount of research has been done to gain an in depth knowledge of amyloid structure. Of the many models for amyloid structure that have been postulated (section 1.1), the cross-β structure has attained most support (Makin *et al.* 2005, Nelson *et al.* 2005).

1.4.1 Amyloid macromolecular structure

Transmission electron microscopy (TEM) and atomic force microscopy (AFM) have revealed much about the macromolecular structure of amyloid. Under the TEM, amyloid fibrils typically appear as relatively straight, unbranched strands of 8–30 nm in width and highly variable lengths, up to several μm, consistent with a substructure of bundled protofilaments of 2–3 nm in diameter (Shirahama and Cohen 1967, Sipe and Cohen 2000, Vestergaard *et al.* 2007). Amyloid fibrils are comprised of protofilaments which are the fibrillar subunits that are clearly visible in micrographs, even before image processing (Makin and Serpell

2004). AFM imaging studies found that the protofilaments have a uniform height which vary when they reach the protofibril and fibril stage (Khurana *et al.* 2003). This signifies the intertwining of protofilaments in the fibrils (Serpell *et al.* 2000), as shown in Figure 1.1 where the SH3 domain forms twisted fibrils in which four protofilaments twist slowly around one another (Jiménez *et al.* 1999). Differing numbers and arrangements of protofilaments may be present under the same experimental conditions (Makin and Serpell 2004). The 3D reconstruction of insulin fibrils depict fibrils formed with two, four and six protofilaments in Figure 1.5 (Jiménez *et al.* 2002). The 4 protofilaments twisted around each other to form a fibril in Figure 1.5 (b) is analogous to the SH3 fibril depicted in Figure 1.1.

Figure 1.5 *Surface representation of 3D maps of the four insulin fibril structures (a) Structure of the fibril with a pair of protofilaments twisting around each other, (b) The four-protofilament compact fibril, (c) The six-protofilament fibril, (d) The twisted ribbon, from (Jiménez* et al*. 2002).*

Cryo-EM images of *ex vivo* amyloid fibrils of Asp67His variant lysozyme showed wavy fibrils, and image analysis indicated the presence of six protofilaments

(Jiménez *et al.* 2001). Chapter 3 will provide further details on the association of protofibrils to form insulin fibrils.

Microscopy studies on amyloid fibril morphology has been supplemented by X-ray fibre diffraction (Makin and Serpell 2005) to derive structural information on amyloid fibrils, which will be discussed in the following sections.

1.4.2 Internal structure of amyloid

At the molecular level, the secondary structure of amyloid fibrils appears to have cross β-sheet structure as revealed by X-ray fibre diffraction (Jiménez *et al.* 1999, Sawaya *et al.* 2007, Sunde and Blake 1997, Sunde *et al.* 1997). The β-strands are arranged perpendicular to the axis of the fibril (approximately 4.7 Å apart) and the β-sheets run parallel to it (approximately 10 Å apart) (Makin *et al.* 2005, Makin and Serpell 2005, Serpell 2000). The signals at 4.7 Å arise from the spacing between hydrogen bonded strands within a sheet and those at 10 Å are indicative of the intersheet spacing. Both of these signals are characteristic of a cross β structure. The backbone hydrogen atoms of the β-sheet provide extensive hydrogen bonding network which, in turn, gives the structure outstanding strength. The "stacks" of β-sheet are short and the amyloid fibril is built up of aligned strands (Makin and Serpell 2005) (Figure 1.6).

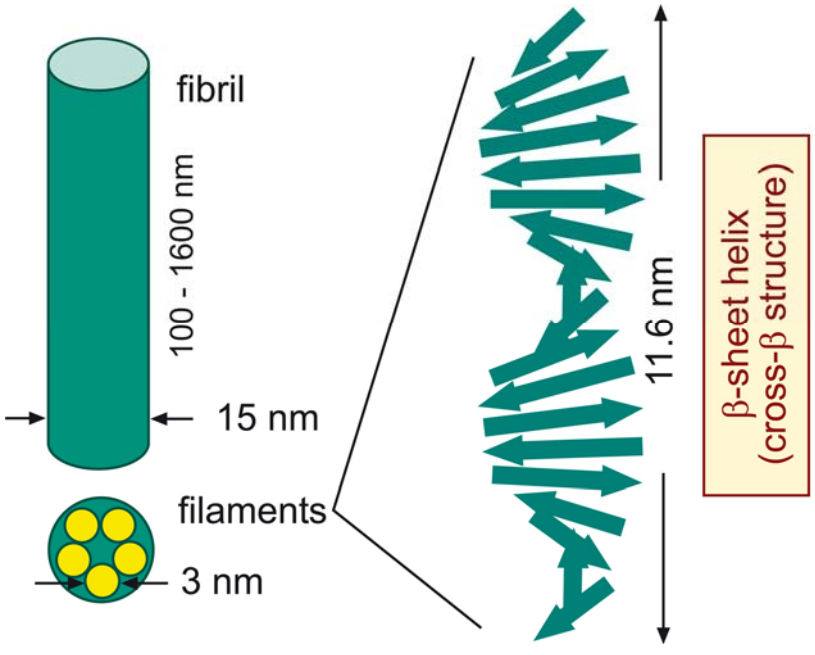

Figure 1.6 *Amyloid fibrils as self-assembling nanostructures, from (Jaskólski 2001).*

1.4.3 High resolution amyloid structural studies

In the last few years, X-ray crystallography and solid-state nuclear magnetic resonance spectroscopy (ssNMR) has been applied to gain insights into the secondary structure of amyloid fibrils (Ritter *et al.* 2005). Crystals prepared from small peptide fragments, with amyloid characteristics, have allowed studies to determine the molecular packing in the cross-β spine (Makin and Serpell 2005, Nelson *et al.* 2005). One example of a well studied peptide is the fragment (GNNQQNY) of the yeast prion protein Sup35p. Its X-ray crystal structure shows that it consists of pairs of parallel β-sheets and each individual peptide molecule contributes to a single β-strand (Figure 1.7 a) (Nelson *et al.* 2005). The region in between the β-sheets is dry, in contrast to the hydration externally. This tight molecular interaction between the pair of β-sheets results from interaction between the side chains of the two sheets to form a 'steric zipper' structure (Figure 1.7 b). The side chain interdigitation within the dry interface is suggested to be the underlying support for the cross-β spine found in amyloid fibrils (Eisenberg *et al.* 2006, Sawaya *et al.* 2007). However, the 'steric zipper' may vary depending on the protein sequence, side-chains, alignment of adjacent strands (parallel/antiparallel) and the separation of the sheets, which subsequently may cause the variations found in the structures of fibrils (Eisenberg *et al.* 2006, Fändrich and Dobson 2002, Sawaya *et al.* 2007). The continued elucidation of amyloid structure at a molecular level reveals that a structural diversity within the cross-β amyloid architecture exists. However, presence of stable β-sheet structures in all amyloid fibrils seems certain. It is possible that proteins with high β-sheet content, may also fall within the amyloid categorisation, hence a collective analysis by X-ray diffraction, ssNMR and EM (electron microscopy), is needed to grasp further understanding of the amyloid core structure (Kajava *et al.* 2005, Kajava *et al.* 2004).

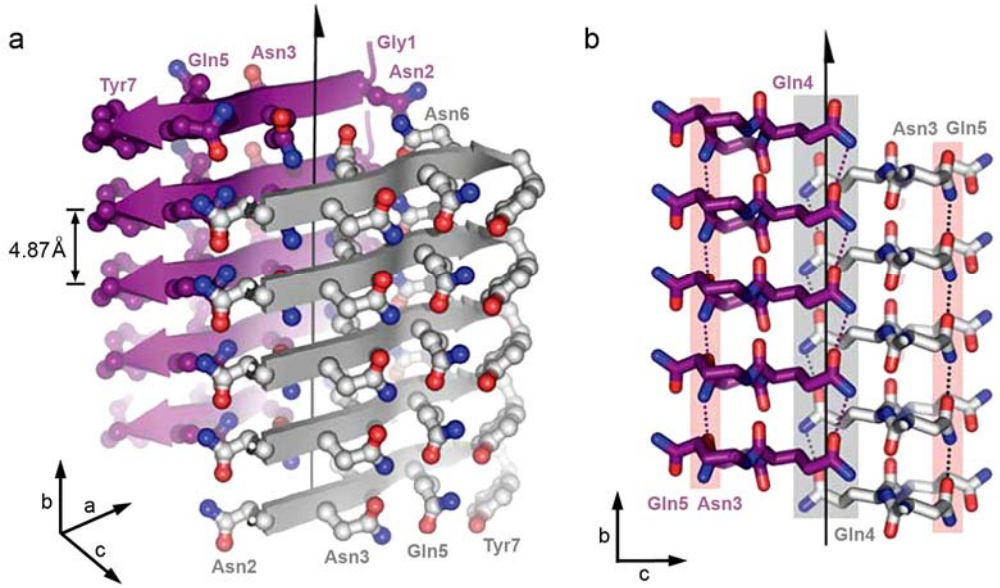

Figure 1.7 *Structure of GNNQQNY. a) "Shows a pair-of-sheets, with the backbone of each β-strand as an arrow with side chains protruding. The dry interface is between the two sheets, and the wet interfaces are on the outside surfaces. Side chains Asn2, Gln4, and Asn6 point inward, forming the dry interface. The 2_1 screw axis of the crystal is shown as the vertical line. It rotates one of the strands of the near sheet 180°C about the axis and moves it up ½ x 4.87 Å so that it is superimposed on one of the strands of the far sheet. b) Shows the steric zipper viewed edge on (down the a-axis). The vertical shift of one sheet, relative to the other, allows interdigitation of the side chains emanating from each sheet. The amide stacks of the dry interface (grey) is at the centre, and those of the wet interface are (pale red) on either side", from (Nelson* et al. *2005).*

1.5 Factors Affecting Protein Amyloid Formation

The process of fibril assembly is driven by non-covalent interactions and is responsive to environmental conditions, which can lead to formation of fibrils with markedly different characteristics, as introduced in section 1.1. For example, glucagon fibrils formed at high concentrations appeared as thin flexible fibrils, in contrast to fibrils formed at low concentrations, which appeared thicker and bundled (Pedersen and Otzen 2008). The environmental conditions

affect both fibril nucleation and fibril growth rates and it is the fibrils with the highest growth rate that are observed at the end of fibrillation trials (Pedersen and Otzen 2008).

This process of amyloid formation *in vitro*, from some peptides and proteins, can be rapid, occurring within a few hours for protein sequences with a high tendency to aggregate. For example, insulin forms fibrils in few hours, at acidic pHs (pH 1.6) and at elevated temperatures (60°C) (Nielsen *et al.* 2001c), and will be discussed in detail in chapters 2 and 3.

1.5.1 Sequence determines protein aggregation propensity

Although all proteins can, in theory, form amyloid, the process itself can be affected by various factors. Intrinsic factors which influence the aggregation propensity of proteins include: the β-sheet propensity, the hydrophobicity, the net charge and the presence of aromatic residues within the protein sequence (Chiti *et al.* 2003, DuBay *et al.* 2004, Lopez de la Paz and Serrano 2004, Pawar *et al.* 2005). The polypeptide 17-H-6 provides an example of a system in which aggregation was controlled by pH adjustment, charge−charge repulsion to obtain distinct nanofibres (Lin *et al.* 2008).

Although a large part of the polypeptide chain may be involved in the fibril structure, it is clear that some amino acid sequences are more prone to aggregation than others, as shown by a variety of studies of peptide assembly into amyloid fibrils *in vitro* (Lopez de la Paz and Serrano 2004). From a systematic analysis of more than 50 protein variants, Chiti *et al*. rationalized the propensities of some sequences to aggregate more rapidly than others, based on the physicochemical characteristics of the polypeptide chain (Chiti *et al.* 2003).

The correlations between amyloid and amorphous aggregation (Chiti *et al.* 2003) (section 1.2), prompted the development of computer algorithms that identify aggregation-prone regions in the amino acid sequence of proteins such as the prion protein, lysozyme, β-microglobulin, α-synuclein and tau (Fernandez-Escamilla *et al.* 2004, Pawar *et al.* 2005). Two examples of the

algorithms which have been developed are Zyggreggator (Pawar *et al.* 2005) and TANGO (Fernandez-Escamilla *et al.* 2004), and attempts were made to characterise the amyloid aggregation propensity of chemically modified proteins in this thesis using the Zyggregator algorithm (chapter 3, section 3.8.2).

1.5.2 Predicting amyloid fibril formation using the algorithm, Zyggregator

The Zyggregator algorithm of Dobson and his co-workers (Pawar *et al.* 2005) identifies aggregation-prone sequences by comparing the aggregation propensity score of a given amino acid sequence with an average propensity calculated for a set of sequences of similar length. Single amino acid mutations in the aggregation prone regions can change the aggregation rates dramatically, while similar changes in other regions may have relatively little effect (Chiti *et al.* 2002, Pawar *et al.* 2005). More specifically, DuBay and co-workers used a seven parameter formula which includes the intrinsic properties of the polypeptide chain (hydrophobicity, charge and the patterns of alternating hydrophobic–hydrophilic residues) and extrinsic factors related to the environment (peptide concentration, pH value and ionic strength of the solution) (DuBay *et al.* 2004). The algorithm takes into consideration both the intrinsic and extrinsic factors of the protein and provides a numeric score of the β–sheet aggregation propensity. This analysis has provided supplementary data for the discussion on the impact of protein sequence modification in chapter 3 which aims to assess the impact of chemical modification on insulin fibril propensity.

1.6 Amyloid Fibrils as Components of Bionanomaterials

Nanotechnology is the study and control of matter at dimensions of 1-100 nm which involves design, fabrication and application of nanomaterials (Koo 2006). Protein aggregates have been of interest in nanotechnology fields through bottom-up approaches for the assembly of fibrils employed in hydrogels and device applications (Hamada *et al.* 2004). Examples include self-assembly of fibrils to construct nanowires (Reches and Gazit 2003, Scheibel *et al.* 2003) and the use of fibrils to promote cell adhesion (Kasai *et al.* 2004). A more recent paper suggests that “an amyloid of a particular protein appears to be an

unusual plastic in some respects, such as in the homogeneous chain lengths of the monomers, the complexity and homogeneity of the side chain sequences, and the amphipathic nature of many polypeptides. Such unique features, combined with our ever-increasing abilities to dissect amyloid structure and the molecular basis of amyloid stability, may provide a level of control over the final product unprecedented in the synthetic plastics field and encourage practical uses of amyloid fibrils in material science and nanotechnology" (Wetzel *et al.* 2007).

Thus, *in vitro* polypeptide association and aggregation can offer attractive avenues for designing desirable structures for material science applications (Arnold 2008, Cherny and Gazit 2008, Gras 2007a, Gras 2007b, Gras *et al.* 2006, Gras *et al.* 2008, Kar *et al.* 2006, Mesquida *et al.* 2006, Petka *et al.* 1998, Qu *et al.* 2000, Waterhouse and Gerrard 2004). A recent analysis summarising/assessing the potential of fibrils led to the construction of a tree diagram (Figure 1.8) (Meade *et al.* 2007). Of the various potential uses for self-assembled protein shown in the tree, one branch depicts the reinforcing properties of fibrils in films, which are the subject of this study. The use of protein fibrils in bionanomaterials is reliant on the nature and properties of fibrils and is discussed in detail in the following sub-sections.

1.6.1 Strength and stability

In addition to their nanometre size and varying structural topographies, discussed in section 1.4.4, amyloids are attractive for their strength and stability. The organisation within the β-sheet structure of amyloid fibrils (Dirix *et al.* 2005, Knowles *et al.* 2006) confers stability at extremes of pH, temperature, or pressure (Dirix *et al.* 2005) and fibril structure is typically preserved in both aqueous and organic solvents. Amyloid fibrils are also resistant to proteolysis (Zurdo *et al.* 2001) and dehydration (Squires *et al.* 2006) making these structures suitable for more extreme conditions than native proteins. The mechanical properties displayed by amyloid fibrils show that fibril strength (~0.6 GPa) is equivalent to steel and the stiffness of fibrils (~3.3 GPa) is equivalent to the natural β-sheet protein silk (Smith *et al.* 2006b) indicating that fibrils are flexible. Additionally, the strength of fibrils under a tensile axial load (Fukuma *et*

al. 2006) has led to the suggestion that fibrils may contribute to the strength of natural adhesives including those utilised by terrestrial algae (Mostaert *et al.* 2006). These properties make fibrils promising candidate for the development of new materials.

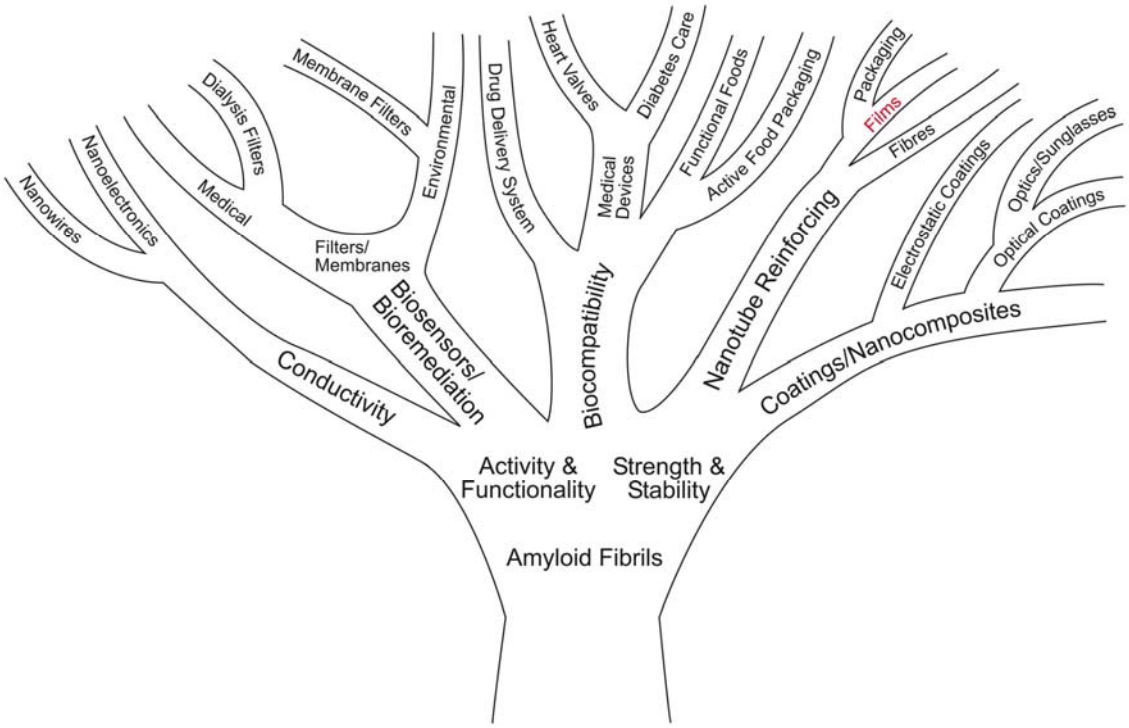

Figure 1.8 *A tree diagram showing the various potential for amyloid fibrils, adapted from (Meade* et al. *2007).*

1.6.2 Sequence versatility

Amyloid fibrils may be constructed from any combination of amino acids so the choice of amino acid sequence included within the fibril core or displayed on the fibril surface can (in theory) be used to manufacture fibrils with desired physical and chemical characteristics (Gras 2007a, Gras 2007b, Gras *et al.* 2008). Selective choice of amino acid side chains may introduce additional functionality to fibrillar materials, such as bioactive groups and enzymes, or for the covalent immobilization of other non-protein groups (Gras *et al.* 2006, Hartgerink 2004). The possibility of making amyloid fibrils composed of two distinct peptides, where the fibril itself assembles from unrelated peptides or proteins (MacPhee

and Dobson 2000), implies that more than one type of functional group can be incorporated on an amyloid fibril at a time (Gras 2007a).

1.6.3 Exploiting proteins in bionanomaterials

The favourable properties of amyloid fibrils including their increasingly recognised use in nature (section 1.1), a size and structure comparable to manmade nano-scale structures such as carbon nanotubes (CNTs) and buckyballs (Katz and Willner 2004) suggest that these structures hold great potential for a number of applications (Donald 2007, Gras 2007b, Gras *et al.* 2006, Gras *et al.* 2008, Hamada *et al.* 2004, Knowles *et al.* 2007, Maji *et al.* 2008, Waterhouse and Gerrard 2004). The use of proteins with their diverse array of biological functionality in composite materials may confer distinct advantages over using non-biological origin analogues, such as CNTs, in such materials. For example, CNTs are difficult to functionalise and may, in themselves, constitute a significant potential environmental hazard (Donaldson *et al.* 2006, Lam *et al.* 2006).

Moreover, the self-association of proteins into β-sheet fibrils has drawn attention for the development of supramolecular structures and functional materials with improved mechanical properties (Hamada *et al.* 2004, Tycko 2004, Zhang 2003). Recent successes include the production of nanowires based on controlled amyloid self-assembly (Scheibel *et al.* 2003). These metal wires were produced using a genetically modified variant of the prion determinant of the yeasts *Saccharomyces cerevisiae* Sup35p. In the first step, the self-assembly of high concentrations of NM fibrils acted as seeds to rapidly induce fibril growth. The exposed cysteine residues of the NM fibrils were derivatised with colloidal gold particles, which were subsequently coated with silver and then gold-enhanced to produce an unbroken network of conductive material spanning the length of fibril. In another study, conductive silver nanowires were produced after casting ionic silver inside the amyloid fibrils formed from a small synthetic peptide (Reches and Gazit 2003). Lindquist and her colleagues (Lindquist *et al.* 2005) claim applications relating to conducting and semi-conducting nano-wires built by controlled self-assembly of amyloid fibrils and selective deposition of metals and semi-conducting materials on these fibres. These achievements

show how the self-assembly process can be controlled to be used to conduct circuit devices on the nanometre scale.

Much discussion around the potential for the use of proteins in materials has originated from work on biological-origin materials. The strength and toughness of natural adhesives, fibres and composites was discussed by Smith and his co-workers in relation to the numbers of sacrificial inter-chain bonds holding a cross-linked multi-chain protein matrix together (Smith *et al.* 1999). The toughness of natural composite materials such as nacre (a composite of calcium carbonate and organic matter comprising protein) was discussed by Smith *et al.* (1999) and later studies (Fukuma *et al.* 2006, Mostaert *et al.* 2006, Mostaert and Jarvis 2007) concluded that the inherent strength of natural adhesives of terrestrial algae were due to the presence of amyloid fibril structures. More specifically, linear protein structures are believed to make stiff and strong fibres, which can be woven or knitted or embedded in a matrix, resulting in strong materials, for example acting as a barrier against crack propagation (Viney 2004).

The development of amyloid fibrils for hydrogels has also been described, based on the conjugation of specific peptide sequences to synthetic polymers. This technology opens up potential future biomedical applications, using hydrogels as biocompatible and/or biodegradable materials with readily controllable physical states (Goeden-Wood *et al.* 2003, Rösler *et al.* 2003). A hydrogel scaffold was designed with chemical and mechanical responsiveness, based on a synthetic peptide designed to undergo intramolecular folding to the β-structure in response to pH (Schneider *et al.* 2002). The folding process promotes self-assembly which allows the gel to respond to shear pressure, while the hydrogel can readily be dissolved by again altering the pH of the environment.

In the nanomaterials related patent literature, Veerman (2006) cites examples of using globular protein fibrils as thickening and foaming agents in food products and has included claims, relating to the use of these products and properties in non-foods such as paints, cosmetics, deodorants and toothpaste (Veerman

2006). *β*-Lactoglobulin forms gels, due to its ability to denature and aggregate. Under differing conditions of pH and ionic strength, *β*-lactoglobulin solutions can form either densely packed particulate gels (Clark *et al.* 2001) or fine-stranded (fibrillar) gels (Euston *et al.* 2007, Langton and Hermansson 1992). Globular aggregates of whey protein isolate and fibril aggregates of ovalbumin from egg white as gels for controlling food properties were found to be promising (Chojnicka *et al.* 2008).

1.6.4 Concerns on the application of amyloid nanofibres

A concern with protein amyloid fibril in bionanomaterials design may be the compatibility and potential toxicity of these materials. Although fibrils are typically associated with amyloid disease *in vivo*, there is evidence that the soluble oligomeric intermediates, not the insoluble well-ordered fibrils, are responsible for cellular toxicity (Bucciantini *et al.* 2002, Hardy and Selkoe 2002, Kayed *et al.* 2003). Mature fibrils may even serve as a rescue mechanism to remove cytotoxic species (Hardy and Selkoe 2002). Recently, it has been found that amyloids can act as a long-acting drug because they are stable depots that ensure a controlled release of the active peptide drug, gonadotropin-releasing hormone, from the amyloid termini (Maji *et al.* 2008).

Furthermore, it has been hypothesised recently that the α-sheet may be the toxic conformer in amyloid diseases (Daggett 2006). The existence of fibrils with natural functions *in vivo* also suggests that controlled interactions between fibrils and cells may be favourable (Fowler *et al.* 2006). These studies further support the thesis aim to investigate the potential of protein amyloid fibrils in bionanomaterials. However, any bionanomaterial developed will need to undergo safety testing prior to its commercial release.

1.6.5 Sources of protein for amyloid fibril

To enable the use of amyloid fibrils in bionanotechnological applications, a ready supply of fibrils is required. However, the vast majority of literature available on the formation of amyloid describes the behaviour of pure proteins *in vitro*. For industrial production of fibrils, there will be a need to source large amounts of amyloid fibrils, which may be prohibitively expensive and make it an

impractical option for material use. With a view to sourcing inexpensive proteins for amyloid forming propensity, fibrils have been formed from inexpensive precursor materials such as crude wheat proteins (Mackintosh *et al.* 2008) and crude bovine eye lens proteins (Garvey *et al.* 2008), potentially decreasing the cost of producing fibrillar materials on a large scale (Larsen *et al.* 2005). This research aims to develop the use of such amyloid fibrils, from crude sources of waste protein, for potential industrial use. In this thesis, methods are developed using insulin as a model protein.

1.7 Lessons from the Development of other β-Sheet Systems

The development of protein based fibrils for bionanomaterials can be informed from work with other β-sheet rich fibre-forming systems, which also offer considerable potential as new materials (Zhang *et al.* 2002). Relevant examples include the short repeating peptide sequences, arginine-alanine-aspartate (RAD) that have been used to produce β-sheet rich scaffolds (Holmes *et al.* 2000). These structures form hydrated gels under physiological conditions, which promote cell differentiation (Kisiday *et al.* 2002) and have been further functionalised incorporating bioactive sequences from laminin and collagen to enhance cell interactions (Genove *et al.* 2005). In addition, self-assembling peptides designed to resemble the chemical properties of the joint lubricant haluronic acid have favourable rheological properties, indicating a potential use as a therapeutic lubricant to assist in osteoarthritis (Bell *et al.* 2006). Nanofibres formed from simple homo-aromatic dipeptide motifs also demonstrate remarkable properties, such as chemical and thermal stability (Adler-Abramovich *et al.* 2006) at temperatures up to 150°C (Sedman *et al.* 2006) suggesting that these fibrils may be used for nanotechnology applications such as scaffolds and drug delivery. In addition, aromatic side chains may be chemically modified, resulting in different fibril morphologies (Reches and Gazit 2006).

The potential to control amyloid fibril morphology by chemical modification provides scope for the development of nanofibres since fibril structure (straight,

curly, ribbon) may affect fibril strength. Chapters 2 and 3 provide a discussion on the chemical modification of bovine insulin and its impact on controlling the structure of insulin nanofibres.

1.8 Film Nanocomposites

The basic physical, chemical, and biological properties of materials are remarkably altered as the size of their constituent grains decreases to a nanometre scale (Wan and Bai 2006). Nanomaterials that contain nanoparticles from a biological source, like protein fibrils, will be referred to as bionanomaterials in this thesis. Nanocomposites are multiphase materials where at least one of the constituent phases has one dimension less than 100 nm (Ajayan *et al.* 2003, Manocha 2006). The promise of nanocomposites lies in their multifunctionality and the feasibility of obtaining unique combinations of properties unachievable with traditional materials (Koo 2006).

1.8.1 Polymer nanocomposites

Polymer nanocomposites consist of a polymeric material and a reinforcing nanoscale material and show improvements in mechanical properties of the polymer, depending on factors such as the polymer matrix, nanocomposite morphology and the type of nanoparticle (Koo 2006). There are different types of commercially available nanoparticles, of which CNTs are attracting considerable interest as reinforcing materials in polymer nanocomposites (Calvert 1999). The driving force for the development of polymer nanocomposites is to control properties of nanomaterials with the introduction of nanometre sized structures, without changing the material chemical composition (Koo 2006).

This thesis investigated the incorporation of amyloid fibrils into a film matrix based on polyvinyl alcohol (PVOH). Nanometre sized fibres can strengthen a polymer matrix and the vast majority of studies have been carried out on CNTs (Bhattacharyya *et al.* 2006, Bhattacharyya *et al.* 2005, Calvert 1999, Coleman

2006). The background literature available on CNTs, protein and polymer nanocomposites were utilised as a platform for investigations in this thesis.

1.8.2 Carbon nanotubes and their functionalisation for nanocomposites

CNTs can be described as a nano-sized tube made up of a graphite sheet (Nepal and Geckeler 2006). Their stiff and robust structure is owed to the carbon-carbon bonds in their graphite-like structures, which are some of the strongest in nature (Thostensona *et al.* 2001). Of the wide spectrum of potential applications, CNTs are attracting considerable interest as reinforcing materials in polymer composites due to their superior structural and transport properties (high strength and flexibility, high thermal and electrical conductivity, and low density) (Calvert 1999, Koo 2006). Mechanical reinforcement of polymers by CNTs requires good interfacial bonding to ensure efficient stress transfer from the polymer matrix to the nanotube lattice. Unlike proteins, CNTs don't intrinsically have any side chain groups on the surface of their walls, to be able interact with a matrix. Studies supporting the modification and functionalisation of CNTs with amino acids and peptides (Figure 1.9) have become important for the bottom-up design of nanotubes (Lin *et al.* 2004). Furthermore, solubilisation *via* chemical modification and functionalisation is effective in imparting biocompatibility to CNTs, especially for the stable conjugation of CNTs with a variety of biological and bioactive molecules like proteins (Lin *et al.* 2004).

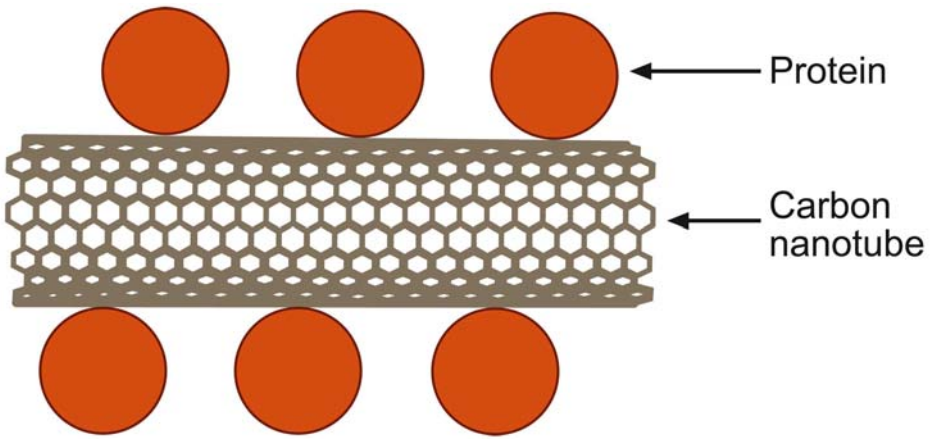

Figure 1.9 *An example of functionalising CNTs with biological molecules like protein from (Lin* et al*. 2004).*

Unlike CNTs, the protein side chains of amyloid are an intrinsic part of their structure and can be functionalised with additional peptide and protein groups or entities such as fluorophores and metalloporphyrins (Baldwin *et al.* 2006, MacPhee and Dobson 2000) allowing fibrils to interact with their environment or living cells. Preliminary studies into bilayered nanotubular structures suggested that hollow tubular arrangements of amyloid can be formed of uniform dimensions with charged curve surfaces representing scaffolds highly accessible for modification (Lu *et al.* 2003). This feature imparts a significant advantage over CNTs, which are limited by the lack of reactivity along their sidewalls (Lin *et al.* 2003).

1.8.3 Polyvinyl alcohol

Polymer nanocomposites have a polymer as the matrix, which will be PVOH in this study, and the nanoparticles, dispersed within it, in this case protein amyloid fibrils. PVOH is a nontoxic, water-soluble, biocompatible, and biodegradable synthetic polymer, which can be widely used in biochemical and biomedical materials. It has good film-forming properties, highly hydrophilic properties, and high mechanical strength, and has been studied as a membrane (Lin *et al.* 2006, Shang and Peng 2007). PVOH is a semicrystalline polymer with hydroxyl groups that give rise to intermolecular and intramolecular hydrogen bonds. PVOH films have a high tensile strength and oxygen barrier properties, comparable to many other polymers (Kim *et al.* 2007). In addition, since PVOH is biocompatible and nontoxic, and exhibits minimal cell adhesion and protein absorption, PVOH membranes have been developed for biomedical applications (Choi *et al.* 2007, Chuang *et al.* 1999, Kobayashi *et al.* 2005, Koyano *et al.* 2000, Oh *et al.* 2004, Qi *et al.* 2004). For instance, PVOH/ polyvinylpyrrolidone/chitosan hydrogels were studied for wound dressing application in rats (Huang and Yang 2008).

PVOH was selected as the model polymer to determine the potential of fibrils as nanocomposite components in this thesis, and the large amount of work done on PVOH provides support for its use as a model in a film forming system. More specifically, the selection of PVOH for investigating the impact of protein fibrils on the mechanical properties of the polymer was motivated by PVOH/protein

based film studies, such as PVOH/wheat (Dicharry *et al.* 2006), PVOH/collagen hydrolysate (Alexy *et al.* 2003), and PVOH/gelatin (Bergo *et al.* 2006, Darder *et al.* 2006, Ma *et al.* 2006, Mendieta-Taboada *et al.* 2008, Su *et al.* 2007, Wang *et al.* 2005, Yi *et al.* 2006)), PVOH/soluble egg shell membrane (Yi *et al.* 2006), PVOH/chitosan (Wang *et al.* 2005), and PVOH/cellulose fibres (Wang and Sain 2007), PVOH/soy protein (Su *et al.* 2007), and PVOH/membrane protein (Ma *et al.* 2006). To improve the mechanical characteristics of protein-based films, these proteins are mixed with synthetic polymers (Tharanathan 2003), such as PVOH. (Chiellini *et al.* 2003) have demonstrated biodegradability of protein blended PVOH films.

1.8.4 Proteins in films

Work to date reveals that films can be made from wheat protein, milk protein, zein protein and other proteins (Budi Santosa and Padua 1999). The biocompatibility, biodegradability, and structural support, plus the availability of an industrial supply of proteins (Aoi *et al.* 2000, Tharanathan 2003) has led to studies on blends of polymers with polypeptides (Takasu 1997) and, more recently, the development of protein-based packaging materials (Tharanathan 2003). In particular, proteins derived from various animal and plant sources have successfully been formed into films and/or coatings (Gounga *et al.* 2007, Lee *et al.* 2008, Naushad and Stading 2007).

Edible films have been produced by heating sunflower proteins to 85°C and solution casting (Meixueir *et al.* 2000). Film formation in such proteins is through intermolecular disulfide bridges and hydrogen bonds, accompanied by surface dehydration. Whey protein isolate and milk protein also produce edible film and coatings with different functionalities and applications (Gounga *et al.* 2007, Khwaldia *et al.* 2004, Sothornvit *et al.* 2007). An example of this type of natural polymers is gelatin, a polypeptide derived from the structural protein collagen, that is able to form tough films (Park *et al.* 2008) and transparent, elastic and thermoreversible gels (Darder *et al.* 2006). The various applications of proteins, both in the functional and aggregated form, discussed in the sections above further support the potential for amyloid fibrils in bionanomaterials (Gras 2007a, Gras 2007b, Gras *et al.* 2006).

1.9 Developing Amyloid Fibril Materials

Potential applications for protein-based materials are far-reaching and include industrial applications as diverse as medicine, health and nutrition, catalysis, electronics, plastics and structural materials (Dobson 2000). As described in section 1.6 (Figure 1.8), limited successes have been described in the literature. The huge potential of amyloid fibrils in bionanomaterials detailed in theory (Arnold 2008, Cherny and Gazit 2008, Gras 2007a, Gras 2007b, Gras *et al.* 2006, Gras *et al.* 2008), signifies a need to carry out investigations to realise the application of protein fibrils in bionanotechnology. To this end, this thesis is aimed at developing a method for making films, comprising amyloid fibrils in a protein-model polymer matrix which may be developed for applications such as biodegradable polymers and membranes and filters for bioremediation and air purification and sensing systems. Applications might also be envisaged in tissue scaffolding (MacPhee and Woolfson 2004).

1.10 Thesis Objectives

A brief overview of the nature of amyloid fibril formation and their properties has been provided in this introduction. For bionanomaterial scientists, protein fibril self-assembly presents an exciting opportunity to create novel bionanomaterials for applications discussed earlier.

The early part of this study proposed to look at protein structures that will form amyloid fibrils, focussing on the little studied area of how protein derivatisation (lysine group modification, disulfide reduction-alkylation, trypsin treatment, chymotrypsin treatment) influences the amyloid fibrils. The goal was to modify bovine insulin (a model protein), knowing that it forms fibrils and can be characterised readily *in vitro*. Initial method development for insulin modification and characterisation of the modified insulin was carried out to prepare samples in milligram quantities for *in vitro* fibril studies. Derivatisations were limited to those potentially applicable on a commercial scale.

This thesis then aimed to test the effect of insulin modification on its aggregation propensity, in a heterogeneous mixture. It was hypothesised that a change in the primary structure of insulin may have an effect on the fibril structure, having identified the role of intrinsic factors in determining the aggregation propensity of proteins (section 1.5). The heterogeneity of the modified insulin was relevant, to provide key information for the later goal of forming fibrils from a cheap and crude source of protein.

The ability of a readily available waste protein (crystallins from bovine eye lenses) to form amyloid was then considered. Bovine eye lens protein was chosen because it was readily available, and possessed many features that appeared promising for the successful induction of amyloid from crude protein extracts. Amyloid fibrils were manufactured from this cheap and crude source of protein to be utilised in later studies of film composites.

The strength and stability of amyloid fibrils opens up the potential for amyloid fibrils to be used as a minor component of a film, and to determine whether the inherent physical properties of individual amyloid fibril structures will have any effects on the bulk physical properties of the films into which they are incorporated. There is scant evidence to date as to what extent changes will be observed in the strength of resulting nanocomposites, when they incorporate very small amounts of fibrils. Accordingly, it was an objective of this study to develop a method to prepare film composite and provide composite materials (films) containing protein amyloid fibrils with better mechanical properties, than the parent material. A laboratory scale method of making films was developed, films were cast with and without fibrils and their strength was measured. The advantage of using waste material is that fibrils could be economically produced on the scale required for many applications. Worldwide there is as yet no significant technological or industrial activity based around the manufacturing or film composite processing of amyloid fibrils. A means to manufacture amyloid fibrils from waste materials may thus open up new opportunities.

1.11 Thesis Overview

Chapter 2 outlines investigations regarding chemical modification of bovine insulin and assessment of the extent of modification via mass spectrometry. Sufficient quantities are prepared to prepare amyloid fibrils from the modified insulin in chapter 3.

Chapter 3 addresses the effect of chemical modification on the aggregation propensity of bovine insulin, present in a heterogeneous mixture *in vitro* and the morphology of the fibrils formed.

Chapter 4 details the development of a small scale method for manufacturing and characterising films incorporating protein fibrils.

Chapter 5 investigates the mechanical effect of incorporating insulin fibrils and crude crystallin fibrils in to PVOH films.

Chapter 6 summarises the major findings of this thesis and future directions to be pursued from this work.

Chapter 7 outlines all experimental procedures undertaken during this thesis.

1.12 References

Adler-Abramovich, L., M. Reches, V. L. Sedman, S. Allen, S. J. B. Tendler, and E. Gazit. 2006. Thermal and chemical stability of diphenylalanine peptide nanotubes: Implications for nanotechnological applications. *Langmuir* 22: 1313-1320.

Aggeli, A., I. A. Nyrkova, M. Bell, R. Harding, L. Carrick, T. C. B. McLeish, A. N. Semenov, and N. Boden. 2001. Hierarchical self-assembly of chiral rod-like molecules as a model for peptide beta-sheet tapes, ribbons, fibrils, and fibers. *Proceedings of the National Academy of Sciences of the United States of America* 98: 11857-11862.

Ahmad, A., V. N. Uversky, D. Hong, and A. L. Fink. 2005. Early events in the fibrillation of monomeric insulin. *Journal of Biological Chemistry* 280: 42669-42675.

Ajayan, P. M., S. S. Schadler, and P. V. Braun. 2003. *Nanocomposite science and technology*. Wiley-VCH GmbH & Co. KGaA, Weinheim.

Alexy, P., D. Bakos, S. Hanzelova, L. Kukolikova, J. Kupec, K. Charvatova, E. Chiellini, and P. Cinelli. 2003. Poly(vinyl alcohol)-collagen hydrolysate thermoplastic blends: I. Experimental design optimisation and biodegradation behaviour. *Polymer Testing* 22: 801-809.

Aoi, K., A. Takasu, and M. Okada. 2000. DNA-based polymer hybrids Part 1. Compatibility and physical properties of poly(vinyl alcohol)/DNA sodium salt blend. *Polymer* 41: 2847-2853.

Arnold, C. 2008. From diseases to devices. *Chemical and Engineering New: Science/Technology* 86: 48-50.

Baldwin, A. J., R. Bader, J. Christodoulou, C. E. MacPhee, C. M. Dobson, and P. D. Barker. 2006. Cytochrome display on amyloid fibrils. *Journal of the American Chemical Society* 128: 2162-2163.

Bell, C. J., L. M. Carrick, J. Katta, Z. Jin, E. Ingham, A. Aggeli, N. Boden, T. A. Waigh, and J. Fisher. 2006. Self-assembling peptides as injectable lubricants for osteoarthritis. *Journal of Biomedical Materials Research Part A* 78A: 236-246.

Bergo, P., R. A. Carvalho, P. J. A. Sobral, F. R. S. Bevilacqua, J. K. C. Pinto, and J. P. Souza. 2006. Microwave transmittance in gelatin-based films. *Measurement Science and Technology* 17: 3261-3264.

Bhattacharyya, S., J.-P. Salvetat, and M.-L. Saboungi. 2006. Reinforcement of semicrystalline polymers with collagen-modified single walled carbon nanotubes. *Applied Physics Letters* 88: 233119-3.

Bhattacharyya, S., C. Sinturel, J. P. Salvetat, and M.-L. Saboungi. 2005. Protein-functionalised carbon nanotube-polymer composites. *Applied Physics Letters* 86: 113104-113107.

Brange, J., L. Andersen, E. D. Laursen, G. Meyn, and E. Rasmussen. 1997a. Toward understanding insulin fibrillation. *Journal of Pharmaceutical Sciences* 86: 517-525.

Brange, J., G. G. Dodson, D. J. Edwards, P. H. Holden, and J. L. Whittingham. 1997b. A model of insulin fibrils derived from the X-ray crystal structure of a monomeric insulin (despentapeptide insulin). *Proteins-Structure Function and Genetics* 27: 507-516.

Brockwell, D. J., and S. E. Radford. 2007. Intermediates: ubiquitous species on folding energy landscapes? *Current Opinion in Structural Biology* 17: 30-37.

Bucciantini, M., E. Giannoni, F. Chiti, F. Baroni, L. Formigli, J. Zurdo, N. Taddei, G. Ramponi, C. M. Dobson, and M. Stefani. 2002. Inherent toxicity of aggregates implies a common mechanism for protein misfolding diseases. *Nature* 416: 507-511.

Budi Santosa, F. X., and G. W. Padua. 1999. Tensile properties and water absorption of zein sheets plasticized with oleic and linoleic acids. *Journal of Agricultural and Food Chemistry* 47: 2070-2074.

Calamai, M., C. Canale, A. Relini, M. Stefani, F. Chiti, and C. M. Dobson. 2005. Reversal of protein aggregation provides evidence for multiple aggregated states. *Journal of Molecular Biology* 346: 603-616.

Calvert, P. 1999. Nanotube composites: A recipe for strength. *Nature* 399: 210-211.

Carrio, M., N. Gonzalez-Montalban, A. Vera, A. Villaverde, and S. Ventura. 2005. Amyloid-like properties of bacterial inclusion bodies. *Journal of Molecular Biology* 347: 1025-1037.

Chapman, M. R., L. S. Robinson, J. S. Pinkner, R. Roth, J. Heuser, M. Hammar, S. Normark, and S. J. Hultgren. 2002. Role of *Escherichia coli* curli operons in directing amyloid fiber formation. *Science* 295: 851-855.

Chen, Y., F. Ding, H. Nie, A. W. Serohijos, S. Sharma, K. C. Wilcox, S. Yin, and N. V. Dokholyan. 2008. Protein folding: Then and now. *Archives of Biochemistry and Biophysics* 469: 4-19.

Cherny, I., and E. Gazit. 2008. Amyloids: Not only pathological agents but also ordered nanomaterials. *Angewandte Chemie International Edition* 47: 4062-4069.

Chiellini, E., A. Corti, S. D'Antone, and R. Solaro. 2003. Biodegradation of poly (vinyl alcohol) based materials. *Progress in Polymer Science* 28: 963-1014.

Chiti, F., and C. M. Dobson. 2006. Protein misfolding, functional amyloid, and human disease. *Annual Review of Biochemistry* 75: 333-366.

Chiti, F., M. Stefani, N. Taddei, G. Ramponi, and C. M. Dobson. 2003. Rationalization of the effects of mutations on peptide and protein aggregation rates. *Nature* 424: 805-808.

Chiti, F., N. Taddei, F. Baroni, C. Capanni, M. Stefani, G. Ramponi, and C. M. Dobson. 2002. Kinetic partitioning of protein folding and aggregation. *Nature Structural Biology* 9: 137-143.

Chiti, F., P. Webster, N. Taddei, A. Clark, M. Stefani, G. Ramponi, and C. M. Dobson. 1999. Designing conditions for *in vitro* formation of amyloid protofilaments and fibrils. *Proceedings of the National Academy of Sciences of the United States of America* 96: 3590-3594.

Choi, J., H. Bodugoz-Senturk, H. J. Kung, A. S. Malhi, and O. K. Muratoglu. 2007. Effects of solvent dehydration on creep resistance of poly(vinyl alcohol) hydrogel. *Biomaterials* 28: 772-780.

Chojnicka, A., S. de Jong, C. G. de Kruif, and R. W. Visschers. 2008. Lubrication properties of protein aggregate dispersions in a soft contact. *Journal Agricultural Food Chemistry* 56: 1274-1282.

Chuang, W.-Y., T.-H. Young, C.-H. Yao, and W.-Y. Chiu. 1999. Properties of the poly(vinyl alcohol)/chitosan blend and its effect on the culture of fibroblast in vitro. *Biomaterials* 20: 1479-1487.

Clark, A. H., G. M. Kavanagh, and S. B. Ross-Murphy. 2001. Globular protein gelation-theory and experiment. *Food Hydrocolloids* 15: 383-400.

Cohen, A. S., and E. Calkins. 1959. Electron microscopic observations on a fibrous component in amyloid of diverse origins. *Nature* 183: 1202-1203.

Coleman, J. N., Khan, U., Gun'ko, Y. K. 2006. Mechanical reinforcement of polymers using carbon nanotubes. *Advanced Materials* 18: 689-706.

Daggett, V. 2006. Alpha-Sheet: The toxic conformer in amyloid diseases? *Accounts of Chemical Research* 39: 594-602.

Dantzker, J. M. 2005. The unfolding of amyloid's true colors. *Public Library of Science Biology* 4: e8.

Darder, M., A. I. Ruiz, P. Aranda, H. Van Damme, and E. Ruiz-Hitzky. 2006. Bio-nanohybrids based on layered inorganic solids: Gelatin nanocomposites. *Current Nanoscience* 2: 231-241.

Dicharry, R. M., P. Ye, G. Saha, E. Waxman, A. D. Asandei, and R. S. Parnas. 2006. Wheat gluten-thiolated poly(vinyl alcohol) blends with improved mechanical properties. *Biomacromolecules* 7: 2837-2844.

Dirix, C., F. Meersman, C. E. MacPhee, C. M. Dobson, and K. Heremans. 2005. High hydrostatic pressure dissociates early aggregates of TTR105-115, but not the mature amyloid fibrils. *Journal of Molecular Biology* 347: 903-909.

Dobson, C. M. 1999. Protein misfolding, evolution and disease. *Trends in Biochemical Sciences* 24: 329-332.

—. 2000. Protein fibrils and their preparation from naturally occurring and non-naturally occurring proteins. Pages 51. *PCT Int. Appl.* (Isis Innovation Ltd., UK). Wo.

—. 2003. Protein folding and misfolding. *Nature* 426: 884-890.

—. 2004a. Experimental investigation of protein folding and misfolding. *Methods Investigating Protein Folding, Misfolding and Nonnative States: Experimental and Theoretical Methods* 34: 4-14.

—. 2004b. Principles of protein folding, misfolding and aggregation. *Seminars in Cell and Developmental Biology* 15: 3-16.

Dobson, C. M., and M. Karplus. 1999. The fundamentals of protein folding: bringing together theory and experiment. *Current Opinion in Structural Biology* 9: 92-101.

Donald, A. M. 2007. Why should polymer physicists study biopolymers? *Journal of Polymer Science, Part B: Polymer Physics* 45: 3257-3262.

Donaldson, K., R. Aitken, L. Tran, V. Stone, R. Duffin, G. Forrest, and A. Alexander. 2006. Carbon nanotubes: A review of their properties in relation to pulmonary toxicology and workplace safety. *Toxicological Science* 92: 5-22.

DuBay, K. F., A. P. Pawar, F. Chiti, J. Zurdo, C. M. Dobson, and M. Vendruscolo. 2004. Prediction of the absolute aggregation rates of amyloidogenic polypeptide chains. *Journal of Molecular Biology* 341: 1317-1326.

Eisenberg, D., R. Nelson, M. R. Sawaya, M. Balbirnie, S. Sambashivan, M. I. Ivanova, A. O. Madsen, and C. Riekel. 2006. The structural biology of protein aggregation diseases: fundamental questions and some answers. *Accounts of Chemical Research* 39: 568-575.

Eisert, R., L. Felau, and L. R. Brown. 2006. Methods for enhancing the accuracy and reproducibility of congo red and thioflavin T assays. *Analytical Biochemistry* 353: 144-146.

Esteras-Chopo, A., L. Serrano, and M. L. de la Paz. 2005. The amyloid stretch hypothesis: Recruiting proteins toward the dark side. *Proceedings of the National Academy of Sciences of the United States of America* 102: 16672-16677.

Euston, S. R., S. Ur-Rehman, and G. Costello. 2007. Denaturation and aggregation of β-lactoglobulin - A preliminary molecular dynamics study. *Food Hydrocolloids* 21: 1081-1091.

Fändrich, M., and C. M. Dobson. 2002. The behaviour of polyamino acids reveals an inverse side chain effect in amyloid structure formation. *The European Molecular Biology Organisation Journal* 21: 5682-5690.

Fändrich, M., M. A. Fletcher, and C. M. Dobson. 2001. Amyloid fibrils from muscle myoglobin. *Nature* 410: 165-166.

Fändrich, M., V. Forge, K. Buder, M. Kittler, C. M. Dobson, and S. Diekmann. 2003. Myoglobin forms amyloid fibrils by association of unfolded polypeptide segments. *Proceedings of the National Academy of Sciences of the United States of America* 100: 15463-15468.

Ferguson, N., J. Becker, H. Tidow, S. Tremmel, T. D. Sharpe, G. Krause, J. Flinders, M. Petrovich, J. Berriman, H. Oschkinat, and A. R. Fersht. 2006. General structural motifs of amyloid protofilaments. *Proceedings of the National Academy of Sciences of the United States of America* 103: 16248-16253.

Fernandez-Escamilla, A.-M., F. Rousseau, J. Schymkowitz, and L. Serrano. 2004. Prediction of sequence-dependent and mutational effects on the aggregation of peptides and proteins. *Nature Biotechnology* 22: 1302-1306.

Fowler, D. M., A. V. Koulov, C. Alory-Jost, M. S. Marks, W. E. Balch, and J. W. Kelly. 2006. Functional amyloid formation within mammalian tissue. *Public Library of Science Biology* 4: e6.

Fukuma, T., A. S. Mostaert, and S. P. Jarvis. 2006. Explanation for the mechanical strength of amyloid fibrils. *Tribology Letters* 22: 233-237.

Galzitskaya, O. V., S. O. Garbuzynskiy, and M. Y. Lobanov. 2006. Prediction of amyloidogenic and disordered regions in protein chains. *Public Library of Science Computational Biology* 2: 1639-1648.

Garvey, M., S. L. Gras, S. Meehan, S. J. Meade, J. A. Carver, and J. A. Gerrard. 2008. Protein nanofibres of defined morphology prepared from mixtures of crude crystallins. *International Journal of Nanotechnology* Submitted.

Genove, E., C. Shen, S. Zhang, and C. E. Semino. 2005. The effect of functionalized self-assembling peptide scaffolds on human aortic endothelial cell function. *Biomaterials* 26: 3341-3351.

Goeden-Wood, N. L., J. D. Keasling, and S. J. Muller. 2003. Self-assembly of a designed protein polymer into β-sheet fibrils and responsive gels. *Macromolecules* 36: 2932-2938.

Gosal, W. S., I. J. Morten, E. W. Hewitt, D. A. Smith, N. H. Thomson, and S. E. Radford. 2005. Competing pathways determine fibril morphology in the self-assembly of β-microglobulin into amyloid. *Journal of Molecular Biology* 351: 850-864.

Gounga, M. E., S.-Y. Xu, and Z. Wang. 2007. Whey protein isolate-based edible films as affected by protein concentration, glycerol ratio and pullulan addition in film formation. *Journal of Food Engineering* 83: 521-530.

Gras, S. L. 2007a. Amyloid fibrils: From disease to design. New biomaterial applications for self-assembling cross-beta fibrils. *Australian Journal of Chemistry* 60: 333-342.

—. 2007b. Protein misfolding: A route to new nanomaterials. *Advanced Powder Technology* 18: 699-705.

Gras, S. L., A. M. Squires, C. M. Dobson, and C. E. MacPhee. 2006. Functionalised fibrils for bio-nanotechnology. *International Conference On Nanoscience and Nanotechnology*, Brisbane, Qld.

Gras, S. L., A. K. Tickler, A. M. Squires, G. L. Devlin, M. A. Horton, C. M. Dobson, and C. E. MacPhee. 2008. Functionalised amyloid fibrils for roles in cell adhesion. *Biomaterials* 29: 1553-1562.

Graveland-Bikker, J. F., and C. G. de Kruif. 2006. Unique milk protein based nanotubes: Food and nanotechnology meet. *Trends in Food Science & Technology, Functionality in Complex Foods* 17: 196-203.

Guijarro, J. I., M. Sunde, J. A. Jones, I. D. Campbell, and C. M. Dobson. 1998. Amyloid fibril formation by an SH3 domain. *Proceedings of the National Academy of Sciences of the United States of America* 95: 4224-4228.

Hamada, D., and C. M. Dobson. 2002. A kinetic study of β-lactoglobulin amyloid fibril formation promoted by urea. *Protein Science* 11: 2417-2426.

Hamada, D., I. Yanagihara, and K. Tsumoto. 2004. Engineering amyloidogenicity towards the developement of nanofibrillar materials. *Trends in Biotechnology* 22: 93-97.

Hardy, J., and D. J. Selkoe. 2002. The amyloid hypothesis of Alzheimer's disease: progress and problems on the road to therapeutics. *Science* 297: 353-356.

Harper, J. D., and P. T. Lansbury, Jr. 1997. Models of amyloid seeding in Alzheimer's disease and scapie: Mechanistic truths and physiological consequences of the time-dependent solubility of amyloid proteins. *Annual Review of Biochemistry* 66: 385-407.

Harrison, R. S., P. C. Sharpe, Y. Singh, and D. P. Fairlie. 2007. Amyloid peptides and proteins in review. *Reviews of Physiology, Biochemistry and Pharmacology* 159: 1-77.

Hartgerink, J. D. 2004. Covalent capture: a natural complement to self-assembly. *Current Opinion in Chemical Biology* 8: 604-609.

Holmes, T. C., S. de Lacalle, X. Su, G. Liu, A. Rich, and S. Zhang. 2000. Extensive neurite outgrowth and active synapse formation on self-assembling peptide scaffolds. *Proceedings of the National Academy of Sciences of the United States of America* 97: 6728-6733.

Huang, M.-H., and M.-C. Yang. 2008. Evaluation of glucan/poly(vinyl alcohol) blend wound dressing using rat models. *International Journal of Pharmaceutics* 346: 38-46.

Iconomidou, V. A., G. Vriend, and S. J. Hamodrakas. 2000. Amyloids protect the silkmoth oocyte and embryo. *Federation of European Biochemical Societies Letters* 479: 141-145.

Jahn, T. R., M. J. Parker, S. W. Homans, and S. E. Radford. 2006. Amyloid formation under physiological conditions proceeds via a native-like folding intermediate. *Nature Structural & Molecular Biology* 13: 195-201.

Jahn, T. R., and S. E. Radford. 2005. The Yin and Yang of protein folding. *Federation of European Biochemical Societies Journal* 272: 5962-5970.

—. 2008. Folding versus aggregation: Polypeptide conformations on competing pathways. *Archives of Biochemistry and Biophysics* 469: 100-117.

Jarrett, J. T., and P. T. Lansbury, Jr. 1993. Seeding "one-dimensional crystallisation" of amyloid: A pathogenic mechanism in Alzheimer's disease and scrapie? *Cell* 73: 1055-1058.

Jaskólski, M. 2001. 3D domain swapping, protein oligomerization, and amyloid formation. *Acta Biochima Polonica* 48: 807-827.

Jiménez, J. L., J. I. Guijarro, E. Orlova, J. Zurdo, C. M. Dobson, M. Sunde, and H. R. Saibil. 1999. Cryo-electron microscopy structure of an SH3 amyloid fibril and model of the molecular packing. *The European Molecular Biology Organisation Journal* 18: 815-821.

Jiménez, J. L., E. J. Nettleton, M. Bouchard, C. V. Robinson, C. M. Dobson, and H. R. Saibil. 2002. The protofilament structure of insulin amyloid fibrils. *Proceedings of the National Academy of Sciences of the United States of America.* 99: 9196-9201.

Jiménez, J. L., G. Tennent, M. Pepys, and H. R. Saibil. 2001. Structural diversity of *ex vivo* amyloid fibrils studied by cryo-electron microscopy. *Journal of Molecular Biology* 311: 241-247.

Kajava, A. V., U. Aebi, and A. C. Steven. 2005. The parallel superpleated beta-structure as a model for amyloid fibrils of human amylin. *Journal of Molecular Biology* 348: 247-252.

Kajava, A. V., U. Baxa, R. B. Wickner, and A. C. Steven. 2004. A model for Ure2p prion filaments and other amyloids: The parallel superpleated β-structure. *Proceedings of the National Academy of Sciences of the United States of America* 101: 7885-7890.

Kar, K., P. Amin, M. A. Bryan, A. V. Persikov, A. Mohs, Y.-H. Wang, and B. Brodsky. 2006. Self-association of collagen triple helic peptides into higher order structures. *Journal of Biological Chemistry* 281: 33283-33290.

Kasai, S., Y. Ohga, M. Mochizuki, N. Nishi, Y. Kadoya, and M. Nomizu. 2004. Multifunctional peptide fibrils for biomedical materials. *Peptide Science* 76: 27-33.

Katz, E., and I. Willner. 2004. Biomolecule-functionalised carbon nanotubes: Applications in nanobioelectronics. *A European Journal of Chemical Physics and Physical Chemistry* 5: 1084-1104.

Kayed, R., E. Head, J. L. Thompson, T. M. McIntire, S. C. Milton, C. W. Cotman, and C. G. Glabe. 2003. Common structure of soluble amyloid oligomers implies common mechanism of pathogenesis. *Science* 300: 486-489.

Kenney, J. K., D. Knight, M. J. Wise, and F. Vollrath. 2002. Amyloidogenic nature of spider silk. *European Journal of Biochemistry* 269: 4159-4163.

Khurana, R., C. Ionescu-Zanetti, M. Pope, J. Li, L. Nielson, M. Ramirez-Alvarado, L. Regan, A. L. Fink, and S. A. Carter. 2003. A general model for amyloid fibril assembly based on morphological studies using atomic force microscopy. *Biophysical Journal* 85: 1135-1144.

Khwaldia, K., C. Perez, S. Banon, S. Desobry, and J. Hardy. 2004. Milk proteins for edible films and coatings. *Critical Reviews in Food Science and Nutrition* 44: 239-251.

Kim, E. M., M. H. Han, Y. J. Lee, D. H. Song, H. K. Lee, O. W. Kwon, D. S. Shin, S. S. Han, S. K. Noh, J. K. Shin, Y.-S. Gal, and W. S. Lyoo. 2007. Characterization of poly(vinyl alcohol) films with various molecular parameters. *Journal of Applied Polymer Science* 106: 3259-3267.

King, C.-Y., P. Tittmann, H. Gross, R. Gebert, M. Aebi, and K. Wuthrich. 1997. Prion-inducing domain 2-114 of yeast Sup35 protein transforms *in vitro* into amyloid-like filaments. *Proceedings of the National Academy of Sciences of the United States of America* 94: 6618-6622.

Kisiday, J., M. Jin, B. Kurz, H. Hung, C. Semino, S. Zhang, and A. J. Grodzinsky. 2002. Self-assembling peptide hydrogel fosters chondrocyte extracellular matrix production and cell division: Implications for cartilage tissue repair. *Proceedings of the National Academy of Sciences of the United States of America* 99: 9996-10001.

Knowles, T. P., A. W. Fitzpatrick, S. Meehan, H. R. Mott, M. Vendruscolo, C. M. Dobson, and M. E. Welland. 2007. Role of intermolecular forces in defining material properties of protein nanofibrils. *Science* 318: 1900-1903.

Knowles, T. P. J., J. F. Smith, A. Craig, C. M. Dobson, and M. E. Welland. 2006. Spatial persistence of angular correlations in amyloid fibrils. *Physical Review Letters* 96: 238301(1)-(4).

Kobayashi, M., Y.-S. Chang, and M. Oka. 2005. A two year *in vivo* study of polyvinyl alcohol-hydrogel (PVA-H) artificial meniscus. *Biomaterials* 26: 3243-3248.

Koo, J. H. 2006. *Polymer nanocomposites: Processing, characterisation and applications*. McGraw-Hill, New York, USA, pg 1-7.

Koyano, T., N. Koshizaki, H. Umehara, M. Nagura, and N. Minoura. 2000. Surface states of PVA/chitosan blended hydrogels. *Polymer* 41: 4461-4465.

Krebs, M. R. H., E. H. C. Bromley, and A. M. Donald. 2005. The binding of thioflavin-T to amyloid fibrils: localisation and implications. *Journal of Structural Biology* 149: 30-37.

Krebs, M. R. H., D. K. Wilkins, E. W. Chung, M. C. Pitkeathly, A. K. Chamberlain, J. Zurdo, C. V. Robinson, and C. M. Dobson. 2000. Formation and seeding of amyloid fibrils from wild-type hen lysozyme and a peptide fragment from the β-domain. *Journal of Molecular Biology* 300: 541-549.

Krishnan, R., and S. L. Lindquist. 2005. Structural insights into a yeast prion illuminate nucleation and strain diversity. *Nature* 435: 765-772.

Kwan, A. H. Y., R. D. Winefield, M. Sunde, J. M. Matthews, R. G. Haverkamp, M. D. Templeton, and J. P. Mackay. 2006. Structural basis for rodlet assembly in fungal hydrophobins. *Proceedings of the National Academy of Sciences of the United States of America* 103: 3621-3626.

Lam, C.-w., J. T. James, R. McCluskey, S. Arepalli, and R. L. Hunter. 2006. A review of carbon nanotube toxicity and assessment of potential occupational and environmental health risks. *Critical Reviews in Toxicology* 36: 189.

Langton, M., and A. M. Hermansson. 1992. Fine-stranded and particulate gels of ß-lactoglobulin and whey protein at varying pH. *Food Hydrocolloids* 5: 523-539.

Larsen, N. G., K. H. Sutton, J. A. Gerrard, and S. H. Waterhouse. 2005. *Amyloid formation*. World Intellectual Property Organization, New Zealand.

Lee, J.-W., S.-M. Son, and S.-I. Hong. 2008. Characterization of protein-coated polypropylene films as a novel composite structure for active food packaging application. *Journal of Food Engineering* 86: 484-493.

Lin, M.-S., L.-Y. Chen, H.-T. Tsai, S. S.-S. Wang, Y. Chang, A. Higuchi, and W.-Y. Chen. 2008. Investigation of the mechanism of β-amyloid fibril formation by kinetic and thermodynamic analyses. *Langmuir* 24: 5802-5808.

Lin, T., V. Bajpai, T. Ji, and L. Dai. 2003. Chemistry of carbon nanotubes. *Australian Journal of Chemistry* 56: 635-651.

Lin, W.-C., D.-G. Yu, and M.-C. Yang. 2006. Blood compatibility of novel poly([gamma]-glutamic acid)/polyvinyl alcohol hydrogels. *Colloids and Surfaces B: Biointerfaces* 47: 43-49.

Lin, Y., S. Taylor, H. Li, K. A. S. Fernando, L. Qu, W. Wang, L. Gu, B. Zhou, and Y.-P. Sun. 2004. Advances toward bioapplications of carbon nanotubes. *Journal of Material Chemistry* 14: 527-541.

Lindquist, S. L., J. Shorter, and T. Scheibel. 2005. *Electrical conductors and devices from prion-like proteins,* US Patent Application no. 11/134,228, USA.

Lopez de la Paz, M., K. Goldie, J. Zurdo, E. Lacroix, C. M. Dobson, A. Hoenger, and L. Serrano. 2002. De novo designed peptide-based amyloid fibrils. *Proceedings of the National Academy of Sciences of the United States of America* 99: 16052-16057.

Lopez de la Paz, M., and L. Serrano. 2004. Sequence determinants of amyloid fibril formation. *Proceedings of the National Academy of Sciences of the United States of America* 101: 87-92.

Lu, K., J. Jacob, P. Thiyagarajan, V. P. Conticello, and D. G. Lynn. 2003. Exploiting amyloid fibril lamination for nanotube self-assembly. *Journal of the American Chemical Society* 125: 6391-6393.

Ma, D., M. Ming, J. Hong, J. Wu, Q. Li, W. Huang, and J. Ding. 2006. A membrane protein/polymer composite film with photochromic response. *Acta Polymerica Sinica* 9: 1078-1082.

Mackintosh, S. H., S. J. Meade, J. P. Healy, K. H. Sutton, N. G. Larsen, A. M. Squires, and J. A. Gerrard. 2008. Wheat glutenin proteins assemble into an amyloid-like structure with unusual structural features. *Journal of Cereal Science* in press.

MacPhee, C. E., and C. M. Dobson. 2000. Formation of mixed fibrils demonstrates the generic nature and potential utility of amyloid nanostructures. *Journal of the American Chemical Society* 122: 12707-12713.

MacPhee, C. E., and D. N. Woolfson. 2004. Engineered and designed peptide-based fibrous biomaterials. *Current Opinion in Solid State and Materials Science* 8: 141-149.

Maji, S. K., D. Schubert, C. Rivier, S. Lee, J. E. Rivier, and R. Riek. 2008. Amyloid as a depot for the formulation of long-acting drugs. *Public Library of Science Biology* 6: e17.

Makin, O. S., E. Atkins, P. Sikorski, J. Johansson, and L. C. Serpell. 2005. Molecular basis for amyloid fibril formation and stability. *Proceedings of the National Academy of Sciences of the United States of America* 102: 315-320.

Makin, O. S., and L. C. Serpell. 2002. Examining the structure of the mature amyloid fibril. *Biochemical Society Transactions* 30: 521-525.

—. 2004. Structural characterisation of islet amyloid polypeptide fibrils. *Journal of Molecular Biology* 335: 1279-1288.

—. 2005. Structures for amyloid fibrils. *Federation of Eurpoean Biochemical Societies Journal* 272: 5950-5961.

Manocha, L. M. 2006. Composites with nanomaterials in K. E. Geckeler and E. Rosenberg, eds. *Functional Nanomaterials*. American Scientific Publishers, Stevensen Ranch, pg 275-286.

McParland, V. J., N. M. Kad, A. P. Kalverda, A. Brown, P. Kirwin-Jones, M. G. Hunter, M. Sunde, and S. E. Radford. 2000. Partially unfolded states of 2-microglobulin and amyloid formation *in vitro*. *Biochemistry* 39: 8735-8746.

Meade, S. J., E. Butler, N. G. Larsen, and J. A. Gerrard. 2007. Pathways towards commercialisation of protein nanotube technologies. Pages 6. Crop & Food Research.

Meixueir, F. A., C. vanGarcia, and F. Silvestre. 2000. Biodegradable films from isolate of sunflower (Helianthus annus) proteins. *Journal of Agricultural and Food Chemistry* 48: 3032–3036.

Mendieta-Taboada, O., P. J. d. A. Sobral, R. A. Carvalho, and A. M. B. Q. Habitante. 2008. Thermomechanical properties of biodegradable films based on blends of gelatin and poly(vinyl alcohol). *Food Hydrocolloids* 22: 1485-1492.

Mesquida, P., E. M. Blanco, and R. A. McKendry. 2006. Patterning amyloid peptide fibrils by AFM charge writing. *Langmuir* 22: 9089-9091.

Mostaert, A. S., M. J. Higgins, T. Fukuma, F. Rindi, and S. P. Jarvis. 2006. Nanoscale mechanical characterisation of amyloid fibrils discovered in a natural adhesive. *Journal of Biological Physics* 32: 393-401.

Mostaert, A. S., and S. P. Jarvis. 2007. Beneficial characteristics of mechanically functional amyloid fibrils evolutionarily preserved in natural adhesives. *Nanotechnology* 18: 044010(1)-(5).

Naushad, E. M., and M. Stading. 2007. *In situ* tensile deformation of zein films with plasticizers and filler materials. *Food Hydrocolloids* 21: 1245-1255.

Necula, M., R. Kayed, S. Milton, and C. G. Glabe. 2007. Small molecule inhibitors of aggregation indicate that amyloid β oligomerization and fibrillisation pathways are independent and distinct. *Journal of Biological Chemistry* 282: 10311-10324.

Nelson, R., and D. Eisenberg. 2006. Recent atomic models of amyloid fibril structure. *Current Opinion in Structural Biology* 16: 260-265.

Nelson, R., M. R. Sawaya, M. Balbirnie, A. O. Madsen, C. Riekel, R. Grothe, and D. Eisenberg. 2005. Structure of the cross-β spine of amyloid-like fibrils. *Nature* 435: 773-778.

Nepal, D., and K. E. Geckeler. 2006. Functionalisation of carbon nanotubes in K. E. Geckeler and E. Rosenberg, eds. *Functional Nanomaterials*. American Scientific Publishers, California.

Nielsen, E. H., M. Nybo, and S.-E. Svehag. 1999. Electron microscopy of prefibrillar structures and amyloid fibrils. *Methods in Enzymology* 309 - Amyloid, Prions, and Other Protein Aggregates: 491-496.

Nielsen, L., S. Frokjaer, J. Brange, V. N. Uversky, and A. L. Fink. 2001a. Probing the mechanism of insulin fibril formation with insulin mutants. *Biochemistry* 40: 8397-8409.

Nielsen, L., S. Frokjaer, J. F. Carpenter, and J. Brange. 2001b. Studies of the structure of insulin fibrils by Fourier transform infrared (FTIR) spectroscopy and electron microscopy. *Journal of Pharmaceutical Sciences* 90: 29-37.

Nielsen, L., R. Khurana, A. Coats, S. Frokjaer, J. Brange, S. Vyas, V. N. Uversky, and A. L. Fink. 2001c. Effect of environmental factors on the kinetics of insulin fibril formation: Elucidation of the molecular mechanism. *Biochemistry* 40: 6036-6046.

Nilsson, M. R. 2004. Techniques to study amyloid fibril formation *in vitro*. *Methods* 34: 151-160.

Oh, K. S., S. K. Han, Y. W. Choi, J. H. Lee, J. Y. Lee, and S. H. Yuk. 2004. Hydrogen-bonded polymer gel and its application as a temperature-sensitive drug delivery system. *Biomaterials* 25: 2393-2398.

O'Nuallain, B., S. Shivaprasad, I. Kheterpal, and R. Wetzel. 2005. Thermodynamics of Aβ(1-40) amyloid fibril elongation. *Biochemistry* 44: 12709-12718.

Park, J. W., W. Scott Whiteside, and S. Y. Cho. 2008. Mechanical and water vapor barrier properties of extruded and heat-pressed gelatin films. *LWT - Food Science and Technology* 41: 692-700.

Pawar, A. P., K. F. DuBay, J. Zurdo, F. Chiti, M. Vendruscolo, and C. M. Dobson. 2005. Prediction of "aggregation-prone" and "aggregation-susceptible" regions in proteins associated with neurodegenerative diseases. *Journal of Molecular Biology* 350: 379-392.

Pearce, F. G., S. H. Mackintosh, and J. A. Gerrard. 2007. Formation of amyloid-like fibrils by ovalbumin and related proteins under conditions relevant to food processing. *Journal of Agricultural and Food Chemistry* 55: 318-322.

Pedersen, J. S., and D. E. Otzen. 2008. Amyloid a state in many guises: Survival of the fittest fibril fold. *Protein Science* 17: 2-10.

Pellarin, R., E. Guarnera, and A. Caflisch. 2007. Pathways and intermediates of amyloid fibril formation. *Journal of Molecular Biology* 374: 917-924.

Perutz, M. F., J. T. Finch, J. Berriman, and A. Lesk. 2002. Amyloid fibers are water-filled nanotubes. *Proceedings of the National Academy of Sciences of the United States of America* 99: 5591-5595.

Petka, W. A., J. L. Harden, K. P. McGrath, D. Wirtz, and D. A. Tirrell. 1998. Reversible hydrogels from self-assembling artificial proteins. *Science* 281: 389-392.

Plakoutsi, G., F. Bemporad, M. Calamai, N. Taddei, C. M. Dobson, and F. Chiti. 2005. Evidence for a mechanism of amyloid formation involving molecular reorganisation within native-like precursor aggregates. *Journal of Molecular Biology* 351: 910-922.

Powers, E. T., and D. L. Powers. 2008. Mechanisms of protein fibril formation: nucleated polymerization with competing off-pathway aggregation. *Biophysical Journal* 94: 379-391.

Qi, M., Y. Gu, N. Sakata, D. Kim, Y. Shirouzu, C. Yamamoto, A. Hiura, S. Sumi, and K. Inoue. 2004. PVA hydrogel sheet macroencapsulation for the bioartificial pancreas. *Biomaterials* 25: 5885-5892.

Qu, Y., S. C. Payne, R. P. Apkarian, and V. P. Conticello. 2000. Self-Assembly of a polypeptide multi-block copolymer modeled on dragline silk proteins. *Journal of the American Chemical Society* 122: 5014-5015.

Radford, S. E. 2000. Protein folding: progress made and promises ahead. *Trends in Biochemical Sciences* 25: 611-618.

Ramirez-Alvarado, M., J. S. Merzel, and L. Regan. 2000. A systematic exploration of the influence of protein stability on amyloid fibril formation *in vitro*. *Proceedings of the National Academy of Sciences of the United States of America* 97: 8979-8984.

Reches, M., and E. Gazit. 2003. Casting metal nanowires within discrete self-assembled peptide nanotubes. *Science* 300: 625-627.

—. 2006. Designed aromatic homo-dipeptides: formation of ordered nanostructures and potential nanotechnological applications. *Physical Biology* 3: S10-S19.

Ritter, C., M.-L. Maddelein, A. B. Siemer, T. Luhrs, M. Ernst, B. H. Meier, S. J. Saupe, and R. Riek. 2005. Correlation of structural elements and infectivity of the HET-s prion. 435: 844-848.

Rösler, A., H.-A. Klok, I. W. Hamley, V. Castelletto, and O. O. Mykhaylyk. 2003. Nanoscale structure of poly(ethylene glycol) hybrid block copolymers containing amphiphilic b-strand peptide sequences. *Biomacromolecules* 4: 859-863.

Sawaya, M. R., S. Sambashivan, R. Nelson, M. I. Ivanova, S. A. Sievers, M. I. Apostol, M. J. Thompson, M. Balbirnie, J. J. W. Wiltzius, H. T. McFarlane, A. O. Madsen, C. Riekel, and D. Eisenberg. 2007. Atomic structures of amyloid cross-β spines reveal varied steric zippers. *Nature* 447: 453-457.

Scheibel, T., J. Bloom, and S. L. Lindquist. 2004. The elongation of yeast prion fibers involves separable steps of association and conversion. *Proceedings of the National Academy of Sciences of the United States of America* 101: 2287-2292.

Scheibel, T., R. Parthasarathy, G. Sawicki, X.-M. Lin, H. Jaeger, and S. L. Lindquist. 2003. Conducting nanowires built by controlled self-assembly of amyloid fibers and selective metal deposition. *Proceedings of the National Academy of Sciences of the United States of America* 100: 4527-4532.

Schneider, J. P., D. J. Pochan, B. Ozbas, K. Rajagopal, L. Pakstis, and J. Kretsinger. 2002. Responsive hydrogels from the intramolecular folding and self-assembly of a designed peptide. *Journal of the American Chemical Society* 124: 15030-15037.

Sedman, V. L., L. Adler-Abramovich, S. Allen, E. Gazit, and S. J. B. Tendler. 2006. Direct observation of the release of phenylalanine from diphenylalanine nanotubes. *Journal of the American Chemical Society* 128: 6903-6908.

Selkoe, D. J. 2003. Folding proteins in fatal ways. *Nature* 426: 900-904.

Serpell, L. C. 2000. Alzheimer's amyloid fibrils: structure and assembly. *Biochimica et Biophysica Acta* 1502: 16-30.

Serpell, L. C., M. Sunde, M. D. Benson, G. A. Tennent, M. B. Pepys, and P. E. Fraser. 2000. The protofilament substructure of amyloid fibrils. *Journal of Molecular Biology* 300: 1033-1039.

Shang, Y., and Y. Peng. 2007. Research of a PVA composite ultrafiltration membrane used in oil-in-water. *Desalination EuroMed 2006 - Conference on Desalination Strategies in South Mediterranean Countries* 204: 322-327.

Shirahama, T., and A. S. Cohen. 1967. High-resolution electron microscopic analysis of the amyloid fibrils. *Journal of Cell Biology* 33: 679-708.

Sipe, J. D., and A. S. Cohen. 2000. Review: History of the amyloid fibril. *Journal of Structural Biology* 130: 88-98.

Smith, A. M., T. R. Jahn, A. E. Ashcroft, and S. E. Radford. 2006a. Direct observation of oligomeric species formed in the early stages of amyloid fibril formation using electrospray ionisation mass spectrometry. *Journal of Molecular Biology* 364: 9-19.

Smith, B. L., T. E. Schaffer, M. Viani, J. B. Thompson, N. A. Frederick, J. Kindt, A. Belcher, G. D. Stucky, D. E. Morse, and P. K. Hansma. 1999. Molecular mechanistic origin of the toughness of natural adhesives, fibres and composites. *Nature* 399: 761-763.

Smith, D. P., S. Jones, L. C. Serpell, M. Sunde, and S. E. Radford. 2003. A systematic investigation into the effect of protein destabilisation on β 2-microglobulin amyloid formation. *Journal of Molecular Biology* 330: 943-954.

Smith, J. F., T. P. J. Knowles, C. M. Dobson, C. E. MacPhee, and M. E. Welland. 2006b. Characterization of the nanoscale properties of individual amyloid fibril. *Proceedings of the National Academy of Science of the United States of America* 103: 15806-15811.

Sothornvit, R., C. W. Olsen, T. H. McHugh, and J. M. Krochta. 2007. Tensile properties of compression-molded whey protein sheets: Determination of molding condition and glycerol-content effects and comparison with solution-cast films. *Journal of Food Engineering* 78: 855-860.

Squires, A. M., G. L. Devlin, S. L. Gras, A. K. Tickler, C. E. MacPhee, and C. M. Dobson. 2006. X-ray scattering study of the effect of hydration on the cross-beta structure of amyloid fibrils. *Journal of the American Chemical Society* 128: 11738-11739.

Stefani, M., and C. Dobson. 2003. Protein aggregation and aggregate toxicity: new insights into protein folding, misfolding diseases and biological evolution. *Journal of Molecular Medicine* 81: 678-699.

Su, J.-F., Z. Huang, K. Liu, L.-L. Fu, and H.-R. Liu. 2007. Mechanical properties, biodegradation and water vapor permeability of blend films of soy protein isolate and poly (vinyl alcohol) compatibilized by glycerol. *Polymer Bulletin* 58: 913-921.

Sunde, M., and C. Blake. 1997. The structure of amyloid fibrils by electron microscopy and X-ray diffraction. *Advances in Protein Chemistry* 50: 123-159.

Sunde, M., L. C. Serpell, M. Bartlam, P. E. Fraser, M. B. Pepys, and C. C. F. Blake. 1997. Common core structure of amyloid fibrils by synchrotron X-ray diffraction. *Journal of Molecular Biology* 273: 729-739.

Takasu, A., Aoi, K., Okada, M. 1997. Polypeptide-synthetic polymer hybrids, 1. Miscibility of poly(vinyl alcohol) with poly(sodium-αβ-D,L-aspartate). *Macromolecular Rapid Communications* 18: 497-502.

Tharanathan, R. N. 2003. Biodegradable films and composite coatings: past, present and future. *Trends in Food Science & Technology* 14: 71-78.

Thompson, M. J., S. A. Sievers, J. Karanicolas, M. I. Ivanova, D. Baker, and D. Eisenberg. 2006. The 3D profile method for identifying fibril-forming segments of proteins. *Proceedings of the National Academy of Sciences of the United States of America* 103: 4074-4078.

Thorn, D. C., S. Meehan, M. Sunde, A. Rekas, S. L. Gras, C. E. MacPhee, C. M. Dobson, M. R. Wilson, and J. A. Carver. 2005. Amyloid fibril formation by bovine milk κ-casein and its inhibition by the molecular chaperones α_s- and β-casein. *Biochemistry* 44: 17027-17036.

Thostensona, E. T., Z. Renb, and T.-W. Choua. 2001. Advances in the science and technology of carbon nanotubes and their composites: a review. *Composites Science and Technology* 61: 1899-1912.

Tycko, R. 2004. Progress towards a molecular-level structural understanding of amyloid fibrils. *Current Opinion in Structural Biology* 14: 1-8.

Uversky, V. N., and A. L. Fink. 2004. Conformational constraints for amyloid fibrillation: the importance of being unfolded. *Biochimica et Biophysica Acta* 1698: 131-153.

Veerman, C. 2006. Method for improving the functional properties of a globular protein, protein thus prepared, use thereof and products containing the protein. US Patent Application 2006/0204454 A1, USA.

Vendruscolo, M., J. Zurdo, C. E. MacPhee, and C. M. Dobson. 2003. Protein folding and misfolding: a paradigm of self-assembly and regulation in complex biological systems. *Philosophical Transactions of the Royal Society of London, Series A: Mathematical, Physical and Engineering Sciences* 361: 1205-1222.

Vestergaard, B., M. Groenning, M. Roessle, J. S. Kastrup, M. v. de Weert, J. M. Flink, S. Frokjaer, M. Gajhede, and D. I. Svergun. 2007. A helical structural nucleus is the primary elongating unit of insulin amyloid fibrils. *Public Library of Science Biology* 5: 1089-1097.

Viney, C. 2004. Self-assembly as a route to fibrous materials: concepts, opportunities and challenges. *Current Opinion in Solid State and Materials Science* 8: 95-101.

Wan, L.-J., and C.-L. Bai. 2006. Nanostructured materials with enhanced magnetic and catalytic properties in K. E. Geckeler and E. Rosenberg, eds. *Functional Nanomaterials*. American Scientific Publishers, California, USA, pg 163-172.

Wang, B., and M. Sain. 2007. Isolation of nanofibers from soybean source and their reinforcing capability on synthetic polymers. *Composites Science and Technology* 67: 2521-2527.

Wang, Q., Y.-M. Du, and L.-H. Fan. 2005. Properties of chitosan/poly(vinyl alcohol) films for drug-controlled release. *Journal of Applied Polymer Science* 96: 808-813.

Waterhouse, S. H., and J. A. Gerrard. 2004. Amyloid fibrils in bionanotechnology. *Australian Journal of Chemistry* 57: 519-523.

Watters, A. L., P. Deka, C. Corrent, D. Callender, G. Varani, T. Sosnick, and D. Baker. 2007. Theory:The highly cooperative folding of small naturally occurring proteins is likely the result of natural selection. *Cell* 128.

Westermark, P., M. D. Benson, J. N. Buxbaum, A. S. Cohen, B. Frangione, S. Ikeda, C. L. Masters, G. Merlini, M. J. Saraiva, and J. D. Sipe. 2005. Amyloid: toward terminology clarification. Report from the nomenclature committee of the international society of amyloidosis. *Amyloid* 12: 1-4.

Wetzel, R., S. Shivaprasad, and A. D. Williams. 2007. Plasticity of amyloid fibrils. *Biochemistry* 46: 1-10.

Wille, H., M. D. Michelitsch, V. Guenebaut, S. Supattapone, A. Serban, F. E. Cohen, D. A. Agard, and S. B. Prusiner. 2002. Structural studies of the scrapie prion protein by electron crystallography. *Proceedings of the National Academy of Sciences of the United States of America* 99: 3563-3568.

Wiseman, R. L., E. T. Powers, and J. F. Kelly. 2005. Partitioning conformational intermediates between competing refolding and aggregation pathways: Insights into transthyretin amyloid disease. *Biochemistry* 44: 16612-16623.

Yi, F., J.-W. Lu, Z.-X. Guo, and J. Yu. 2006. Mechanical properties and biocompatibility of soluble eggshell membrane protein/poly(vinyl alcohol) blend films. *Journal of Biomaterials Science, Polymer Edition* 17: 1015-1024.

Zhang, S. 2003. Fabrication of novel biomaterials through molecular self-assembly. *Nature Biotechnology* 21: 1171-1178.

Zhang, S., D. M. Marini, W. Hwang, and S. Santoso. 2002. Design of nanostructured biological materials through self-assembly of peptides and proteins. *Current Opinion in Chemical Biology* 6: 865-871.

Zurdo, J., J. I. Guijarro, and C. M. Dobson. 2001. Preparation and characterization of purified amyloid fibrils. *Journal of the American Chemical Society* 123: 8141-8142.

Modification and Characterisation of Insulin

This chapter aimed to assess the impact of chemical modification on the ability to form amyloid fibrils for a model protein, insulin. The spectrum of possible chemical modifications of proteins is wide, and therefore a representative selection is considered here. Previous studies on the impact of chemical modification on the aggregation propensity of proteins have been, for the most part, motivated by the need to understand the impact of protein modification *in vivo* (Dobson 2003, Naiki *et al.* 1997, Rochet and Lansbury Jr 2000, Uversky and Fink 2004). This chapter, presents the results of the modification of a model protein, insulin, with a view to accelerating the formation of amyloid fibrils, for potential use in bionanomaterials.

2.1 Background

Post-translational phosphorylation (Ecroyd *et al.* 2007), glycation (Obrenovich and Monnier 2004), acetylation, truncation, oxidative stress (Dear *et al.* 2007) and conformational changes (Colon *et al.* 2007) have all been shown to play a role in the series of events leading to fibrillation. The effect of chemical modification on protein aggregation *in vitro* has been part of studies contributing towards an understanding of the mechanism of protein aggregation *in vivo* (Ahmad *et al.* 2003, Ahmad *et al.* 2004, Arora *et al.* 2004, Brange *et al.* 1997a, Jansen *et al.* 2005, Jiménez *et al.* 2002, Khurana *et al.* 2003, Sluzky *et al.* 1991, Uversky *et al.* 2003). For example, α-synuclein aggregation plays a key role in the etiology of Parkinson's disease and *in vitro* studies reveal that the nitration of tyrosine inhibits α-synuclein fibrillation at neutral pH (Uversky *et al.* 2005). Similarly, the phosphorylation of αβ-crystallin regulates its chaperone activity *in vitro*, which may alleviate the pathogenic effects associated with protein conformational diseases (Ecroyd *et al.* 2007). The impact of glycosylation on

the propensity of prion peptides to form fibrils has been shown to depend on the site of glycosylation and the nature of the sugar (Chen *et al.* 2002), the O-linked α-GalNAc at Ser-135 suppresses the formation of amyloid fibril formation of the prion peptide, whereas the peptide with the same sugar at Ser-132 shows the opposite effect. More recently, glycosylation was found to suppress fibrillation of chicken cystatin (He *et al.* 2006). Furthermore, glycation favours the formation of β-sheets in albumin (Bouma *et al.* 2003, Obrenovich and Monnier 2004). However, it has been shown that phosphorylation and glycation of tau protein *in vitro* do not promote fibril nucleation but instead favour fibril growth once they have been nucleated (Necula and Kuret 2004). Despite a bulky hydrophobic group on its C-terminal, prion peptide still formed fibrils, but this derivatisation prevented the lateral association of filaments into higher order structures (Breydo *et al.* 2007). These findings suggest that post translational modification affects both the kinetic status and thermodynamic stability of fibril formation; it may or may not favour the formation of β-structure relative to the native conformation. This is consistent with the complicated relationship shown between fibril formation and protein sequences (Lopez de la Paz and Serrano 2004, Pawar *et al.* 2005).

Chapter 1 detailed the properties of fibrils, and their potential use in bionanomaterials. However, a reliance on purified, expensive protein could potentially represent a major obstacle for industrial fibril production, as sourcing large volumes of pure protein may prove to be costly and hence a nonviable option for materials use. The use of fibrils on an industrial scale will require large amounts of proteins from inexpensive sources. Amyloid fibril formation from crude, and/or partially purified proteins would reduce costs for manufacture on a large scale. As such, in this chapter, we were not only interested in studying the fibril forming ability of purified modified insulin but the potential of fibril formation from modified insulin mixtures, which model the crude starting materials in industrial processes using unpurified material as a starting point for manufacture.

In order to fully assess the potential of chemical modification and sample heterogeneity on the propensity of a protein to form amyloid fibrils *in vitro*, a number of areas needed to be addressed, including selection of an appropriate protein and development of a range of methods to generate and then characterise the derivatised protein. This chapter describes these methods and reports on the crude products obtained by a range of chemical modifications of insulin. For all the chemical modifications to be discussed in this chapter, bovine insulin was modified on a scale to obtain samples in sufficient quantities for fibril studies in chapter 3.

2.2 Bovine Insulin, the Model Protein

2.2.1 Insulin aggregation

Bovine insulin has been used to study the process of amyloid formation for a number of years (reviewed in Brange *et al.* 1997a) with the most common fibril formation conditions involving elevated temperatures and acidic pH. Additionally, organic solvents and agitation have been identified as conditions that lead to insulin fibril formation (Ahmad *et al.* 2003, Ahmad *et al.* 2004, Ahmed *et al.* 2003, Arora *et al.* 2004, Brange *et al.* 1997b, Devlin *et al.* 2006, Jansen *et al.* 2005, Jansen *et al.* 2004, Jiménez *et al.* 2002, Khurana *et al.* 2003, Nielsen *et al.* 2001a, Nielsen *et al.* 2001c, Sluzky *et al.* 1991, Uversky *et al.* 2003, Waugh 1946, Waugh *et al.* 1953). A number of compounds added to the solution have also been shown to have an influence on the kinetics of amyloid fibril formation, with Neilsen *et al*. (2001c) providing a comprehensive review on the effects of a selection of environmental factors. The presence of strong denaturants such as guanidine hydrochloride and urea (Ahmad *et al.* 2003, Ahmad *et al.* 2004) also cause insulin to form ordered amyloid-like aggregates with distinct staining properties.

Since it was realised that commonly observed insulin fibrils had the generic amyloid structure that is associated with many other human diseases (Dische *et al.* 1988, Sluzky *et al.* 1991, Storkel *et al.* 1983) several research groups have focused their attention on understanding the process of insulin amyloid fibril

formation (Brange *et al.* 1997c, Devlin *et al.* 2006, Fandrich 2007, Hong *et al.* 2006, Hong and Fink 2005, Jiménez *et al.* 2002, Mauro *et al.* 2007, Uversky *et al.* 2003, Vestergaard *et al.* 2007). Insulin fibrils have been studied in considerable depth in recent years and there is a substantial body of evidence to show that they contain the signature β-sheet structure diagnostic of amyloid fibrils (Bouchard *et al.* 2000, Burke and Rougvie 1972, Devlin *et al.* 2006, Fandrich 2007, Jiménez *et al.* 2002, Mauro *et al.* 2007, Nielsen *et al.* 2001b, Yu *et al.* 1974). Although a lot of work has been done on insulin and its ability to fibrillise, the molecular mechanism of the fibrillation is still not fully understood (Ahmad *et al.* 2005, Brange *et al.* 1997b, Mauro *et al.* 2007). Early work on insulin fibrils prepared from native insulin and modified insulin revealed similar X-ray diffraction patterns, suggesting that there is not much difference in the structure of fibrils (Koltun *et al.* 1954). However, this work pre-dated a full appreciation of the amyloid form.

2.2.2 Insulin structure

Bovine insulin is a compact globular protein having a molecular weight of about 5.7 kDa. It is composed of two polypeptide chains, the 21 residue A-chain and the 30 residue B-chain, linked together by two interchain disulfide bonds and a third intramolecular disulfide bridge within the A chain (Baker *et al.* 1988, Blundell *et al.* 1972, Derewenda *et al.* 1990) (Figure 2.1). In solution, insulin exists as an equilibrium mixture of monomers, dimers, tetramers, hexamers, and possibly higher associated states (Nielsen *et al.* 2001c). It is thought that the fibril precursor is an insulin monomer, since conditions that promote monomer formation include low pH and high temperatures also promote self-assembly (Brange *et al.* 1997a).

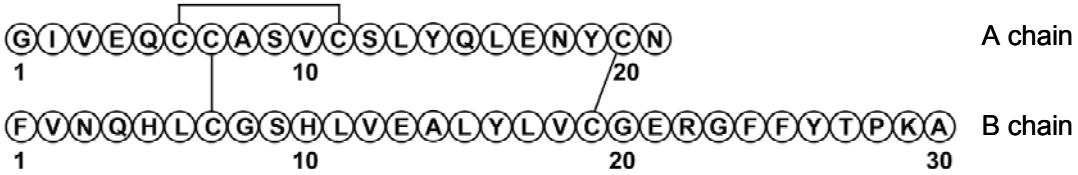

Figure 2.1 *Primary structure of bovine insulin from (Hong and Fink 2005).*

It is proposed that the critical step in insulin fibrillation involves disruption of the native protein contacts (Ahmad *et al.* 2005, Uversky and Fink 2004). NMR studies on the structure of human insulin, when exposed to amyloidogenic conditions, show that the N-termini of the A and B chains are separated from the core, which leads to the exposure of a hydrophobic surface, which in turn may provide the initial interaction surface for aggregation (Hua and Weiss 2004). Brange and his co-workers (Brange *et al.* 1997b, Brange *et al.* 1987) showed that the propensity of fibril formation increases with increasing truncation of the C-terminal region of the B chain, indicating a region of the B chain is critical in the intermolecular association events that lead to insulin fibril formation. The removal of residues from the C-terminal region of insulin native structure *via* protein engineering causes exposure of non polar groups normally in the core of the protein (Brange *et al.* 1997b).

In terms of its structure, insulin is constrained by the three disulfide bridges, all of which are retained in insulin fibrils (Brange *et al.* 1997a). As such, these constraints limit the conformational space that can be accessed by the protein, which, in turn, limits the possible arrangements of the protein in the amyloid fibrils (Jiménez *et al.* 2002).

2.2.3 Insulin chemical modification

An extensive literature search revealed a substantial body of literature on the chemical derivatisation of insulin, carried out for the most part to elucidate structure-function relationships of the native fold (Brandenburg *et al.* 1971, Massaglia *et al.* 1968, Suckau *et al.* 1992, Zahn *et al.* 1972). The chemical modification of several functional groups, such as carboxyl and amino groups and histidine and tyrosine residues, were shown not to prevent fibrillation in insulin in early work (Koltun *et al.* 1954), although the derivatisation of side chain amino acids led to a decreased rate of fibrillation (Blundell *et al.* 1972, Koltun *et al.* 1954). However, Koltun and his co-workers had not characterised insulin fibrils as amyloid in those early works. More recently, treatment of bovine insulin with cyanogens resulted in crosslinking between Ala-30 and His-5 at physiological conditions which caused insulin to form amyloid fibrils (Winters 2002).

The glycosylation of insulin has been shown to stabilise its native structural form, by suppressing self-association tendencies (Baudys *et al.* 1995). Whether this also influences the tendency to form amyloid does not appear to have been investigated, although other derivatisations, such as the attachment of low molecular weight monomethoxypoly(ethylene glycol) derivatives, have significantly enhanced insulin's resistance to fibrillation (Hinds and Kim 2002).

For this research, emphasis was placed on establishing how chemical modification might influence amyloid fibril formation in insulin molecules. A range of modifications was considered, based on various factors including the complexity of the methods, availability of reagents and suitability for use on a commercial scale. Three approaches were taken to insulin modification:

i) derivatisation of the single lysine residue with acetic anhydride
ii) reduction and derivatisation of the disulfide bonds with iodoacetic acid (IAA) and 4-vinylpyridine (4-VP).
iii) treatment with enzymes, specifically trypsin and chymotrypsin

In this chapter, the modification of insulin *via* each of the three approaches is described. The impact of these modifications on the ability to form amyloid fibrils is described in chapter 3.

2.2.4 Characterising bovine insulin

Bovine insulin was obtained commercially and the purity of the batch (Sigma Chemicals (Lot 054K1375)) was assessed using Nu polyacrylamide gel electrophoresis (NuPAGE) and liquid chromatography-mass spectrometry (LC-ESI-MS) analysis.

Figure 2.2 compares two purchased batches of insulin including the batch used subsequently in this study and shows no difference in the two batches of bovine insulin; both batches have an insulin band at about 5.7 kDa. The pH (1.6-8) of the insulin solution does not change the position of the insulin bands relative to the MW marker, an important consideration for the analysis of different modifications which may be soluble at different pHs.

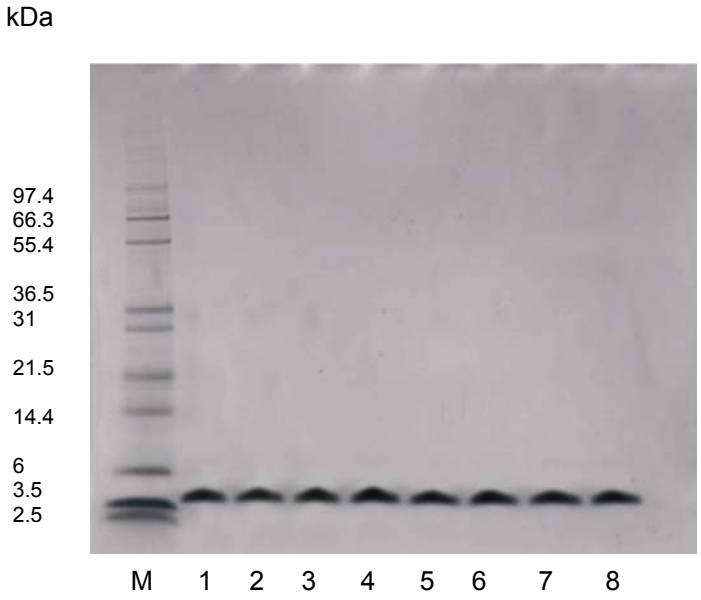

Figure 2.2 *Bovine insulin SDS-PAGE (non-reducing) analysis on a Bis-Tris 4-12% gel, 5 µl was loaded at 0.5 mg/ml protein. Lane M = molecular weight marker, (Lanes 1-4 are bovine insulin from batch Lot no. 103K1440 used for this study, at different pHs), Lane 1= 0.025 M HCl with 0.1 M NaCl buffer pH 1.6, Lane 2 = 0.025 M HCl pH 2, Lane 3 = 50 mM phosphate buffer pH 7, Lane 4 = 50 mM phosphate buffer pH 8, (Lanes 6-9 are bovine insulin from 5 g batch Lot no. 054K1375 previously used in the laboratory, at different pHs), Lane 5 = 0.025 M HCl with 0.1 NaCl buffer pH 1.6, Lane 6 = 0.025 M HCl pH 2, Lane 7 = 50 mM phosphate buffer pH 7, Lane 8 = 50 mM phosphate buffer pH 8.*

LC-ESI-MS of bovine insulin was carried out to verify purity and molecular weight. Figure 2.3 below shows a liquid chromatogram and ESI-MS mass spectrum of the insulin monomer. The liquid chromatogram shows a single peak for bovine insulin which elutes at 13.05 min with m/z value of 1147.5. Having a charge of +5, the experimentally determined molecular mass of insulin is 5732.5 Da. Thus the commercial sample of insulin was pure and underivatised and the molecular mass, with a standard deviation of 2, was consistent with that predicted from the amino acid sequence of 5733.5 Da .

a)

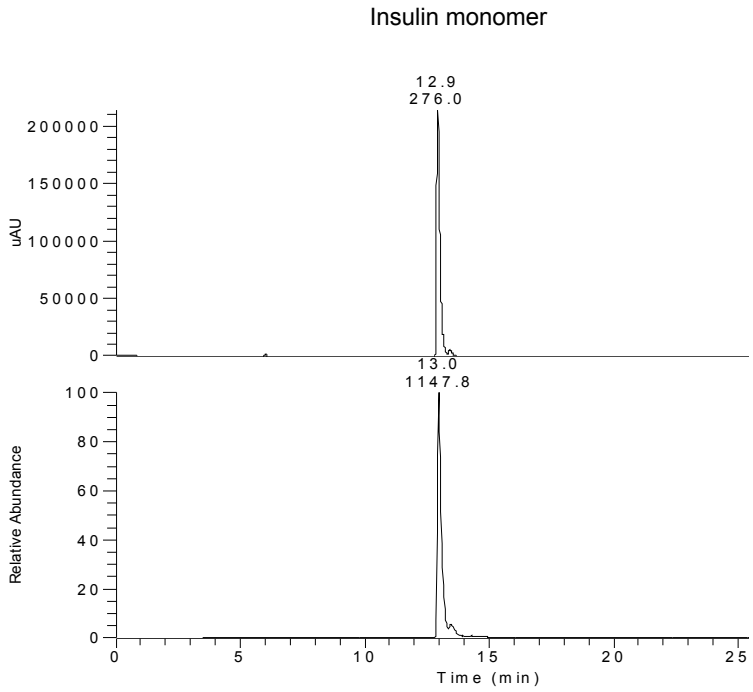

b)

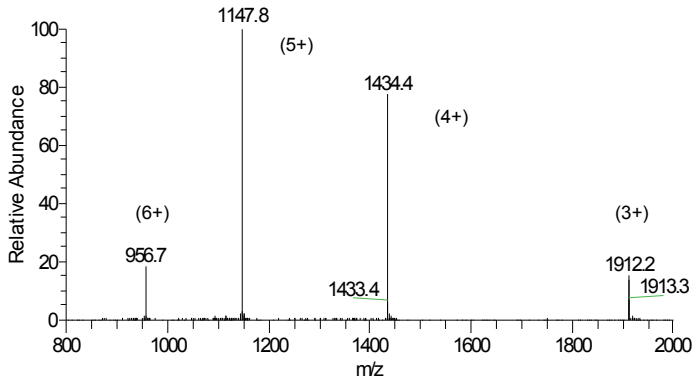

Figure 2.3 *Spectra from LC-ESI-MS analysis of 10 µl injection of 0.1 mg/ml insulin solution. a) Insulin was resolved on a Zorbex 2 column with mobile phase A and B (A: 0.2% formic acid in H_2O, B: 0.2% formic acid in acetonitrile) and the eluent was introduced to mass spectrometer via electrospray. Ions were scanned over a range of 800-2000 m/z $[M+H]^+$. b) Full scan mass spectra of the insulin LC peak present in the total ion current (TIC) chromatogram, the multiply charged peaks were detected by the ESI-MS, manually deconvoluted based on the high resolution mass scans (Zoom scan, which provided charge state information). The charge state for insulin peak is shown in parentheses.*

2.3 Amino Group Acetylation of Bovine Insulin

Acetylation has the effect of neutralising the charge of the amino groups at neutral pH and charge is one of the intrinsic factors believed to affect aggregation propensity. Figure 2.4 shows the possible sites for amino group acetylation in bovine insulin, which has 3 available amino groups for acetylation, 2 on the N-termini (glycine at A1 and phenylalanine at B1) and one on the side chain of lysine on B29.

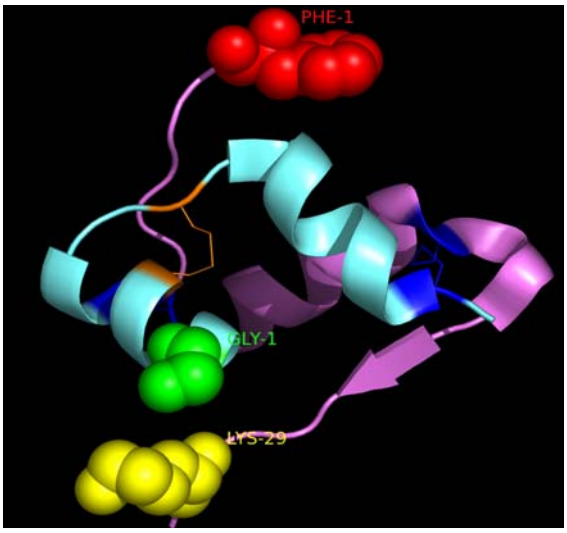

Figure 2.4 *Ribbon representation of the native bovine insulin monomer structure. The coordinates are from the crystal structure of the T6 hexameric crystal structure (PDB file 2A3G), but only the monomer is shown. The A chain is shown in teal, the B-chain in purple with the space filled labelled residues showing the available sites for acetylation (lysine-yellow, glycine-green, phenylalanine-red). The intrachain disulfide bond is shown in orange and the two interchain disulfide bonds are shown in dark blue. Figure was generated using PyMol (DeLano 2002).*

Early attempts at non-selective acetylation of insulin amino groups produced a mixture of products which had a low resolution by chromatography. As a result, selective acetylation of the lysine side chain amino group was thought as a better means of insulin amino derivatisation. Acylating agents chosen were reported to be specific and react rapidly under mild conditions (Riordan and Vallee 1972a). The reactivity of the amino groups to electrophilic attack,

depends on the local environment of the residues (Blundell *et al.* 1972). However, the *O*-acetylation of hydroxyl groups of amino acids such as tyrosine is also possible (Riordan and Vallee 1972a, Riordan and Vallee 1972b). This section outlines attempts to selectively acetylate the lysine group of bovine insulin at B29 and assess the impact on fibrillation. The acetylation of lysine with acetic anhydride is well studied and is illustrated in Figure 2.5 (Hermanson 1996).

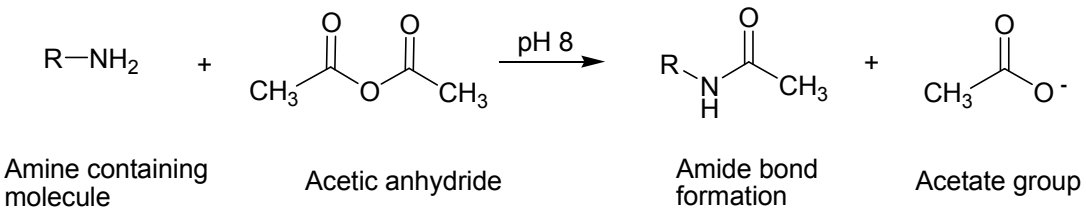

Figure 2.5 *Acetic anhydride reacts with amines to form amide bond derivatives, adapted from (Hermanson 1996).*

Amino group acetylation reactions of bovine insulin were carried out as described by Zahn *et al*. (1972) and Blundell *et al*. (1972). The route, shown in Figure 2.6, for acetylation was expected to yield insulin monoacetylated at the lysine residue. The modified insulin samples described in Figure 2.6 were tested for fibril formation and will be discussed in chapter 3, section 3.4.

2.3.1 Blocking insulin N-terminals with citraconic anhydride

Citraconic anhydride (2-methylmaleic anhydride) is a reversible acylation agent, designed for temporarily masking amine groups. It reacts with amines at alkaline pH values (7-8) to form amide linkages with an extending terminal carboxylate (Figure 2.7). The amide bonds can be hydrolysed at acidic (pH 3-4) pH to release the citraconic acid and liberate the amine (Dixon and Perham 1968, Habeeb and Atassi 1970).

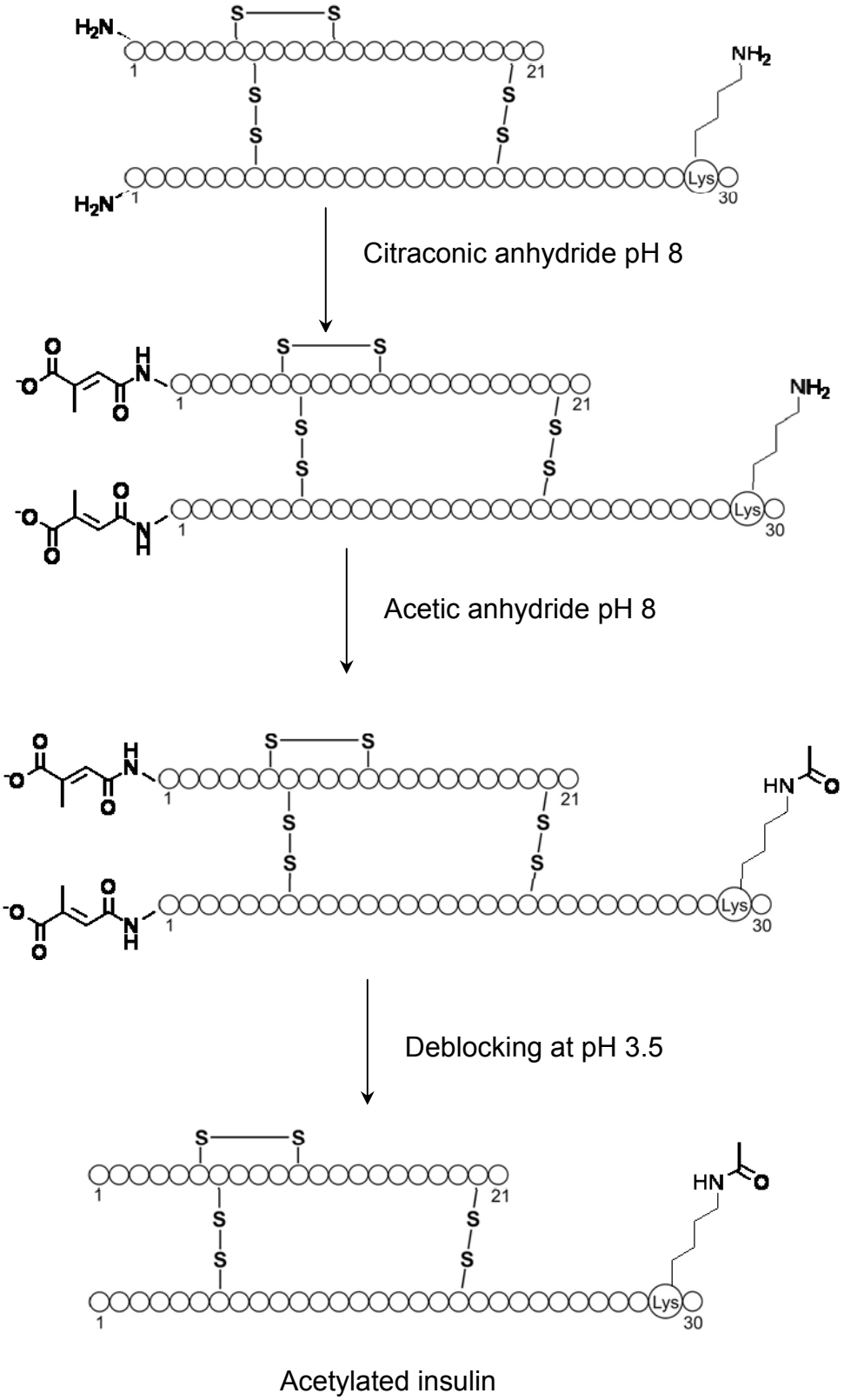

Figure 2.6 *Preparation of insulin derivatives modified at B29 ε-amino group, adapted from (Zahn* et al*. 1972).*

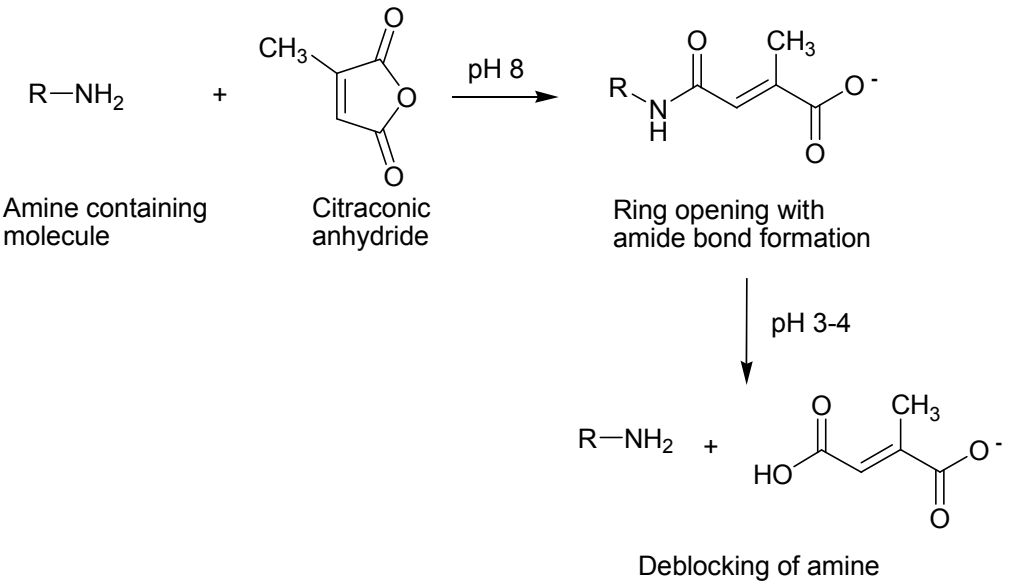

Figure 2.7 *Citraconic anhydride can be used to block amine groups reversibly because the amide bond formed is unstable to acidic conditions, from (Hermanson 1996).*

With respect to the scheme shown in Figure 2.6, the first step was to block the N-terminal amino group with citraconic anhydride, leaving the lysine residue free to be acetylated. Insulin was made up to 1 mg/ml concentration with potassium phosphate buffer (100 mM) and reacted with a 50 fold molar excess (per amino group) of citraconic acid anhydride, according to the method of (Havelund *et al.* 1995) at two pHs, 7 and 8, then characterised by ESI-MS. The predicted increase in mass due to the attachment of a citraconic group was 112.1 Da.

The degree of citraconylation was determined by measuring the increase in MW *via* ESI-MS. The ESI-MS of the citraconylated insulin at pH 7 showed that there was some unmodified insulin still present (Figure 2.8) in the sample and that the MW of insulin increased by 113.5 (+5 charge state) and 224.2 (+4 charge state) (Table 2.1). This indicated that there was a crude mixture of mono and dicitraconylated insulin and some unmodified insulin. In contrast, there was no indication of any unmodified insulin present in the insulin modified at pH 8 (Figure 2.9).

a)

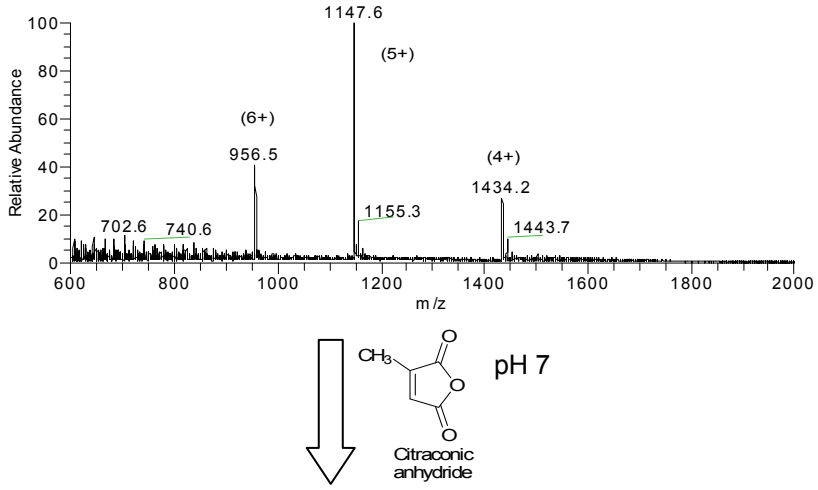

b)

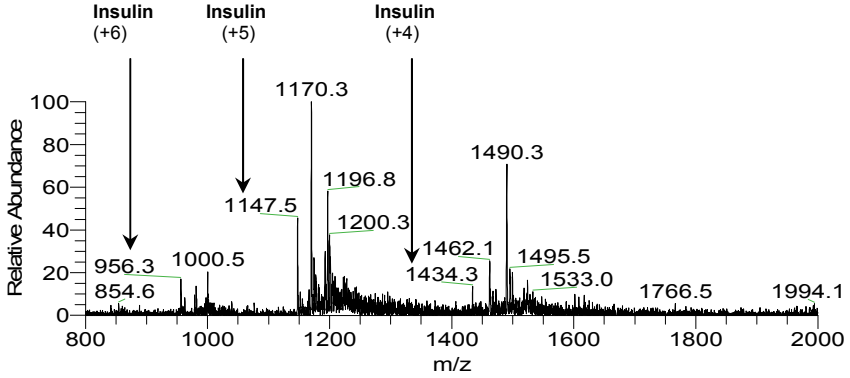

Mass fragmentation of parent ion at m/z 1170.3

c)

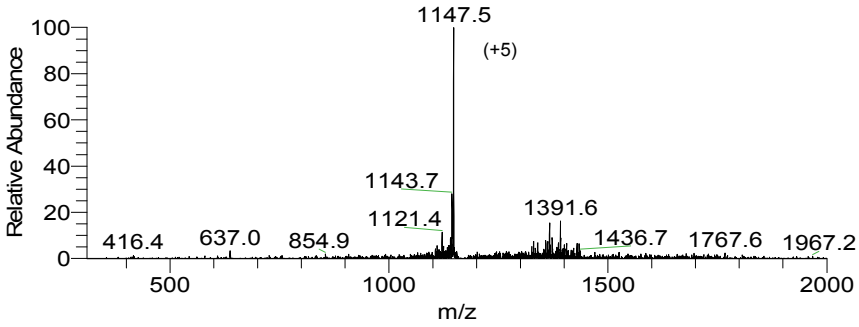

Figure 2.8 *ESI-MS of insulin solution before (a) and after (b) citraconylation was performed using an electrospray mass spectrometer operated in positive ion mode. Labels in b) show the presence of unmodified insulin. (c) ESI spectrum of citraconylated bovine insulin at pH 7 showing mass fragmentation of the parent ion at m/z 1170.3. Each of the m/z value is labelled above its corresponding charged states. The multiply charged peaks detected by the ESI-MS experiment were manually deconvoluted based on the high resolution mass scans (Zoom scan which provided charge state information).*

a)

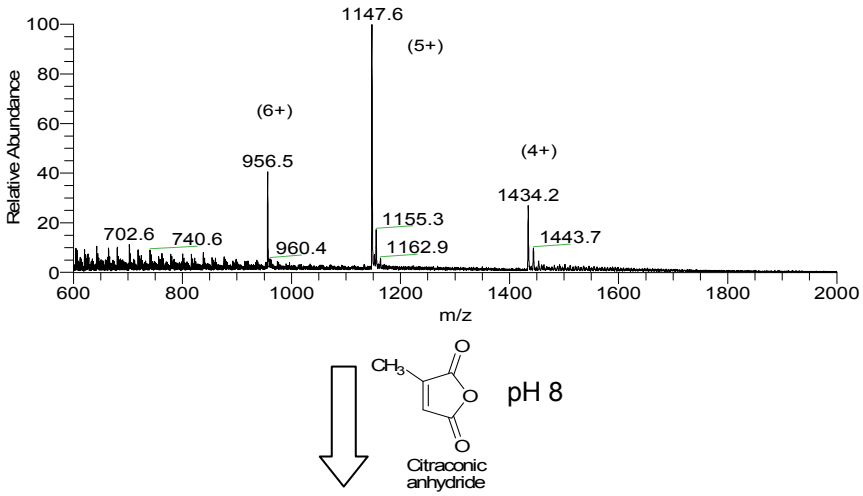

b)

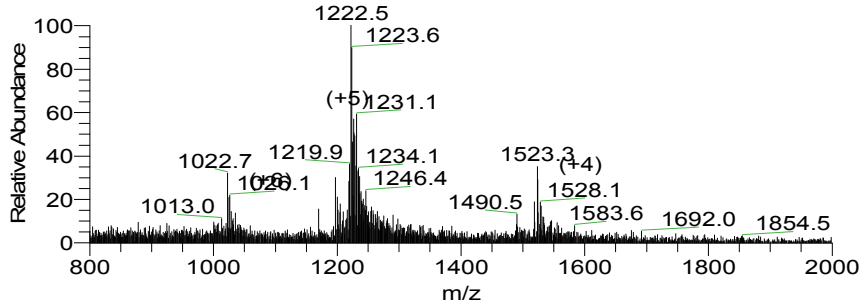

Mass fragmentation of parent ion at m/z 1222.5

c)

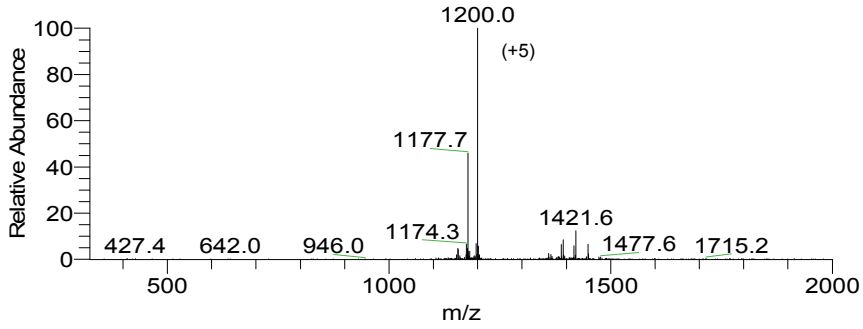

Figure 2.9 *ESI spectrum of citraconylated bovine insulin at pH 8, a) insulin control, b) crude citraconylated insulin and c) shows mass fragmentation of the parent ion at m/z 1222.5 in b). Each of the m/z values labelled above its corresponding charge states.*

The reaction went further when citraconylation was carried out at pH 8, with an increased mass of 357 (+5 charge state) and 397.2 (+4 charge state) (Table 2.1). The increase in mass was related to the addition of 3 citraconic groups (336 ± 2) plus the Na^+ (+23) and K^+ (+39) adduct ions, quite common in electrospray ionisation (Iavarone *et al.* 2004). Hence mass fragmentation of the parent ions at (M+5H) was carried out and the MW of the fragments lost

calculated (Figure 2.8 for pH 7 and Figure 2.9 for pH 8). The fragmentation confirmed the attachment of at least one citraconic anhydride to insulin at pH 7 and pH 8. Future reactions were done at pH 8, to maximise the modification of two amino groups and minimise the presence of unmodified insulin in the product.

As discussed in the introduction, the heterogeneous nature of the product was relevant as a mimic of the crude protein extracts likely to be used in industrial production, as sourcing large volumes of pure protein of the required size may prove to be costly and hence a nonviable option for materials use. Thus further time-consuming attempts to purify the components of the mixture were not made. A reasonable quantity (~20 mg) of acetylated insulin was prepared to carry out fibril formation studies in chapter 3.

Ion description	**m/z observed**	**MW calculated**	***Δ Mass**	**Mass fragmented from parent ion (M+5H)**
Bovine insulin pH 7	1147.5 (M+5H) 1434.3 (M+4H)	5732.5 5733.2	0 (±1)	na
Citraconylated insulin pH 7	1170.3 (M+5H) 1490.3 (M+4H)	5846.5 5957.2	113.5 224.2	114
Bovine insulin pH 8	956.5 (M+6H) 1147.5 (M+5H) 1434.3 (M+4H)	5733.0 5732.5 5733.2	0 (±1)	na
Citraconylated insulin pH 8	1022.7 (M+6H) 1222.5 (M+5H) 1523.3 (M+4H)	6130.2 6107.5 5957.2	374.5 356.7 397.2	112.5 224.0

Table 2.1 *Effect of citraconylation on the MW of insulin at pH 7 and pH 8.* MW of 5733 for insulin monomer was used to calculate Δ Mass after modification.*
na = not applicable

2.3.2 Acetylating citraconylated bovine insulin and determining the extent of amino group acetylation

Acetylation reactions of the crude citraconylated insulin from section 2.3.1 were carried out in 50 mM potassium phosphate buffer with the pH maintained at 8 (chapter 7, section 7.3) and the extent of acetylation was determined by LC-ESI-MS analysis. Having selectively citraconylated the two N-termini, the lysine was acetylated with a 10-fold molar excess of acetic anhydride. Lysine residues are reasonably good nucleophiles at pH 8.0, and therefore react with the carbonyl group of the acetic anhydride to form an amide bond with the acetate group being the side product (Hermanson 1996). As per Figure 2.10, the addition of acetyl is predicted to increase the MW weight by 42 atomic units.

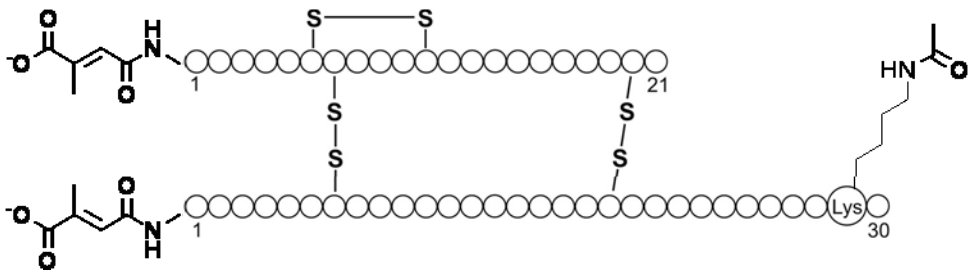

Figure 2.10 *A schematic representative of the insulin molecule, showing the attachment of 2 citraconic groups and 1 acetyl group.*

The liquid chromatogram shows a small peak at 6.8 min in the modified insulin sample and at 5.3 min in the insulin control (Figure 2.11), it was present in all chromatograms obtained during insulin acetylation reactions and will be discussed in a later section (2.3.4).

The control sample was put through all the buffer treatments and incubations without the derivatising agents, and it will be referred to as the 'insulin control' throughout chapters 2 and 3 to distinguish it from the insulin standard, which was the commercial sample, stored frozen.

The analysis also revealed that the crude citraconylated acetylated insulin peaks elute after the insulin peak (Figure 2.11). The LC-ESI mass spectrum showed a distribution of multiply protonated molecular ions, similar to that of unmodified insulin, although the modified insulin had a charged state of +4, while that of unmodified insulin was +5, consistent with the loss of an amino group. The citraconylated insulin sample, which was acetylated at 10-fold molar excess of anhydride per lysine, yielded a mass increase from 42 to 126 atomic mass units (Table 2.2), corresponding to one to three acetyl groups. The results also show the dicitraconylated insulin detected in the ESI-MS (Table 2.1) was absent after acetylation and it is assumed that it was a minor component of the citraconylated insulin. Table 2.2 shows the sixth component had a citraconyl group as well as 3 acetyl groups attached to it, which may be indicative of the *O*-acetylation of one of the five tyrosine residues present in bovine insulin.

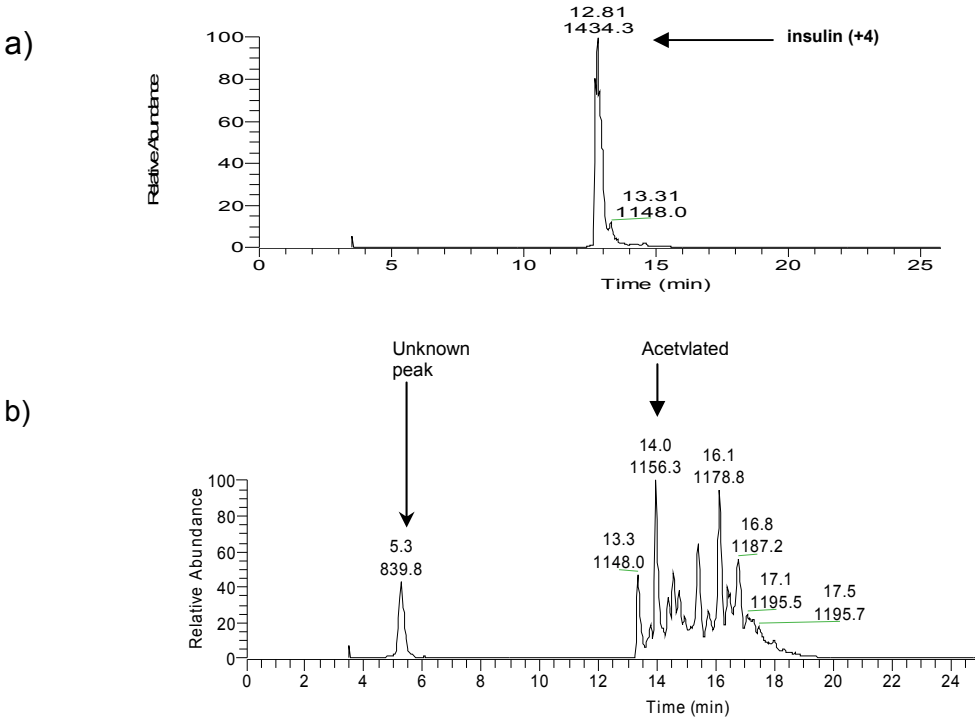

Figure 2.11 *LC-ESI-MS of (a) non-modified insulin and (b) citraconylated acetylated insulin. The m/z corresponds to each LC peak present in the total ion current (TIC) chromatogram. The samples were monitored at 280 nm PDA detector on the LC system. A: Full ESI-MS, shows a m/z of 1147.73, charge state of +5, molecular weight determined as 5734 Da. B: Full ESI-MS of the modified insulin peaks, have a charge state of +4. The six most abundant peaks on TIC have been identified in accordance with their molecular weights.*

	m/z	MW	Change in MW	Expected protein peak identification
1	1147.9	5734.5	-	Insulin monomer
2	1156.3	5776.5	42.0	Monoacetyl insulin
3	1164.7	5818.5	84.0	Diacetyl insulin
4	1170.3	5846.5	112	Monocitraconyl insulin
5	1178.8	5889	154.5 (112.5+42.0)	Monoacetyl monocitraconyl insulin*
6	1187.2	5931	196.5 (112.5+42.0+42.0)	Diacetyl monocitraconyl insulin*
7	1195.6	5973	238.5 (112.5+42.0+42.0+42.0)	Triacetyl monocitraconyl insulin

Table 2.2 *Effect of acetylation on the molecular weight of citraconylated insulin.*Indicates MW for components which elute at 2 different retention times on liquid chromatography, due to the difference in their sites of modification.*

2.3.3 Attempts to identify the unknown peak

The unknown peak eluting earlier (RT=5.3 min) than the modified insulin peaks (RT=12.8-18 min) was present in the liquid chromatography of the unmodified and modified insulin sample chromatograms throughout this study (Figure 2.11). The intensity of the unknown peak varied relative to the intensity of the modified insulin peak. Attempts were made to identify the source of the unknown peak *via* the EI mass spectra. The peak was scanned from 190-350 nm using the photo diode array detector (PDA) source on the X-calibur software (Figure 2.12). The absorbance of the molecule(s) was found to be of a broad range, with the maximum at 246 nm. The mass spectrum does not show a single m/z score but has a range of signals at a suppressed intensity (Figure 2.13). The mass spectra for the unknown peak were inconsistent along the distribution of the peak itself. It was assumed that the molecule possibly has m/z below 800, suggesting that it cannot be a protein, but phthalates.

A literature search revealed that generally the EI spectra of phthalates lack a molecular ion and are characterised by an abundant base peak at m/z 149 (Ende and Spiteller 1982, Kumar 1999). In addition, low abundance ions in the

higher mass range have also been assigned to phthalate esters. Phthalate esters tend to migrate from plastic sources into the environment (Williams 2004) as they are not chemically bound to the polymer. The possible source of contamination in the insulin samples during its amino group acetylation can be postulated to be polymeric in nature due to the broad PDA absorbance and its low ionisation. The procedure for insulin acetylation involved usage of plastic tubing/materials which were part of the autotitrator utilised to carry out the reactions (citraconylation followed by acetylation), which may have exclusively contributed to this contamination. As expected, this particular peak was absent from the insulin standard since it was tested straight from the standard jar (Figure 2.5). Attempts to run the modified insulin in negative ion mode on LC-MS, to analyse the unknown peak were unsuccessful as it still did not ionise. The peak was not investigated any further and presumed to be artifactual.

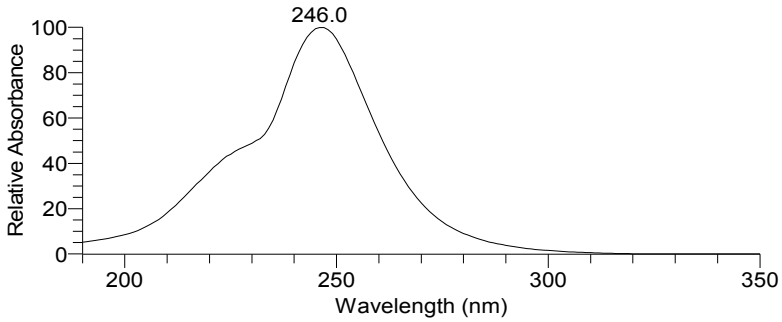

Figure 2.12 *PDA spectrum (190-350 nm) of the LC-ESI-MS peak at RT 5.3 min, shows that it has a maximum absorbance at 246 nm.*

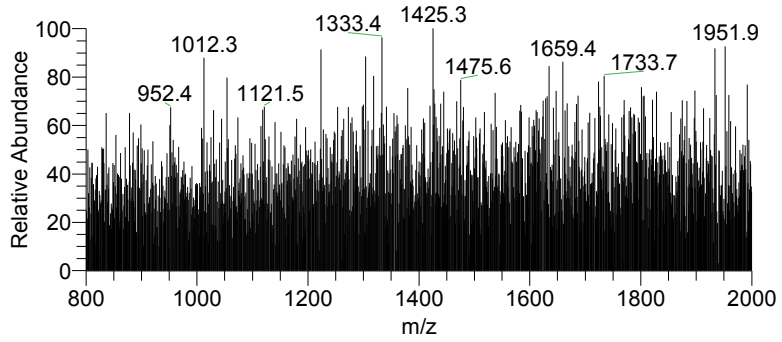

Figure 2.13 *ESI-MS full mass spectrum of the unknown peak at RT 5.3 min, the spectra differed with the retention time variation of 0.01 min. The unknown peak was extracted from the LC-ESI-MS data in Figure 2.11.*

2.3.4 Deprotecting of insulin N-terminals at pH 3.5 (de-citraconylation)

With reference to the insulin amino group acetylation scheme shown early in this chapter (Figure 2.6), insulin was successfully modified to crude citraconylated acetylated insulin. The heterogeneous product was composed of nine different components modified to different degrees (Table 2.3), of which three components had the same MW, but differed in their LC peaks, which indicates their different sites of modification. The next step was to deprotect the insulin N-termini (Blundell *et al.* 1972, Zahn *et al.* 1972) since the citraconylation reaction is reversible (Figure 2.7) (Atassi and Habeeb 1972, Brinegar and Kinsella 1981).

The lability of the citraconyl blocking group under various conditions was explored. Specifically, the effects of time and temperature on de-citraconylation of insulin amino groups were determined by treating samples at pH 3.5 in 75 mM citrate phosphate buffer (Dixon and Perham 1968, Habeeb and Atassi 1970). The samples were incubated at 20°C and 30°C for 0, 5, 10, 12, 24, 48, 72, 96 hr and analysed on LC-ESI-MS to determine the change in MW. Loss of the citraconic groups was expected. However, the LC-ESI-MS data obtained for the samples deprotected at 20°C did not show a decrease in MW (data not shown).

The LC-ESI-MS data obtained for the samples deblocked at 30°C were analysed and the MW of the sample components were calculated from the m/z score of each peak. The sample components were quantified based on the LC peak areas. The calculated MW was identified, with the degree of insulin modification that was expected. Deblocking of citraconic groups from crude citraconylated acetylated insulin was achieved at 30°C after 24 and 48 hr of acid (pH 3.5) treatment (Figure 2.14).

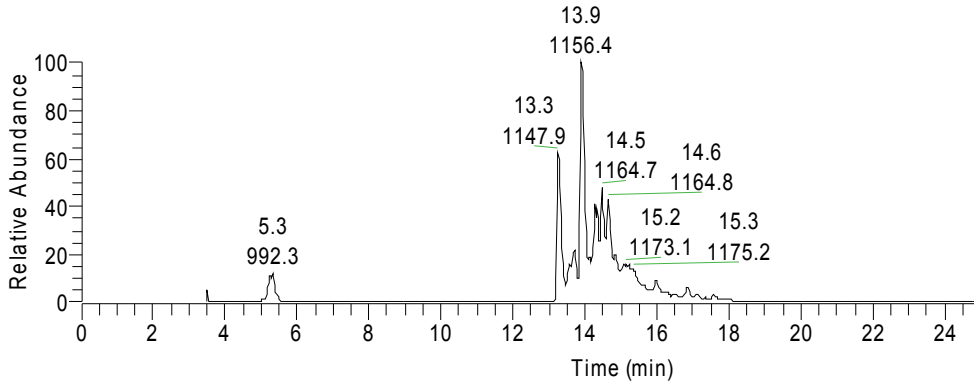

Figure 2.14 *Total ion chromatograms (TIC) of crude citraconylated acetylated insulin after de-citraconylation, 48 hr treatment at pH 3.5. LC-MS was performed using an electrospray mass spectrometer operated in positive ion mode. Ions were scanned over a range of 800-2000 m/z* $[M+H]^+$*).*

The bar graphs at 0 hr in Figure 2.15 show that at the outset of the acid treatment, the citraconylated acetylated insulin sample had nine components (a, c, d, f, g, h, I, j, k) in the mixture. Monoacetyl insulin (b,c), and monoacetyl monocitraconyl insulin (g,h) and diacetyl monocitraconyl (i,j) were graphed separately since they differed in their retention times.

Acid treatment of the sample (Figure 2.17 f, g, h, i, j, k) for 24 and 48 hr led to the loss of all citraconic groups in the nine components of the sample. The data show that after de-citraconylation, only five components (a, b, c, d, e) remained in the mixture of acetylated insulin, the components differing in the degree of acetylation (mono, di, tri). Sample component peaks with similar MW but different LC peaks were noticed as well. For example, there were two mono acetyl insulin peaks (b, c), one eluted at 13.8 min and the other at 14.1 min, suggesting different sites of acetylation.

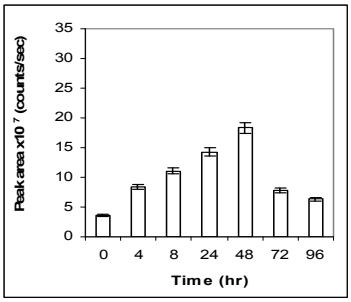

(a) insulin

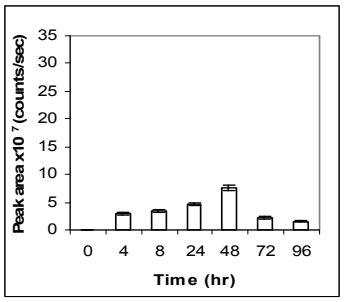

(b) monoacetyl insulin

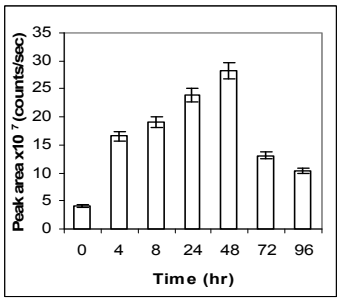

(c) monoacetyl insulin

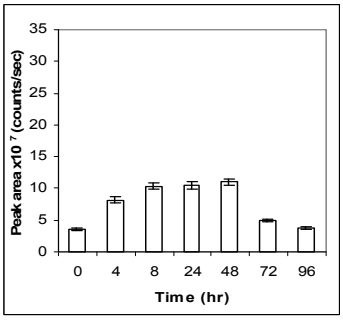

(d) diacetyl insulin

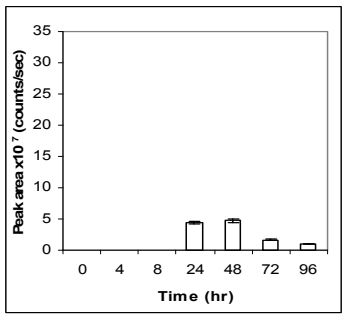

(e) triacetyl insulin

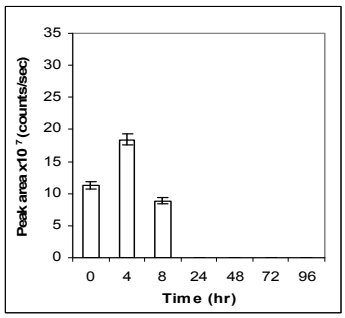

(f) monocitraconyl insulin

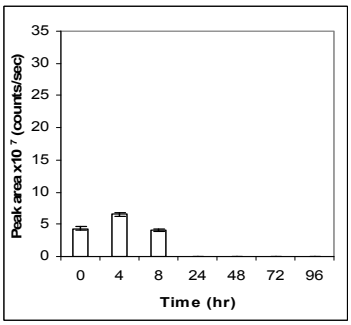

(g) monoacetyl monocitraconyl insulin

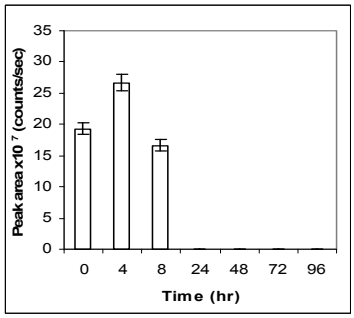

(h) monoacetyl monocitraconyl insulin

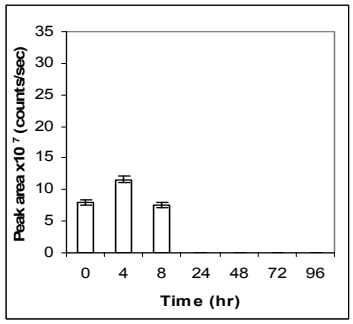

(i) diacetyl monocitraconyl insulin

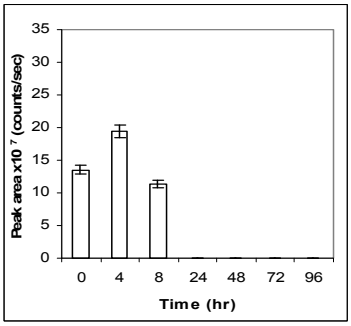

(j) diacetyl monocitraconyl insulin

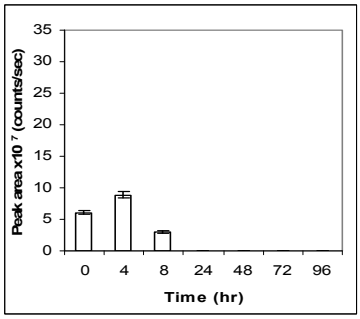

(k) triacetyl monocitraconyl insulin

Figure 2.15 *Removal of citraconyl group from citraconylated acetylated insulin at 30ºC over time. Separate bar graphs are labelled with the different components of citraconylated acetylated insulin. Peak areas were quantified from LC-MS spectra. MW calculated from m/z score for each peak. Error bars show % error of the mean from duplicate samples.*

It was also inferred that over the incubation period there was an increase in the peak area of the unmodified insulin present in the modified samples after deprotection at 24 and 48 hr of acid treatment. This can be attributed to the loss of the citraconyl groups from citraconylated insulin under acidic conditions. Deprotected samples at 24 and 48 hr of acid treatment contain mono, di, tri acetyl insulin which may differ in their site of acetylation. The results also showed that deprotection at 72 hr and beyond caused a decrease in the peak areas of the modified insulin fractions, indicating loss of proteins, presumably *via* aggregation.

Citraconylated acetylated insulin required an acid treatment at 30°C for at least 24-48 hr to remove the citraconic anhydride group and obtain acetylated insulin, which was then tested for its aggregation propensity as discussed in the next chapter. Quantitative analysis of the LC-ESI-MS peak areas from Figure 2.15 revealed that 24% of the insulin was unmodified and that the largest proportion of the modified insulin was monoacetyl insulin at the retention time of 14.1 min (37% of the sample). Samples tested in chapter 3 for fibril formation were crude citraconylated acetylated insulin and crude acetylated insulin.

2.3.5 Determination of the site of insulin acetylation

The crude acetylated insulin, composed largely of mono acetyl insulin, was sequenced on LC-ESI-MS/MS to find the site of the acetyl group. Crude acetylated insulin was reduced and alkylated prior to trypsin digestion and sequencing by LC-ESI-MS/MS. The reduction alkylation was needed to break and cap the disulfides, to ensure complete digestion of the protein so that the peptide fragments could be identified by MS (Hale *et al.* 2004).

Trypsin has well defined cleavage specificity at the carboxy terminal side of lysine and arginine. It typically yields peptides with an average length of about ten amino acid residues (Olsen *et al.* 2004). Studies in the 1960s on the trypsin digestion of bovine insulin (Bromer and Chance 1967, Carpenter 1966, Carpenter and Baum 1962, Young and Carpenter 1961) have shown the products to be alanine (C-terminus of B chain), a heptapeptide (B chain

residues 23-29) and desoctapeptide-insulin. The expected site of trypsin cleavage for bovine insulin is shown in Figure 2.16.

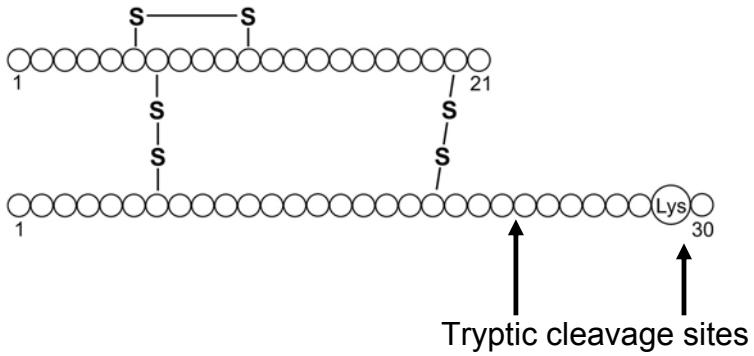

Figure 2.16 *Insulin amino acid sequence showing the two sites of trypsin cleavage.*

The mass sequencing of the trypsin-digested crude acetylated insulin was predicted to yield insulin B chain with an acetylated lysine. A control sample of unmodified insulin was also reduced and alkylated before trypsin digestion and then sequenced by LC-ESI-MS/MS.

To observe a fragment ion by mass spectrometry, the parent molecule has to be fragmented and the resulting fragments must acquire a positive charge to be detected. The spine of a peptide contains three types of bond, C-C, C-N, and N-C. Any of these bonds may be broken in the mass spectrometer and 2 of the ions resulting from the breakage are named B, and Y (Wedd 2007). Figure 2.17 shows the mechanisms by which the commonly found B and Y ions may become charged.

The acquired MS/MS spectra for each sample were searched using the SEQUEST algorithm (under license from the University of Washington, (BioWorks Browser© v3.2 EF2, Thermo Electron Corp., CA, USA) against the in-house protein database (MacCoss *et al.* 2002, Moore *et al.* 2002). BioWorks 3.2 features the SEQUEST protein search algorithm, which automatically identifies peptides by comparing experimental mass spectrometry (MS/MS) data with standard protein databases. Searches were performed with trypsin

specified as the enzyme with an allowance for missed cleavage of one amino acid, for potential hindrance to cleavage of the acetylated lysine B29. Data were filtered and scored against SEQUEST database consisting of bovine insulin A and B chains and trypsin with the expected variable amino acid modifications of alkylation (+58) on cysteine (C) and acetylation (+42) on N-terminal amines and lysine (K). Possible peptide combinations were then filtered to show only matches with greater than 30% Y and B ion confirmation and a preliminary score (Sp) of greater than 200. An explanation of scoring is provided in section 7.6.3.4 (Novatia 2008).

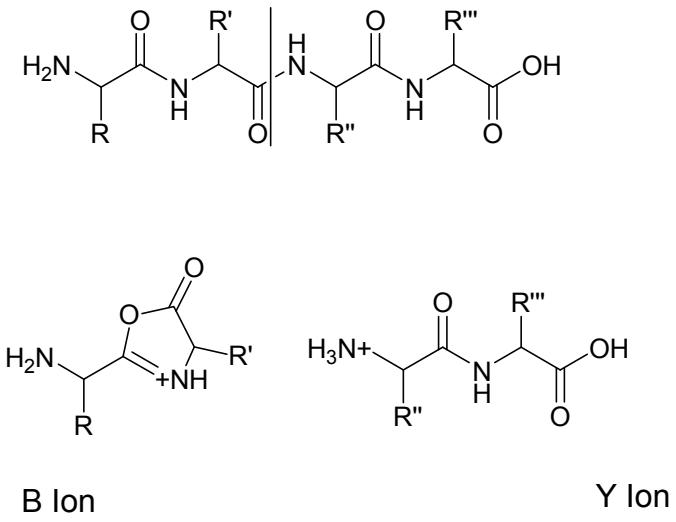

Figure 2.17 *Formation and charging of B and Y ions (Wedd 2007).*

The ion value gives a measure of the number of experimental ions that matched with the theoretical ions for the peptide listed. For example, 8/10 says that the LC-MS/MS spectrum contained 8 out of 10 predicted ions for the peptide. 100% coverage of the predicted ions is rare, but 70% or 80% coverage is common (Joyce, pers. comm.). The scan range limitations or the low mass cut-off feature of the ion trap might drop off ions at either end of the spectrum (Joyce, pers. comm.). The ion link showed the MS/MS spectrum labeled with the theoretical ions from the matched peptides.

Combinations of cysteine alkylation with and without N-terminal acetylation were identified, but lysine acetylation did not appear to be present. Results are summarised in Figure 2.18 and reveal that the glycine on the N-terminus of the insulin A chain was acetylated in the crude acetylated insulin.

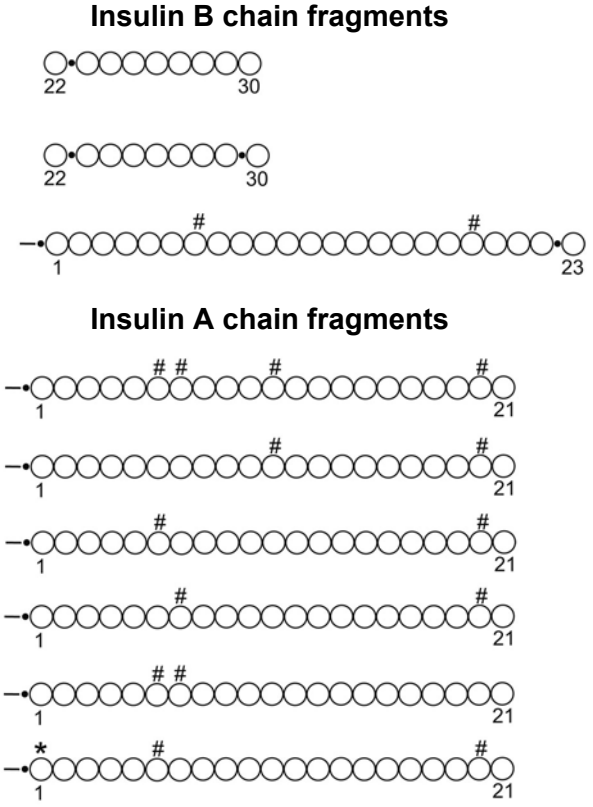

Figure 2.18 *Prominent fragments and modifications for crude acetylated insulin digest. Sample was injected in a 10 µl aliquot. Separation was performed on a Zorbax-300SB-C8, column with a mobile flow rate of 300 µl/min. The mobile phase consisted of water (A) and acetonitrile (B) both containing 0.2% formic acid (FA). An elution gradient of 95% A held for 5 min then switched to 70% A with a linear gradient to 20% A over 45 min was applied. The column was then re-equilibrated with 95% (A). Eluent was dispersed with electrospray ionisation (ESI) in the positive mode for ionisation of the peptides into the ion-trap mass analyser from 400-2000 m/z. Full scan normal/zoom data were automatically filtered to select M+2H and M+3H peptide states for* MS^2 *fragmentation to produce fragments suitable for sequence analysis. Any undefined charge states were not selected for fragmentation. Note: •Denotes point of enzyme cleavage,* $^{\#}$ *Alkylation, *N-terminal acetylation.*

These findings demonstrate that the glycine on insulin A chain was unexpectedly not protected by citraconic group and hence was most susceptible to acetylation using this procedure. This is in accordance with the results of Lindsay and Shall (1971) who also found that acetylation of insulin with hydroxysuccinimide esters increasingly favours reaction at the glycine residue on increasing pH. Modifications of the A1 group by acetyl (Zahn *et al.* 1972), acetoacetyl (Lindsay and Shall 1969), have crystal structures which indicate that they form hexamers and can have similar structures to insulin but circular dichroism indicates that acetylation at A1 may induce conformational changes in solution (Blundell *et al.* 1972, Lindsay and Shall 1971). This is of much interest, knowing that a change in the polarity, the secondary structure propensity or the net charge of the polypeptide determine a protein's ability to form amyloid (Chiti *et al.* 2002, Fink 1998, Lopez de la Paz *et al.* 2002, Lopez de la Paz and Serrano 2004). These crude modified insulin samples were analysed in fibril trials and are described in chapter 3.

2.4 Reductive Alkylation of Bovine Insulin

This section describes the second approach to derivatise insulin, which was reductive alkylation of insulin disulfide bonds. The role of disulfide (S-S) bridges in proteins is to add stability in the changing extracellular environment; in general, if all the disulfide bonds in a protein are reduced, both the structure and the function are lost completely (Thornton 1981). This is true for insulin (Figure 2.1), where breaking the disulfide linkages of insulin results in an extensive unfolding (Markus 1964, Thornton 1981, Waugh 1948), with the conformational change accompanying the reduction being the direct consequence of the release from the restriction imposed on the native structure by these bonds (Fukada and Takahashi 1980, Markus 1964).

Reduction of disulfide bridges is conducive to a greater molecular flexibility and a dramatic increase in the exposure of hydrophobic regions. To study the role of the disulfide bridges in insulin, all disulfides were reduced with dithioerythritol (DTE) and the free cysteines were blocked with IAA and 4-VP. These are

frequently used alkylating agents: IAA yielding S-carboxymethyl cysteine and 4-VP yielding S-pyridylethyl cysteine (Simpson 2003). Iodoacetic introduces a hydrophobic moiety to the cysteine while the 4-VP introduces a negative nature to the side chain of the protein. The molecular weight change of insulin before and after the reduction and alkylation processes was determined by LC-ESI-MS. The ability of the reduced and alkylated insulin to self-assemble into amyloid fibrils was monitored and will be discussed in chapter 3.

2.4.1 Reduction and characterisation of bovine insulin

Bovine insulin (10 mg/ml) was reduced with DTE at pH 8.0, in 8 M urea using a published method (Shechter *et al.* 1973). DTE reduces all accessible biological disulfides and maintains free thiols in solution even in the presence of oxygen (Hermanson 1996) (Figure 2.19).

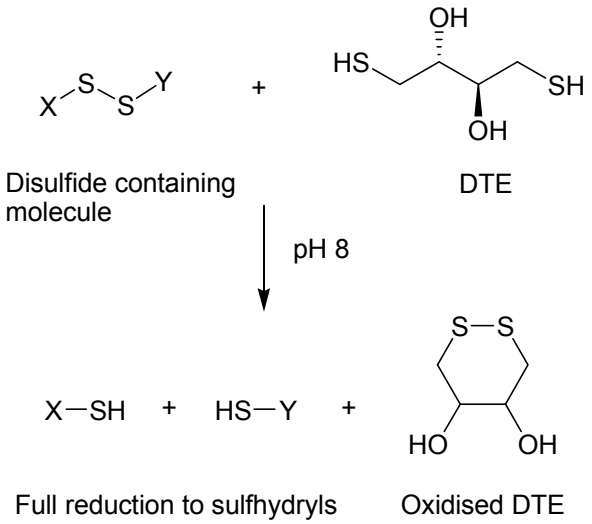

Figure 2.19 *DTE reduction of disulfides (Hermanson 1996).*

2.4.2 Carboxymethylation and pyridylethylation of reduced insulin

For the alkylation process, the reduced insulin was further modified by either carboxymethylation or pyridylethylation. Figure 2.20 (a) and (b) show the carboxymethylation of a reduced cysteine by IAA and pyridylethylation.

a)

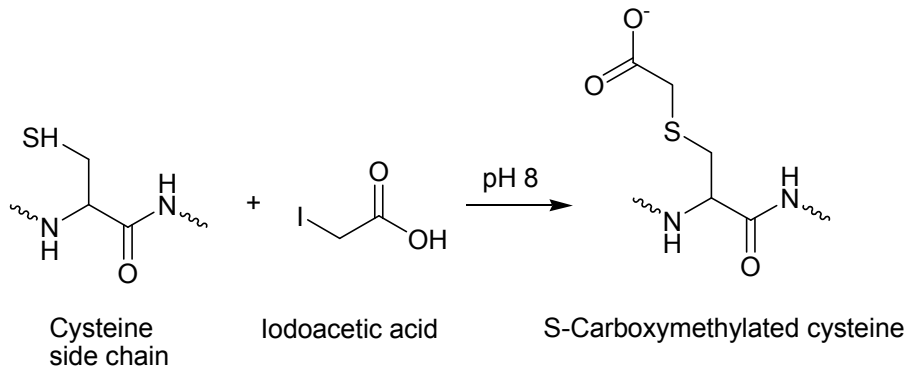

b)

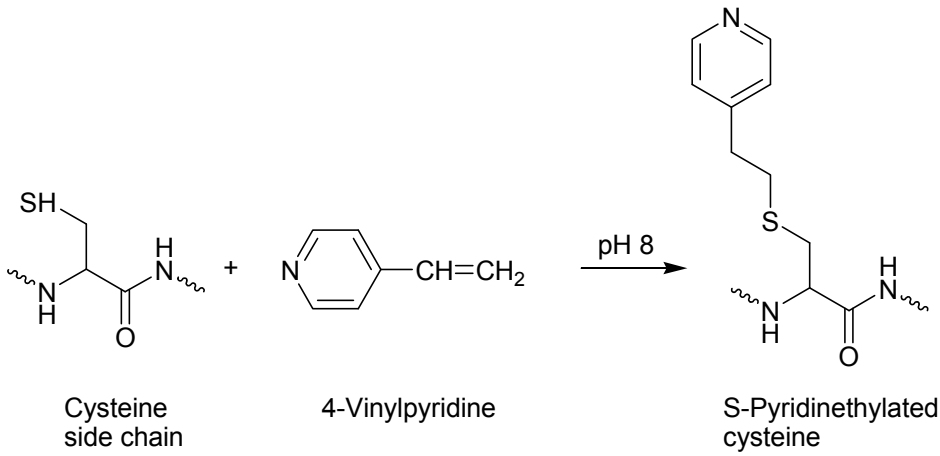

Figure 2.20 *Modification of free SH groups by a) iodoacetic acid b) 4-vinylpyridine (Friedman 2001).*

2.4.3 Characterising the reduced alkylated insulin

The reduced insulin samples (before and after carboxymethylation) were gel filtered using a Sephadex G-25 column to remove salts. For control purposes, the starting material was also gel filtered (insulin control).

The addition of 4-VP to the crude reduced insulin resulted in the formation of a white precipitate of reduced pyridylethylated insulin (RPE) which was centrifuged at 5000 rpm for 10 min to separate supernatant from the pellet. The RPE supernatant was also gel filtered. An example of the gel filtration chromatography column profile obtained is shown in Figure 2.21. The protein

peaks corresponding to insulin control, reduced insulin, reduced-carboxymethylated (RCM) insulin and RPE insulin were pooled separately, were lyophilised and stored at 4°C. LC-ESI-MS analysis was used to confirm the identity of the pooled fractions corresponding to the peaks on the gel filtration profile. The RPE pellet was solubilised in HCl (25 mM) at pH 2 for LC-ESI-MS. After the characterisation of the insulin control and the modified insulin on LC-ESI-MS, samples were tested for aggregation propensity, as discussed in chapter 3.

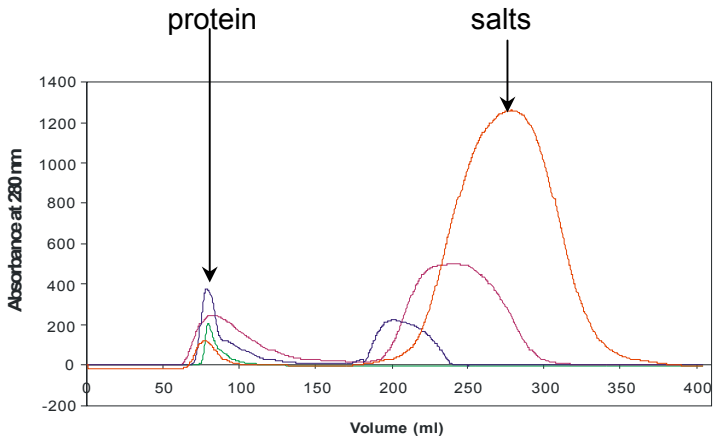

Figure 2.21 *Gel filtration chromatography of soluble derivatised insulin samples on a Sephadex G-25 column (2.6 cm x 100 cm) equilibrated in 50 mM ammonium bicarbonate pH 7.9. The chromatogram shows peaks corresponding to insulin control (green), reduced insulin (blue), RCM insulin (pink) and RPE insulin supernatant (red).*

2.4.4 Determining the extent of insulin reduction alkylation

LC-ESI-MS was used to analyse insulin before and after disulfide reduction as well as after S-carboxymethylation and S-pyridylethylation. The mass of the insulin increased by ~58 as a result of the introduction of one carboxymethyl group for each SH group and by ~106 for the pyridylethylation (Table 2.4). As discussed in section 2.2.2 of this chapter, insulin contains three disulfide bonds (Figure 2.1); the two interchain bonds are more reactive than the intrachain disulfide bond with their reactivities ranging in the order: A7-B7>A20-B17>A6-A11 (Blundell *et al.* 1972).

LC-ESI-MS profiles of insulin after reduction, reduction carboxymethylation, and reduction pyridylethylation (supernatant and pellet) are shown in Figure 2.22. The insulin control was also analysed and Figure 2.22 (a) shows a single peak of insulin with m/z score labelled as 1147.7, with the MW calculated to be 5733.5 Da at a charge of +5. This was expected and shown earlier in section 2.1. Reduction of insulin disulfides with DTE produced a crude mixture of separated insulin chains A and B, including some unmodified insulin (Figure 2.22 b). Analysis of the LC-ESI-MS data showed the presence of some unmodified insulin (5733 Da), insulin A chain (2335 Da) and B chain (3398 Da) (Figure 2.22 b).

a) Insulin control

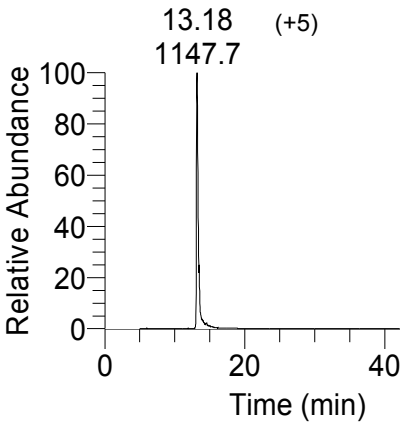

b) Crude reduced insulin

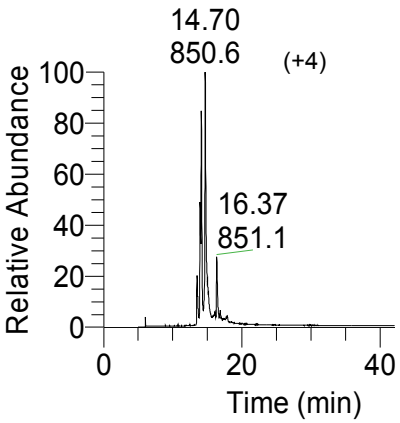

c) Crude reduced carboxymethylated insulin

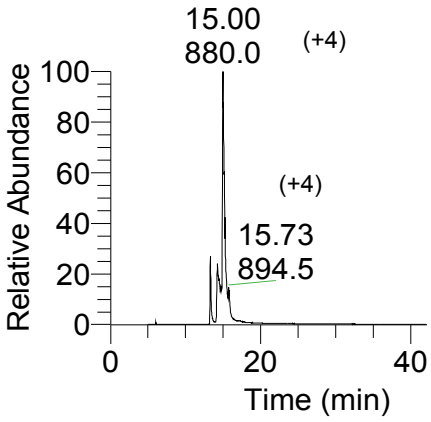

d) Crude reduced pyridylethylated insulin supernatant

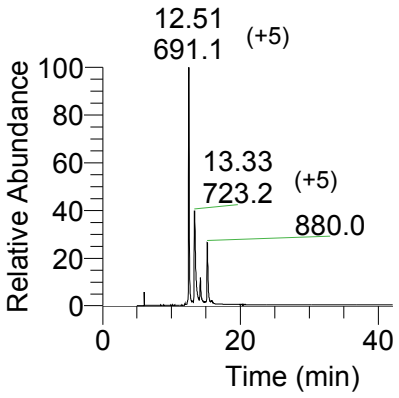

e) Crude reduced pyridylethylated insulin, pellet

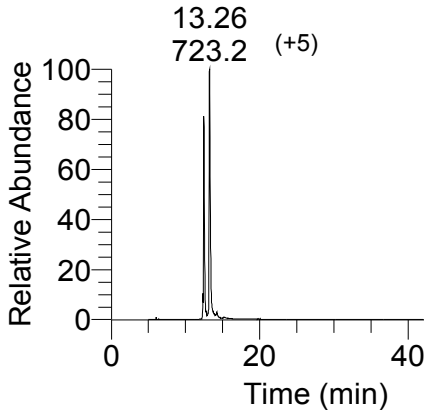

Figure 2.22 *A 10 µl aliquot of modified and unmodified insulin was injected onto the Thermofinnigan Micro AS system for LC-ESI-MS. (Thermo-Finnigan LTQ mass spectrometer described as a 2D linear quadrupole iontrap, San Jose, CA, USA). A triple play (full scan, Zoom scan, CID with 35% collisional energy) data-dependent acquisition method with dynamic exclusion was performed using the Xcalibur software. Spectra were processed using the base peak ion chromatogram and a seven-point Gaussian smoothing function. The multiply charged peaks detected by the ESI-MS experiment were manually deconvoluted based on the high resolution mass scans (Zoom scan which provided charge state information). Each peak shows its retention time and m/z score of the protein component.*

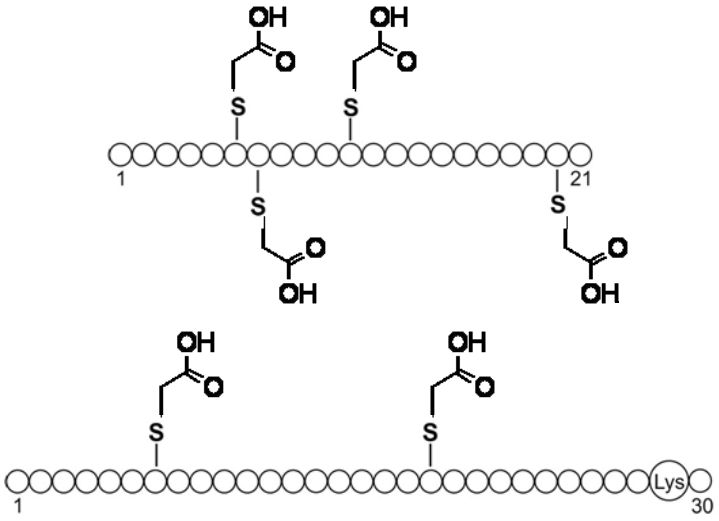

Figure 2.23 *Separate insulin chains (A chain 1-21, B chain 1-30) showing the modification of the liberated SH groups with iodoacetic acid.*

Calculations from the LC-ESI-MS data in Figure 2.22 (c) show that insulin A chain has increased in MW from 2338 Da to 2568 Da, confirming the attachment of four carboxymethyl groups (58 Da per carboxymethyl) to the four cysteine molecules present on the A chain (Table 2.3). Figure 2.22 (c) also shows an increment in the MW of the peak representing the insulin B chain (MW=3516 Da) which suggests that the two cysteines on the insulin B chain have been carboxymethylated (Table 2.3). The unmodified insulin was carried over from the reduction step to the RCM insulin mixture, indicated by the peak corresponding to MW 5733.4 Da in Figure 2.22 (c).

As discussed earlier, pyridylethylation of the crude reduced insulin led to a crude RPE supernatant and pellet. The two fractions were analysed separately on LC-ESI-MS for comparison purposes. The RPE pellet was solubilised in HCl (25 mM) at pH 2 for LC-ESI-MS. Figure 2.22 (c) and (d), both showed the loss of the unmodified insulin peak from the chromatogram. 4-VP produced hydrophobic insulin A and B chains, with an elution pattern on LC-ESI-MS chromatogram different from that of the unmodified insulin, which was expected. The pellet had a mixture of S-pyridylethylated insulin A and B chain and the supernatant sample was largely composed of insulin A chain (Figure 2.22 d, e and Table 2.3).

There is an increase in the MW of insulin A and B chain which confirms that it has 4 and 2 pyridylethyl groups attached to the respective reduced cysteines (Table 2.3). The pellet profile has a higher intensity for both S-pyridylethylated insulin A and B chain, while the supernatant has a more intense peak for S-pyridylethylated A chain than the B chain. This reflects the partial separation of the two chains: the supernatant mainly contained the A chain, and the pellet consists of both the A and B chain.

Ion description	MW calculated	Δ MW	Sequence
Insulin monomer	5733.4	NA	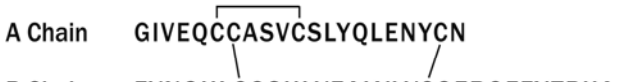
Reduced insulin	5733.4 2335.3 3398.3 3399.9 10196.9	NA	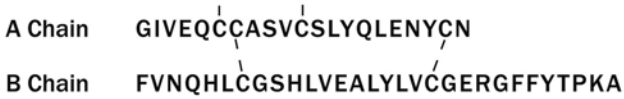
RCM insulin (A and B chain)	5733.4	0.0	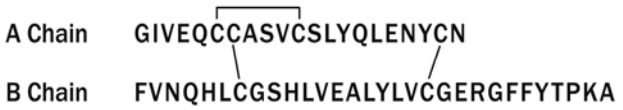
	2571.6	236 (4 x 59)	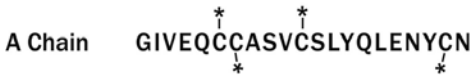
	3516.1	118 (2 x 59)	
RPE insulin (A and B chain)	2760.4	425 (4 x 106)	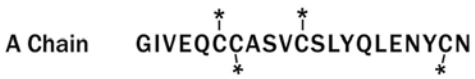
	3610.4	212 (2 X 106)	

Table 2.3 *Effect of reduction, reduction S-carboxymethylation, reduction S-pyridylethylation on insulin molecular weight. Note:* represents the carboxymethyl/pyridylethyl group attached to insulin, with a MW of 58 ±1 Da or 106±1 Da. MW of insulin A and B chain without any modification is, A chain = 2337.9 Da, B chain = 3397.7 Da modification.* Δ *MW =* $MW_{after\ modification} - MW_{before\ modification}$

Overall, the insulin intermolecular and intramolecular disulfide bonds were reduced and alkylated (carboxymethylated, pyridylethylated) to obtain crude mixtures of RCM and RPE insulin samples for testing aggregation propensity in chapter 3. In addition, there was an insulin control sample and reduced insulin, which were also tested in aggregation trials.

2.5 Trypsin Digestion of Bovine Insulin

Insulin was digested with trypsin (section 2.3.5, Figure 2.18) on a large scale to obtain digests in reasonable quantities (20 mg) for fibril studies in chapter 3. Insulin was treated with trypsin at a ratio of 1:50, enzyme to protein ratio at pH 8.5 (37ºC) for 4 hr (Sigma-Aldrich 2007). Half of the sample digested in the first 4 hr was retained and the rest was digested sequentially for 12 more hours, with 4 hr per enzyme addition, to obtain totally digested insulin, without any undigested insulin in the mixture. Samples were digested in 500 µl fractions, in Eppendorfs. The insulin standard was also treated under the same conditions without the enzyme, and will be referred to as the insulin control. LC-ESI-MS analysis of the insulin control and trypsin treated insulin is shown in Figure 2.24. Mass spectrometry revealed that the intial enzyme digestion (Figure 2.24 b) resulted in insulin cleavage to produce 2 peptides with m/z, 859 and 965. Table 2.4 shows the peptide sequences that were obtained, in addition to the undigested insulin present in the trypsin treated sample.

a)

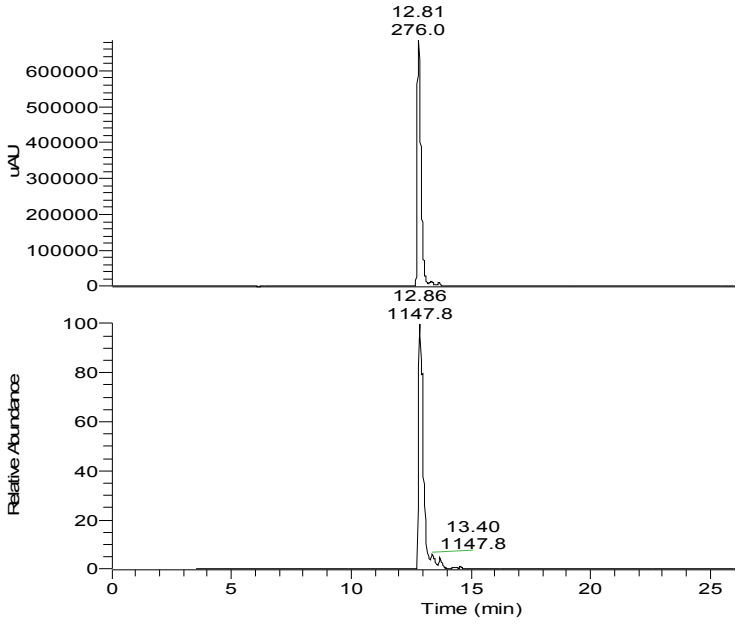

b)

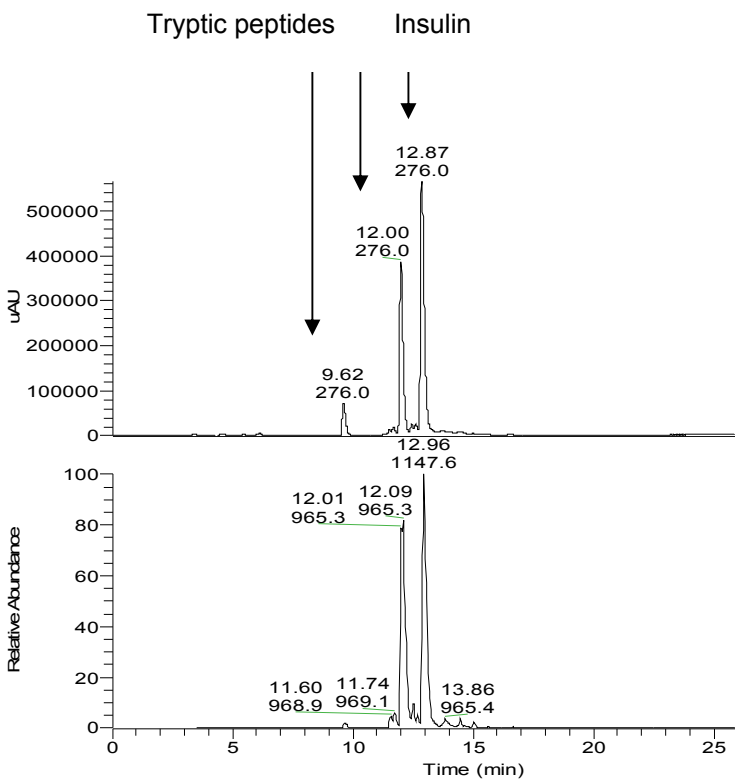

Figure 2.24 *LC-ESI-MS analysis of (a) insulin control and (b) trypsin treated insulin (4 hrs, 1:50, enzyme:protein ratio). Labels show the m/z score representing tryptic peptides, undigested insulin.*

Sequential addition of trypsin to insulin led to the total digestion of insulin to produce 3 tryptic peptides with m/z 859, 965, 1133 (Figure 2.24 b). The insulin fragments (Table 2.4) produced in a crude mixture from these experiments were freeze dried and tested for aggregation propensity in chapter 3.

a)

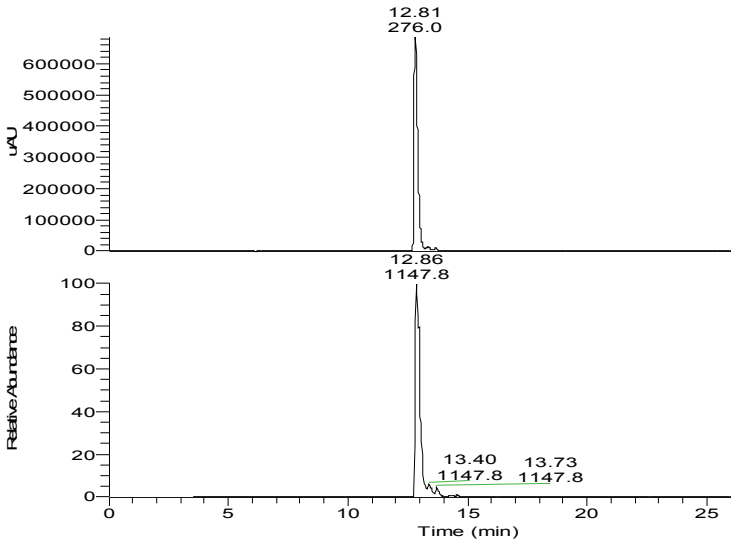

b)

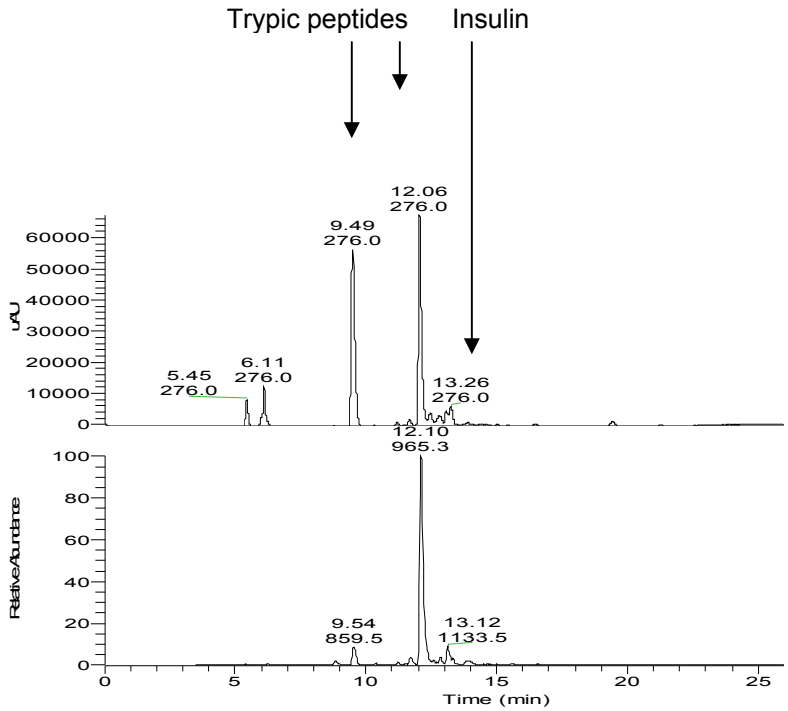

Figure 2.25 *LC-ESI-MS analysis of (a) insulin control and (b) trypsin treated insulin (4 hrs of 4 sequential treatments at 1:50, enzyme:protein ratio). Labels show the m/z score representing tryptic peptides.*

Elution time (min)	Ion description	m/z observed	Sequence
12.9	Insulin monomer	1147.8 (M+5H)	A Chain GIVEQCCASVCSLYQLENYCN B Chain FVNQHLCGSHLVEALYLVCGERGFFYTPKA
9.5	Tryptic peptide	859.6 (M+H)	B Chain (R)GFFYTPK(A)
12.2	Tryptic peptide	965.3 (M+5H)	A Chain GIVEQCCASVCSLYQLENYCN B Chain FVNQHLCGSHLVEALYLVCGER(G)
13.1	Tryptic peptide	1133.7 (M+5H)	A Chain GIVEQCCASVCSLYQLENYCN B Chain FVNQHLCGSHLVEALYLVCGERGFFYTPK

Table 2.4 *Effect of trypsin digestion on bovine insulin molecular weight and sequence*

2.6 Chymotrypsin Digestion of Bovine Insulin

This section illustrates the effect of chymotrypsin on insulin cleavage, to obtain peptide fragments for fibril studies in chapter 3. Insulin was treated with chymotrypsin at a ratio of 1:50, enzyme to protein ratio, at pH 8.5 (37°C) for 4 hr (Sigma-Aldrich 2007). Insulin standard was also treated under the same buffer conditions without the enzyme (insulin control).

The general strategy to analyse the digested fragments of insulin *via* LC-MS/MS involved the following steps (Yen *et al.* 2002): (1) chymotrypsin digestion of insulin at pH 8.5 to obtain peptides; (2) complete reduction with dithioerythritol and alkylation by IAA to label the cysteine residues of the peptides; (3) LC-ESI-MS/MS analysis of the resulting peptides to identify the fragments. A diagram of this scheme is shown in Figure 2.26. Treatment with DTE and IAA was necessary because it is more difficult to analyse fragments for disulfide-bonded peptides than those completely reduced and alkylated. This step was not necessary for the trypsin cleavage of insulin in section 2.5 since the trypsin employed specifically cleaved insulin to produce the 3 expected peptide fragments, while chymotrypsin cleaved at more than its expected sites of cleavage to produce fragments which were difficult to identify prior to the insulin reduction and alkylation.

The acquired MS/MS spectra for insulin control and the chymotryptic digest of insulin were searched using the SEQUEST (under license from the University of Washington) algorithm on the BioWorks Browser© v3.2 EF2 (Thermo Electron Corp., CA, USA) against the in-house insulin database (MacCoss *et al.* 2002, Moore *et al.* 2002). Searches were performed with chymotrypsin specified as the enzyme with an allowance for up to two missed cleavage sites.

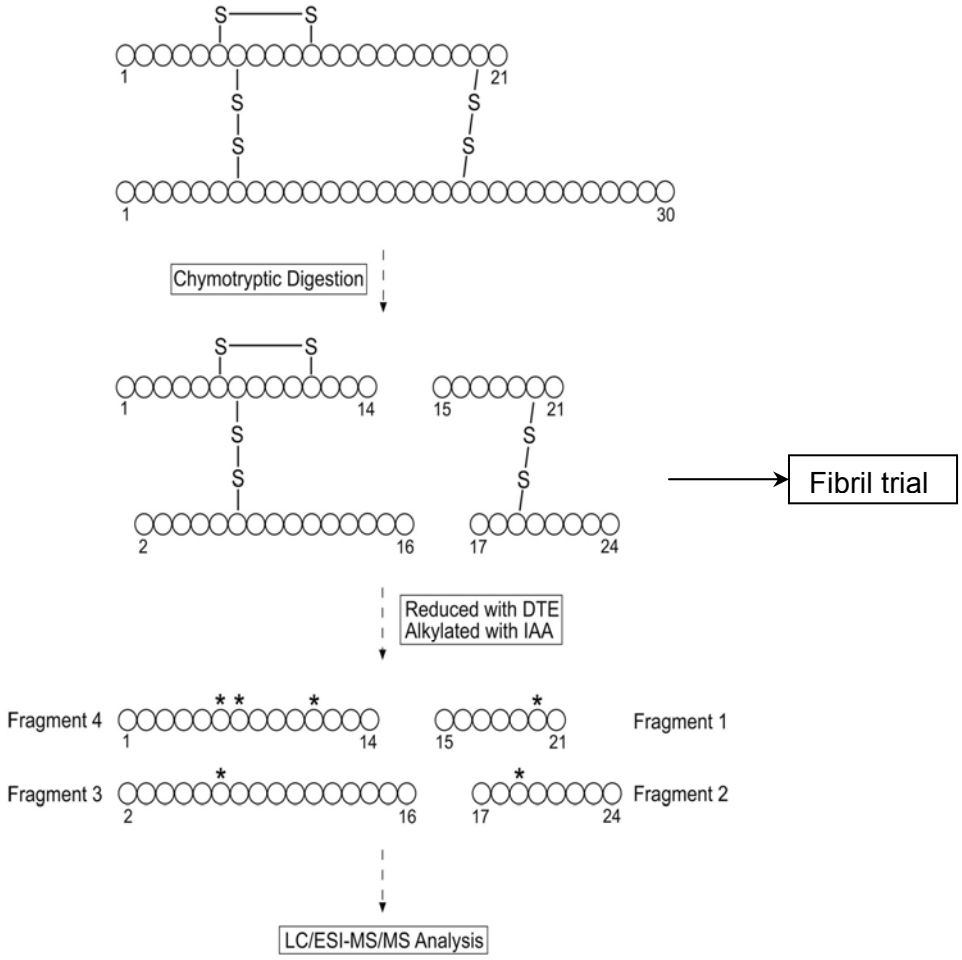

Figure 2.26 *Scheme of the experimental protocol, with modifications from the literature (Yen* et al. *2002).* **carboxymethylated.*

LC-ESI-MS ion chromatograms and spectra of the insulin control and chymotrypsin treated insulin are shown in Figure 2.27 a. SEQUEST search for the insulin control treated with the buffer (without enzyme) showed the presence of the separated A and B chains of insulin, with the cysteines carboxymethylated (Table 2.5). These data confirm the presence of undigested insulin in the insulin control. SEQUEST identified a list of peptide sequences (Table 2.5) for the chymotrypsin treated insulin (Figure 2.27 b). The four fragments expected from the chymotryptic digest of insulin (Figure 2.26) were present in the sample (Table 2.6). The table also shows that the chymotrypsin, had missed cleavages, by one or two amino acids, which led to more than the four expected fragments. The presence of separated insulin chain B chain, with the cysteines modified (Table 2.6), suggests that undigested insulin B chain is present in the chymotrypsin treated sample.

RT (min)	m/z $(M+nH)^{n+}$	MW	Sequence	Insulin chains
36.8	1285^{2+}	2568	GIVEQ*C*CASV*CSLYQLENY*CN	A chain
41.2	880^{4+} 1173^{3+} 1758^{2+}	3516	FVNQHL*CGSHLVEALYLV*CGERGFFYTPKA	B chain

Table 2.5 *Major peptide components from insulin reduced and carboxymethylated, A chain with the 4 cysteines carboxymethylated, B chain with the two cysteines carbxymethylated. RT is retention time.*Indicates carboxymethyl group.*

A)

B)

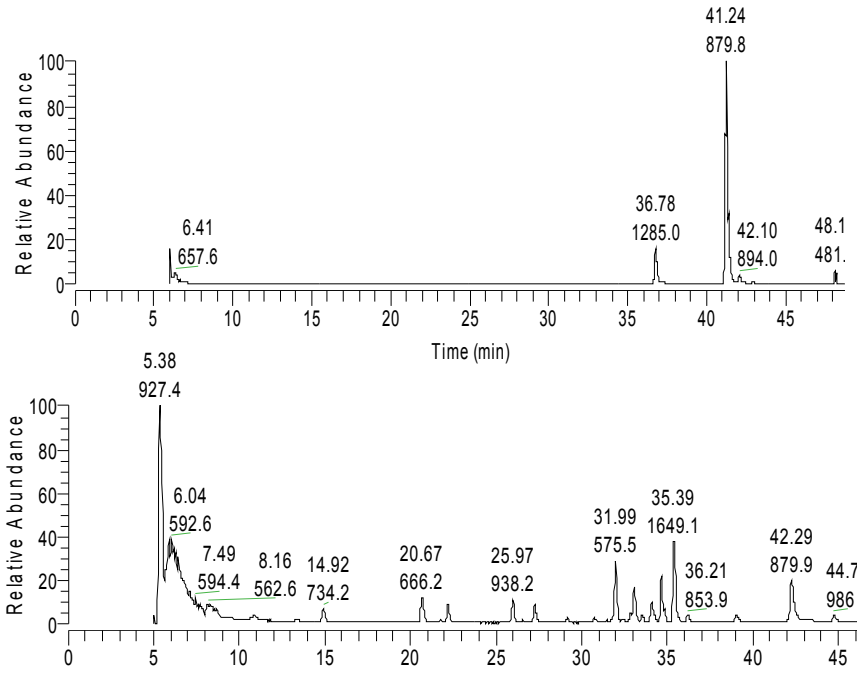

Figure 2.27 *Total ion chromatograms (TIC) of insulin control (A) and chymotrypsin treated insulin (B) Samples were at 1 mg/ml. The m/z score corresponding to each peak is labelled. LC-ESI-MS was performed using an electrospray mass spectrometer operated in positive ion mode. Ions were scanned over a range of 800-2000 m/z $[M+H]^+$).*

Chymotrypsin digestion of insulin led to the successful preparation of a crude mixture of insulin peptide fragments in reasonable quantity for fibril studies in chapter 3. The insulin control was also tested.

RT, min	m/z $(M+nH)^{n+}$	Sequence	
10-12	579	YTPKA	
13.17 - 13.70	610	F.VNQHL.C	
20.84 - 20.86	**941**		Fragment 1
20.88 - 21.59	666	Y.QLENY.C	
21.61 - 21.78	1166	F.VNQHLC*GSHL.V	
21.81 - 21.87	825	L.VC*GERGF.F	
22.00 - 22.52	757	-.FVNQHL.C	
22.55 - 22.99	726	F.FYTPKA	
25.66 - 25.81	1313	.FVNQHLC*GSHL.V	
25.84 - 26.32	938		Fragment 2
26.35 - 26.80	594	L.VEALY.L	
29.03 - 29.37	987	L.C*GSHLVEAL.Y	
30.26 - 30.39	1102	L.YLVC*GERGF.F	
30.42 - 30.53	1533	L.VC*GERGFFYTPKA	
30.66 - 30.81	1578	F.VNQHLC*GSHLVEAL.Y	
31.73 - 31.80	972	L.VC*GERGFF.Y	
31.82 - 31.92	1150	L.C*GSHLVEALY.L	
31.98 - 32.13	1150	L.C*GSHLVEALY.L	
32.72 - 32.94	1725	.FVNQHLC*GSHLVEAL.Y	
32.96 - 33.37	1741		Fragment 3
33.43 - 33.72	1486	-.GIVEQC*C*ASVC*SL.Y	
33.95 - 34.20	1086	Y.LVC*GERGFF.Y	
34.79	1263	L.C*GSHLVEALYL.V	
35.21 - 35.60	1649		Fragment 4
36.95 - 37.16	1249	L.YLVC*GERGFF.Y	
38.00 - 38.11	1263	L.C*GSHLVEALYL.V	
42.2	**880**	**FVNQHL*CGSHLVEALYLV*CGERGFFYTPKA**	**B chain**
46.5-46.7	986	C*GSHLVEAL	

Table 2.6 *Peptide matches from insulin chymotrypsin digest. *Indicates the carboxymethyl group attached to the cysteines. •Denotes point of enzyme cleavage The four peptide components that were expected (Figure 2.28) are labelled.*

2.7 Summary

Chemical modifications of insulin discussed in this chapter yielded heterogeneous mixtures of products in most cases, simulating the sorts of mixtures that might be relevant in an industrial process using crude protein extracts. The products obtained in sufficient quantities for use in chapter 2 and 3 are listed below (Figure 2.28):

a)* Crude citraconylated acetylated insulin

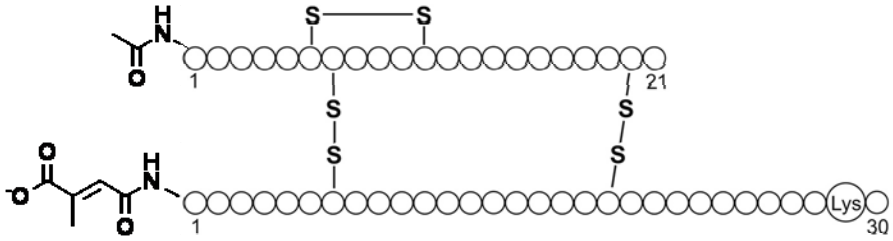

b) Crude acetylated insulin

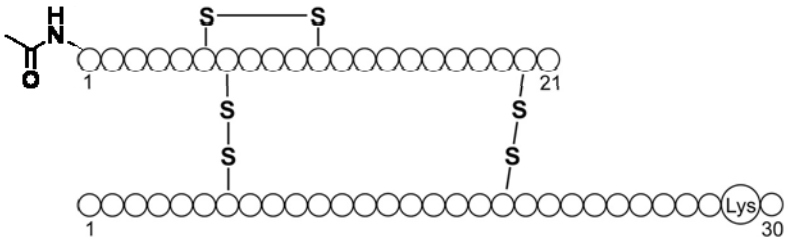

c) Crude reduced carboxymethylated insulin

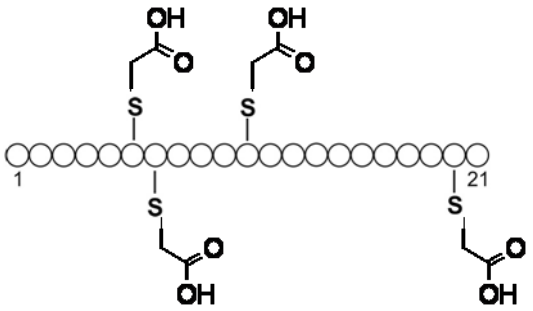

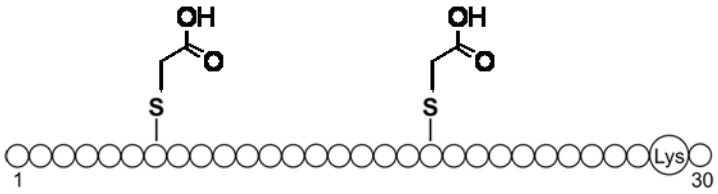

d) Crude reduced pyridylethylated insulin (pellet and supernatant)

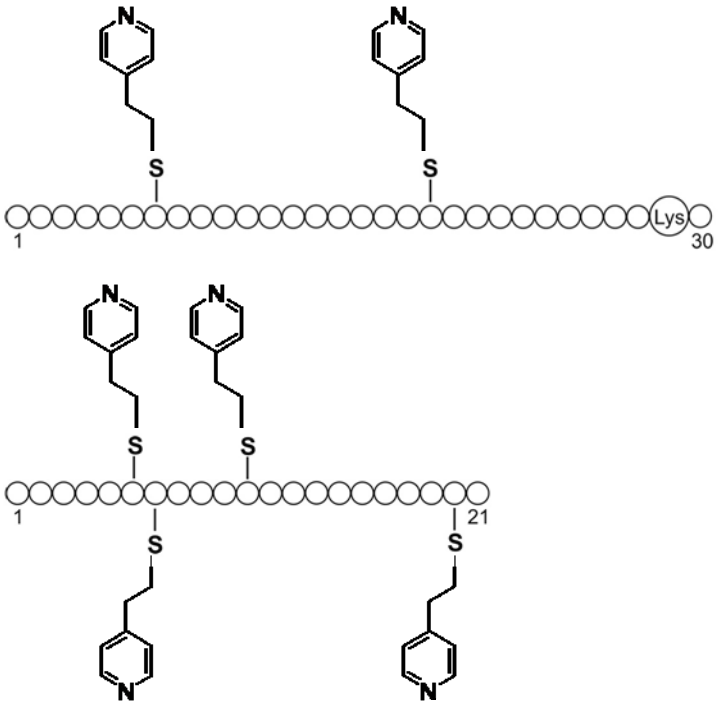

e) Crude tryptic digest of insulin

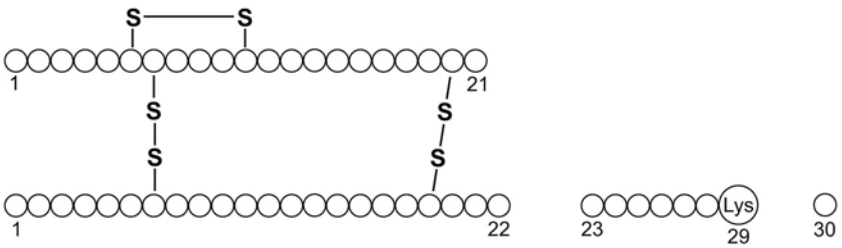

f) Crude chymotryptic digest of insulin

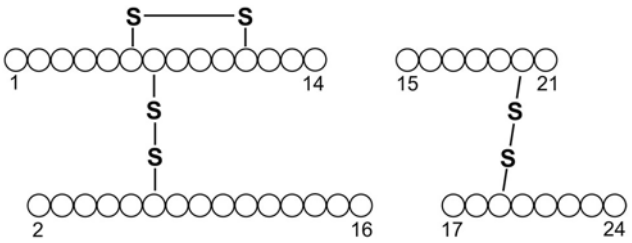

Figure 2.28 *Structures showing modified insulin products obtained: (a) citraconylated acetylated insulin with 1 sites of citraconyl group attachment, (b) glycine acetylated insulin, (c) reduced carboxymethylated insulin, (d) reduced pyridylethylated insulin, (e) tryptic digest of insulin, (f) chymotryptic digest of insulin. * Note: The site of citraconyl group attachment was not confirmed, and has been presumed in the structure shown.*

The crude citraconylated acetylated insulin, was largely composed of three forms of insulin, in decreasing levels, monoacetyl monocitraconyl insulin > monocitraconyl insulin > diacetyl monocitraconyl insulin. The crude acetylated insulin mixture also was composed of three forms of insulin, in decreasing levels, monoacetyl insulin > unmodified insulin > diacetyl insulin. Both of these mixtures of acetylated insulin were obtained in sufficient quantities and then subjected to aggregation trials.

In addition, reduction alkylation of bovine insulin led to the preparation of crude reduced carboxymethylated insulin and crude reduced pyridylethylated insulin (precipitate and supernatant), including the respective insulin control samples. These samples were also tested for aggregation propensity in chapter 3.

Two forms of crude enzymatic digests of insulin were obtained, with trypsin digestion and chymotrypsin digestion of insulin.

All of the crude modified insulin samples summarised in this section were tested for aggregation propensity in chapter 3 to determine the ability of amyloid fibril to form in heterogeneous mixtures of modified insulin.

2.8 References

Ahmad, A., I. S. Millett, S. Doniach, V. N. Uversky, and A. L. Fink. 2003. Partially folded intermediates in insulin fibrillation. *Biochemistry* 42: 11404-11416.

—. 2004. Stimulation of insulin fibrillation by urea-induced intermediates. *Journal of Biological Chemistry* 279: 14999-15013.

Ahmad, A., V. N. Uversky, D. Hong, and A. L. Fink. 2005. Early events in the fibrillation of monomeric insulin. *Journal of Biological Chemistry* 280: 42669-42675.

Ahmed, A., I. S. Millett, S. Doniach, V. N. Uversky, and A. L. Fink. 2003. Partially folded intermediates in insulin fibrillation. *Biochemistry* 42: 11404-11416.

Arora, A., C. Ha, and C. Park, Beum. 2004. Inhibition of insulin amyloid formation by small stress molecules. *Federation of European Biochemical Societies Letters* 564: 121-125.

Atassi, M. Z., and F. S. A. Habeeb. 1972. Reaction of proteins with citraconic anhydride. *Methods in Enzymology* XXV: 547-553.

Baker, E. N., T. L. Blundell, J. F. Cutfield, S. M. Cutfield, E. J. Dodson, G. G. Dodson, D. M. Crowfoot Hodgkin, R. E. Hubbard, N. W. Isaacs, C. D. Reynolds, K. Sakabe, N. Sakabe, and N. M. Vijayan. 1988. The structure of 2Zn pig insulin crystals at 1.5 angstrom resolution. *Philosophical Transactions of the Royal Society of London. Series B, Biological Sciences* 319: 369-456.

Baudys, M., T. Uchio, D. Mix, D. Wilson, and S. W. Kim. 1995. Physical stabilization of insulin by glycosylation. *Journal of Pharmaceutical Sciences* 84: 28-33.

Blundell, T. L., G. G. Dodson, D. C. Hodgkin, and D. A. Mercola. 1972. Insulin: the structure in the crystal and its reflection in chemistry and biology. *Advances in Protein Chemistry* 26: 379-402.

Bouchard, M., J. Zurdo, E. J. Nettleton, C. M. Dobson, and C. V. Robinson. 2000. Formation of insulin amyloid fibrils followed by FTIR simultaneously with CD and electron microscopy. *Protein Science* 9: 1960-1967.

Bouma, B., L. M. J. Kroon-Batenburg, Y.-P. Wu, B. Brunjes, G. Posthuma, O. Kranenburg, P. G. de Groot, E. E. Voest, and M. F. B. G. Gebbink. 2003. Glycation induces formation of amyloid cross-β structure in albumin. *Journal of Biological Chemistry* 278: 41810-41819.

Brandenburg, D., H.-G. Gattner, M. Weinert, L. Herbertz, H. Zahn, and A. Wollmer. 1971. Structure and function studies with derivatives and analogs of insulin and its chains. Pages 363-376. *Diabetes 1970-Proceedings of the Seventh Congress of the International Diabetes Federation*. Excerpta Medica, Amsterdam, International Congress Series No.231.

Brange, J., L. Andersen, E. D. Laursen, G. Meyn, and E. Rasmussen. 1997a. Toward understanding insulin fibrillation. *Journal of Pharmaceutical Sciences* 86: 517-525.

Brange, J., G. G. Dodson, D. J. Edwards, P. H. Holden, and J. L. Whittingham. 1997b. A model of insulin fibrils derived from the X-ray crystal structure of a monomeric insulin (despentapeptide insulin). *Proteins-Structure Function and Genetics* 27: 507-516.

Brange, J., J. F. Hansen, S. Havelund, and S. G. Melberg. 1987. Studies of the insulin fibrillation process in B. P, ed. *Advanced models for the therapy of insulin-dependent diabetes*. Raven Press, New York, pg 85-90.

Brange, J., J. Whittingham, D. Edwards, Z. You-Shang, A. Wollmer, D. Brandenburg, G. Dodson, and J. Finch. 1997c. Insulin structure and diabetes treatment. *Current Science* 72: 470-476.

Breydo, L., Y. Sun, N. Makarava, C.-I. Lee, V. Novitskaia, O. Bocharova, J. P. Y. Kao, and I. V. Baskakov. 2007. Nonpolar substitution at the C-terminus of the prion protein, a mimic of the glycosylphosphatidylinositol anchor, partially impairs amyloid fibril formation. *Biochemistry* 46: 852-861.

Brinegar, A. C., and J. E. Kinsella. 1981. Reversible modification of lysine in β-lactoglobulin using citraconic anhydride. *International Journal of Peptide and Protein Research* 18: 18-25.

Bromer, W. W., and R. E. Chance. 1967. Preparation and characterisation of desoctapeptide-insulin. *Biochimica et Biophysica Acta* 133: 219-223.

Burke, M. J., and M. A. Rougvie. 1972. Cross-β protein structures. I. Insulin fibrils. *Biochemistry* 11: 2435-2439.

Carpenter, F. H. 1966. Relationship of structure to biological activity of insulin as revealed by degradative studies. *American Journal of Medicine* 40: 750-758.

Carpenter, F. H., and W. E. Baum. 1962. Rates of production of alanine and heptapeptide and of loss of biological activity during digestion of insulin with trypsin. *Journal of Biological Chemistry* 237: 409-412.

Chen, P.-Y., C.-C. Lin, Y.-T. Chang, S.-C. Lin, and S. I. Chan. 2002. One O-linked sugar can affect the coil-to-β structural transition of the prion peptide. *Proceedings of the National Academy of Sciences of the United States of America* 99: 12633-12638.

Chiti, F., M. Calamai, N. Taddei, M. Stefani, G. Ramponi, and C. M. Dobson. 2002. Studies of the aggregation of mutant proteins *in vitro* provide insights into the genetics of amyloid diseases. *Proceedings of the National Academy of Sciences of the United States of America* 99: 16419-16426.

Colon, W., Z. Lai, S. L. McCutchen, G. J. Miroy, C. Strang, and J. W. Kelly. 2007. FAP mutations destabilize transthyretin facilitating conformational changes required for amyloid formation. *Ciba Foundation Symposium 199 - The Nature and Origin of Amyloid Fibrils*: 228-242.

Dear, D. V., D. S. Young, J. Kazlauskaite, F. Meersman, D. Oxley, J. Webster, T. J. T. Pinheiro, A. C. Gill, I. Bronstein, and C. R. Lowe. 2007. Effects of post-translational modifications on prion protein aggregation and the propagation of scrapie-like characteristics *in vitro*. *Biochimica et Biophysica Acta (BBA) - Proteins & Proteomics* 1774: 792-802.

DeLano, W. L. 2002. The PyMOL molecular graphics system (2002) on world wide web http://www.pymol.org.

Derewenda, U., Z. S. Derewanda, G. G. Dodson, and R. E. Hubbard. 1990. Insulin Structure. *Insulin*. Springer-Verlag, Berlin, pg 23-39.

Devlin, G. L., T. P. J. Knowles, A. Squires, M. G. McCammon, S. L. Gras, M. R. Nilsson, C. V. Robinson, C. M. Dobson, and C. E. MacPhee. 2006. The component polypeptide chains of bovine insulin nucleate or inhibit aggregation of the parent protein in a conformation-dependent manner. *Journal of Molecular Biology* 360: 497-509.

Dische, F. E., C. Wernstedt, G. T. Westermark, P. Westermark, M. B. Pepys, J. A. Rennie, S. G. Gilbey, and P. J. Watkins. 1988. Insulin as an amyloid-fibril protein at sites of repeated insulin injections in a diabetic patient. *Diabetologia* 31: 158-161.

Dixon, H. B. F., and R. N. Perham. 1968. Reversible blocking of amino groups with citraconic anhydrides. *Biochemical Journal* 109: 312-314.

Dobson, C. M. 2003. Protein folding and misfolding. *Nature* 426: 884-890.

Ecroyd, H., S. Meehan, J. Horwitz, J. A. Aquilina, J. L. P. Benesch, C. V. Robinson, C. E. Macphee, and J. A. Carver. 2007. Mimicking phosphorylation of beta crystallin affects its chaperone activity. *Biochemical Journal* 401: 129-141.

Ende, M., and G. Spiteller. 1982. Contaminants in mass spectrometry. *Mass Spectrometry Review* 1: 29-62.

Fandrich, M. 2007. Absolute correlation between lag time and growth rate in the spontaneous formation of several amyloid-like aggregates and fibrils. *Journal of Molecular Biology* 365: 1266-1270.

Fink, A. L. 1998. Protein aggregation: folding aggregates, inclusion bodies and amyloid. *Folding & Design* 3: R9-R23.

Friedman, M. 2001. Application of the S-pyridylethylation reactions to the elucidation of the structures and functions of proteins. *Journal of Protein Chemistry* 20: 431-453.

Fukada, H., and K. Takahashi. 1980. Calorimetric study of the reduction of the disulfide bonds in insulin. *Journal of Biochemistry (Tokyo)* 87: 1111-1117.

Habeeb, A. F. S. A., and M. Z. Atassi. 1970. Enzymic and immunochemical properties of lysozyme. Evaluation of several amino group reversible blocking reagents. *Biochemistry* 9: 4939-4944.

Hale, J. E., J. P. Butler, V. Gelfanova, Y. J.-S. and, and M. D. Knierman. 2004. A simplified procedure for the reduction and alkylation of cysteine residues in proteins prior to proteolytic digestion and mass spectral analysis. *Analytical Biochemistry* 333: 174-181.

Havelund, S., J. B. Halstroem, I. Jonassen, A. S. Andersen, and J. Markussen. 1995. Acylated derivatives of human insulin with improved solubility and stability for treatment of diabetes. Pages 99. *PCT Int. Appl.* (Novo Nordisk A/S, Den.). Wo.

He, J., Y. Song, N. Ueyama, A. Saito, H. Azakami, and A. Kato. 2006. Prevention of amyloid fibril formation of amyloidogenic chicken cystatin by site-specific glycosylation in yeast. *Protein Science* 15: 213-222.

Hermanson, G. T. 1996. *Bioconjugate Techniques*. Academic Press, San Diego, USA, pg 76-80, 126-129.

Hinds, K. D., and S. W. Kim. 2002. Effects of PEG conjugation on insulin properties. *Advanced Drug Delivery Reviews* 54: 505-530.

Hong, D.-P., A. Ahmad, and A. L. Fink. 2006. Fibrillation of human insulin a and b chains. *Biochemistry* 45: 9342-9353.

Hong, D.-P., and A. L. Fink. 2005. Independent heterologous fibrillation of insulin and its β-chain peptide. *Biochemistry* 44: 16701-16709.

Hua, Q.-x., and M. A. Weiss. 2004. Mechanism of insulin fibrillation: The structure of insulin under amyloidogenic conditions resembles a protein-folding intermediate. *Journal of Biological Chemistry* 279: 21449-21460.

Iavarone, A. T., O. A. Udekwu, and E. Williams. 2004. Buffer loading for counteracting metal salt-induced signal suppression in electrospray ionization. *Analytical Chemistry* 76: 3944-3950.

Jansen, R., W. Dzwolak, and R. Winter. 2005. Amyloidogenic self-assembly of insulin aggregates probed by high resolution atomic force microscopy. *Biophysical Journal* 88: 1344-1353.

Jansen, R., S. Grudzielanek, W. Dzwolak, and R. Winter. 2004. High pressure promotes circularly shaped insulin amyloid. *Journal of Molecular Biology* 338: 203-206.

Jiménez, J. L., E. J. Nettleton, M. Bouchard, C. V. Robinson, C. M. Dobson, and H. R. Saibil. 2002. The protofilament structure of insulin amyloid fibrils. *Proceedings of the National Academy of Sciences of the United States of America.* 99: 9196-9201.

Khurana, R., C. Ionescu-Zanetti, M. Pope, J. Li, L. Nielson, M. Ramirez-Alvarado, L. Regan, A. L. Fink, and S. A. Carter. 2003. A general model for amyloid fibril assembly based on morphological studies using atomic force microscopy. *Biophysical Journal* 85: 1135-1144.

Koltun, W. L., D. F. Waugh, and R. S. Bear. 1954. An X-ray diffraction investigation of selected type of insulin fibrils. *American Chemical Society* 76: 413-417.

Kumar, R. 1999. A mass spectral guide for quick identification of phthalate esters. *American Laboratory*: 32-35.

Lindsay, D. G., and S. Shall. 1969. Acetoacetylation of insulin. *Biochemical Journal* 115: 587-595.

—. 1971. The acetylation of insulin. *Biochemical Journal* 121: 737-745.

Lopez de la Paz, M., K. Goldie, J. Zurdo, E. Lacroix, C. M. Dobson, A. Hoenger, and L. Serrano. 2002. De novo designed peptide-based amyloid fibrils. *Proceedings of the National Academy of Sciences of the United States of America* 99: 16052-16057.

Lopez de la Paz, M., and L. Serrano. 2004. Sequence determinants of amyloid fibril formation. *Proceedings of the National Academy of Sciences of the United States of America* 101: 87-92.

MacCoss, M. J., C. C. Wu, and J. R. I. Yates. 2002. Probability-based validation of protein identifications using a modified SEQUEST algorithm. *Analytical Chemistry* 74: 5593-5599.

Markus, G. 1964. Electrolytic reduction of the disulfide bonds of insulin. *Journal of Biological Chemistry* 239: 4163-4170.

Massaglia, A., F. Pennisi, U. Rosa, S. Ronca-Testoni, and C. A. Rossi. 1968. The effect of chemical modifications induced in insulin on the reactivity of the interchain disulphide bonds towards to sodium sulphite. *Biochemical Journal* 108: 247-255.

Mauro, M., E. F. Craparo, A. Podesta, D. Bulone, R. Carrotta, V. Martorana, G. Tiana, and P. L. San Biagio. 2007. Kinetics of different processes in human insulin amyloid formation. *Journal of Molecular Biology* 366: 258-274.

Moore, R. E., M. K. Young, and T. D. Lee. 2002. Qscore: an algorithm for evaluating SEQUEST database search results. *Journal of the American Society for Mass Spectrometry* 13: 378-86.

Naiki, H., N. Hashimoto, S. Suzuki, H. Kimura, K. Nakakuki, and F. Gejyo. 1997. Establishment of a kinetic model of dialysis-related amyloid fibril extension *in vitro*. *Amyloid* 4: 223-232.

Necula, M., and J. Kuret. 2004. Pseudophosphorylation and glycation of tau protein enhance but do not trigger fibrillisation in vitro. *Journal of Biological Chemistry* 279: 49694-49703.

Nielsen, L., S. Frokjaer, J. Brange, V. N. Uversky, and A. L. Fink. 2001a. Probing the mechanism of insulin fibril formation with insulin mutants. *Biochemistry* 40: 8397-8409.

Nielsen, L., S. Frokjaer, J. F. Carpenter, and J. Brange. 2001b. Studies of the structure of insulin fibrils by Fourier transform infrared (FTIR) spectroscopy and electron microscopy. *Journal of Pharmaceutical Sciences* 90: 29-37.

Nielsen, L., R. Khurana, A. Coats, S. Frokjaer, J. Brange, S. Vyas, V. N. Uversky, and A. L. Fink. 2001c. Effect of environmental factors on the kinetics of insulin fibril formation: Elucidation of the molecular mechanism. *Biochemistry* 40: 6036-6046.

Novatia, L. 2008. What constitutes a good "hit" from a SEQUEST search [online]. *Available:http://www.enovatia.com/stories/storyReader$64* [accessed 12th May, 2008].

Obrenovich, M. E., and V. M. Monnier. 2004. Glycation stimulates amyloid formation. *Science of Aging Knowledge Environment* 2004: pe3.

Olsen, J. V., S.-E. Ong, and M. Mann. 2004. Trypsin cleaves exclusively C-terminal to arginine and lysine residues. *Molecular Cell Proteomics* 3: 608-614.

Pawar, A. P., K. F. DuBay, J. Zurdo, F. Chiti, M. Vendruscolo, and C. M. Dobson. 2005. Prediction of "aggregation-prone" and "aggregation-susceptible" regions in proteins associated with neurodegenerative diseases. *Journal of Molecular Biology* 350: 379-392.

Riordan, J. F., and B. L. Vallee. 1972a. Acetylation. *Methods in Enzymology* XXV: 494-499.

—. 1972b. O-Acetyltyrosine. *Methods in Enzymology* XXV: 500-505.

Rochet, J.-C., and P. T. Lansbury Jr. 2000. Amyloid fibrillogenesis: themes and variations. *Current Opinion in Structural Biology* 10: 60-68.

Shechter, Y., A. Patchornik, and Y. Burstein. 1973. Selective reduction of cystine I-VI11 in α-lactalbumin of bovine milk. *Biochemistry* 12: 3407-3413.

Sigma-Aldrich. 2007. Trypsin, Proteomics Grade, Sigma: Product Code T 6567, 2007. *Technical Bulletin*.

Simpson, R. J. 2003. *Proteins and Proteomics: A Laboratory Manual*. Cold Spring Harbor Laboratory Press, Cold Spring Habor, New York.

Sluzky, V., J. A. Tamada, A. M. Klibanov, and R. Langer. 1991. Kinetics of insulin aggregation in aqueous solutions upon agitation in the presence of hydrophobic surfaces. *Proceedings of the National Academy of Sciences of the United States of America* 88: 9377-9381.

Storkel, S., H. M. Schneider, H. Muntefering, and S. Kashiwagi. 1983. Iatrogenic, insulin-dependent, local amyloidosis. *Laboratory Investigation* 48: 108-111.

Suckau, D., M. Mak, and M. Przybylski. 1992. Protein surface topology-probing by selective chemical modification and mass spectrometric peptide mapping. *Proceedings of the National Academy of Sciences of the United States of America* 89: 5630-5634.

Thornton, J. M. 1981. Disulphide bridges in globular proteins. *Journal of Molecular Biology* 151: 261-287.

Uversky, V. N., and A. L. Fink. 2004. Conformational constraints for amyloid fibrillation: the importance of being unfolded. *Biochimica et Biophysica Acta* 1698: 131-153.

Uversky, V. N., L. Nielsen Garriques, I. S. Millett, S. Frokjaer, J. Brange, S. Doniach, and A. L. Fink. 2003. Prediction of the association state of insulin using special parameters. *Journal of Pharmaceutical Sciences* 94: 847-858.

Uversky, V. N., G. Yamin, L. A. Munishkina, M. A. Karymov, I. S. Millett, S. Doniach, Y. L. Lyubchenko, and A. L. Fink. 2005. Effects of nitration on the structure and aggregation of [alpha]-synuclein. *Molecular Brain Research Molecular Mechanisms in Parkinson's Disease* 134: 84-102.

Vestergaard, B., M. Groenning, M. Roessle, J. S. Kastrup, M. v. de Weert, J. M. Flink, S. Frokjaer, M. Gajhede, and D. I. Svergun. 2007. A helical structural nucleus is the primary elongating unit of insulin amyloid fibrils. *Public Library of Science Biology* 5: 1089-1097.

Waugh, D. F. 1946. A fibrous modification of insulin. I. The heat precipitate of insulin. *Journal of the American Chemical Society* 68: 247-250.

—. 1948. Regeneration of insulin from insulin fibrils by the action of alkali. *Journal of the American Chemical Society* 70: 1850-1857.

Waugh, D. F., D. F. Wilhelmson, S. L. Commerford, and M. L. Sackler. 1953. The nucleation and growth reactions of selected types of insulin fibrils. *Journal of the American Chemical Society* 75: 2592-600.

Wedd, N. S. 2007. Tandem Peptide Spectrum Interpretation [online]. Available:http://www.weddslist.com/ms/tandem.html [accessed 22 November, 2007].

Williams, S. 2004. Ghost peaks in reversed-phase gradient HPLC: a review and update. *Journal of Chromatography A* 1052: 1-11.

Winters, M. S. 2002. Probing protein-protein interactions *in vitro* and *in vivo* with cyanogens. *Department of Chemistry of the College of Science and Arts*. University of Cincinnati, pg 119.

Yen, T.-Y., H. Yan, and B. A. Macher. 2002. Characterizing closely spaced, complex disulfide bond patterns in peptides and proteins by liquid chromatography/electrospray ionization tandem mass spectrometry. *Journal of Mass Spectrometry* 37: 15-30.

Young, J. D., and F. H. Carpenter. 1961. Isolation and characterisation of products formed by the action of trypsin on insulin. *Journal of Biological Chemistry* 236: 743-748.

Yu, N.-T., B. H. Jo, R. C. Chang, and J. D. Huber. 1974. Single-crystal raman spectra of native insulin: Structures of insulin fibrils, glucagon fibrils, and intact calf lens. *Archives of Biochemistry and Biophysics* 160: 614-622.

Zahn, H., D. Brandenburg, and G. Hans-Gregor. 1972. Molecular basis of insulin action: Contributions of chemical modifications and synthetic approaches. *Diabetes* 21: 468-475.

The Impact of Modification on Insulin Aggregation and Fibril Formation

As described in chapter 1, there are a range of diagnostic measures for amyloid fibrils including their characteristic positive interaction with amyloid detecting dyes such as ThT and their morphology, as observed by microscopy techniques. In this chapter, ThT binding and TEM are used to assess whether the heterogeneous mixtures of modified insulin, characterised in chapter 2, form amyloid fibrils when subjected to partially denaturing environmental conditions known to fibrillise native insulin. These heterogeneous mixtures are typical of crude protein mixtures likely to be available as cheap starting materials for industrial fibril production.

3.1 Effect of Association States and Oligomerisation on Insulin Fibrillation

Several studies have shown that the formation of insulin fibrils is preceded by the assembly of partially folded insulin monomers into relatively small oligomers (Ahmad *et al.* 2005, Bouchard *et al.* 2000, Nettleton *et al.* 2000). The pathway for the formation of insulin fibrils can be described by a simple model hexamer→ modified monomer→ fibrils shown in Figure 3.1 (Ahmad *et al.* 2003, Nielsen *et al.* 2001a, Nielsen *et al.* 2001b).

The fully formed insulin fibrils are morphologically distinct and consist of between two and six protofilaments interwined into a braided fibrillar structure as described in chapter 1, section 1.4.1 (Jiménez *et al.* 2002). A model for the molecular packing of three protofilaments of the insulin molecule within the fibril is shown in Figure 3.2 C.

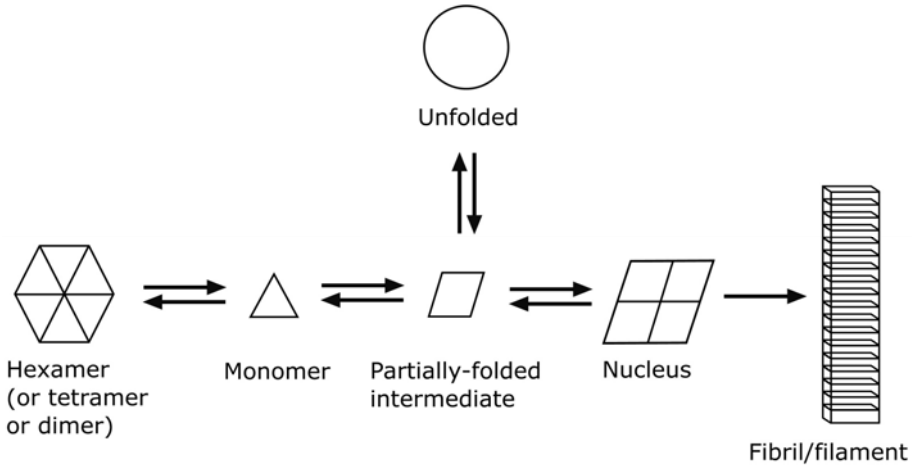

Figure 3.1 *Model for insulin fibrillation (different shapes represent different conformations. The nucleus is shown schematically and consists of a number of subunits), adapted from (Nielsen* et al. *2001b).*

In its native state, insulin is predominantly α-helical (chapter 2, Figure 2.4); the monomer self-assembles into dimers, tetramers, and hexamers, depending on the concentration and the solvent conditions (Hua and Weiss 2004, Nettleton *et al.* 2000). Insulin exists as a monomer in 20% acetic acid (pH 1.6, 100 mM NaCl), a dimer in 25 mM HCl (pH 1.6, 100 mM), a tetramer at pH 3 (20 mM formate buffer, 100 mM NaCl) and a hexamer at pH 7.4 (20 mM phosphate buffer, 100 mM NaCl) (Nielsen *et al.* 2001b). Thus, for fibril formation to occur, the hexameric or tetrameric associated states of insulin at neutral pH, or the dimers at low pH, must initially dissociate into monomeric molecules, which are in equilibrium with a partially folded conformation that undergoes oligomerisation to form the critical nucleus (Figure 3.1). This step is assumed to involve a number of non-native oligomeric precursors, accounting for the lag phase observed in the kinetics of fibrillation (Jahn and Radford 2008).

Although one cannot completely exclude the possibility that fibrils may grow by addition of individual insulin monomers, the model described in Figure 3.2 assumes that elongation of protofilaments is directed by insulin oligomer association. Figure 3.2 displays a model with a central cavity in which the cross-section contains eight helical oligomers. Fourteen repeats of the length of these eight helical oligomers would form a full turn of one protofilament across three fibril repeating units. Two protofilaments presumably intertwine to form the

protofibrils, yielding an average protofibril diameter of about 10 nm. Finally, three protofibrils intertwine to form the mature insulin fibril.

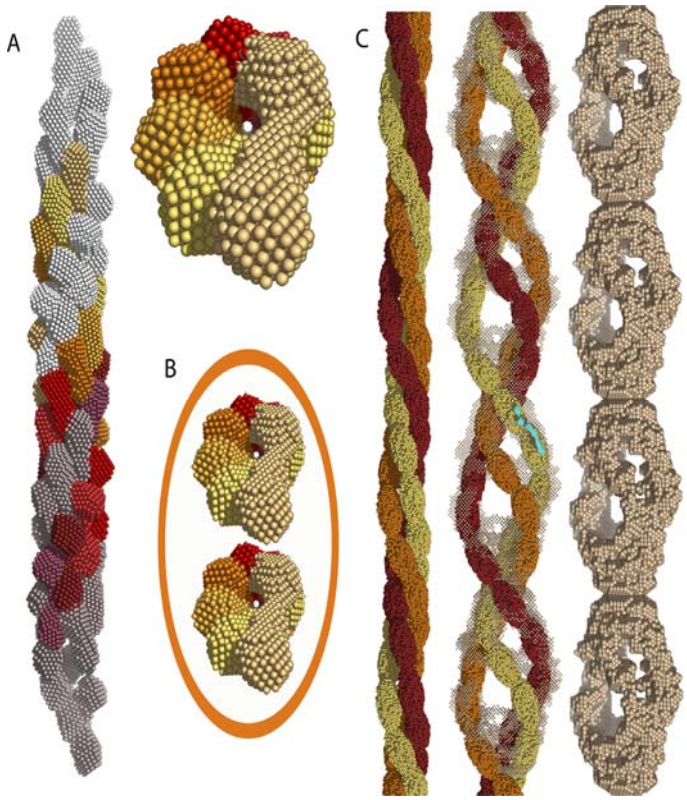

Figure 3.2 *Model for assembly of the distinct insulin oligomers into protofilaments, protofibrils, and fibrils, generated using small-angle x-ray scattering (SAXS):*
(A) Eight helical oligomers (shown in a colour scale from purple through red to light yellow) intertwine to form the protofilament. Eight additional precursors in grey nuances form the open ends of the model. Side and top views are shown.
(B) Two protofilaments presumably intertwine to form the protofibrils, with an average diameter of 10 nm (top view, intertwining not depicted). An orange ellipse marks the outer boundaries of one protofibril.
(C) Three protofibrils (shown in orange, yellow, and red) intertwine to form the mature insulin amyloid fibril ~ 30 nm. Shown are side and front views. An oligomer (blue) is superimposed onto the fibril mode , from (Vestergaard et al*. 2007).*

It can be assumed that the helical oligomer is both the structural nucleus and the elongating building block of insulin amyloid fibrils. The final morphology of the mature fibril is dependent on the conditions under which the fibril was formed and can change subtly between treatment conditions (chapter 1, section 1.5), and even within the same sample (Whittingham *et al*. 2002).

3.2 Standard Insulin Fibril Formation and ThT Assay

ThT, is a fluorescent dye that is frequently used as a specific probe to detect amyloid fibril formation *in vitro* (LeVine 1993, Naiki *et al.* 1989). Prior to its chemical modification, the standard insulin purchased for this study was subjected to conditions, low pHs and at high temperatures, known to cause fibrillation (Nielsen *et al.* 2001b, Waterhouse 2003). Fibrils were then characterised using the ThT assay on either a spectrofluorometer or a plate reader for *in situ* fibril ThT assays (Nielsen *et al.* 2001b). Incubations were carried out in conditions known to favour the monomeric form of insulin, pH 1.6, 20% acetic acid solution (Uversky *et al.* 2003).

3.2.1 Small scale fibril formation and ThT assay

The spectrofluorometric method involved two separate steps: firstly, to form fibrils over time of protein incubation at elevated temperatures and secondly, to characterise the rate of fibrillation using the ThT assay. The results obtained from this procedure for a standard insulin fibrillation are presented in Figure 3.3. The observed ThT fluorescence intensity had a classic sigmoid pattern (Figure 3.3) (Nielsen *et al.* 2001b). It also showed the typical fibril formation process, with a lag phase of ~1.5 hr. At the end of the lag phase, a sudden increase in fibril concentration was observed. Eventually, the process reached saturation when most soluble proteins were converted into fibrils. The maximum fluorescence intensity observed on the spectrofluorometer was 630 relative fluorescence units (Figure 3.3).

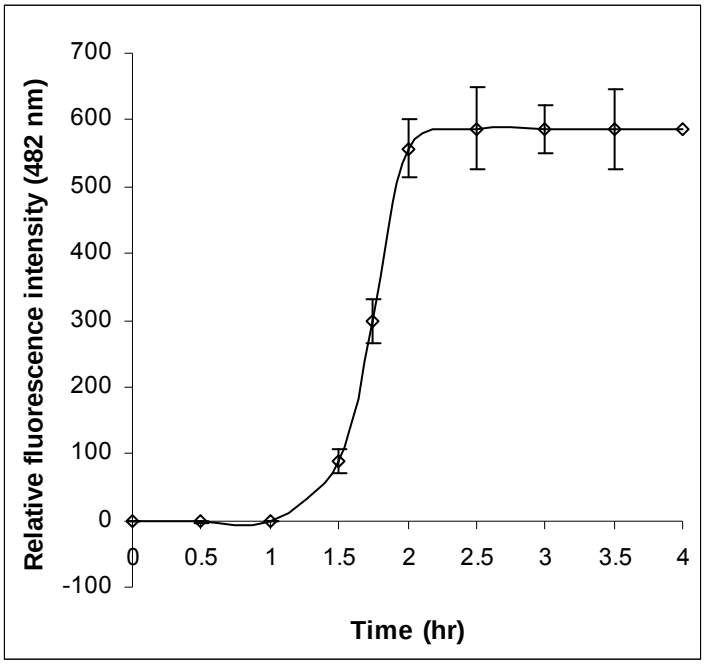

Figure 3.3 *The behaviour of insulin, over time of fibrillation at 5.7 mg/ml, in 20% acetic acid, 100 mM NaCl, (pH 1.6) at 60°C. For the ThT assay, samples were assayed in triplicate in Tris buffer (pH 7.5) with ThT, final concentration of insulin in the assay was 0.02 mg/ml. Error bars represent the standard deviation of the mean. The curve was fitted according to the method of Nielsen* et al*. (2001c), the data show a lag time of 1.5 hr.*

3.2.2 *In situ* fibril formation and ThT assay

In order to facilitate the rapid screening of many samples over time, a high throughput method was developed using 96 well plates. ThT was included in the acid and fibril formation monitored in real time. Since ThT may influence the amyloid forming process in the *in situ* method, it was important to compare this method to that described above, where the ThT assay was carried out after fibrils had formed.

In situ fibril ThT fluorescence measurements were carried out on the 96 well plate reader. This procedure was chosen as it allows a relatively large number of samples to be assayed using small reaction volumes of 200 µl. Insulin fibrils were formed within a few hours of incubation at 60ºC. Fibrillation was monitored by measuring fluorescence at 482 nm over time of incubation until maximum ThT signal was obtained (Figure 3.4).

In situ insulin fibrillation with ThT binding illustrated that the increase in ThT fluorescence intensity again followed the classic sigmoidal pattern (Figure 3.4), similar to Figure 3.3. From the kinetic analysis of the time course ThT assay, it was found that, at 5.7 mg/ml, insulin had a lag phase of 1.7 hr, which is in reasonable agreement with the first method.

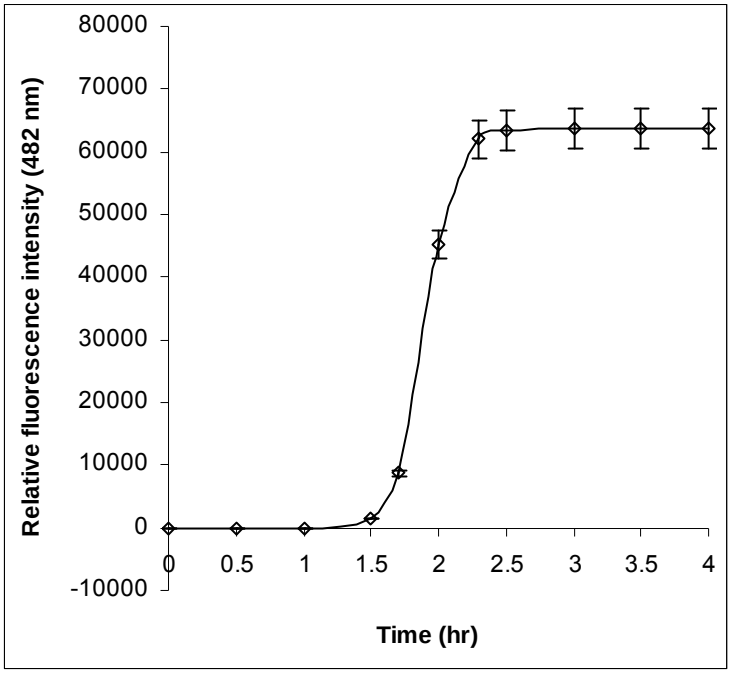

Figure 3.4 *Behaviour of insulin at 5.7 mg/ml, at 60ºC in 20% acetic acid (100 mM NaCl) only, fibril formed* in situ *in the plate reader. Samples were analysed in triplicate and the curve fitted according to the method of Nielsen* et al*. (2001c). Fluorescence was measured at a final concentration of 5.7 mg/ml insulin and 5-10 µM ThT. The maximum fluorescence intensity obtained on the plate reader was 63870, close to the maximum reading of the instrument (65000).*

3.2.3 Summary of the two methods for ThT fibrillation

The above results obtained for insulin fibrillation at 5.7 mg/ml, in 20% acetic (pH 1.6) and 60°C, shows that both methods gave similar lag times (Figure 3.3, Figure 3.4). The *in situ* method was thus used for rapid screening of the insulin samples and allowing more investigations with the limited quantities of modified samples available. Since the conditions were different between the two methods, direct comparison was not possible. This is because, between the two

different methods for ThT assay above, there is also a significant difference in the pH at which the ThT assay is carried out. In the small scale fibrillation method, the growth of fibrils was carried out at pH 1.6 but the assay was done at pH 7.5, the pH at which ThT binding to β-sheets is at its optimum (Nielsen *et al.* 2001b). In contrast, in the plate reader method, the ThT binding took place *in situ*, at pH 1.6.

Even though histological dyes like ThT and Congo red (CR) have been commonly used as indicators of the presence of amyloid fibrils, the relationship between fluorescence intensity and amount of amyloid fibril remain unclear (LeVine 1999). It has been demonstrated that the ThT fluorescence maximum is dependent on the pH, for example, murine senile amyloid protein, amyloid protein A (Naiki *et al.* 1989) and the β-amyloid protein (LeVine 1993) are reported to display different maximum fluorescence levels in solutions at different pH levels. ThT fluorescence when bound to insulin amyloid fibrils was found to be maximal at approximately pH 8, in a 50 mM Tris, 100 mM NaCl buffer, close to the pH 7.5 Tris-NaCl used in previous work in the literature (Nielsen *et al.* 2001b, Waterhouse 2003).

The impact of pH and amyloid concentration on fluorescence at 482 nm, was determined by investigating the linearity range of concentrations of insulin fibrils with ThT fluorescence at 482 nm.

3.2.4 The impact of pH and insulin fibril concentration on ThT fluorescence

Fibrils formed after 4 hr of incubation at 60ºC, pH 1.6 (Figure 3.4) were diluted separately in the two different buffers used for each method. Figure 3.5 illustrates that the fluorescence of the fibril solutions, at both pHs 1.6 and 7.5, increased with increasing insulin concentration until reaching a the maximum fluorescence reading. Overall, the fluorescence values were higher at pH 7.5 as compared to those obtained at pH 1.6. This was expected due to the higher binding capacity of insulin fibrils to ThT dye at a higher pH (Nielsen *et al.* 2001b,

Sabaté *et al.* 2008). However, another study specified that the ThT binding capacity is unaffected by pH (Groenning *et al.* 2007).

At pH 7.5, fluorescence intensity increased rapidly with increasing insulin concentration until 0.12 mg/ml, after which it remained at the maximum value of the instrument. A linear relationship was found between the insulin concentration ranging from 0.004 mg/ml up to 0.10 mg/ml and ThT fluorescence, having a correlation coefficient (R^2) of 0.99 (Figure 3.5). At pH 1.6, the linear range extended to 0.8 mg/ml, after which fluorescence remained at the maximum value.

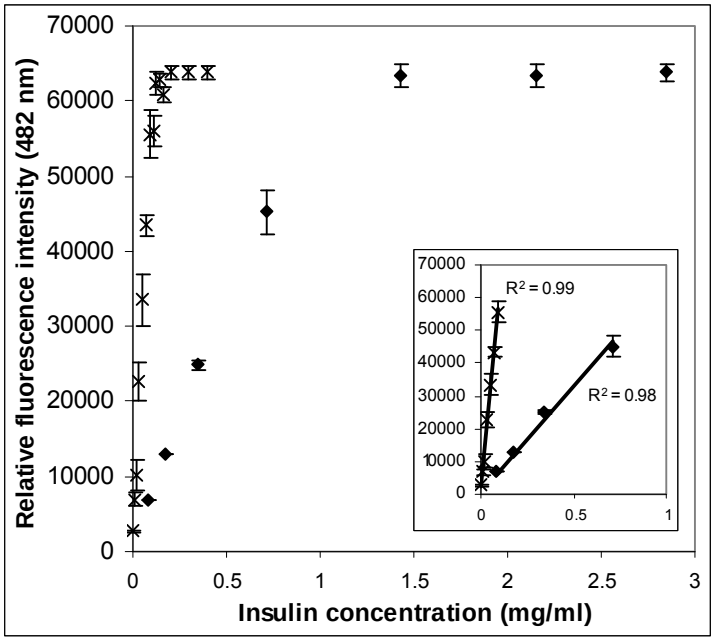

Figure 3.5 *Effect of insulin fibril concentration on ThT fluorescence at 482 nm, in 50 mM Tris, 100 mM NaCl pH 7.5 (crosses) and 20% acetic acid, 100 mM NaCl, pH 1.6 (shaded diamonds). Insulin fibrils were initially formed at 5.7 mg/ml pH 1.6, 20% acetic acid, 100 NaCl, at 60ºC for 4 hr in plate reader. The data have been corrected for background from fluorescence intensity measurements obtained in the absence of ThT. Insert: Comparison of insulin linear range for ThT assay conditions, at pH 1.6 (crosses) and pH 7.5 (shaded diamonds). Samples were analysed in triplicate. Error bars represent the standard error of the mean.*

3.2.5 The effect of pH on preformed insulin fibrils

In addition to altering the relative fluorescence of ThT when bound to the amyloid fibrils, the effect of pH on the fibrils themselves was investigated. Fibril formation was investigated in HCl, since early TEM work revealed that the fibrils formed in HCl were more distinctive than those formed in 20% acetic acid. In consideration of this, insulin fibrils formed in HCl were intended to be used in chapter 4 and 5 of this thesis. To our knowledge, there has not been any study that shows the immediate impact of altering the pH on insulin fibrils preformed at pH 1.6, in HCl.

Insulin fibrils were prepared at pH 1.6 in HCl (25 mM, 100 m NaCl) on a ~ 400 mg scale. It was found that adjustment of the fibril pH had a dramatic effect on the structure of the fibrils when examined by TEM. It is known that amyloid fibrils, when viewed on the TEM, generally share an elongated unbranched fibrillar appearance, but they often have a mixture of different morphologies, depending on various factors including pH (chapter 1.5, section 1.2).

The characterisation of insulin fibrils at a high concentration of 11.4 mg/ml (worked out for bionanomaterial study) via ThT assay showed that no fibrils were present in the insulin before fibrillation (Table 3.1) which was in agreement with the TEM examination (Figure 3.6 A). Table 3.1 illustrates that the increase in pH had no effect on insulin fibril fluorescence readings. However, the result showed a loss in fluorescence when the pH of the fibrils was reduced back to 2 from 6.5 via dialysis.

Sample	ThT (+/-)
Insulin control in 25 mM HCl (100 mM NaCl, pH 1.6), before fibrillation (A)	-
Fibrils prepared in 25 mM HCl (100 mM NaCl, pH 1.6), at 60ºC for 12 hr (B)	+
Insulin fibrils after dialysis at pH 2 (C)	+
Insulin fibrils after dialysis at pH 3.5 (D)	+
Insulin fibrils after dialysis at pH 4.5 (E)	+
Insulin fibrils after dialysis at pH 6.5 (F)	+
Insulin fibrils after dialysis in pH 6.5, re-dialysed in pH 2 (G)	-

Table 3.1 *Effect of dialysing insulin fibrils at different pHs on ThT fluorescence at 482 nm, in 50 mM Tris, 100 mM NaCl, pH 7.5. Samples were at 11.4 mg/ml. Samples were tested in triplicate.*

Insulin fibrils produced at 11.4 mg/ml (pH 1.6), were short, unbranched rod like structures (Figure 3.6 B). The increase in pH from 1.6 to 6.5, led to the loss of the distinct, unbranched, rod like fibrils. Figure 3.6 indicates that the fibrils may have a tendency to clump together, with increasing pH.

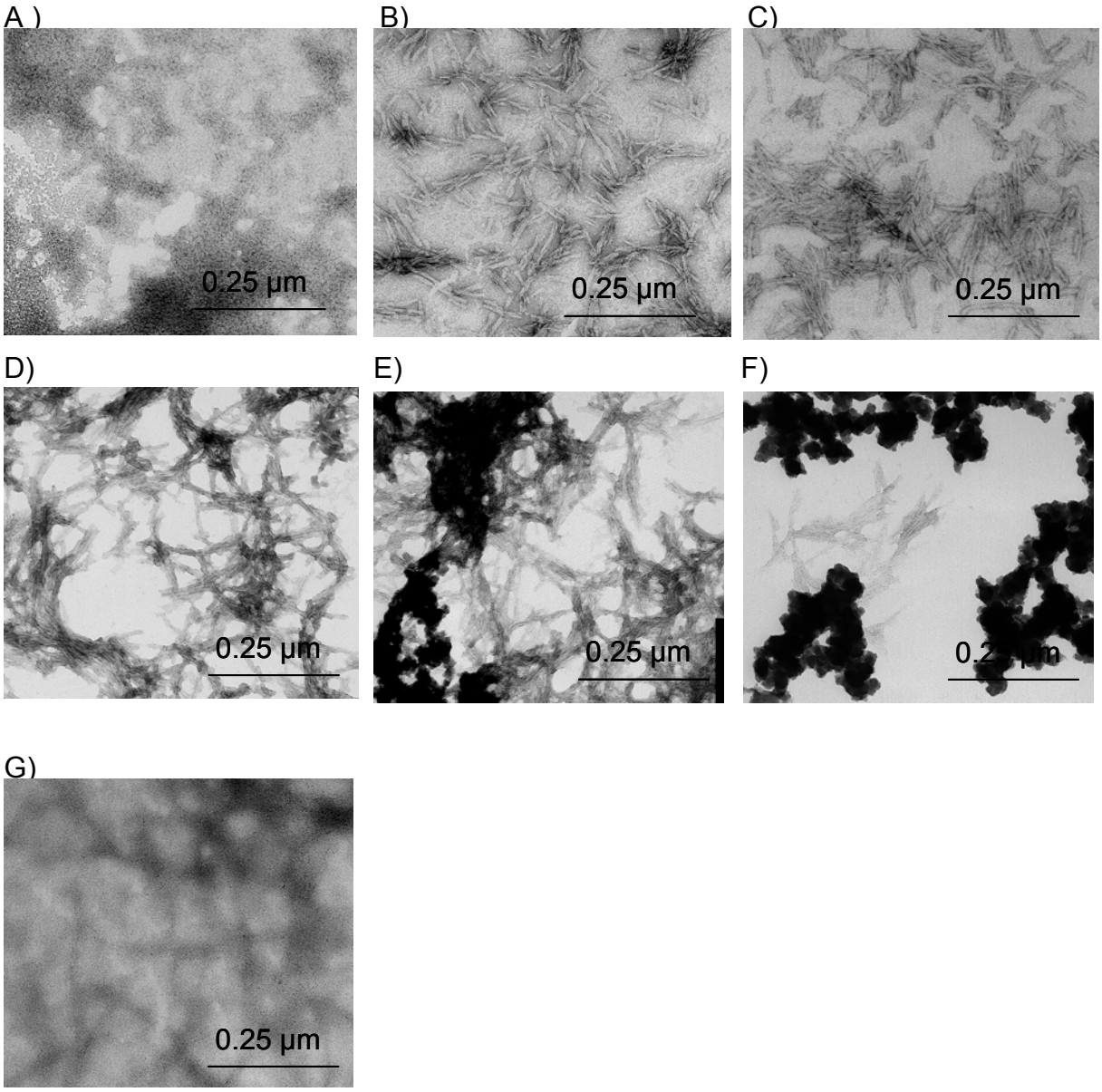

Figure 3.6 *Electron micrographs showing the impact of pH on insulin fibrils. Samples were at 11.4 mg/ml: (A) insulin control in 25 mM HCl (100 mM NaCl, pH 1.6) before fibrillation, (B) insulin fibrils in 25 mM HCl (100 mM NaCl, pH 1.6) at 60 ºC for 12 hr, (C) insulin fibrils after dialysis at pH 2, (D) pH 3.5, (E) pH 4.5, (F) pH 6.5 and (G) insulin fibrils after dialysis in pH 6.5, re-dialysed in pH 2. All samples had been frozen at -80°C for 24 hr before TEM examination. These images are a representation of triplicate samples. Images have been reproduced in larger forms in the Appendix.*

The loss of fibril morphology demonstrated in Figure 3.6 relates to the early findings on insulin fibrils, where treatment with alkali gave a crystalline product similar to native insulin (Waugh 1948). The results found in these experiments showed that insulin fibrils needed to be kept at pHs below 6, for the large scale preparation of fibril in bionanomaterials (chapters 4 and 5).

3.3 Investigation of the Propensity of the Crude Modified Insulin to form Fibrils

The following modified insulin samples, as characterised in chapter 2, were investigated:

- crude citraconylated insulin
- crude acetylated insulin
- crude reduced insulin
- crude reduced carboxymethylated insulin
- crude reduced pyridylethylated insulin precipitate
- crude reduced pyridylethylated insulin supernatant
- crude tryptic digest of insulin (partially and total digested)
- crude chymotryptic digest of insulin

All samples were initially tested for solubility under native insulin fibrillation conditions (Nielsen *et al.* 2001b). It was found that all of the modified crude insulin samples were soluble at pH 1.6, except RCM and RPE supernatant which were solubilised at pH 7.4, which provided some constraints on the conditions employed for fibrillation. Having examined the preliminary conditions for solubility of the modified insulin, they were tested for fibril formation and each chemical modification is discussed separately in the next sections.

3.4 The Effect of Acetylation on Insulin Aggregation

Figure 3.7 compares fibrillation patterns of the insulin standard, insulin control and crude acetylated insulin, monitored by ThT fluorescence. The insulin control was put through all the changes and incubations as the treated sample (chapter

2, section 2.3.2), but without the addition of the acetylating agent. The small scale incubation method was used to form fibrils due to the unavailability of a plate reader at this stage of this project. Analysis of the ThT curves showed that the fibrillation of insulin at 5.7 mg/ml, with and without acetylation, is characterised by lag times of 2.4 and 7.2 hr, repectively, compared to 1.5 hr in the insulin standard. The low yield of fibrils and the reduced rate of fibril formation in the modified insulin mixture are evident from Figure 3.7. Interestingly, the insulin control had a significantly longer lag time than the insulin standard under these conditions.

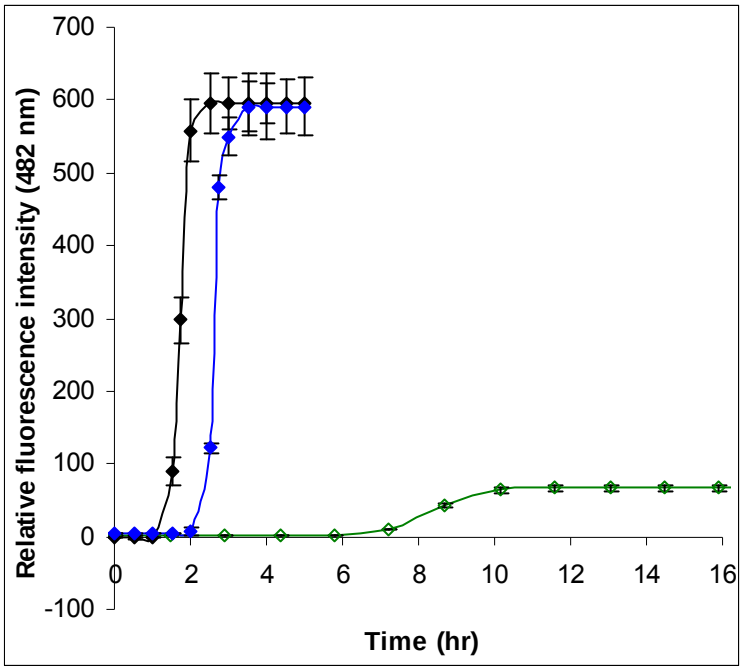

Sample	Lag time (hr)
Insulin standard	1.5 ± 0.2
Insulin control	2.4 ± 0.4
Crude acetylated insulin	7.2 ± 3

Figure 3.7 *Kinetics of fibril formation of insulin standard (black), insulin control (blue) and crude acetylated insulin (green). Fibrils were formed at 5.7 mg/ml, in 20% acetic acid, 100 mM NaCl, (pH 1.6) at 60°C. For the ThT assay, samples were assayed in triplicate Tris buffer (pH 7.5) with ThT, final concentration of protein in the assay was 0.02 mg/ml. The curves were fitted according to the method of Nielsen* et al. *(2001c). Error bars represent the standard deviation of the mean of three measurements*.

It has been shown earlier in this study that the crude acetylated insulin largely consists of unmodified insulin (24%) and monoacetyl insulin (37%) (chapter 2, section 2.3.4). The ThT data are consistent with fibril formation by the

unmodified insulin present in the insulin-mixture, with the acetylated insulin unreactive. The fluorescence intensity units are indicative of 13% of fibrils formed by the acetylated insulin mixture. This may be due to the 24% of insulin present in mixture leading to its much lower concentration in the assay solution (0.005 mg/ml), which led to a lower yield. However, if pure insulin still undergoes fibrillation in a heterogeneous sample, this has potential relevance to an industrial process, where the presence of impurities in proteins won't necessarily prevent the fibrillating species from forming fibrils.

3.4.1 Identity of the protein in the aggregate

The ThT assay for crude acetylated insulin was consistent with the possibility that the unmodified insulin present in the crude derivatised insulin mixture is forming fibrils (Figure 3.7) with the derivatised insulin remaining in solution. An additional experiment was performed to determine the content of the soluble crude acetylated insulin during the course of its aggregation. Crude acetylated insulin solution was subsampled every 30 min during its incubation at 60°C under fibril forming conditions. The subsamples of the fibrillating solutions were centrifuged and the supernatant analysed for the presence of protein *via* LC-ESI-MS (Figure 3.8).

The TIC showed that the intensity of the protein peaks from the fibril supernatant reduced during the course of fibrillation, as expected. The results obtained demonstrate the loss of crude acetylated insulin from the supernatant of its fibril forming solutions (Figure 3.8).

The peak areas of the insulin and monoacetyl insulin component of the crude acetylated insulin fibril forming solution were calculated from the TIC profiles. Arrows in Figure 3.8 (A) indicate the insulin peak and the monoacetyl insulin peak. The peak areas from both components were plotted against the time course of fibrillation to measure the level of the proteins over the course of the aggregation (Figure 3.9).

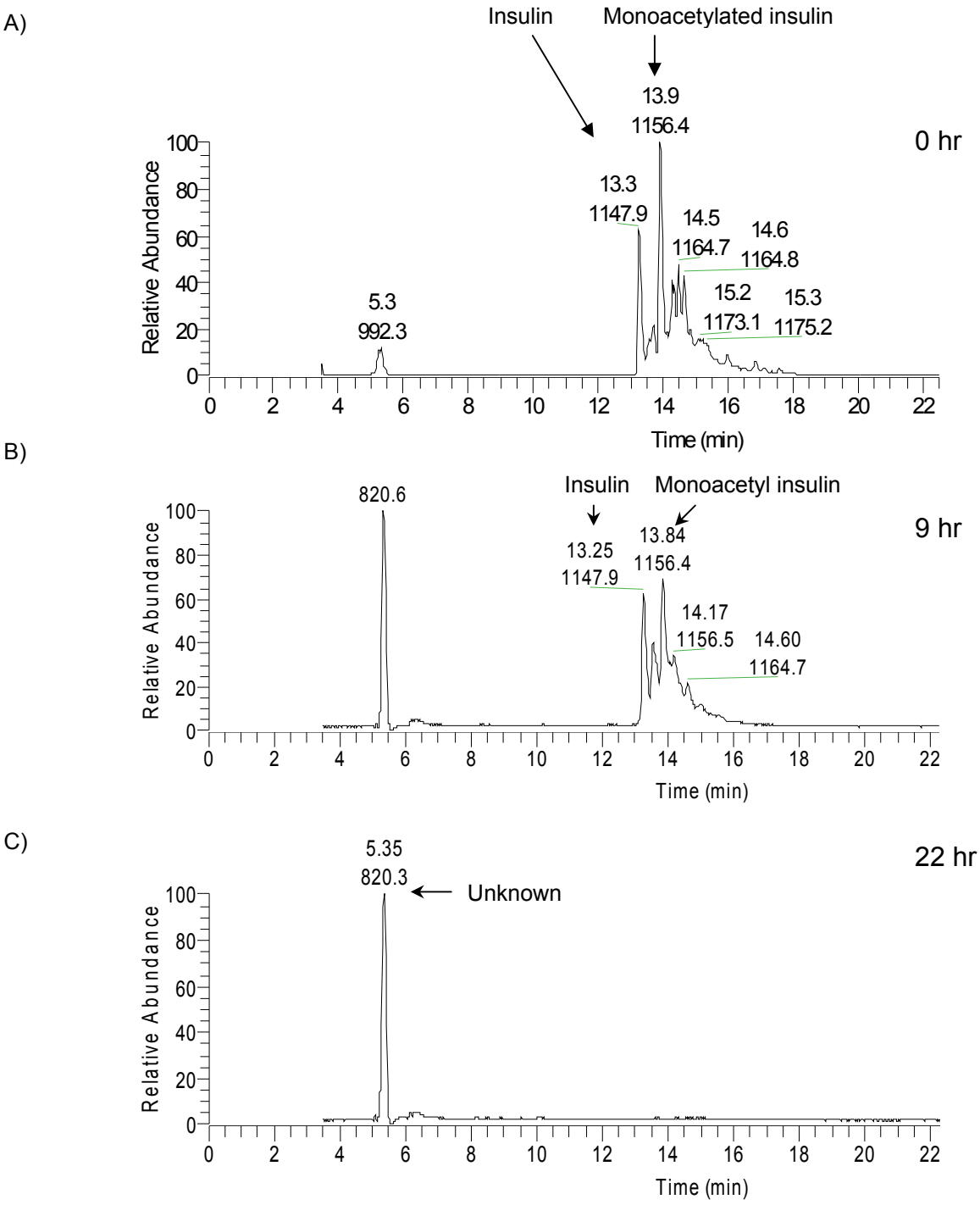

Figure 3.8 *Total ion chromatograms (TIC) of crude acetylated insulin solution at pH 1.6 obtained by LC-ESI-MS in positive ion mode.analysis of: (A) 0 hr incubation, (B) 9 hr of incubation, (C) 22 hr of incubation. LC-ESI-MS was performed using an electrospray mass spectrometer operated in positive ion mode. Ions were scanned over a range of 800-2000 m/z* $[M+H]^+$ *and data were collected in full scan with a secondary dependent scan event to select data for ultrazoom mapping.*

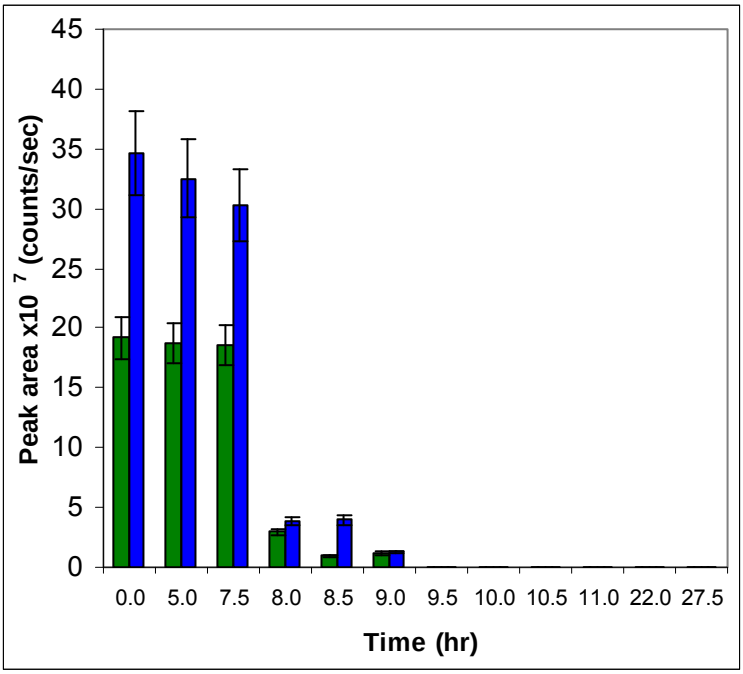

Figure 3.9 *LC-ESI-MS of crude acetylated insulin solution over the course of its aggregation. Analysis of samples taken out from the 60ºC incubator as a function of time: 0 hr to 27.5 hr. Bars represent (green) insulin peak (m/z 1147.9, RT 13.0 min) and (blue) monoacetyl insulin peak (m/z 1156.3 RT 13.8 min).*

There was no preferential loss of unmodified insulin as compared to derivatised insulin. These results suggest that either unmodified insulin was forming fibrils whereas the acetylated insulin was forming amorphous aggregate, or that both species were forming fibrils and amorphous aggregate. Further work would be required to distinguish between these possibilities.

3.4.2 *In situ* ThT assay of crude citraconylated acetylated insulin and crude acetylated insulin

The *in situ* ThT assay was used for these experiments, since this required less sample compared to the small scale incubation method, enabling tests of both the crude citraconylated acetylated insulin and the crude acetylated insulin, plus the insulin standard and control samples. There were two types of unmodified insulin control samples, one underwent treatment up to the stage of obtaining crude citraconylated insulin and the other control was treated under the conditions required to obtain the crude acetylated insulin. Due to the limited

quantity of modified insulin prepared a lower concentration of 2.9 mg/ml was used. Figure 3.10 shows sigmoid curves for all of the samples.

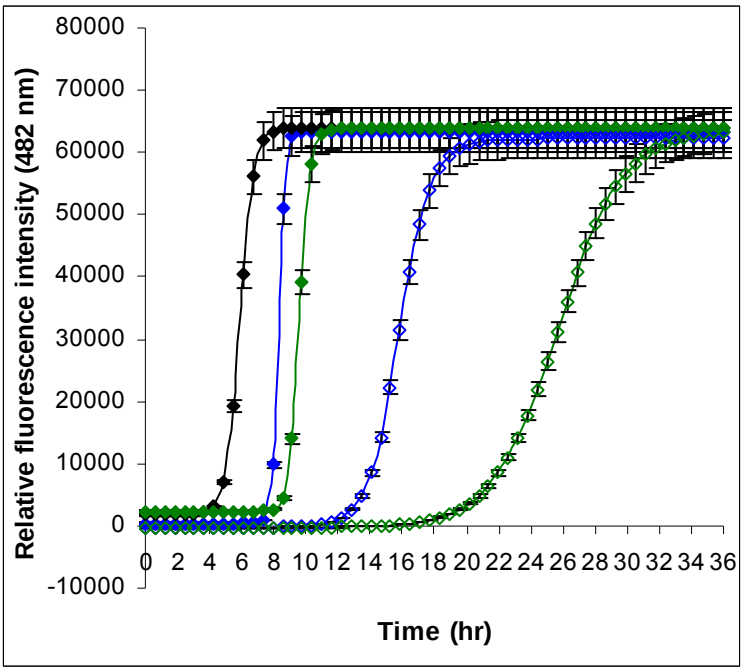

Sample	Lag time (hr)
Insulin standard	2
Insulin control (for citraconylated and acetylated insulin)	6
Crude citraconylated acetylated insulin	10
Insulin control (for acetylated insulin)	15
Crude acetylated insulin	25

Figure 3.10 *Time profiles for ThT induced fluorescence of: insulin standard (black diamonds), insulin control for crude citraconylated insulin (blue diamonds), insulin control for crude acetylated insulin (green diamonds), crude citraconylated insulin (unfilled blue diamonds), crude acetylated insulin (unfilled green diamonds) incubated at 60ºC. All samples were prepared at a concentration of 2.9 mg/ml in 20% acetic acid (100 mM NaCl, pH 1.6). Each reading represents an average of triplicate well readings, with the error bars representing standard error. The maximum fluorescence is due to instrumental limitations and is not representative of yield.*

When compared to the fresh insulin standard fibrillation, both of the insulin controls have a longer lag phase (Figure 3.10). Since all protein solution concentrations were measured by a Nanodrop (A_{280}) prior to assaying, it can be suggested that the controls were affected by the buffer treatments with both

having longer lag phases. The buffer treatments undergone by the insulin controls may have an impact on their association states, which in turn may have affected their oligomerisation.

The crude citraconylated acetylated insulin and the crude acetylated insulin; both had a longer lag phase compared to their respective insulin control (Figure 3.10). This is in accordance with results obtained from the small scale method in section 3.5.1. Overall, acetylation led to an increase in the lag phase of insulin fibrillation and a decrease in fibril yield when exposed to 20% acetic acid (pH 1.6, 100 mM NaCl).

3.4.3 TEM examination of fibrils

Fibrils formed in section 3.4.2 were examined using TEM to confirm the presence of amyloid fibrils and assess if the modification had influenced fibril morphology. The fibrils distinguishable by TEM (Figure 3.11) are described in Table 3.2. The pictures show that the fibrils are of varying lengths and have irregular appearance due to varying degrees of lateral aggregation and twisting (Burke and Rougvie 1972).

Treatment	Morphology
(A) None	long, twisted, and entangled
(B) Buffer at pH 8, for 1.5 hr	long, twisted, and entangled
(C) Buffer at pH 8, for 1.5 hr (with citraconic acid followed by acetic anhydride)	long, twisted, and entangled
(D) Buffer at pH 8, for 1.5 hr and dialysed in pH 3.5 at 30°C for 48 hr, insulin control	shorter and less entangled
(E) Buffer at pH 8, for 1.5 hr (with citraconic acid followed by acetic anhydride), dialysed in pH 3.5, at 30°C for 48 hr (deblocking)	shorter and less entangled

Table 3.2 *Effect of buffer and reagent treatment on insulin fibril morphology.*

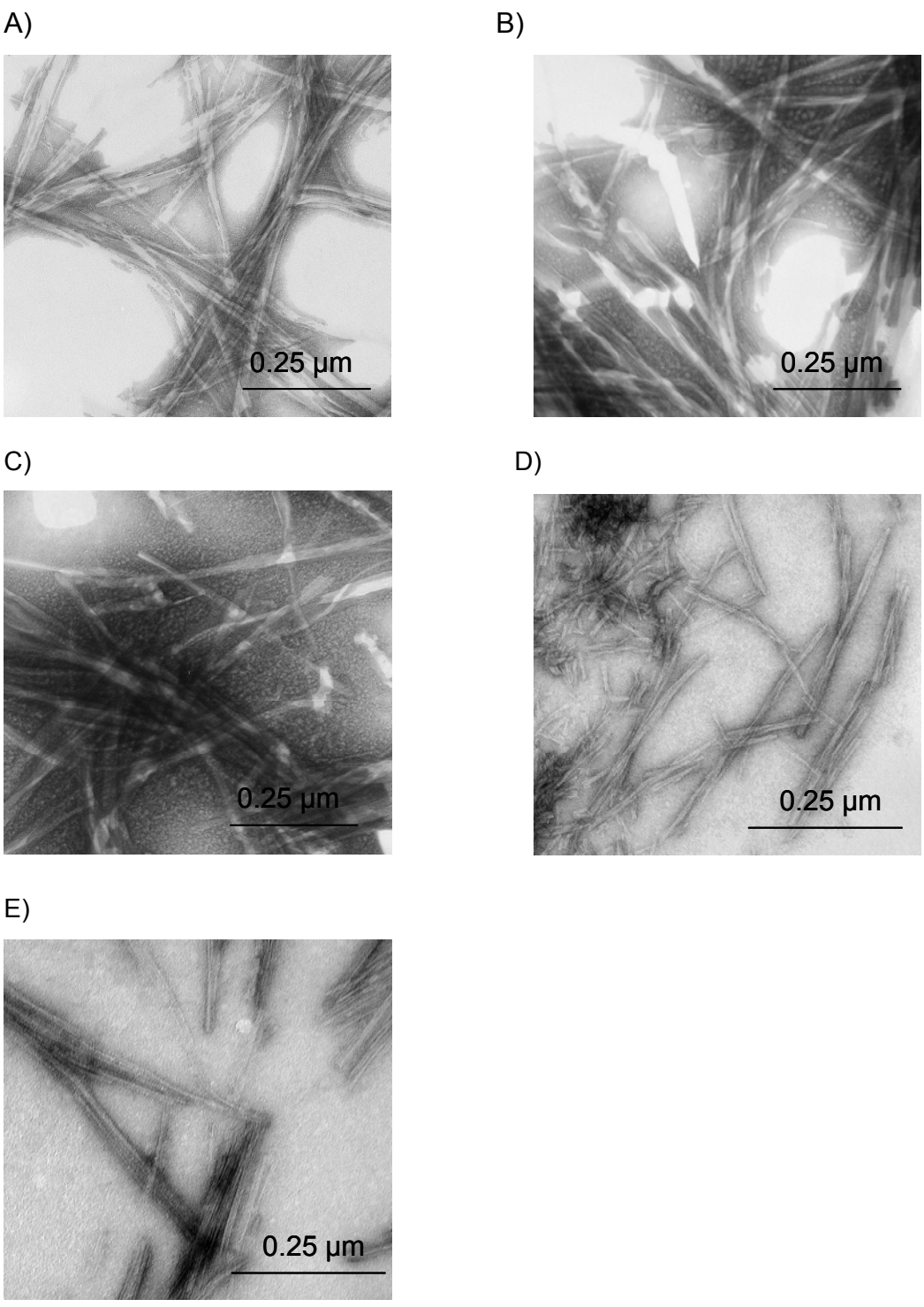

Figure 3.11 *Electron micrographs of fibrils obtained from insulin before and after modification. These images are a representation of triplicate samples. Small scale fibrillation in 20% acetic acid at 5.7 mg/ml, 60ºC in oven: (A) standard insulin, (B) insulin control, (C) crude citraconylated acetylated insulin, (D) insulin control, (E) crude acetylated insulin.*

It is interesting to note that the insulin still forms fibrils in a heterogeneous mixture of acetylated insulin, albeit at a slower rate.

3.5 The Effect of Reduction Alkylation on Insulin Aggregation

3.5.1 Previous studies on protein disulfide reduction and fibrillation

Insulin was reduced and alkylated to determine whether fibril formation is facilitated by disruption of disulfide bridges that enhance the structural stability for the native protein. Though insulin is amyloidogenic in the wild-type form, such enhanced stability conferred by the disulfide bonds is known to delay fibrillation in some proteins (Ramirez-Alvarado and Regan 2002). The A and B chains of bovine insulin have been found to form fibrils in isolation from each other, with unique morphologies in comparison to intact bovine insulin (Devlin *et al.* 2006). Similarly, in reduced human insulin, which has three different amino acids to bovine insulin (A-8 Thr, A-10 Ilc, B-30 Ala), both the A and the B chain form fibrils at acidic and neutral pHs. The A chain fibrillates without a lag phase, whilst the B chain exhibits a pH dependent lag phase (Hong *et al.* 2006). Fibrillation in a mixture of bovine insulin and its B-chain peptide showed that mixtures of the two peptides form fibrils in distinctly separate processes (Hong and Fink 2005). However, Devlin *et al*. (2006) also suggested that the impact of the insulin chains on fibrillation depends on their physical state, since the soluble A and the B chain may inhibit the intact insulin from forming fibrils due to a complex formation between insulin and the separate chains.

In β_2-macroglobulin, unfolding was achieved by disulfide reduction, which destabilised the intermediate state by increasing the flexibility of the molecule (Katou *et al.* 2002) but the intrachain disulfide bond was found to be essential for β_2-macroglobulin amyloid formation. Similarly, Mait and Surewcz (2001) found that the removal of prion peptide disulfide bridge destabilised the native protein and resulting in partial unfolding and formation of insoluble aggregates (Maiti and Surewicz 2001).

Moreover, it was found that disulfide reduction in Bence Jones protein (Klafki *et al.* 1993) and lysozyme (Takase *et al.* 2002) resulted in fibril formation. These findings support the hypothesis that disulfide bond modification of protein can have a significant impact on fibril formation.

3.5.2 Investigation of insulin amyloid formation, before and after reduction carboxymethylation

The carboxymethylation reaction was chosen due to the high specificity of iodoacetic acid for sulfhydryl cysteine modifications (Hermanson 1996). The reduced insulin and reduced carboxymethylated (RCM) insulin were initially tested for their solubility under the conditions known to solubilise standard insulin, pH 1.6. Both the reduced insulin and RCM insulin were insoluble in acidic buffers, but were soluble at pH 7.4, at 5.7 mg/ml, conditions under which insulin exists as a hexamer. Since native insulin has a low solubility at neutral pHs, solubility tests were carried out at a range of low insulin concentrations, in order to find a concentration at which native insulin is soluble. This was necessary to enable comparison between unmodified and modified insulin samples. All samples were soluble at 1 mg/ml and below, hence *in situ* ThT assay was carried out at 1 mg/ml and 0.1 mg/ml for comparison (Figure 3.12 A and B).

Fluorescence measured over time in Figure 3.12 (A) and (B) shows a sigmoid curve for crude RCM insulin, indicative of β-sheet formation. At the low concentration of 0.1 mg/ml in graph A, there was a lag phase of about 4 hrs before an increase in fluorescence. Graph (A) also shows an increase in the rate of fibril formation by the insulin standard, after 32 hr of incubation. There was no indication of fibril formation with the insulin control and reduced insulin at 0.1 mg/ml. The difference between insulin standard and control ThT fluorescence, may be due to the low concentration of protein utilised, since amyloid formation at pH 7.4 is significantly affected by protein concentration (Waterhouse 2003). This result for insulin is consistent with previous studies at pH 7.4, where no fibrils were formed within 24 hr without stirring (Nielsen *et al.* 2001b). However, RCM insulin behaved differently when compared to

unmodified insulin, with amyloid fibril formation apparently occurring at a much faster rate than unmodified insulin under the same conditions.

A)

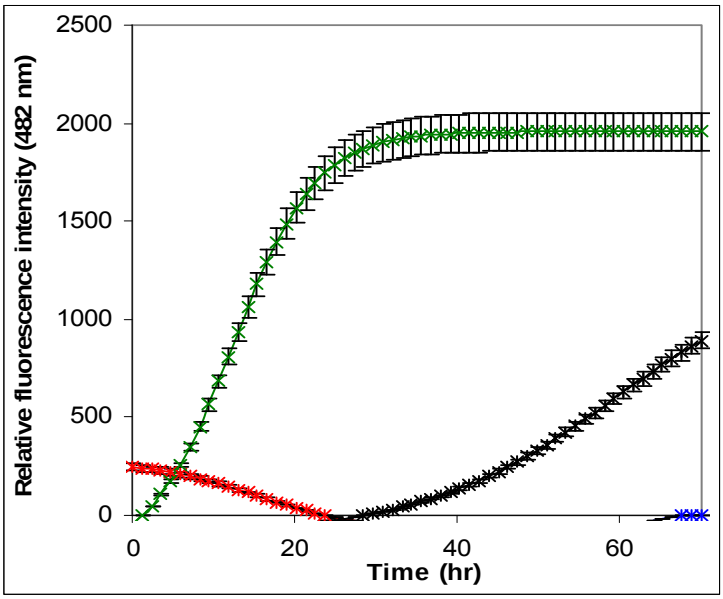

B)

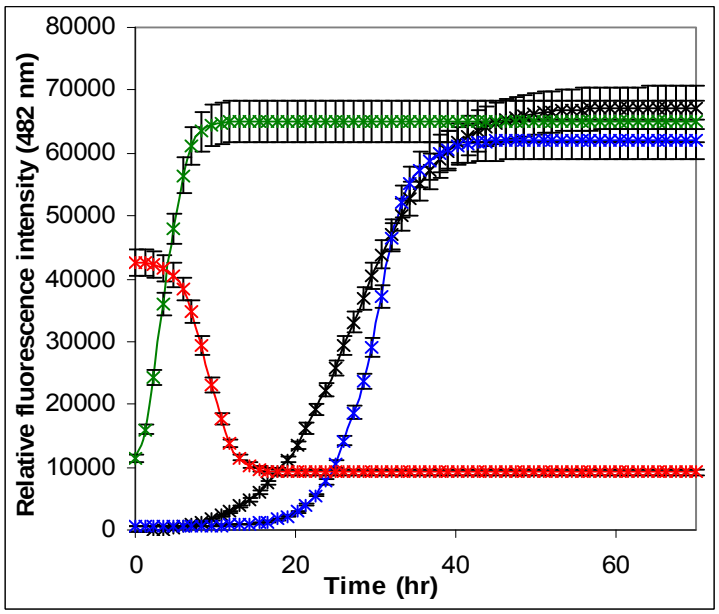

Figure 3.12 *Influence of reduction carboxymethylation on insulin fibril formation at 60ºC monitored by ThT fluorescence. Insulin was dissolved in 50 mM potassium phosphate buffer and 100 mM NaCl at pH 7.4 at: (A) 0.1 mg/ml and (B) 1 mg/ml. Fluorescence measurements were carried out,* in situ *with ThT (200 µM) in phosphate buffer. Graph A and B: black = insulin standard, blue = insulin control, red = crude reduced insulin, green = crude RCM insulin.*

A further fibrillation trial was carried out at 1 mg/ml protein concentration in order to determine the effect of concentration on RCM insulin fibril formation (Figure 3.12 B). RCM insulin lacked the lag phase, and showed a significant increase in fluorescence over the early hours of its incubation. Insulin standard and control, both showed an increase in ThT fluorescence, though the lag phase for insulin standard (16 hr) was shorter than for the control (25 hr). The reduced insulin showed a reduction in fluorescence over time until it reached a plateau, which was not indicative of fibril formation but instead may be due to the sample precipitating out of the solution (a white precipitate was observed in the plate wells). All insulin samples ThT assayed in Figure 3.12, were examined on the TEM (Figure 3.13).

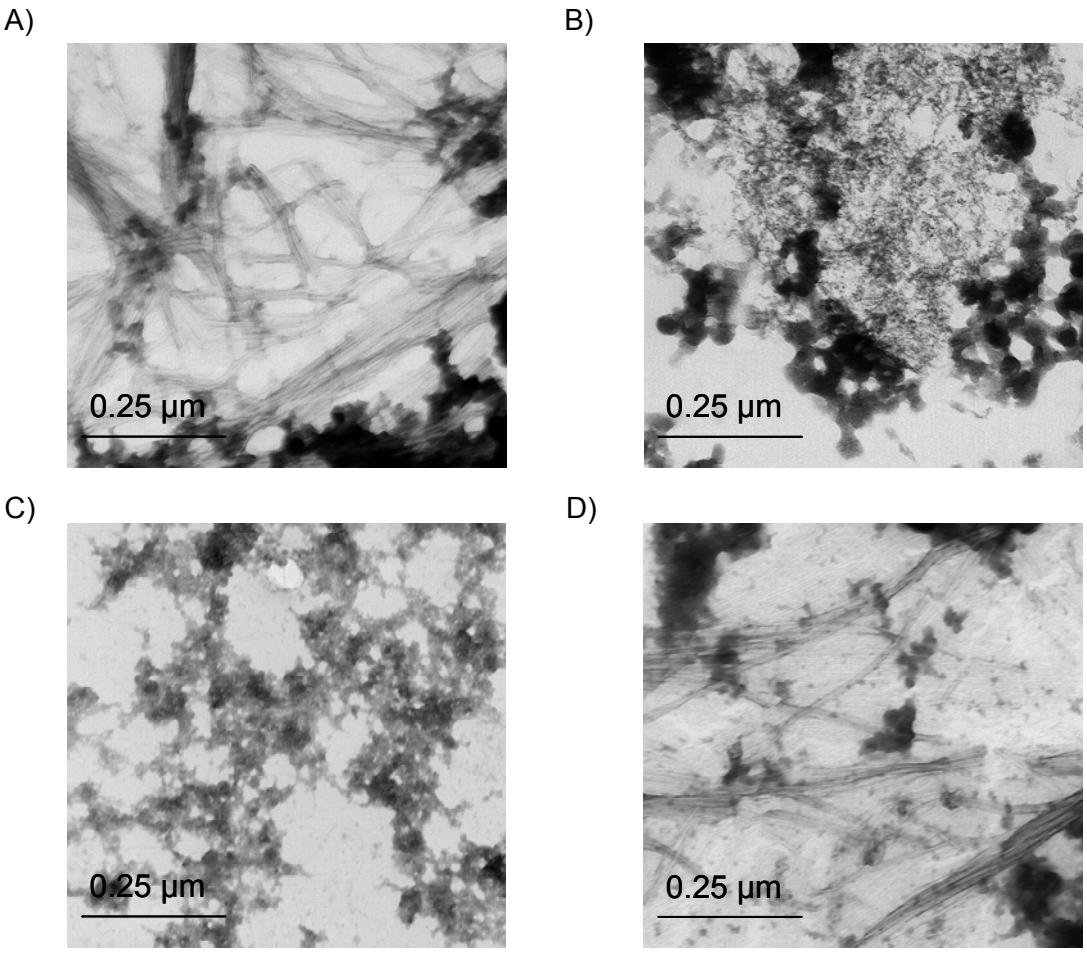

Figure 3.13 *TEM image of fibrils obtained from: A) insulin standard, B) insulin control, C) crude reduced insulin, D) RCM insulin, at pH 7.4 (50 mM phosphate buffer, 100 mM NaCl), 0.1 mg/ml, incubated* in situ *at 60ºC for 72 hr. These images are a representative of triplicate samples.*

The results corroborated the ThT data, showing fibrils present in the insulin standard and RCM insulin samples only. The structure of fibrils illustrated in Figure 3.13 was very similar in A and D, long, with thin and unbranching nanofibres of varying lengths.

From the samples fibrillised at 1 mg/ml in Figure 3.14, insulin standard, control and reduced sample all showed the presence of long, unbranched fibrils, sparingly scattered around the grids, in addition to the presence of some amorphous aggregates (Figure 3.14).

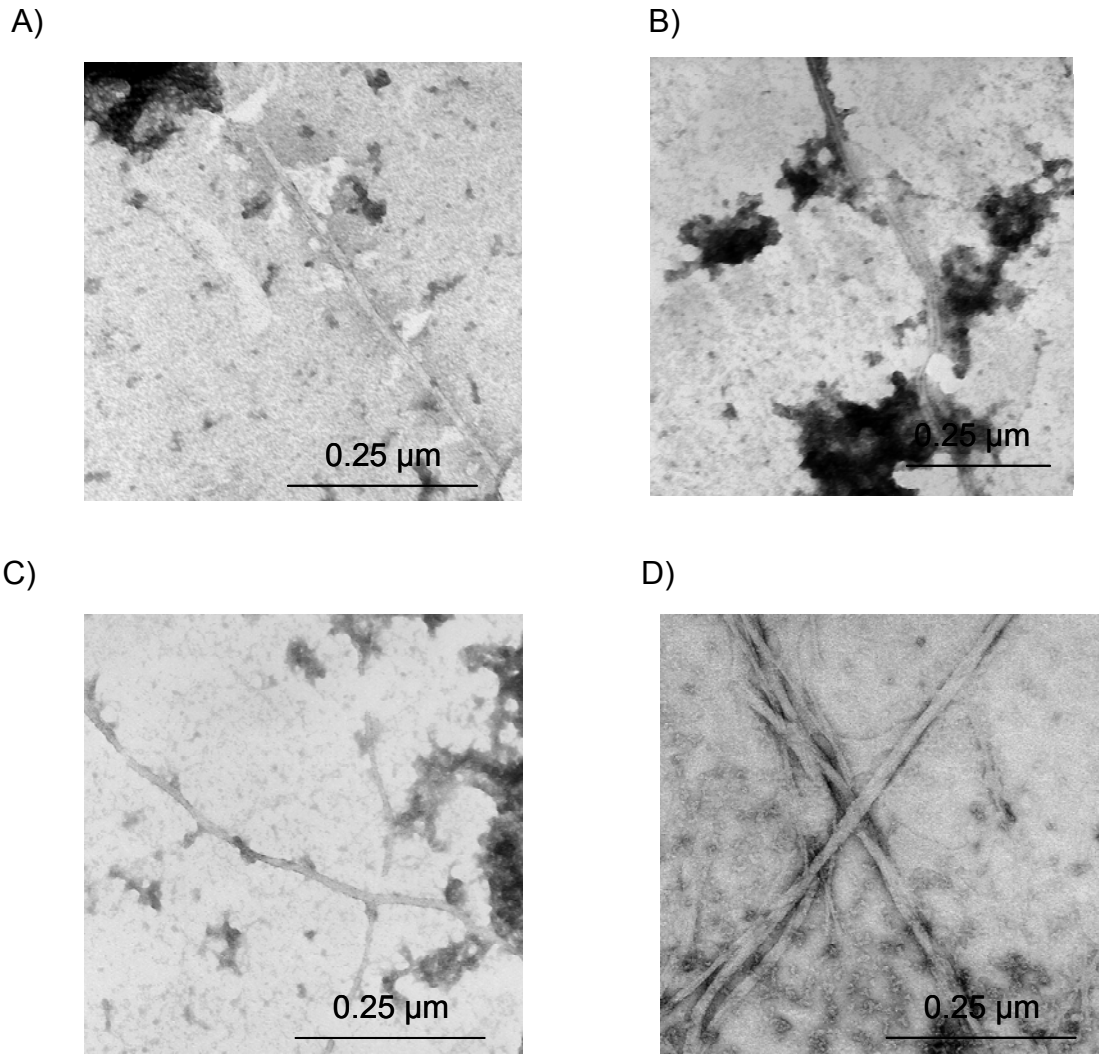

Figure 3.14 *TEM image of fibrils obtained from: A) insulin standard, B) insulin control, C) crude reduced insulin, D) RCM insulin, at 1 mg/ml, pH 7.4 (50 mM phosphate buffer, 100 mM NaCl). These images are a representation of triplicate samples.*

Conversely, the RCM insulin sample revealed straight, distinct fibrils with protofilaments twisted around in each other, as well as short wavy fibrils (Figure 3.14 D). This fibril morphology of RCM insulin at 1 mg/ml is significantly different to that obtained at 0.1 mg/ml in Figure 3.13 D. The straight fibrils were also wider in diameter (~20 nm) compared to that obtained at 0.1 mg/ml (~10 nm).

The microscopy results confirmed that insulin formed fibrils readily after reduction-carboxymethylation at pH 7.4, and the structure of the fibrils was dependent on protein concentration. There was a marked acceleration in the propensity of bovine insulin to form fibrils without a lag phase post reduction-carboxymethylation. This was similar to the results obtained with the fibrillation of human insulin A chain, which showed a rapid increase in ThT fluorescence without a lag phase at pH 7.2 (Hong *et al.* 2006). However, the distinctively straight, long nanofibres showing twists in its association (Figure 3.14 D) were found to be unique in comparison to its control counterparts.

Moreover, fibrillation studies with RCM κ-casein, a milk protein, has shown that it forms fibrils much more readily when compared to the native κ-casein (Thorn *et al.* 2005). It was suggested that the loss of disulfide bonds, may have led to the increase in the number of dissociated species in solution that is available to form fibrils. However, RCM κ-casein fibrils are assumed to form by the dissociation of an amyloidogenic precursor from an oligomeric state instead of the nucleation-dependent mechanism (Ecroyd *et al.* 2008).

3.5.3 The impact of reduction pyridylethylation on insulin amyloid formation

As outlined in chapter 2, a precipitate was obtained after insulin reduction and pyridylethylation, referred to as RPE insulin. A quick ThT testing of the precipitate obtained showed the presence of β-sheet at pH 1.6, and TEM indicated that there were wavy fibrils present. Further tests were done to verify these results.

Figure 3.15 shows that there is no difference in the fibrillation pattern of insulin standard and control under the conditions tested, and an increase in fluorescence with time was observed for both. RPE insulin precipitate showed a fluorescence of 30000 units at time 0, which suggested the presence of fibrils before incubation. Since the RPE insulin precipitate was insoluble in 20% acetic acid, and was partially soluble in HCl, fibrillation was carried in 0.025 M HCl. The behaviour of insulin standard and control was typical of insulin amyloid formation at acidic pHs, forming amyloid in a few hours. The insulin control in this section had been treated in Tris-HCl buffer at pH 8 for 1 hr before subjected to gel filtration, under similar conditions as the modified insulin.

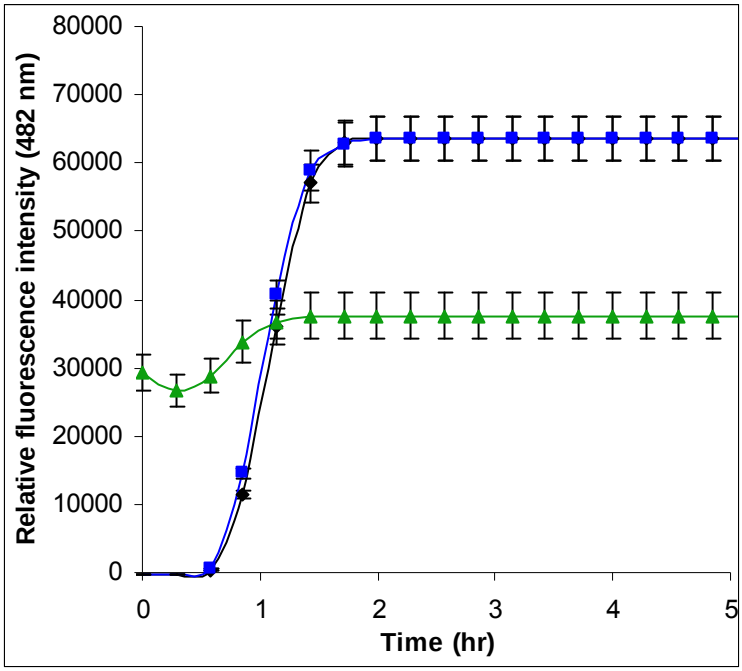

Figure 3.15 *Influence of reduction pyridylethylation on insulin fibril formation at 60ºC monitored by ThT fluorescence. Insulin (2 mg/ml) was dissolved in 25 mM HCl and 100 mM NaCl at pH 1.6. Fluorescence measurements were carried out experimentally,* in situ *with ThT (200 µM). Samples are represented as: black= insulin standard, blue = insulin control, green = crude RPE insulin precipitate. Crude reduced insulin was not tested since it is insoluble in HCl at pH 1.6.*

TEM examination of insulin standard and control showed similar structural features for the fibrils; narrow long and short tubular structures (Figure 3.16 A and B). RPE insulin precipitate was insoluble at 5.7 mg/ml and fibrillation was

carried out at the lower concentration of 2 mg/ml, at which it dissolved. The insulin fibrils formed at a concentration of 2 mg/ml looked more distinct and were not as straight as those obtained at 5.7 mg/ml (Figure 3.23 A and B), which may have been due to the differences in concentration. RPE insulin precipitate, at 0 hr and at 5 hr of incubation was also examined (Figure 3.16 C and D). Examination of RPE insulin precipitate showed that clumps of aggregates were present before incubation (Figure 3.16 A), which may have been responsible for the positive ThT fluorescence at 0 hr. After RPE insulin incubation at 60ºC, it showed fibrils which were well separated and distinctly wavy.

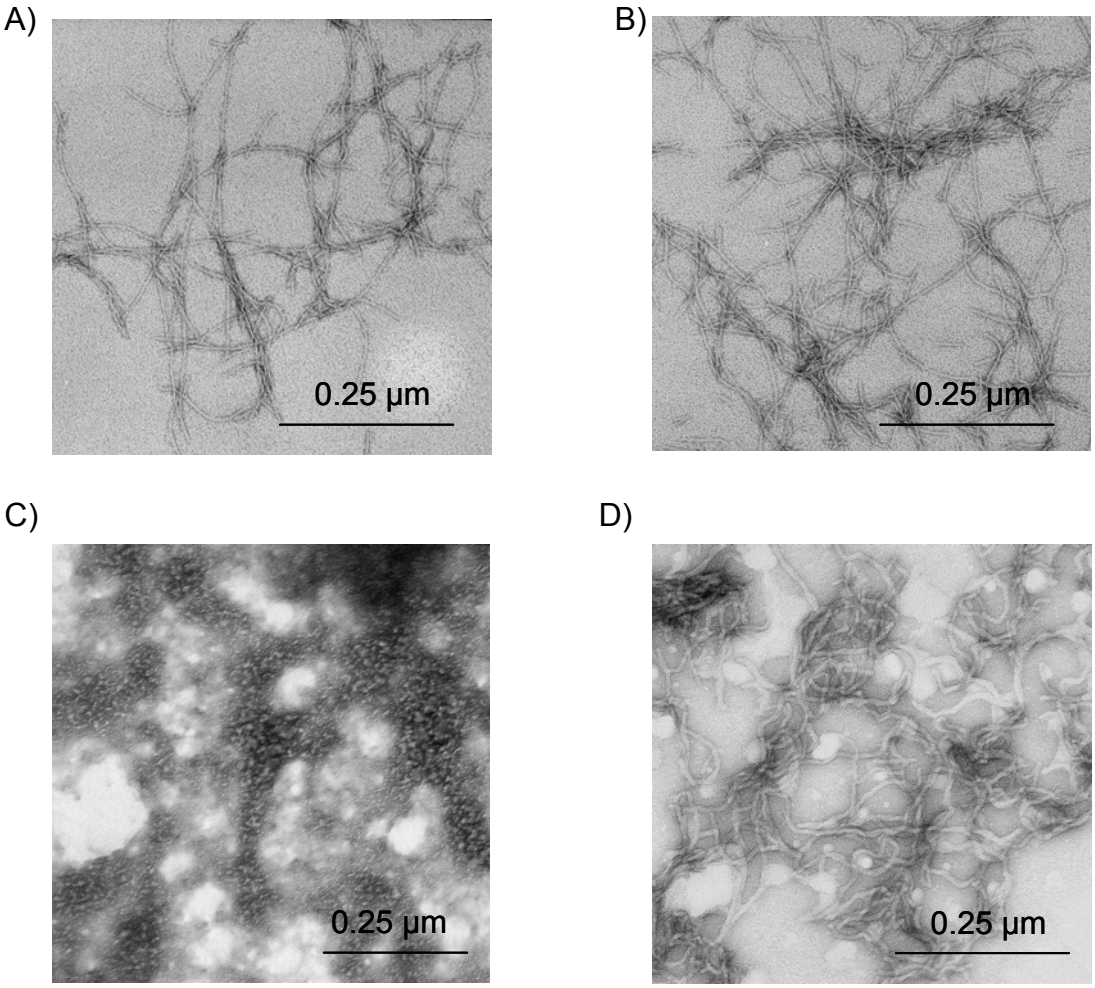

Figure 3.16 *Electron micrographs of fibrils obtained from, A) insulin standard, B) insulin control, C) precipitated RPE insulin at time 0 hr, D) precipitated insulin after 5 hr of incubation, at 2 mg/ml. These images are a representation of triplicate samples.*

RPE supernatant also gave a positive test with ThT dye, before incubation at 60ºC (Figure 3.17). There was an increase in fluorescence over time for about 1 hr until a plateau was reached. The reduced insulin sample assayed did not show any ThT binding, which may have to do with its solubility in the buffer since a white precipitate was observed in the sample wells at the end of the assay.

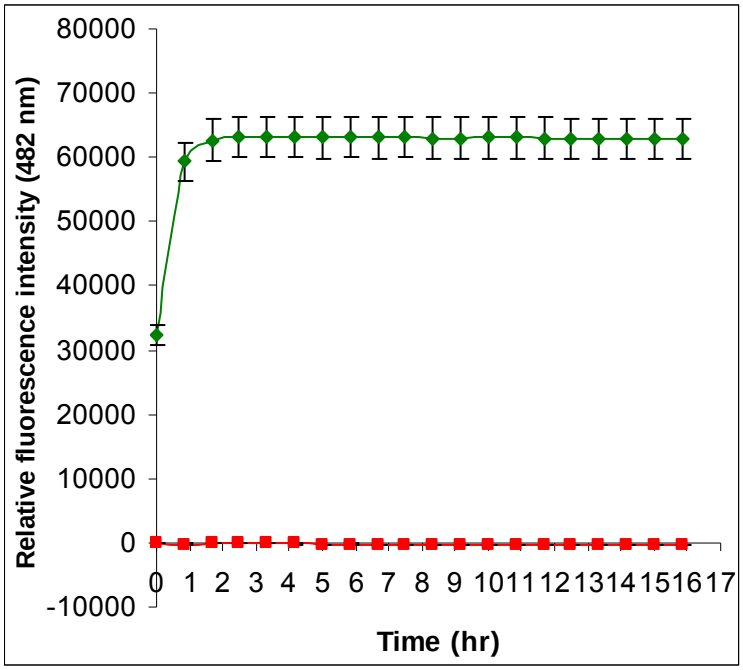

Figure 3.17 *Influence of reduction pyridylethylation on insulin fibril formation at 60ºC monitored by ThT fluorescence. RPE insulin supernatant (2 mg/ml) was dissolved in pH 7.4 phosphate buffer, 100 mM NaCl. Fluorescence measurements were carried out experimentally,* in situ *with ThT (200 µM). Samples are represented as: green= RPE supernatant, red= reduced insulin. Insulin standard and control was not tested since it is insoluble at 2 mg/ml in pH 7.4.*

Figure 3.18 illustrates the presence of wavy fibrils in the RPE insulin supernatant, very similar to those observed in the RPE precipitate. However, the fibrils obtained from the supernatant had a higher degree of waves within them. Insulin fibril morphology (long, unbranched) had changed after modification (reduction pyridylethylation). This may have been due to the fact

that RPE insulin precipitate and supernatant both have a mixture of insulin and A and B chains (chapter 2). The ThT data were indicative of the presence of β-sheets in the sample at time 0, hence it can be concluded that fibrillation was induced during insulin pyridylethylation at pH 8. However, the RPE insulin (precipitate and supernatant) showed an increase in fluorescence over time of its incubation at 60°C and the fibril morphology examination showed that wavy fibrils were formed due to the modification.

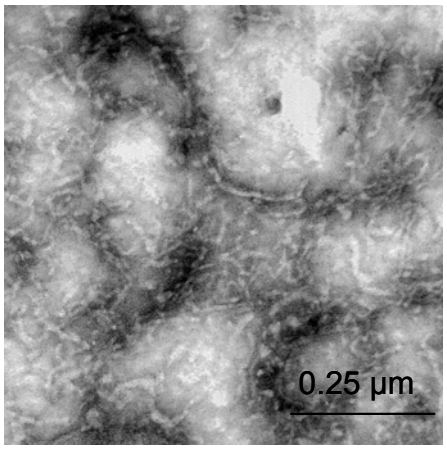

Figure 3.18 *Electron micrographs of fibrils obtained from RPE insulin supernatant (2 mg/ml) was dissolved in pH 7.4 phosphate buffer, 100 mM NaCl , incubated at 60 for 5 hr. This image is representative of triplicate samples.*

3.6 The Effect of Trypsin Digestion on Insulin Aggregation

The mixture of insulin fragments obtained after trypsin digestion of insulin (partial and total digestion) were soluble in 20% acetic acid (pH 1.6). Fibrillation tests were performed at 5.7 mg/ml and at 45ºC *in situ* (Figure 3.19 A). The insulin control was found to have a significantly longer lag phase than that of insulin standard. Results showed a decrease in the fluorescence intensity of insulin after partial digestion and negligible fluorescence after total digestion of insulin. This suggested that it is the undigested insulin in the crude digested mixture which is responsible for low fluorescence obtained in the partially digested insulin fragments.

A)

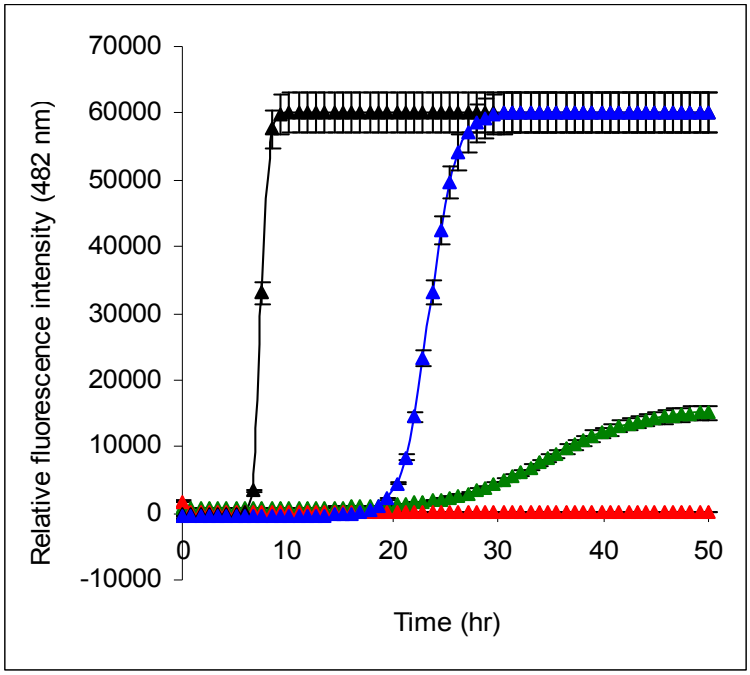

B)

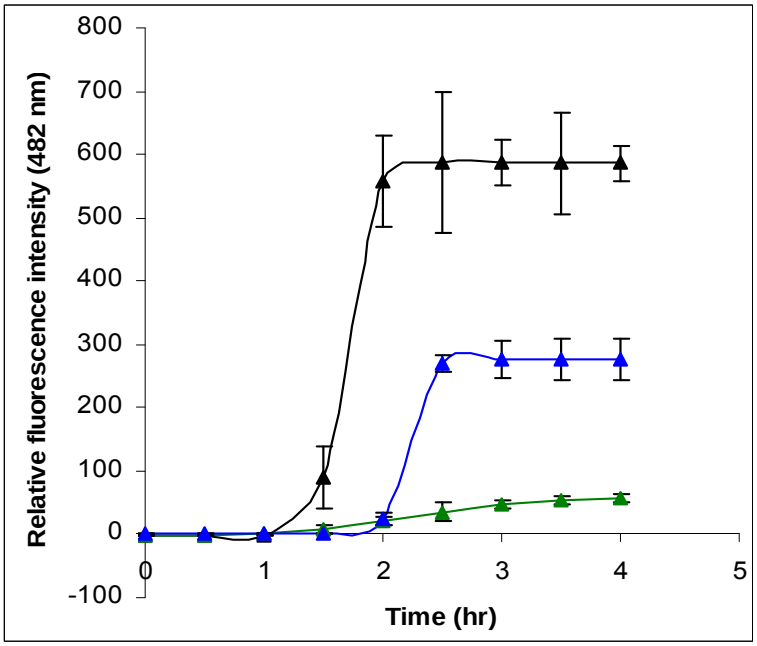

Figure 3.19 *Influence of trypsin digestion on insulin fibril formation at: (A) 45ºC and (B) 60ºC, monitored by ThT fluorescence. Insulin (5.7 mg/ml) was dissolved in 20% acetic acid and 100 mM NaCl at pH 1.6. (A)* In situ *fluorescence measurements were taken in 20% acetic acid buffer. Samples: black= insulin standard, blue= insulin control, green= partially digested insulin, red= totally digested insulin. (B) Fibrillation was carried out on small scale incubation in Tris buffer (50 mM, 100 mM NaCl). Samples: black= insulin standard, blue= insulin control, green = partially digested insulin.*

It was found (Figure 3.19 A) that the totally digested insulin (peptide fragments) do not form amyloid when present in a mixture at pH 1.6 (20% acetic acid, 100 mM NaCl). However, fibrillation occurred more readily with insulin in which the B-chain C termini were truncated, which confirmed that the B-chain C terminus does not have a role in self assembly (Brange *et al.* 1997).

Similar results were found when a small scale fibrillation trial was carried out on insulin trypsin digest at 60°C, and Figure 3.19 (B) illustrates that the insulin standard had a lag time of 1 hr while the insulin control had a longer lag time of 2 hr with reduced fluorescence. The partially treated insulin also showed a very low fluorescence for ThT dye binding over the time of its incubation and the totally digested insulin did not show any positive response to ThT dye, in agreement with data from *in situ* studies in Figure 3.19 (B). TEM examination was carried out to confirm inhibition of amyloid formation, in crude trypsin digested insulin.

TEM observation of insulin samples obtained from the fibril trial (Figure 3.20), showed long narrow fibrils present in the insulin standard sample similar to the insulin control, except the standard was more densely packed with fibrils. There was no indication of fibrils present in the partially digested samples when observed on the TEM, although there was a positive fluorescence signal (100 A.U.) shown by the sample. This could be due to the low concentration of unmodified insulin forming fibrils in negligible amounts within the peptide fragments. Literature suggests that insulin fibrillation can be inhibited or stimulated with polypeptides that are chemically similar to insulin, for example the soluble form of the insulin A and B chain form a complex with insulin, preventing fibrillation (Devlin *et al.* 2006).

A)

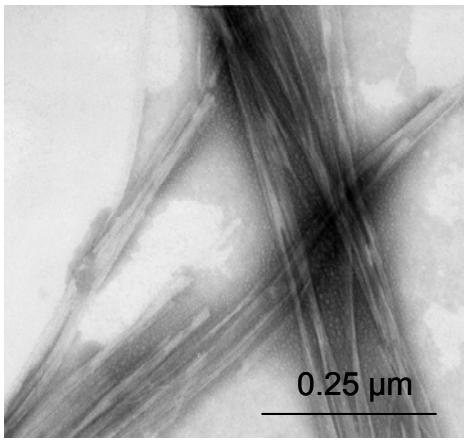

B)

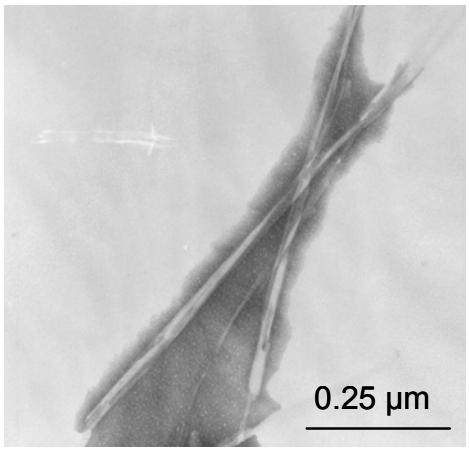

C)

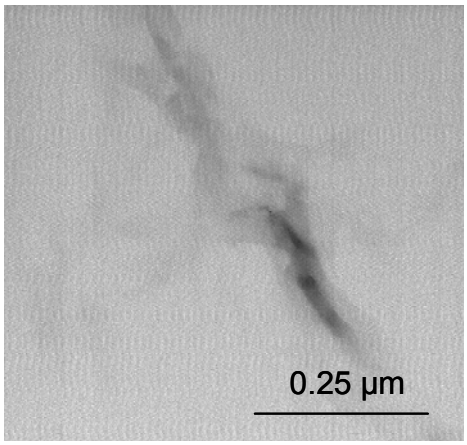

Figure 3.20 *Electron micrographs of fibrils obtained from; (A) insulin standard, (B) insulin control, (C) partially trypsin treated insulin. Protein at 5.7 mg/ml was dissolved in 20% acetic acid, 100 mM NaCl at pH 1.6 and incubated at 60ºC. These images are a representation of triplicate samples.*

3.7 The Effect of Chymotrypsin Digestion on Insulin Aggregation

ThT assay of insulin digested with chymotrypsin showed that it formed fibrils both in acetic acid and HCl (Figure 3.21 A and B). There was no lag phase observed for the digest in both acids tested. The high fluorescence intensity at 0 hr in HCl suggested that fibrils (Figure 3.21 B) were present at the start of the assay, and this was confirmed with TEM (Figure 3.23 D).

A)

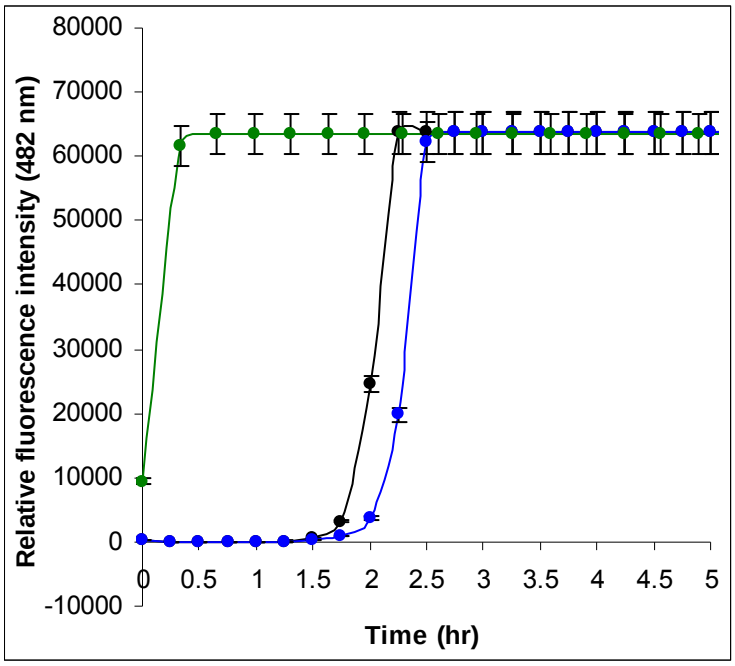

B)

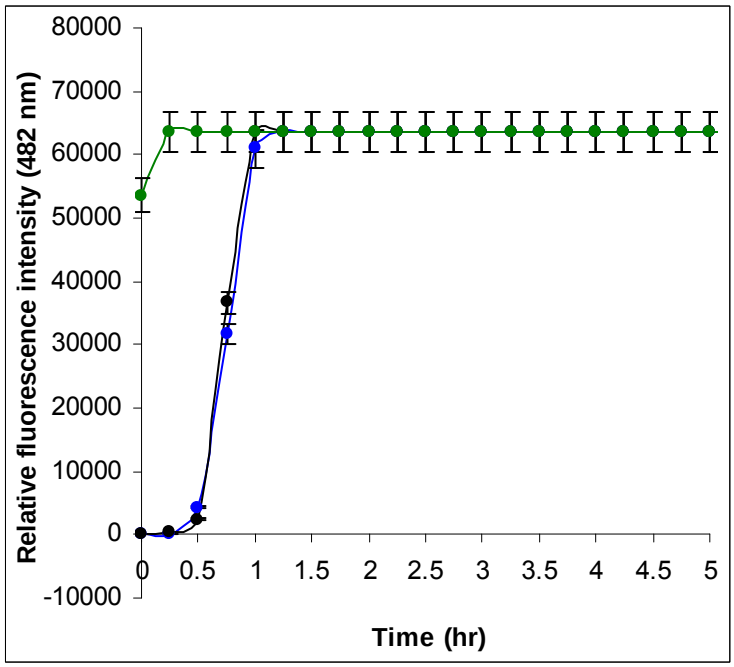

Figure 3.21 *Influence of chymotrypsin digestion on insulin fibril formation at 60ºC monitored by ThT fluorescence. Insulin (5.7 mg/ml) was dissolved in: (A) 20% acetic acid (100 m M NaCl) at pH 1.6, (B) 25 mM HCl (100 mM NaCl) at pH 1.6. Fluorescence measurements were carried out experimentally,* in situ *with ThT (200 µM). Samples in graphs A and B are: green= crude chymotryptic digest of insulin, black= insulin standard, blue= insulin control.*

The insulin control had a slightly longer lag phase (2 hr) compared to the standard (1.5 hr) in acetic acid (Figure 3.21 A), but both showed a similar behaviour in HCl (Figure 3.21 B).

TEM examination of the samples after 3 hrs of fibrillation in acetic acid showed that both the insulin standard and control had long narrow, unbranched fibrils with some twists amongst them (Figure 3.22 A and B). The chymotryptic digest of insulin in Figure 3.22 (C) showed similar fibril structure to the standard except the fibril edges were not as distinct as the standard.

A)

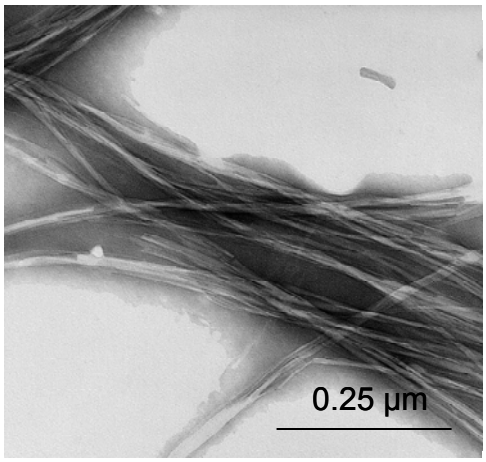

B)

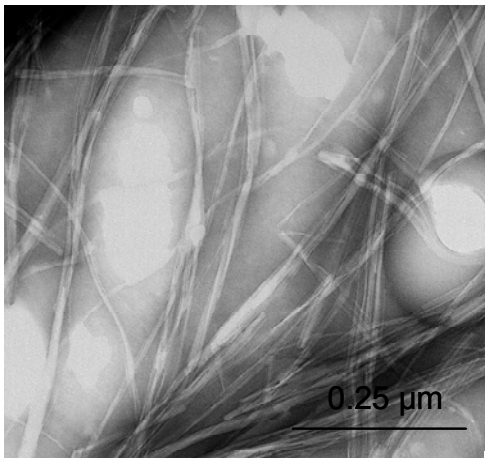

C)

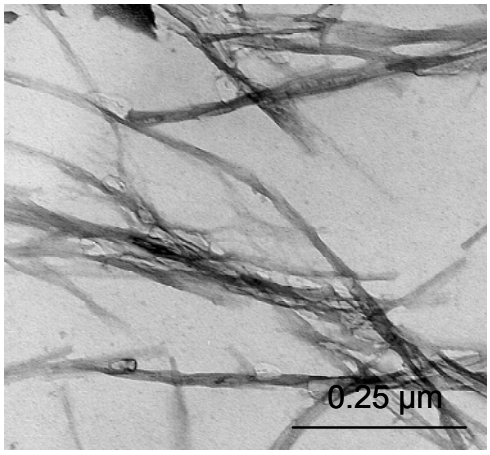

Figure 3.22 *Electron micrographs of fibrils obtained from: A) insulin standard, B) insulin control, C) crude chymotryptic digest of insulin, at 3 hr of incubation at 60ºC. Protein at 5.7 mg/ml was dissolved in 1.6 (20% acetic acid, 100 mM NaCl).*

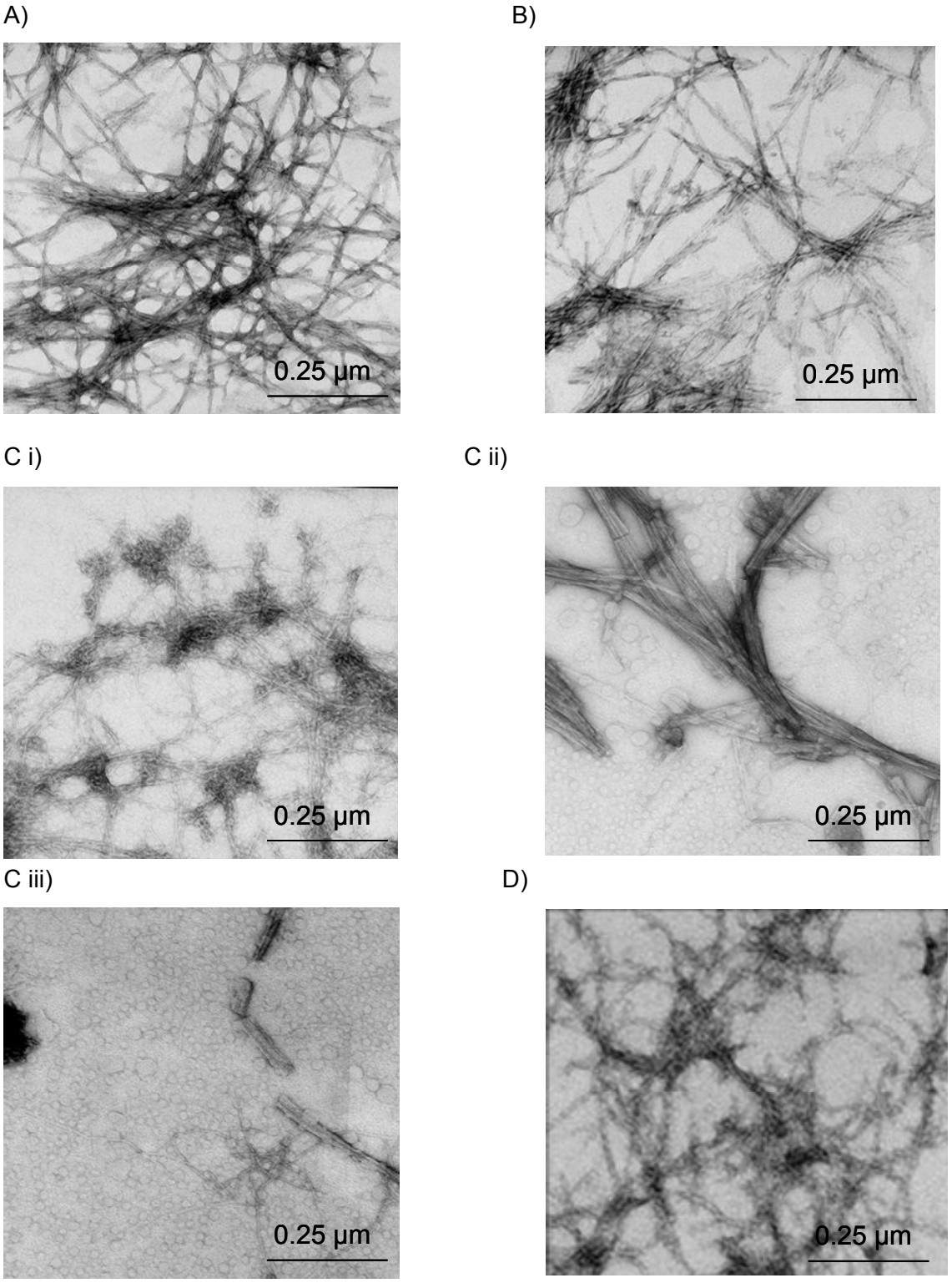

Figure 3.23 *Electron micrographs of fibrils obtained from: A) insulin standard at 3 hr, B) insulin control at 3 hr, C) i) ii) iii) crude chymotryptic digest of insulin at 3 hr, D) crude chymotryptic digest of insulin at 0 hr, of incubation at 60°C. Protein at 5.7 mg/ml was dissolved at pH 1.6 (25 mM HCl, 100 mM NaCl).*

TEM work for the samples fibrillised in the HCl buffer, showed that the insulin standard, control and digest (Figure 3.23 A, B and C(i)), contained similar long narrow fibrils. Interestingly, the chymotryptic digest revealed fibrils that varied from long and narrow to short, thick rod-like structures (Figure 3.24 C (i), (ii), (iii)). This heterogeneity in the fibrils was not visible at 0 hr (Figure 3.23 D) hence the short thick fibrils had formed after incubation at 60ºC. The different types of fibril morphology could be due to the varying peptide fragments (section 2.6, chapter 2) present in the crude mixture of insulin digest. However, it is known that insulin B chain fibril morphology is concentration dependent, and it can contain some monomers that associate to form mature fibrils and some soluble oligomers that form protofilaments and not mature fibrils (Hong *et al.* 2006). Thus Figure 3.23 (C) may be indicative of the presence of both mature fibrils and thin protofilaments in the insulin digest.

3.8 Discussion

3.8.1 Impact of insulin oligomeric state

The impact of chemical modifications and buffer treatments on the insulin standard was monitored and experiments showed that the behaviour of insulin was affected to varying degrees. The lag time for standard insulin fibrillation was elevated by some of the buffer treatments, tabulated in Table 3.3. The impact of exposing insulin at pH 8 for 1 hr led to an increase in the lag time from 2 hr to 6 hr, which further increased to 15 hr after treatment at pH 3.5 for 48 hr. All data tabulated suggested that exposing insulin to pH 8 caused a delay in the time it normally takes to break down to a monomer and form a nucleus for fibril formation. As mentioned earlier, insulin exists as a hexamer form at neutral pHs. Insulin fibril morphology remained unchanged after the buffer treatments except that shorter and less entangled fibrils were noticed in the sample designated with an asterisk (Table 3.3).

Under these conditions, the RCM insulin may no longer form a hexamer, and it is possible that it exists at a lower oligomeric state than the standard insulin at pH 7.5, and is able to form fibrils at faster rate than insulin standard. The

fibrillation of the insulin B-chain peptide has been shown to be independent of pH, and it assumed that there is no pH-dependent oligomer (e.g. hexamer) dissociation involved (Hong and Fink 2005).

Buffer/incubation history	**Fibrillation of insulin control at 60 ºC, acetic acid buffer, 5.7 mg/ml**	**Fibrillation of insulin control at 60ºC, acetic acid buffer, 2.9 mg/ml**	**Fibrillation of insulin control 45 ºC, acetic acid buffer, 5.7 mg/ml**
None	insulin standard lag time= 1.7 hr	insulin standard lag time= 2 hr	insulin standard lag time= 7.5 hr
Potassium phosphate buffer at pH 8, with stirring at 21ºC for 30 min, followed by dialysis at pH 8 for 6 hr at 0ºC	na	insulin standard lag time= 6 hr	na
Potassium phosphate buffer at pH 8, with stirring at 21ºC for 30 min with subsequent stirring at 0ºC for 1 hr, followed by incubation at pH 3.5 for 48 hr 30ºC, and dialysis at pH 8 for 6 hr at 0 ºC	*insulin standard lag time= 24 hr	insulin standard lag time= 15 hr	na
Ammonium bicarbonate buffer at pH 8.5, 37ºC for 4 hr followed by pH 3.5 at -80ºC for 48 hr	na	na	insulin control lag time= 21 hr

Table 3.3 *Shows the impact of buffer treatment on the lag time of insulin during fibrillation. na= not applicable. * Contained shorter and less entangled fibrils.*

3.8.2 Prediction of the aggregation propensity of proteins by Zagg score

3.8.2.1 Insulin

The chemical modifications carried out in this study had an impact on the lag time for insulin fibril formation, as well as the morphology of insulin fibrils in some cases. To explore this phenomenon in more detail, the Zagg score for unmodified insulin and modified insulin was calculated and compared (Table 3.4). The possible relationship between the scores and aggregation propensities found in this study was then investigated.

As discussed in chapter 1 (section 1.5), at each position in a polypeptide chain we can consider all possible amino acid replacements and determine the intrinsic *Z*-score for aggregation (*Z*agg). This enables comparisons to be made between the aggregation propensities of different polypeptide sequences (Pawar *et al.* 2005). The Zagg scores of known protein and peptide sequences show that mutated proteins with a higher score than the wild type correlate with an increased propensity to aggregate (Pawar *et al.* 2005). However, Zagg assumes that a completely unfolded protein which may limit the results (Pawar *et al.* 2005).

The algorithm is not designed to explore the impact of chemical modification; however, an estimation of the Zagg for the modified insulin was made by approximating the modified amino acids with a similar natural amino acid. Specifically, the acetylated glycine residue was approximated as alanine, leucine, and isoleucine residues in the intact insulin sequence. In insulin A and B chains, the cysteines were approximated with glutamic acid and phenylalanine residues. The Zagg scores for the wild type and the modified (intact insulin, insulin A and B chains) were calculated at pH 1.6 and pH 7. The wild type Zagg score were compared to the Zagg scores obtained for the modified insulin sequence.

The Zagg score of bovine insulin was found to be 1.38 at pH 1.6, but there was an increase in the Zagg score when alanine, leucine and isoleucine were

replaced for the glycine in the sequence. This predicts that attachment of a residue with more hydrophobic acetyl groups at A1 may induce an increase in the aggregation propensity of insulin. This does not agree with the data obtained from the acetylation on insulin which slowed down the aggregation.

The Zagg score, predicts that at pH 1.6, the insulin A chain has a higher propensity to form fibrils compared to intact insulin and the relative aggregation propensity can be ordered as such: A chain>native insulin>B chain. At pH 7, the Zagg score of the A chain was higher than both the intact insulin and the B chain. When the cysteine residues were replaced with glutamic acid, to mimic the RCM insulin, it was found that the Zagg score of the wild type insulin A and B chain were higher than the mutated insulin chains. This suggested a lower propensity for both the modified insulin A and B chains to aggregate. This does not correlate with the experimental results obtained for RCM insulin, which readily formed fibrils at a neutral pH.

The Zagg score for the replacement of the cysteines with phenylalanine, to mimic RPE insulin was also analysed at both pHs of 1.6 and 7. The Zagg scores showed an increase between the wild type (A and B chains) and the modified insulin (A and B chains) sequences at both pH 1.6 and 7. This correlates with the experimentally observed results for RPE insulin.

According to the Zagg scores obtained in Table 3.4, the tryptic peptide (A1-A21, B1-B23) has a higher propensity to aggregate compared to native insulin. The truncated insulin fragments can be arranged in the order of aggregation propensity; tryptic peptide (A1-A21, B1-B23)> tryptic peptide (A1-A21, B1-B29)> tryptic peptide (B24-B30). The tryptic peptides of insulin showed a reduction in observed fibril forming propensity. The Zagg scores of both the chymotryptic peptides are higher than the wild type insulin and this is supported by the results obtained in Figure 3.23, which shows that the digests formed fibrils readily, suggesting that the algorithm has some value in predicting aggregation potential.

Modification	**Primary sequence of bovine insulin after the modification**	**Zagg score pH 1.6**	**Zagg score pH 7**
Native insulin (A1-A21, B1-B30)	GIVEQCCASVCSLYQLENYCNFVNQHLCGSHLVEALYLVCGERG FFYTPKA	1.38	1.60
Ala for Gly at A1	**A**IVEQCCASVCSLYQLENYCNFVNQHLCGSHLVEALYLVCGERG FFYTPKA	1.39	na
Lys for Gly at A1	**L**IVEQCCASVCSLYQLENYCNFVNQHLCGSHLVEALYLVCGERG FFYTPKA	1.45	na
Ileu for Gly at A1	**I**IVEQCCASVCSLYQLENYCNFVNQHLCGSHLVEALYLVCGERGF FYTPKA	1.48	na
Insulin A chain	GIVEQCCASVCSLYQLENYCN	1.87	1.70
Insulin B chain	FVNQHLCGSHLVEALYLVCGERGFFYTPKA	0.91	1.60
Glu for Cys Insulin A chain	GIVEQ**EE**ASVESLYQL**E**NY**E**N	na	-0.64
Glu for Cys Insulin B chain	FVNQHL**E**GSHLVEALYLV**E**GERGFFYTPKA	na	0.60
Phe for Cys Insulin A chain	GIVEQ**FF**ASV**F**SLYQLENY**F**N	2.00	1.90
Phe for Cys Insulin B chain	FVNQHL**F**GSHLVEALYLV**F**GERGFFYTPKA	1.00	1.70
Tryptic peptide (A1-A21, B1-B29)	GIVEQCCASVCSLYQLENYCNFVNQHLCGSHLVEALYLVCGERG FFYTPK	1.38	na
Tryptic peptide (A1-A21, B1-B23)	GIVEQCCASVCSLYQLENYCNFVNQHLCGSHLVEALYLVCGER	1.50	na
Tryptic peptide (B24-B30)	GFFYTPKA	0.82	na
Chymotryptic peptide	GIVEQCCASVCSLYFVNQHLCGSHLVEALY	1.81	na
Chymotryptic peptide	QLENYCNLYLVCGERGF	1.37	na

Table 3.4 *Effect of mutating amino acids of the insulin chain, separating insulin A and B chain and truncating bovine insulin chain, on the aggregation propensity of the protein evaluated by Zagg score.*

3.8.2.2 Bovine eye lens and wheat proteins

Since the algorithm showed some success in predicting improved aggregation propensity in modified insulin, it was applied to two potential large scale sources of proteins of interest to the wider research programme: wheat proteins and bovine crystallins both of which have been shown to form amyloid proteins from crude extracts (Garvey *et al.* 2008, Mackintosh *et al.* 2008), to obtain a measure of their aggregation propensity in Tables 3.5 and 3.6.

Bovine eye lens is an example of a waste protein, which can be sourced for fibrils to be made on a reasonable scale and will be further discussed in chapter 4 and 5. The α-, β-, and γ- proteins are the major structural proteins in the eye lens, which form fibrils under mildly denaturing conditions *in vitro* (Meehan *et al.* 2004). The Zagg scores calculated for bovine eye lens α- and β- sequences showed that the α-crystallins are more prone to aggregate when compared to β-crystallins. This was unexpected since α-crystallins act as chaperones for themselves as well as for other crystallins. They also take longer to form fibrils *in vitro* when compared to the β-crystallins (Meehan *et al.* 2004).

Bovine eye lens proteins	**Zagg score at pH 2**
P02470[1-173], Alpha-crystallin A chain	-0.29
P02510[1-175], Alpha-crystallin B chain	0.17
P02510[1-175], Alpha-crystallin B chain	0.10
P11843[1-215], Beta-crystallin A3	0.06
P26444[2-197], Beta-crystallin A2	-0.42
P11842[2-210], Beta-crystallin A4	-0.41
P07318[2-253], Beta-crystallin B1	-0.98
P02522[2-205], Beta-crystallin B2	-1.32
P19141[2-211], Beta-crystallin B3	-1.74
P06504[2-178], Beta-crystallin S	-0.08

Table3.5 *Zagg scores obtained for various crystallins of bovine eye lens.*

For high molecular weight glutenins (HMW) in wheat (Mackintosh *et al.* 2008), the Zagg scores found were negative, which indicates a low propensity to form aggregates. This is consistent with the very long timeframe required to form amyloid like structures in this case.

The results obtained show that it may not be possible to utilise the Zyggregator to predict the ability of protein to form fibrils in a heterogeneous mixture, as Devlin and his co-workers (Devlin *et al.* 2006) found that the propensity of insulin to form fibrils in a mixture of chemically related peptides depends on peptide conformation. The impact of buffer treatments on insulin fibril forming propensity also suggest that the algorithms are may require further development to be of use in these studies.

Wheat high molecular weight (HMW) glutenins	**Zagg score at pH 7**
GLT0_WHEAT(P10387) Glutenin, high molecular weight subunit DY10 precursor	-3.00
GLT1_WHEAT (P02861) Glutenin,high molecular weight subunit PC256 (Fragment)	-1.20
GLT2_WHEAT(P02862) Glutenin, high molecular weight subunit PC237 (Fragment)	-0.15
GLT3_WHEAT(P08488) Glutenin, high molecular weight subunit 12 precursor	-0.30
GLT4_WHEAT(P08489) Glutenin, high molecular weight subunit PW212 precursor	-3.30
GLT5_WHEAT(P10388) Glutenin, high molecular weight subunit DX5 precursor	-1.07

Table 3.6 *Zagg score obtained for various HMW glutenin sequences.*

3.8.3 Fibril morphology, rate and yield

Results from this chapter suggest that insulin fibril formation is possible in heterogeneous matrix, depending on the type of chemical derivatisation.

Acetylation of insulin caused an increase in the lag phase and a reduction in the yield of the fibrils. Since the fibrils formed by the acetylated insulin mixture were short and straight similar to the insulin control, it was assumed that the unmodified insulin in the mixture had formed fibrils and the acetylated component of the mixture formed amorphous aggregates.

Reduction carboxymethylation of insulin led to the loss of the lag phase during fibrillation and enabled the rapid formation of straight fibrils with twists at pH 7.4, which also had some small wavy fibrils, unlike the unmodified insulin. The method allowed production of fibrils at a faster rate than for the native protein.

Reduction pyridylethylation of insulin led to the formation of wavy fibrils, compared to the self assembly of native insulin into non wavy fibrils, suggesting that chemical modification may provide a means of manipulating fibril morphology.

Enzymatic digestion of insulin had varying effects on its fibrillation. Trypsin digests with some undigested insulin, showed an increase in the lag phase and a reduction in the yield of fibrils. Straight, long, unbranched fibrils obtained were similar to the insulin standard. The trypsin digest without any undigested insulin showed no fibrillation. Chymotrypsin digestion of insulin led to the formation of a heterogeneous mixture of fibrils. The morphology of fibrils varied from thin, straight and long structures to thick, short fibrils.

3.9 Summary

This chapter has demonstrated that bovine insulin forms fibrils in crude heterogeneous mixtures of chemically modified insulin. It also showed how the various chemical modifications employed affected insulin fibrillation lag phase,

rate, yield and fibril morphology. This study also provides evidence that insulin can form fibrils of varying morphologies, in heterogeneous mixtures. These finding suggests the feasibility of using crude sources of protein such as bovine eye lens in bionanotechnology (Garvey *et al.* 2008). The ability to control morphology of crude mixtures of protein fibrils is a potentially desirable characteristic in bionanotechnology, where multiple uses may be required from a single crude protein source.

3.10 References

Ahmad, A., I. S. Millett, S. Doniach, V. N. Uversky, and A. L. Fink. 2003. Partially folded intermediates in insulin fibrillation. *Biochemistry* 42: 11404-11416.

Ahmad, A., V. N. Uversky, D. Hong, and A. L. Fink. 2005. Early events in the fibrillation of monomeric insulin. *Journal of Biological Chemistry* 280: 42669-42675.

Bouchard, M., J. Zurdo, E. J. Nettleton, C. M. Dobson, and C. V. Robinson. 2000. Formation of insulin amyloid fibrils followed by FTIR simultaneously with CD and electron microscopy. *Protein Science* 9: 1960-1967.

Brange, J., G. G. Dodson, D. J. Edwards, P. H. Holden, and J. L. Whittingham. 1997. A model of insulin fibrils derived from the X-ray crystal structure of a monomeric insulin (despentapeptide insulin). *Proteins-Structure Function and Genetics* 27: 507-516.

Burke, M. J., and M. A. Rougvie. 1972. Cross-β protein structures. I. Insulin fibrils. *Biochemistry* 11: 2435-2439.

Devlin, G. L., T. P. J. Knowles, A. Squires, M. G. McCammon, S. L. Gras, M. R. Nilsson, C. V. Robinson, C. M. Dobson, and C. E. MacPhee. 2006. The component polypeptide chains of bovine insulin nucleate or inhibit aggregation of the parent protein in a conformation-dependent manner. *Journal of Molecular Biology* 360: 497-509.

Ecroyd, H., T. Koudelka, D. C. Thorn, D. M. Williams, G. Devlin, P. Hoffmann, and J. A. Carver. 2008. Dissociation from the oligomeric state is the rate-limiting step in fibril formation by κ-casein. *Journal of Biological Chemisty* 283: 9012-9022.

Garvey, M., S. L. Gras, S. Meehan, S. J. Meade, J. A. Carver, and J. A. Gerrard. 2008. Protein nanofibres of defined morphology prepared from mixtures of crude crystallins. *International Journal of Nanotechnology* Submitted.

Groenning, M., M. Norrman, J. M. Flink, M. van de Weert, J. T. Bukrinsky, G. Schluckebier, and S. Frokjaer. 2007. Binding mode of thioflavin T in insulin amyloid fibrils. *Journal of Structural Biology* 159: 483-497.

Hermanson, G. T. 1996. *Bioconjugate Techniques*. Academic Press, San Diego, USA, pg 76-80, 126-129.

Hong, D.-P., A. Ahmad, and A. L. Fink. 2006. Fibrillation of human insulin a and b chains. *Biochemistry* 45: 9342-9353.

Hong, D.-P., and A. L. Fink. 2005. Independent heterologous fibrillation of insulin and its β-chain peptide. *Biochemistry* 44: 16701-16709.

Hua, Q.-x., and M. A. Weiss. 2004. Mechanism of insulin fibrillation: The structure of insulin under amyloidogenic conditions resembles a protein-folding intermediate. *Journal of Biological Chemistry* 279: 21449-21460.

Jahn, T. R., and S. E. Radford. 2008. Folding versus aggregation: Polypeptide conformations on competing pathways. *Archives of Biochemistry and Biophysics* 469: 100-117.

Jiménez, J. L., E. J. Nettleton, M. Bouchard, C. V. Robinson, C. M. Dobson, and H. R. Saibil. 2002. The protofilament structure of insulin amyloid fibrils. *Proceedings of the National Academy of Sciences of the United States of America.* 99: 9196-9201.

Katou, H., T. Kanno, M. Hoshino, Y. Hagihara, H. Tanaka, T. Kawai, K. Hasegawa, H. Naiki, and Y. Goto. 2002. The role of disulfide bond in the amyloidogenic state of β_2-microglobulin studied by heteronuclear NMR. *Protein Science* 11: 2218-2229.

Klafki, H. W., A. I. Pick, I. Pardowitz, T. Cole, L. A. Awni, H. U. Barnikol, F. Mayer, H. D. Kratzin, and N. Hilschmann. 1993. Reduction of disulfide bonds in an amyloidogenic Bence Jones protein leads to formation of "amyloid-like" fibrils *in vitro*. *Biological Chemistry Hoppe-Seyler* 374: 1117-1122.

LeVine, H., III. 1993. Thioflavin T interaction with synthetic alzheimer's disease beta-amyloid peptides: Detection of amyloid aggregation in solution. *Protein Science* 2: 404-410.

LeVine, H., III. 1999. Quantification of β-sheet amyloid fibril structures with thioflavin T. *Methods in Enzymology* 309: 274-284.

Mackintosh, S. H., S. J. Meade, J. P. Healy, K. H. Sutton, N. G. Larsen, A. M. Squires, and J. A. Gerrard. 2008. Wheat glutenin proteins assemble into an amyloid-like structure with unusual structural features. *Journal of Cereal Science* in press.

Maiti, N. R., and W. K. Surewicz. 2001. The Role of Disulfide Bridge in the Folding and Stability of the Recombinant Human Prion Protein. *Journal of Biological Chemistry* 276: 2427-2431.

Meehan, S., Y. Berry, B. Luisi, C. M. Dobson, J. A. Carver, and C. E. MacPhee. 2004. Amyloid fibril formation by lens crystallin proteins and its implications for cataract formation. *Journal of Biological Chemistry* 279: 3413-3419.

Naiki, H., K. Higuchi, M. Hosokawa, and T. Takeda. 1989. Fluorometric determination of amyloid fibrils in vitro using the fluorescent dye, thioflavin T. *Analytical Biochemistry* 177: 244-249.

Nettleton, E. J., P. Tito, M. Sunde, M. Bouchard, C. M. Dobson, and C. V. Robinson. 2000. Characterization of the oligomeric states of insulin in self-assembly and amyloid fibril formation by mass spectrometry. *Biophysical Journal* 79: 1053-1065.

Nielsen, L., S. Frokjaer, J. Brange, V. N. Uversky, and A. L. Fink. 2001a. Probing the mechanism of insulin fibril formation with insulin mutants. *Biochemistry* 40: 8397-8409.

Nielsen, L., R. Khurana, A. Coats, S. Frokjaer, J. Brange, S. Vyas, V. N. Uversky, and A. L. Fink. 2001b. Effect of environmental factors on the kinetics of insulin fibril formation: Elucidation of the molecular mechanism. *Biochemistry* 40: 6036-6046.

Pawar, A. P., K. F. DuBay, J. Zurdo, F. Chiti, M. Vendruscolo, and C. M. Dobson. 2005. Prediction of "aggregation-prone" and "aggregation-susceptible" regions in proteins associated with neurodegenerative diseases. *Journal of Molecular Biology* 350: 379-392.

Ramirez-Alvarado, M., and L. Regan. 2002. Does the location of a mutation determine the ability to form amyloid fibrils? *Journal of Molecular Biology* 323: 17-22.

Sabaté, R., I. Lascu, and S. J. Saupe. 2008. On the binding of thioflavin-T to HET-s amyloid fibrils assembled at pH 2. *Journal of Structural Biology* 162: 387-396.

Takase, K., T. Higashi, and T. Omura. 2002. Aggregate formation and the structure of the aggregates of disulfide-reduced proteins. *Journal of Protein Chemistry* 21: 427-433.

Thorn, D. C., S. Meehan, M. Sunde, A. Rekas, S. L. Gras, C. E. MacPhee, C. M. Dobson, M. R. Wilson, and J. A. Carver. 2005. Amyloid fibril formation by bovine milk κ-casein and its inhibition by the molecular chaperones α_s- and β-casein. *Biochemistry* 44: 17027-17036.

Uversky, V. N., L. Nielsen Garriques, I. S. Millett, S. Frokjaer, J. Brange, S. Doniach, and A. L. Fink. 2003. Prediction of the association state of insulin using special parameters. *Journal of Pharmaceutical Sciences* 94: 847-858.

Vestergaard, B., M. Groenning, M. Roessle, J. S. Kastrup, M. v. de Weert, J. M. Flink, S. Frokjaer, M. Gajhede, and D. I. Svergun. 2007. A helical structural nucleus is the primary elongating unit of insulin amyloid fibrils. *Public Library of Science Biology* 5: 1089-1097.

Waterhouse, S. H. 2003. MSc. Thesis. Controlling amyloid fibril growth. *School of Biological Sicences*. University of Canterbury, Christchurch.

Waugh, D. F. 1948. Regeneration of insulin from insulin fibrils by the action of alkali. *Journal of the American Chemical Society* 70: 1850-1857.

Whittingham, J. L., D. J. Scott, K. Chance, A. Wilson, J. Finch, J. Brange, and G. G. Dodson. 2002. Insulin at pH 2: Structural analysis of the conditions promoting insulin fibre formation. *Journal of Molecular Biology* 318: 479-490.

The development of a laboratory scale method for film manufacture and characterisation

4.1 Background

In chapter 1, the background and importance of amyloid fibrils in bionanomaterials was discussed. Chapter 2 and 3 investigated and established chemical methods to modify bovine insulin and gain control of the morphology of bovine insulin nanofibres. In this chapter, a nanocomposite film manufacture method was established. The impact of film manufacturing steps and drying was characterised. The potential of adding amyloid fibrils to a polymer matrix system was also investigated. In chapter 5, proof of principle that amyloid fibrils from two different sources of proteins may make a difference to bionanomaterial properties was sought.

There has been much interest in the potential application of amyloid fibrils (chapter 1, section 1.6) with efforts in the past decade seeking to understand protein fibril growth (Dobson 2004, Jahn and Radford 2008, Nielsen *et al.* 2001, Radford 2000, Tycko 2004) and to produce fibrils in an economic way, in particular with a view to exploring applications such as nanocomposites (Cherny and Gazit 2008, Garvey *et al.* 2008, Gras 2007, Waterhouse and Gerrard 2004, Waterhouse *et al.* 2003).

Polymers are useful as a matrix to produce nanocomposites with enhanced properties (Cadek *et al.* 2002, Cadek *et al.* 2004, Calvert 1999, Coleman 2006, Guo *et al.* 2007, Lau *et al.* 2006, Schadler *et al.* 1998, Zhang *et al.* 2003). Of the various polymers that serve as a matrix, PVOH was chosen for this study as

previously described in chapter 1, section 1.8.2. The primary issues in the development of the PVOH + protein fibril composites were the production of amyloid fibrils on an appropriate scale, the choice of a polymer as a matrix, the choice of method for film manufacture, and the effect of polymer-fibril mixing on the stability of the protein fibrils and protein control.

As introduced in chapter 1, bovine insulin is the model protein in this thesis hence this chapter is largely based on the use of insulin to develop a film manufacture method. However, methods successfully established with bovine insulin were applied to crystallins, a cheap, industrial waste material that have been shown to form amyloid fibrils (Garvey *et al.* 2008) and will be discussed in part in this chapter and explored further in chapter 5.

4.2 Production of Amyloid Fibrils for Films

As shown in chapter 3, protein fibrils can be produced in a variety of morphologies, long, short, twisted, straight and ribbon like, to name a few. In this study fibrils were produced from two different protein sources, insulin and crystallins.

4.2.1 Insulin fibrils

The ability of bovine insulin to form fibrils readily under denaturing conditions *in vitro*, was described in detail in chapter 3. For this chapter, insulin fibrils were prepared in HCl (25 mM, 100 mM NaCl, pH 1.6). The fibrils prepared in HCl were reproducibly unbranched and straight and distinct on the TEM, which facilitated its characterisation in films. These nanofibres ranged from 8-30 nm in diameter with varying lengths of several micrometers (chapter 3, Figure 3.6).

4.2.2 Crystallin fibrils

Bovine eye lenses were obtained from Canterbury Meat Packers Seafield Plant and stored at -20°C prior to protein extraction in this study. Protein extraction and fibril formation was performed using optimised conditions from a recent study in our research group (Garvey *et al*. 2008). Several bovine eye lens were

homogenised in a Tris buffer (50 mM, pH 7.2) and centrifuged to obtain a clear supernatant which was composed of the crude crystallins.

The crystallins were diluted to 22 mg/ml in 2,2,2-trifluoroethanol (TFE) (10%, pH 2) and incubated at 60°C to form fibrils. A NuPAGE gel was run to determine the molecular weight of the proteins in the crystallins. Figure 4.1 shows that the crystallin control (Lane 1) are 20-28 kDa, which is consistent with the findings of Garvey *et al.* (2008). They are made up of primarily the α-, β- and γ-crystallin proteins (Kapphahn *et al.* 2003). The β- component protein bands were identified in Lane 1 at ~26 kDa and the α-, γ-crystallin bands ranged from 17-25 kDa. After the fibrillation of the crystallins, the fibrils were centrifuged and the supernatant was run on NuPAGE (Figure 4.1, Lane 2). The gel shows the loss of proteins bands after protein fibrillation.

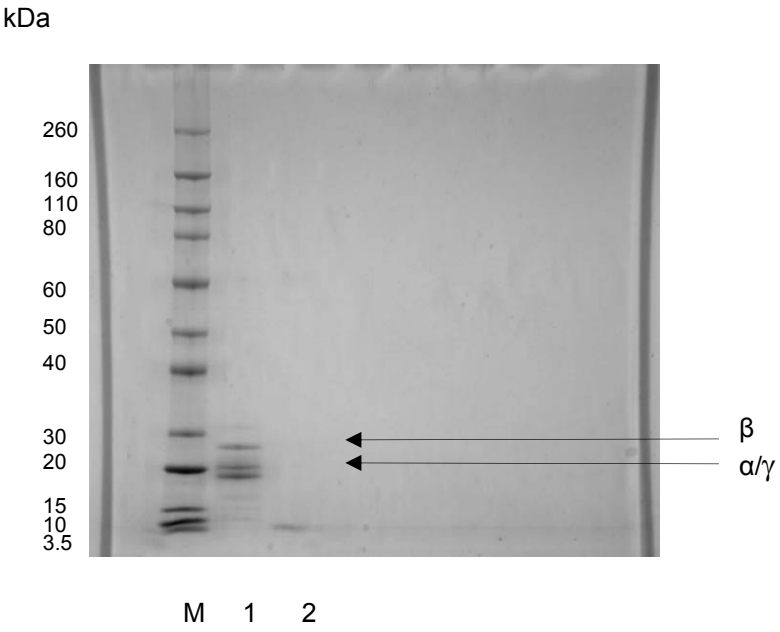

Figure 4.1 *Crude crystallin NuPAGE (reducing) analysis on a Bis-Tris 4-12% gel, 5 µl was loaded at 0.44 mg/ml protein. Lane M = molecular weight marker, Lane 1 = native crude crystallin protein, Lane 2 = crude crystallin fibril supernatant.*

Crystallins are known to have high β-sheet content in their structure. The crystallins have a relatively high affinity for the ThT dye in their native form (Meehan *et al.* 2004) therefore there is a high ThT background reading in the fibrillisation incubation. Time courses on *in situ* fibrillation incubations were not monitored by ThT. However, incubations of crystallins in 10% TFE at pH 2

showed a measurable increase in ThT fluorescence (Figure 4.2 a). The ThT assay observations were supported by TEM examination of the crystallin fibrils which showed a variety of different morphologies (Figure 4.2 b, c, d).

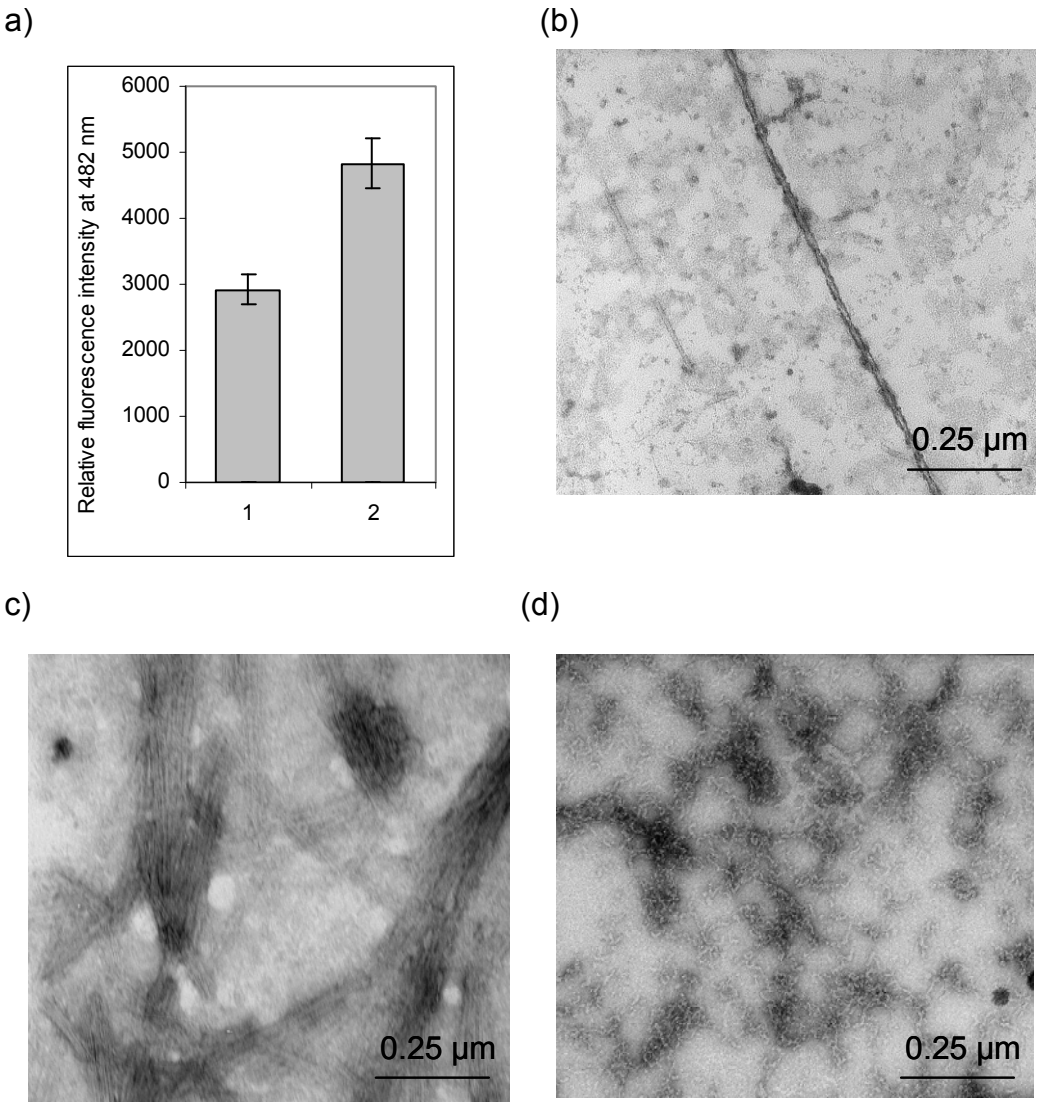

Figure 4.2 *ThT fluorescence (a) and TEM image (b-d) of crude crystallin fibrils, after 4 weeks of incubation at 22 mg/ml in 10% TFE (pH 2) at 60°C. For the ThT assay, samples were assayed in triplicate, Column 1: crystallin control, Column 2: crystallin fibrils. The assay was carried in Tris buffer (pH 7.5) with ThT and the final concentration of crystallin in the assay was 7 mg/ml. Error bars represent the standard deviation of mean. TEM shows (b) twisted fibril, (c) straight fibrils in sheeted conformation and (d) short curly fibril, all obtained from the same sample. Some amorphous aggregates were also observed (picture not shown).*

TEM images in Figure 4.2 (b), (c), (d) show that the fibrils are largely composed of straight and curly fibrils. The long straight unbranching fibrils form from the α-crystallins and short flexible curly fibrils from the β- and γ-crystallin fractions (Garvey *et al.* 2008, Meehan *et al.* 2004). However, the relative concentration of crystallin proteins in crude mixtures may dictate the fibril morphology (Garvey *et al.* 2008). For the purpose of this work, a mixture of morphologies is assumed.

4.2.3 Pre-treatment of fibrils

All fibrils were dialysed at pH 4 (12 mM HCl) with 3 changes of the solution, at room temperature. This was done to minimise the salt in the composites and obtain a consistent pH of 4 (12 mM HCl) at which fibrils were stable. It was found in chapter 3 that pHs above 4 led to the aggregation of insulin fibrils into clumps, which may affect their dispersion in the polymer matrix. Hence all the fibril solutions prepared in this composite study were kept at pH 4. TEM examination of the crystallin and insulin fibrils at pH 4 showed that the fibrils remained unchanged.

Control solutions of the unfibrillised protein were also prepared at 11.4 mg/ml (12 mM HCl, pH 4) as a point of comparison to the fibrillised proteins. Since insulin is insoluble at pH 4, it was dissolved in a minimum volume of 25 mM HCl (pH 2) and made up to volume with pH 4 (12 mM HCl). Crystallin proteins were made up at pH 4 (12 mM HCl) without 10% TFE. All unfibrillised protein will be referred to as protein (insulin/crystallin) control in this chapter and chapter 5.

Additional controls of buffers used for the 2 different protein fibrillisations, HCl and 10% TFE were diluted at pH 4 to obtain control solutions for making control films with PVOH. The diluted solutions will be referred to as no protein (insulin/crystallin) control in this chapter and chapter 5.

4.3 Preparation of Polyvinyl Alcohol for Films

PVOH was chosen to be the polymer matrix for nanocomposite film manufacture in this thesis (described in detail in chapter 1, section 1.8.4). The polymer contains a unit of chemical structure which is represented by (-CH_2CHOH-) (Sakurada 1985). It is a semicrystalline polymer with hydroxyl groups that give rise to intermolecular and intramolecular bonding (Kim *et al.* 2007). The PVOH utilised in this project was partially hydrolysed (86.5-89.0%) and had a MW of 115 kDa. A PVOH aqueous solution (5% w/v) was prepared in water by dissolving PVOH at 80°C. PVOH solutions were used within 3 days of its preparation since the solution gradually became turbid upon standing at room temperature for longer time periods. The turbidity may be indicative of increasing viscosity and secondary bond formation between PVOH chain in the aqueous solution (Sakurada 1985) which had to be minimised by using fresh PVOH solutions.

4.4 Incorporating Proteins into PVOH

Development of a PVOH-fibril composite was based on literature examples of carbon nanotube (CNT) studies, since the incorporation of CNTs into polymers can potentially provide materials with increased modulus and strength (Zhang *et al.* 2003). Polymer-CNT composites can be developed as fibres, films and bulk structures, of which films are one of the predominant materials for development work (Manocha 2006). Of the several ways to disperse nanostructures in polymers (Manocha 2006), a direct mixing of the polymer, PVOH and the amyloid fibrils in solution was chosen to minimise agitation and maintain protein stability.

Solution casting is a small scale laboratory film production process (Petersson and Oksman 2006) which was selected for this study. The method has previously been used for the production of nanocomposites with nano-sized fillers (Petersson and Oksman 2006). In this thesis, a rectangular gel casting tray (7 cm wide x 10 cm length and 1.5 cm in depth) was utilised to obtain an

appropriate sized film (Figure 4.3) for mechanical characterisation in chapter 5. A bubble leveller was used to ensure that all trays were levelled during the solvent evaporation stage to minimise variation in the thickness of films.

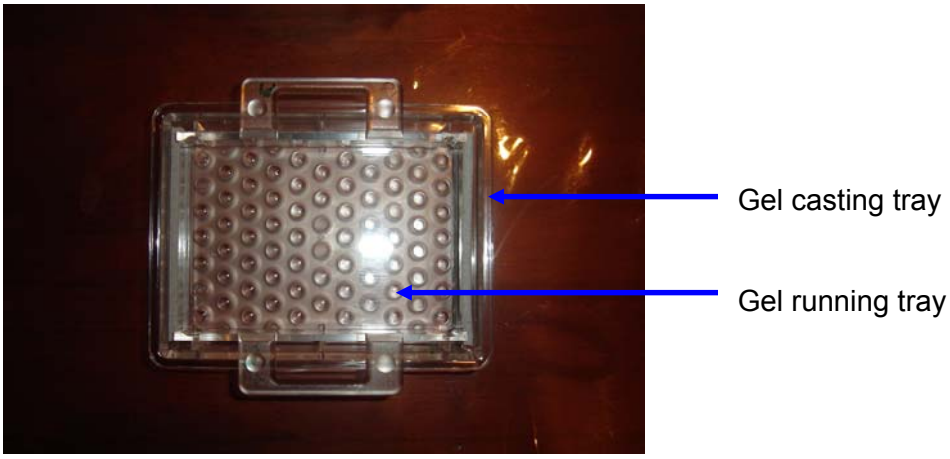

Figure 4.3 *Gel casting tray used to cast films (7 x10 cm).*

Protein amyloid fibril solutions were suspended at pH 4 as obtained after dialysis. The fibrils were then added to 5% PVOH solution (pH~5.8) to obtain a final concentration of 2.5% (w/v) PVOH solution and 0.6% (w/v) fibril. The pH was adjusted with dilute NaOH or dilute HCl to pH 4. Control solutions with and without protein were also mixed with PVOH in the same way, for comparison. The mixtures of PVOH + protein fibrils, PVOH + protein control, PVOH + no protein control were swirled gently for 2 min to obtain a uniform dispersion and poured into separate casting trays. Care was taken to minimise air bubbles during mixing and pouring into casting dishes. The water was then allowed to evaporate and a polymer film was formed over 5 days of evaporation at room temperature. Films were carefully peeled off the casting trays and left to equilibrate at room temperature for 48 hr (Figure 4.4) before further testing. The images show that the PVOH + no protein control and PVOH + protein control film are clear and transparent in comparison to the opaque PVOH + insulin fibril film showing white insulin fibrils dispersed within the film.

All films referred to as hydrated films in this chapter and chapter 5, have been formed by solvent evaporation method (air drying at room temperature) followed by 48 hr equilibration. Any subsequent conditioning or drying of the hydrated films will be specified.

Figure 4.4 *Digital images of 2.5% PVOH composite films: (a) PVOH + no insulin control, (b) PVOH + 0.6% insulin control, (c) PVOH + 0.6% insulin fibrils.*

4.5 Investigating the Impact of Processing Method on Proteins in Nanocomposites

Since there had not been any previous literature reports on the incorporation of protein fibrils into a polymer matrix, it was important to investigate the impact of the polymer-fibril mixing on the protein control and protein fibrils and ensure that the fibrils remained intact. ThT assay, TEM and CR staining with polarising light microscopy were utilised to ascertain if fibrils were retained in the PVOH + fibril films, and whether there was any indication of amyloid formation in the control PVOH + protein control films.

4.5.1 Characterising insulin fibrils in the nanocomposites by ThT and TEM

The ThT assay was carried out on PVOH + insulin mixtures to determine the impact of processing on the insulin fibrils and insulin control. Figure 4.5 shows the intensity of ThT fluorescence and suggests that the dialysis and mixing of insulin fibrils with PVOH did not affect the β-sheet content (columns 4 and 5). Similarly the insulin control was not affected by the steps involved in preparing a PVOH-native insulin mixture, since the ThT fluorescence remained negligible (columns 1 and 2), pre and post PVOH mixing.

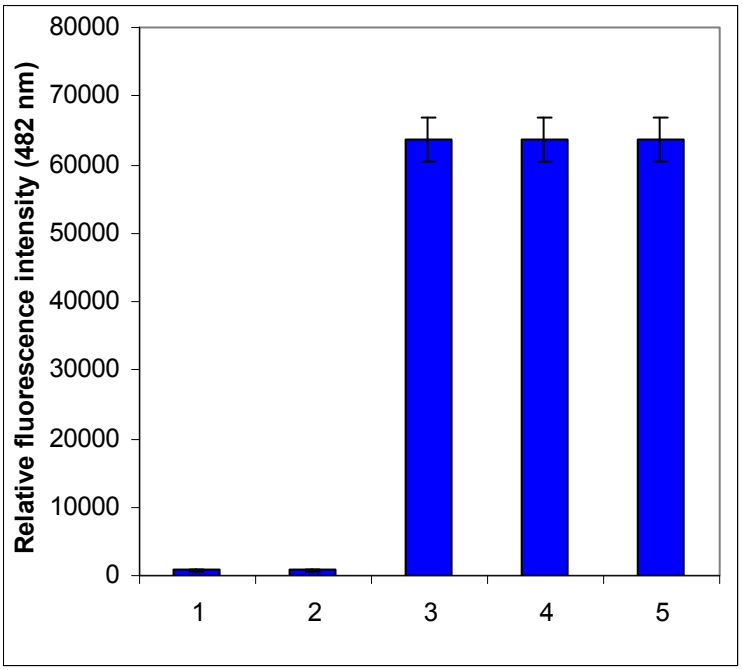

Figure 4.5 *ThT assay of casting solutions with insulin control and insulin fibrils, with and without PVOH. Lane 1: 0.6% insulin control, Lane 2: 2.5% PVOH + 0.6% insulin control, Lane 3: 0.6% insulin fibrils before dialysis, Lane 4: 0.6% insulin fibrils after dialysis in 12 mM HCl, Lane 5: 2.5% PVOH + 0.6% insulin fibrils. All PVOH + protein solutions were made up with dialysed protein solutions at pH 4. Insulin fibrils were prepared in 25 mM HCl (100 mM NaCl, pH 1.6), at 60°C for 24 hr. ThT assay was carried out* in situ *on the plate reader, in triplicates, with 198.4 µl of protein solution and 1.6 µl of (2.5 mM) ThT in the wells.*

The TEM micrographs of the two composite solutions from Figure 4.5 (Lane 2 and 5) prior to casting are shown in Figure 4.6. In the images, observation of the proteins and protein nanofibres is made particularly difficult by the presence (and thickness) of the PVOH, which strongly reduces the image contrast. Figure 4.6 (a) shows that native insulin is present in the form of dark globular aggregates in the films. Figure 4.6 (b) shows dark contrast, which may have a nanofibre network, but the image is not distinct. However, further characterisation of the composite solutions was carried out using CR and examination of films under cross polarised light.

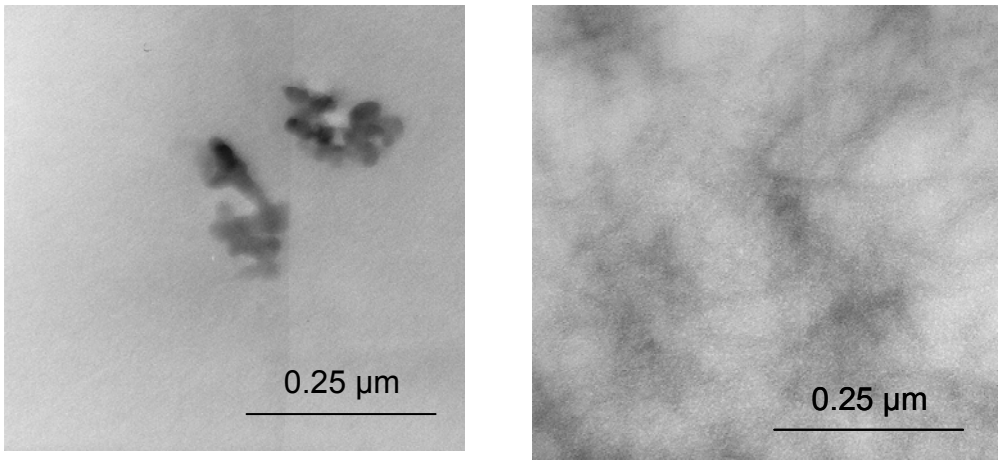

Figure 4.6 *TEM analysis of the 2.5% PVOH composite mixture. (a) PVOH + 0.6% insulin control, (b) PVOH + 0.6% insulin fibrils. Insulin control and fibrils had been dialysed before mixing with PVOH.*

4.5.2 Using CR to detect amyloid in PVOH nanocomposites

Further attempts were made to investigate the stability of insulin control and insulin fibrils in PVOH films using CR, which has a structure as shown in Figure 4.7. CR dye is a diazo dye of symmetrical structure (Puchtler *et al.* 1962) which forms hydrophobic interactions with the β-sheets of the fibrils (Westermark *et al.* 1999). Light microscopic studies demonstrated that the birefringence of amyloid deposits increases intensely after staining with CR (Puchtler and Sweat 1965).

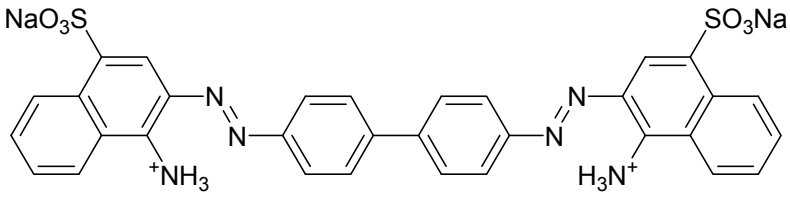

Figure 4.7 *The structure of Congo red.*

Insulin (control and fibrils) solutions were stained with CR dye prior to mixing with PVOH and casting. Staining was carried out by adding CR at 1 mg/ml to the solutions used to make the protein control and protein fibrils respectively. The solutions were allowed to equilibrate for 30 min to allow the CR to bind. The protein solutions were dialysed to remove any unbound CR. Figure 4.8 shows the PVOH films with insulin fibrils at varying levels.

(a) (b) (c) (d)

Figure 4.8 *2.5% PVOH-insulin fibrils composites with CR in casting dishes, while the water was evaporated from the solutions. (a) PVOH + no fibril control, (b) PVOH + 0.2% insulin fibrils, (c) PVOH + 0.4 % insulin fibrils, (d) PVOH + 0.6% insulin fibrils.*

Films composed of PVOH + no protein control, PVOH + insulin control, PVOH + insulin fibrils with CR were viewed with a light microscope fitted with a cross polarising lens. The CR dye emits a bright yellow-green birefringence under polarised light when bound to amyloid fibrils (Puchtler and Sweat 1965) . Figure 4.9 demonstrates the CR binding on 2.5% PVOH films with and without the insulin fibrils and insulin control. PVOH + no protein control films showed no

yellow-green birefringence observed in the controls when examined under unpolarised light.

The films with insulin fibrils (Figure 4.9 f) showed yellow-green birefringence under the cross polarised lens, confirming the presence of amyloid fibrils in the films. No yellow-green birefringence was observed for PVOH + insulin control films under cross polarised light (Figure 4.9 d). The film manufacture method did not induce fibrillation of the insulin control. Similarly the PVOH + no protein control film showed no amyloid present (Figure 4.9 b).

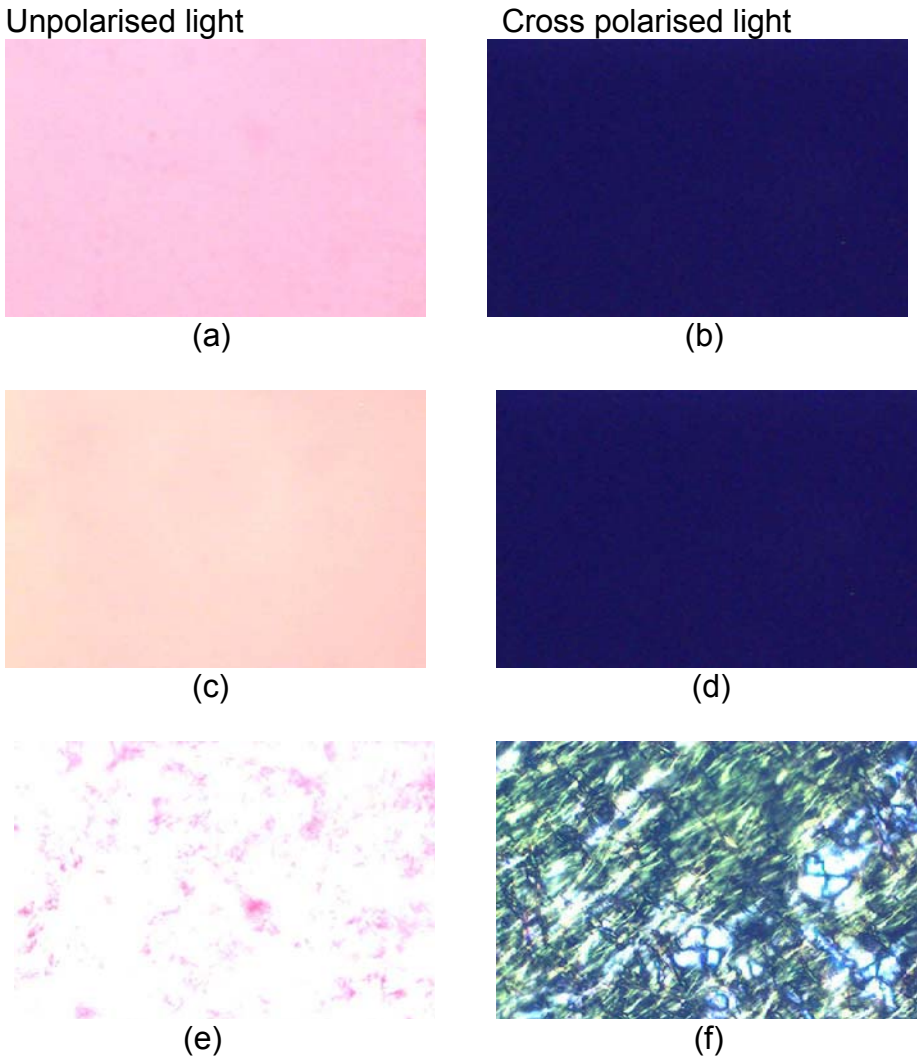

Figure 4.9 *PVOH films when viewed under unpolarised and cross polarised lens. Images are at 40x magnification: (a) and (b) PVOH + no protein control + CR, (c) and (d) PVOH + insulin control + CR, (e) and (f) PVOH + insulin fibrils + CR. Fibrils were prepared in HCl (25 mM HCl, 100 mM NaCl). Protein solutions were dialysed and the buffer was diluted at pH 4.*

The impact of film manufacture method on crude crystallin protein was also assessed by CR. Figure 4.10 shows that the PVOH + crystallin fibrils (Figure 4.10 d) do not show a yellow-green birefringence similar to the crystallin control films. This can be attributed to the low concentration of fibrils in the crystallins and CR requires a significant level of amyloid fibrils to be able to bind. However, CR served as a diagnostic tool for *in vitro* detection of amyloid in polymer nanocomposites such as PVOH + insulin fibril film method development work.

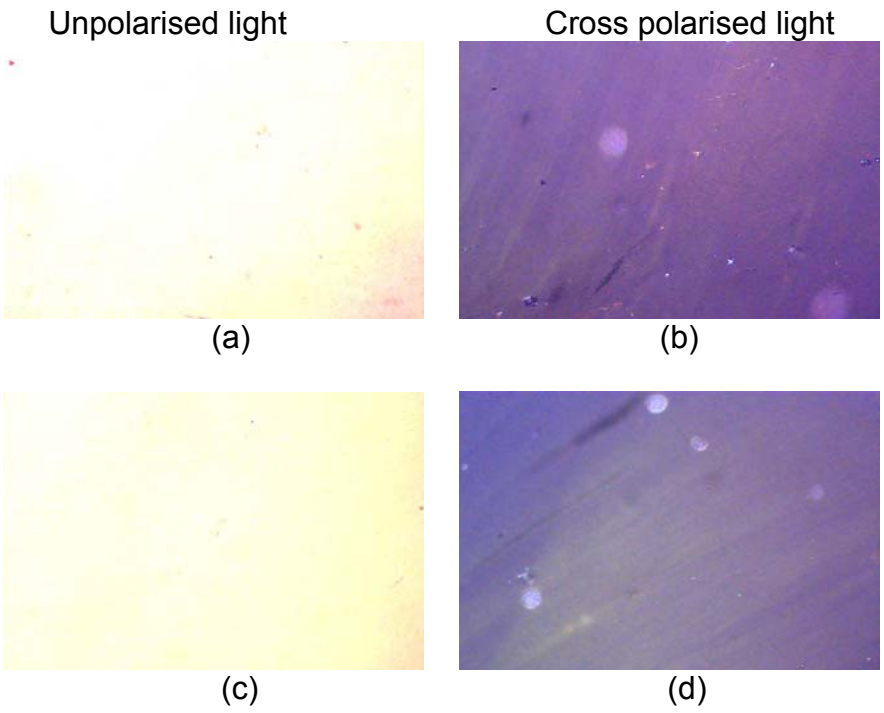

Figure 4.10 *2.5% PVOH films when viewed under unpolarised and cross polarised lens. Images were taken 10x magnification: (a) and (b) PVOH + crystallin control + CR, (c) and (d) PVOH + crystallin fibrils + CR. Fibrils were prepared in 10% TFE and final concentration in the films were 0.6%. Protein solutions were dialysed and the buffer was diluted at pH 4.*

.

4.6 Background on Polymer Mechanical Properties

In this thesis, efforts were made to measure the impact of protein nanofibres on PVOH mechanical properties since promising results have been found by introducing other nanostructures in polymer systems (Aoi *et al.* 2000a, Aoi *et al.*

2000b, Bhattacharyya *et al.* 2006, Bhattacharyya *et al.* 2005, Safadi *et al.* 2002, Zhang *et al.* 2003). The mechanical properties of interest generally comprise the polymer strength, elongation, modulus and toughness, which measure how well a material resists deformation. To measure these properties, the composite has to be placed under stress and its response to the stress characterised. This can be done by tensile strength measurement and thermo-mechanical analysis, which are widely employed to measure the mechanical properties of composites (Aoi *et al.* 2000a, Bhattacharyya *et al.* 2006, Bhattacharyya *et al.* 2005, Cadek *et al.* 2004, Chang and Kim 2007, Mi *et al.* 2007, Park *et al.* 2001, Peng *et al.* 2007, Ryan *et al.* 2006, Safadi *et al.* 2002, Zhang *et al.* 2003).

Strength is measured by the force that is needed to break a sample, and more specifically tensile strength refers to the force required when the material is under tension (Sionkowska 2005). The tensile strength in this study was measured on an Instron Universal Testing Machine (UTM) (Figure 4.11), where the machine stretches the sample and it measures the amount of force that it is exerting and the stress (force/cross sectional area) that the sample is experiencing.

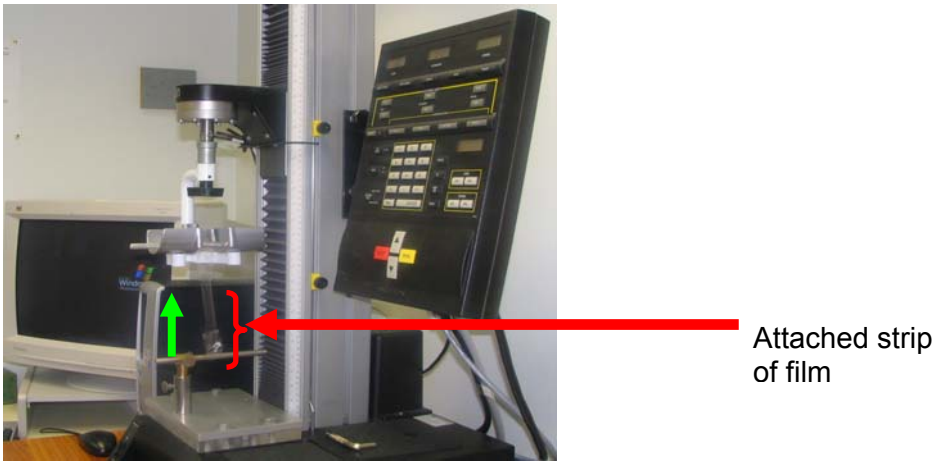

Figure 4.11 *Image of Instron (UTM) testing machine showing a film strip attached for uniaxial elongation (green arrow).*

The UTM continues to increase the amount of force, and stress, on the sample until it breaks. The force needed to break the sample is the tensile strength of the material. The elongation is a type of deformation that a material undergoes under stress and the toughness is the amount of energy that is needed to break a sample, measured by the area under the stress-strain curves. Figure 4.12 shows a force-extension curve, normally obtained by an UTM, demonstrating 3 types of curves with distinctive material properties. The curve shows that a strong material can be identified by a large force and a minor extension while a strong material may possess a large force and extension. Weak materials are signified by a small increase in force with a large extension. Figure 4.12 also indicates that the dynamic mechanical analysis (DMA) testing (described below and in chapter 5) is done at low force regions.

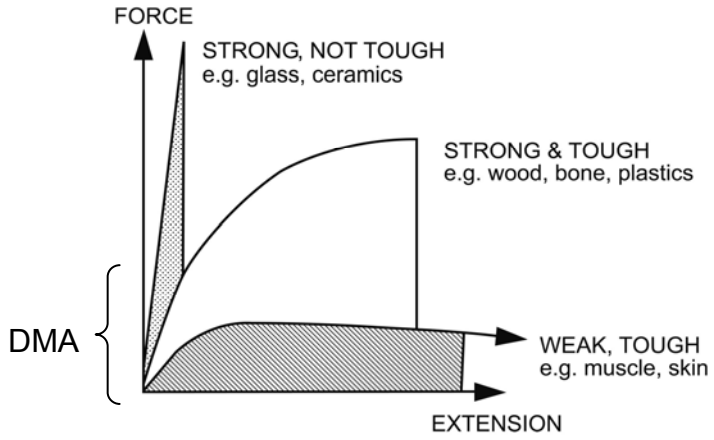

Figure 4.12 *Nominal force-extension plot showing several materials of contrasting strength and toughness from (Rosenthal 1999).*

The mechanical properties of nanocomposites are dependent on the interface between nanostructures and their matrix (Adam and Alan 2001). This is because the nanostructures have a high surface area. Studies have shown that some types of CNTs provide better nanotube-matrix adhesion than others (Manocha 2006). A good adhesion allows effective stress transfer from the nanostructures to the polymer, for example in PVOH/CNT composites (Cadek *et al.* 2002). Hence the mechanical properties of bionanocomposites such as

the PVOH + protein fibril films may also depend on the extent of stress transfer between the PVOH and the protein.

In preliminary experiments, the direct impact of the protein (0.2%-0.6%) on the PVOH polymer was evaluated by the tensile strength and strain to failure on an UTM. The stress-strain curve provides information on the strength, elongation and toughness of the films and forms the preliminary discussion in this chapter (sections 4.7.1, 4.9 and 4.10.2) and provides baseline data for the DMA work.

More detailed information about the behaviour of the films was obtained by DMA analysis (Figure 4.13). DMA testing is relevant to the initial slope of the stress-strain test profile obtained from the UTM (Figure 4.12) (Staiger, pers. comm.). The slope of the initial curve represents the elastic modulus of the material, which under tension is the Young's modulus (Nielsen 1974). DMA analysis is most useful to study polymer viscoelasticity, because polymers are partially elastic and partially viscous (Nielsen 1974). They exist in 2 distinct states with different physical properties: at low temperatures they exhibit the glass state, the material is hard and rigid, but at high temperatures a rubbery state is exhibited, which is flexible and extendible. Thus DMA is carried out over a range of temperatures.

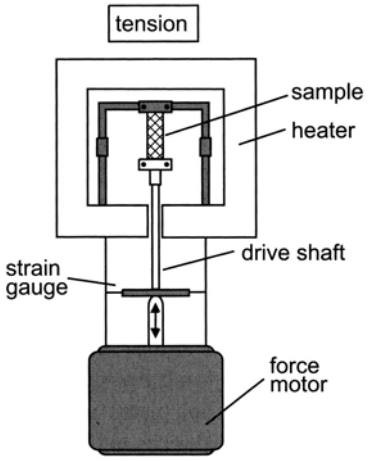

Figure 4.13 *A schematic of a DMA showing the test arrangement in tension mode, from (Ehrenstein* et al*. 2004).*

During the DMA test, an oscillating force is applied continuously to a sample and the resulting displacement of the sample is measured. Sample deformation under oscillating load is monitored against time, temperature or frequency of oscillation and the sample storage modulus (E′) and loss modulus (E″) and loss factor Tan δ are obtained (Figure 4.14). E′ is directly associated with elastic response and is a measure of the stiffness of the material (Yang *et al.* 2004) and E″ measures the energy dissipated per cycle of vibration. The ratio of E″/E′ is the loss Tangent (Tan δ), which describes the damping properties of a material. A high Tan δ is characteristic of a material with non-elastic behaviour, while a low value of Tan δ is characteristic of a more elastic material. Since Tan δ measures the ratio of energy dissipated to maximum energy stored, a decrease in Tan δ means more energy is stored in the material (Yang *et al.* 2004). The maximum value of the Tan δ or E″ modulus is the glass transition temperature T_g (Ehrenstein *et al.* 2004), which defines the limit between the glassy and the rubbery state (Roos and Karel 1991).

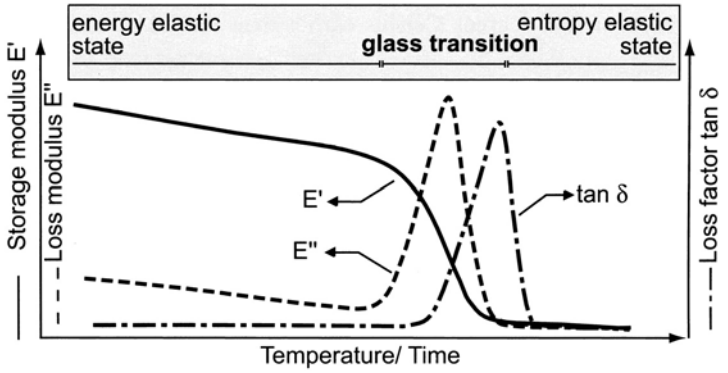

Figure 4.14 *A diagram showing the typical DMA curves for an amorphous polymer, from (Ehrenstein* et al*. 2004).*

Thus DMA was used to obtain information as to whether protein addition affects the mechanical relaxation processes of the PVOH films. The impact of both insulin and crude crystallin proteins was determined at a level of 0.6%, in a 2.5% PVOH film. Experiments were conducted by increasing the DMA temperature at 2°C/min at a constant deformation frequency of 1 Hz, under stress in tension (stretching) mode. Initial tests were carried out at a wide

temperature range of -150°C to 150°C but were narrowed to 25°C to 150°C since the desired PVOH profiles were obtainable within this range. The DMA data were supplemented by characterisation with differential scanning calorimetry-thermogravimetric analysis (DSC-TGA), X-ray diffraction (XRD) and scanning electron microscopy (SEM) imaging.

4.7 Characterisation of PVOH Films

Preliminary studies on PVOH films were based on preparing hydrated PVOH films without any additives.

4.7.1 Effect of film thickness on tensile strength

In the initial studies, a series of experiments were done to develop a reliable film casting method. The moisture level (measured by % weight loss on drying) was found to be 10 ± 3% for all the hydrated films tested in this section. During the method development work, PVOH films were cast at varying thicknesses (0.03-0.08 mm). Tensile testing of 2.5% PVOH films showed that the thickness of the films affected the stress and elongation of the samples (Figure 4.15). As the thickness of the films increased, from 0.03 mm to 0.08 mm, the stress values decreased while the elongation increased (Figure 4.15 a and b). A decrease in stress occurred when the thickness of films was further increased from 0.08 to 0.12 mm but the elongation increased further (Figure 4.15 a and b). The linear increase in % elongation values with increasing film thickness is in agreement with the results obtained with whey protein isolate films (Longares *et al.* 2004).

Film thickness is one of parameters that could affect physicochemical properties of the films, such as gas permeability (McCaig and Paul 2000) and mechanical properties (Jansson and Thuvander 2004). The data suggested that the thick PVOH films were more flexible than the thin films. The decrease in film strength with thickness was unexpected since stress is a measure of force per cross section area of specimen, which is predicted to be proportional to film thickness. However, the results were in agreement with the previous studies (Jansson and Thuvander 2004, Pongjanyakul and Puttipipatkhachorn 2008). The higher

strength of thin films than the thick films, may have been due to higher crystallinity of the thin films (Pongjanyakul and Puttipipatkhachorn 2008).

(a)

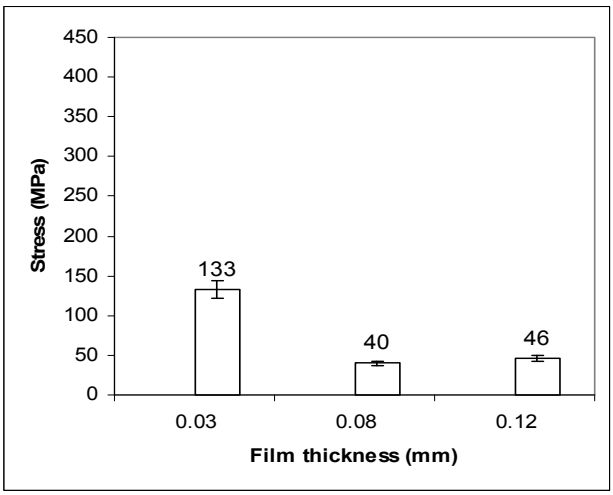

(b)

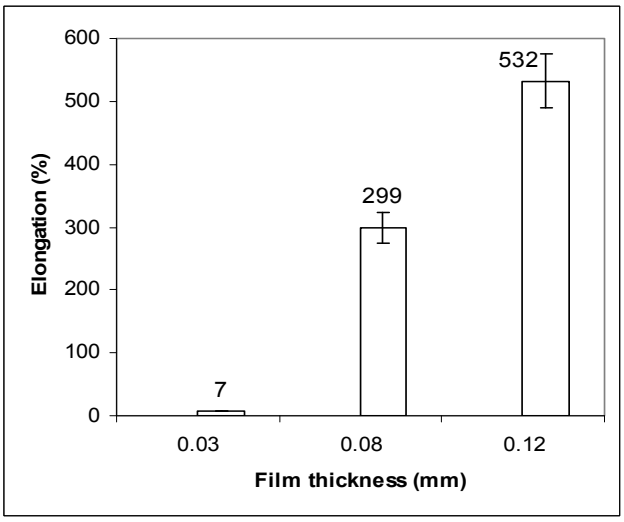

Figure 4.15 *Effect of film thickness on the stress (a) and elongation (b) of 2.5 % PVOH films. Films were dried for 5 days at ambient conditions and tested in replicates of five; Data show average values with % standard error of the mean.*

4.7.2 Impact of moisture on the viscoelastic behaviour of PVOH films

Preliminary testing of hydrated PVOH film without any additive encountered reproducibility issues in the UTM and DMA data for replicate samples. This was thought to be due to water in the PVOH films. Attempts were therefore made to improve reproducibility by vacuum drying the films and measuring the impact on

the viscoelastic behaviour. Thus vacuum dried films will be referred to as dried films in this chapter and chapter 5.

4.7.2.1 Drying

Films were dried in a vacuum oven at 60°C for 0 hr to 72 hr to determine the loss of moisture over time. Figure 4.16 shows that a plateau is reached after 16 hr of drying films, after which no further loss of water from the PVOH film was observed. Consequently, films were vacuum dried for at least 24 hr at 60°C when measuring the mechanical properties for dry films.

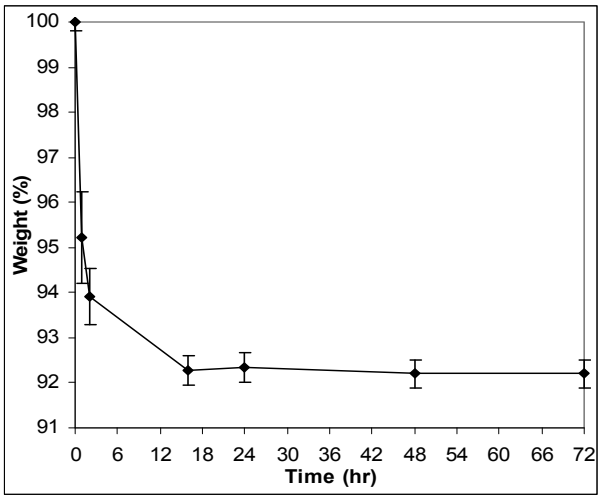

Figure 4.16 *Effect of drying 2.5% PVA films at 60°C in a vacuum oven, over time. Samples in triplicate were obtained from three films cast separately and 9 strips of films were tested. Error bars represent standard deviation of the 9 measurements.*

4.7.2.2 Impact on viscoelasticity

DMA analysis of hydrated and dried PVOH films without any additives was carried out as a function of drying time (Aoi *et al.* 2000b, Park *et al.* 2001). Figure 4.17 (a), (b) and (c) provide evidence that all the parameters, stiffness, loss modulus and the Tan δ profiles of PVOH films are affected by the water content. The stiffness (Figure 4.17 a) and the loss modulus (Figure 4.17 b) increased with the length of drying and decreasing hydration. The increase in Tan δ intensity in Figure 4.17 (c) suggests an increase in molecular slippage within the films (Nielsen 1974).

a)

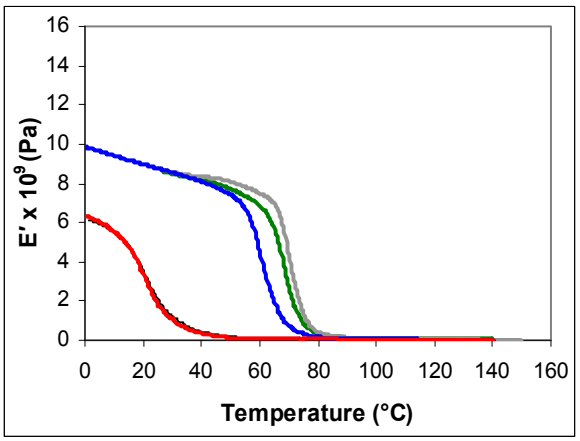

b)

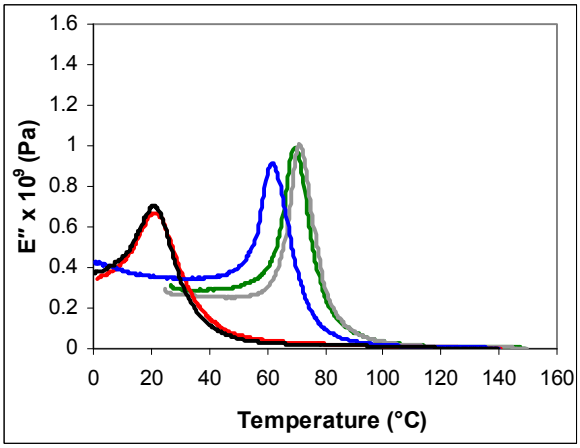

Time (hr)	T_g (°C)
0	23 ± 0.1
5	23 ± 0.1
16	64 ± 0.1
24	73 ± 0.2
48	73 ± 0.2

(c)

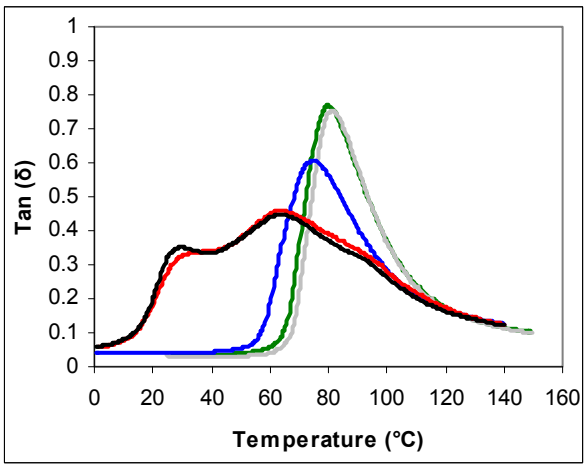

Figure 4.17 *E' curve (a) and E" curve (b) and Tan δ (c) of 2.5% PVOH films measured by DMA. Graph represents samples which have been dried for 0 hr (black), 5 hr (red), 16 hr (blue), 24 hr (green) and 48 hr (grey). Films were dried at 60°C in a vacuum oven. The T_g is the value indicated by the peaks of E" curves (b).*

The T_g was determined from the peak of the E″ curve (Ehrenstein *et al.* 2004) and was found to increase from 23°C in the hydrated films, to 73°C for dried PVOH films. T_g increased with the length of drying time to a maximum T_g value of 73°C. The T_g values obtained for the dried films in this experiment are similar to the literature, where the T_g of PVOH was reported to be between 68-85°C (Aoi *et al.* 2000b, Cassu and Felisberti 1999, Park and Russell 2001, Sakurada 1985).

Figure 4.17 (c), also shows that moisture/level of hydration affects the shape of the DMA (Tan δ) curves. Water can act as a plasticiser and cause the T_g to shift to lower temperatures (Ehrenstein *et al.* 2004). To standardise the effect due to differing moisture levels, films were dried prior to mechanical testings.

4.8 Impact of Fibril Forming Solutions on PVOH Films

Since HCl and TFE were utilised in the preparation of the protein fibrils, it was necessary to determine the impact of these compounds on PVOH films. The 25 mM HCl (100 mM NaCl) and 10% TFE solution were diluted with 12 mM HCl (pH 4) to simulate the dialysis of the protein fibrils.

4.8.1 Visual examination

PVOH films prepared were examined to determine the impact of TFE and HCl on the visual characteristics of the films. It was found that the PVOH films with added water and no protein controls (12 mM HCl) were similar with a uniform and clear appearance. The 10% TFE did not affect the appearance of PVOH films. However, the addition of undiluted solution used to make insulin fibrils (25 mM HCl, 100 mM NaCl, pH 1.6) led to the rough and uneven appearance of a film (Table 4.1). This may be due to the low pH or the sodium ions.

Film samples	Visual
PVOH + water	Clear, smooth surface
PVOH + HCl (25 mM HCl, 100 mM NaCl)	Clear, with roughness in mid regions on both sides
PVOH + diluted HCl (12 mM HCl)	Clear, smooth surface
PVOH + 10% TFE	Clear, smooth surface
PVOH + diluted TFE (12 mM HCl)	Clear, smooth surface

Table 4.1 *Comparing the impact of buffers on PVOH film characteristics.*

4.8.2 Thermal analysis: viscoelastic behaviour

DMA analysis was performed on dried PVOH films: (1) PVOH + no insulin control, (2) PVOH + no crystallin control, (3) PVOH + no insulin with 25 mM HCl (100 mM NaCl), and (4) PVOH + no crystallin with 10% TFE. The stiffness, loss modulus and the Tan δ profiles are shown in Figure 4.18 (a), (b) and (c). The PVOH + no crystallin, and PVOH + no insulin, control films had higher stiffness compared to the films with undiluted HCl and TFE. The T_g of both the no protein control films were found to be at 72°C. The 10% TFE, lowered the T_g of PVOH to 67°C. Overall, Figure 4.18 confirms that the dialysis of protein solutions is ideal to minimise their impact on the viscoelastic behaviour of the PVOH films.

4.8.3 Thermogravimetric analysis

Another technique that is useful to determine the thermal stability of materials, is thermogravimetric analysis (TGA) (Ehrenstein *et al.* 2004). TGA was carried out on all film samples in this study using a simultaneous DSC-TGA. It involved a continuous weight measurement as the film sample temperature increased from 25°C to 600°C at 10°C/min in an inert nitrogen environment. Preliminary TGA was carried out to assess the impact of the solutions used to make protein fibrils (25 mM HCl (100 mM NaCl) and 10% TFE) on the thermal stability of the nanocomposite system.

(a)

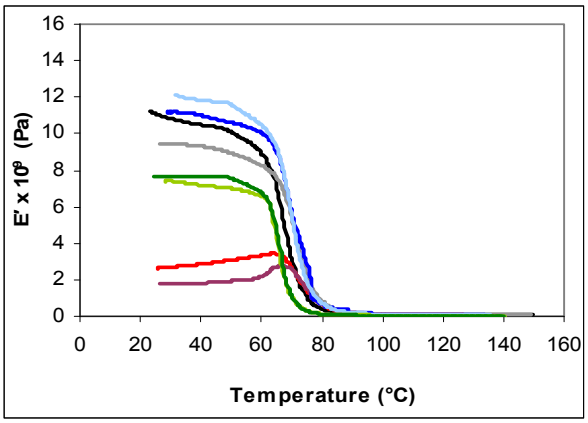

(b)

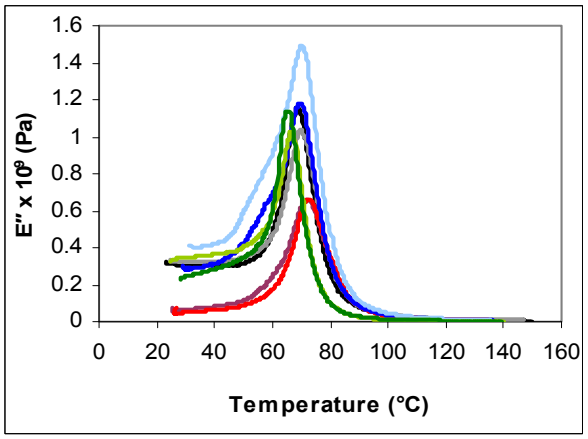

Sample	T_g (°C)
PVOH + no insulin control	72 ± 0.2
PVOH + no crystallin control	72 ± 0.2
PVOH + no insulin with 25 mM HCl (100 mM NaCl)	72 ± 0.2
PVOH + no crystallin with 10% TFE	67 ± 0.1

(c)

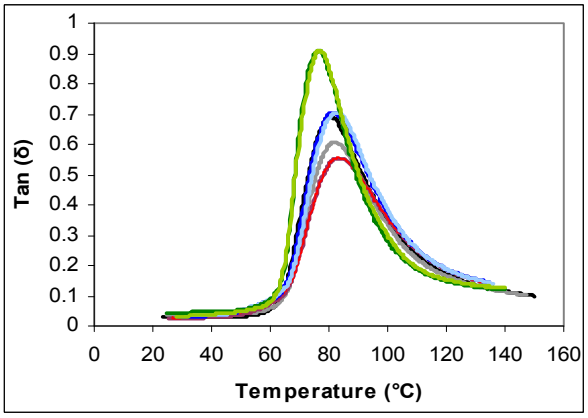

Figure 4.18 *(a) E' curve, (b) E" curve and (c) Tan δ of 2.5% PVOH + no protein control films and PVOH + no protein with 10% TFE or 25 mM HCl (100 mM NaCl) measured by DMA. Sample are: PVOH + no insulin control replicate 1 (black) and replicate 2 (grey), PVOH + no insulin with 25 mM HCl (100 mM NaCl) replicate 1 (red), replicate 2 (plum), PVOH + no crystallin with 10% TFE replicate 1 (green), replicate 2 (lime green), PVOH + no crystallin control replicate 1 (blue), replicate 2 (pale blue). Samples had been dried at 60°C in vacuum oven for 24 hr. The T_g is the value indicated by the peaks of E" curves (b).*

The degradation temperature for each sample was determined from the slope of the TGA profiles, using the TGA computer software SDT 800 V20. Table 4.2 shows that PVOH has a degradation temperature from 288 to 293 ± 2°C, in the PVOH + water film and PVOH + no insulin control and PVOH + no crystallin control films. The solutions used to make protein fibrils in this study did not affect the degradation temperature of PVOH films. However, the undiluted 25 mM HCl (100 mM NaCl) led to a decrease in the thermal stability of the PVOH to 280°C. The decomposition temperature of PVOH decreased further on the addition of 10% TFE (pH 2).

Samples	**Degradation Temperature (°C)**
PVOH + water film	293 ± 1
PVOH + no insulin with 25 mM HCl (100 mM NaCl) film	280 ± 3
PVOH + no insulin control film	290 ± 1
PVOH + no crystallin with 10% TFE film	240 ± 2
PVOH + no crystallin control film	288 ± 2

Table 4.2 *Effect of buffers on the thermal degradation temperature of PVOH films.*

4.9 Impact of Proteins on the Tensile Properties of Hydrated PVOH films

Preliminary tensile studies on the UTM, were based on measuring the impact of adding 0.2% fibrils to PVOH films. A low amount of fibrils were used initially to observe its impact on the strength of PVOH.

The impact of the incorporation of 0.2% insulin and crystallin into 2.5% PVOH films is shown in Figure 4.19. The stress of PVOH films without any protein was found to be 133 ± 14 MPa. The stress of the PVOH films was lowered with the addition of insulin control. There was no significant change in the stress of the PVOH film with the addition of insulin fibrils (Figure 4.19 a). The elongation of

the PVOH films was increased with the addition of native insulin as well as insulin fibrils (Figure 4.19 b); however the increase conferred by the insulin control was substantial compared to insulin fibrils.

(a)

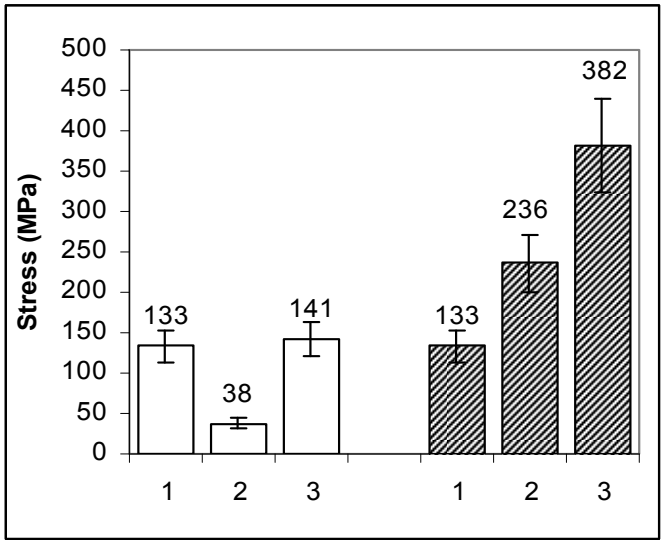

(b)

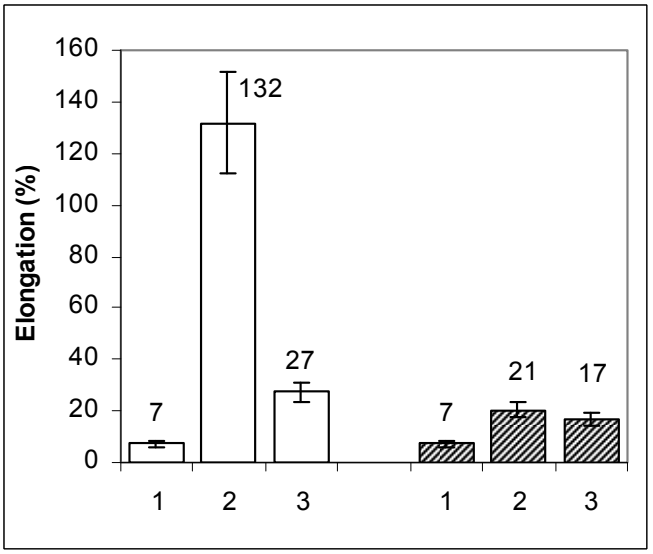

Figure 4.19 *Effect of 0.2% insulin on 2.5% PVOH films tensile properties (a) stress and (b) elongation. In both graphs: unshaded bars = insulin, shaded bars = crystallin proteins and the columns represent, PVOH + no insulin/crystallin control (Column 1), PVOH + protein control (Column 2), and PVOH + protein fibrils (Column 3). Films were 0.03 mm in thickness. Error bars represent % standard deviation of mean.*

In contrast to the impact of insulin on the behaviour of PVOH films, the crystallins caused a significant increase in the stress of the films, in both the control and fibrillised form with more stress conferred by the fibrillised protein. The elongation of the PVOH films was also increased by the addition of the crystallin protein, though by a lower amount that the insulin control.

The addition of insulin control caused PVOH films to become more elongated than the rest of the composites. The large increase in the stress caused by the addition of crystallin fibrils is a promising result and suggests that crystallins may increase the strength of PVOH films.

4.10 The Impact of Insulin Addition on PVOH Films by DMA

Insulin was added at a higher concentration of 0.6%, to determine its impact on the PVOH film mechanical properties. The level of insulin fibrils in the PVOH matrix was increased from 0.2% in the preliminary study (section 4.9) to 0.6% since nanocomposite studies with CNTs show incorporation of CNTs at significantly higher levels for investigations on their effect on PVOH films (Safadi *et al.* 2002, Zhang *et al.* 2003). The costs associated with bovine insulin allowed a maximum of 0.6% to be incorporated into the PVOH films for this study. The viscoelastic properties were measured in both the hydrated and dried states of the films.

4.10.1 Viscoelastic properties of hydrated films

Figure 4.20 a and b show that the stiffness and the loss modulus, E″ profile of PVOH shift toward a higher temperature region, due to the addition of the insulin, in both the control and the fibril form. This is indicative of an increase in the T_g of PVOH (Figure 4.20 b) and suggested that the PVOH required a higher temperature to transit from a glassy to a rubbery polymer, due to the presence of insulin in the films. The decrease in stiffness due to the insulin addition (Figure 4.20 a) shows that the insulin is making the PVOH films less stiff compared to the PVOH without insulin.

(a)

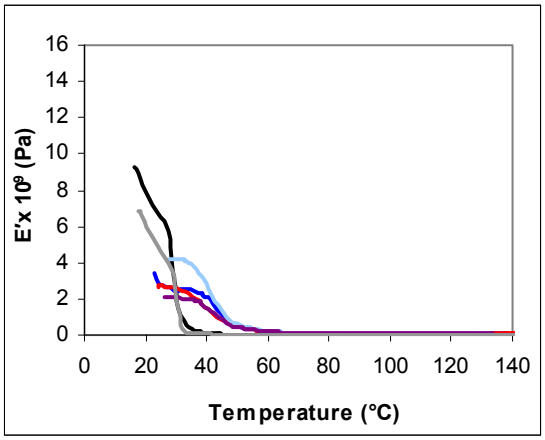

Sample	E′ at 30°C (x10^9) Pa
PVOH + no insulin control	6.3 ± 1.3
PVOH + 0.6% insulin control	4.0 ± 1.8
PVOH + 0.6% insulin fibrils	2.0 ± 0.4

(b)

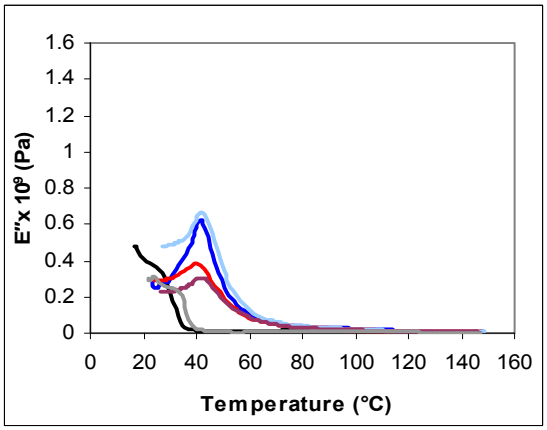

Sample	T_g (°C)
PVOH + no insulin control	30 ± 3
PVOH + 0.6% insulin control	42 ± 0.3
PVOH + 0.6% insulin fibrils	42 ± 1

(c)

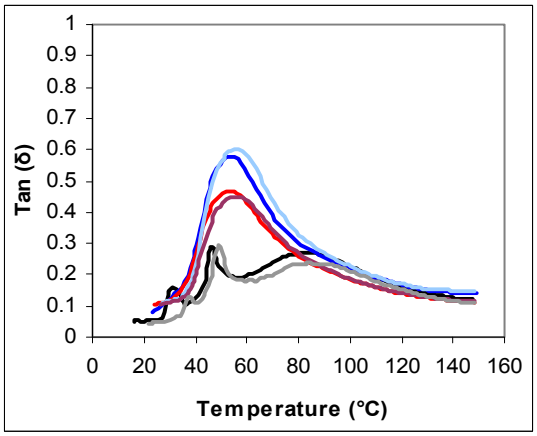

Sample	Tan δ at 57°C
PVOH + no insulin control	0.17 ± 0.5
PVOH + 0.6% insulin control	0.58 ± 0.1
PVOH + 0.6% insulin fibrils	0.45 ± 0.1

Figure 4.20 *(a) E' curve, (b) E" curve and (c) Tan δ curve of 2.5% PVOH films with and without insulin measured by DMA. Graph represents hydrated film samples, PVOH + no insulin control (black and grey), PVOH + 0.6% insulin control (blue and pale blue) and PVOH + 0.6% insulin fibrils (red and plum). The E' values at 30°C (a), T_g values from E" peak (b) and the Tan δ intensities (c) are tabulated at the respective curves.*

The effect of insulin control and insulin fibrils on the value of Tan δ is shown in figure 4.20 c. The Tan δ peaks observed for PVOH + insulin control/fibril films show that their Tan δ intensities are higher (40°C-77°C) than those obtained for PVOH + no insulin control. This suggested that the hydrated PVOH + insulin films had more molecular slipping than PVOH + no insulin control films. However, PVOH + insulin fibril films had a lower Tan δ when compared to the PVOH + insulin control, which suggested that the PVOH with insulin fibrils may possess a lower extent of molecular slipping than PVOH with insulin control.

4.10.2 Dried films

The results obtained earlier in Figure 4.17 suggested that the moisture in the films were having an effect on thermal analysis, hence the PVOH films with insulin were also dried under vacuum prior to analysis. The hydrated films were cut into 60 mm x 7 mm rectangular strips, dried in a vacuum oven at 60°C for 24 hr before tensile testing.

4.10.2.1 Effect on tensile strength

Figure 4.21 (a) and (b) show data on the effect of insulin (control and fibrils) on the dried PVOH film tensile properties. The stress was increased with the addition of insulin control to the dry PVOH film but was reduced with the fibril addition (Figure 4.21 a) in contrast to the results obtained with the hydrated films with 0.2% insulin (Figure 4.19). This suggested that the insulin fibril addition reduced the strength of the PVOH films. The PVOH film elongation was markedly reduced upon insulin addition (Figure 4.21 b).

(a)

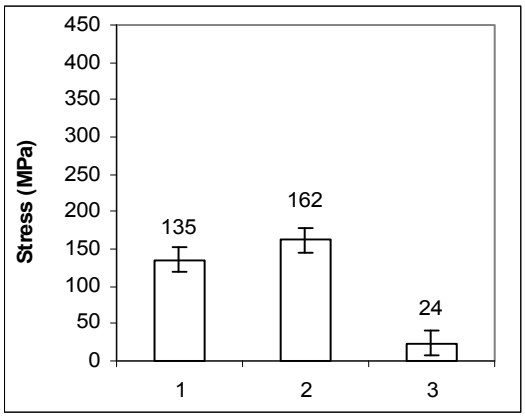

(c)

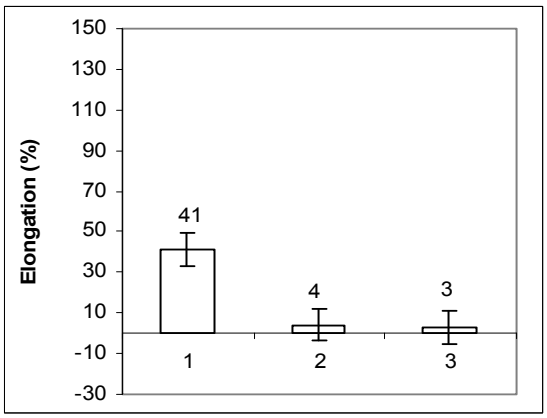

Figure 4.21 *Effect of 0.6% insulin on 2.5% PVOH films tensile properties: (a) stress and (b) elongation. Graph (a) and (b) show: (Lane 1) PVOH + no insulin control, (Lane 2) PVOH + insulin control, (Lane 3) PVOH + insulin fibrils. Data values are an average of triplicate measurements and error bars represent standard deviation of the mean. Samples had been dried at 60°C in vacuum oven for 24 hr.*

Interestingly, the PVOH film behaviour changed from a tough hydrated film (Figure 4.19) to a brittle dried film (Figure 4.21). These findings suggest that water may affect the elongation properties of the PVOH + insulin control/fibril film.

4.10.2.2 Effect on viscoelastic properties

PVOH + no insulin control, PVOH + insulin control and PVOH + insulin fibrils films were tested on the DMA to analyse the impact of 0.6% insulin on dried PVOH films. Figure 4.22 (a) shows the storage moduli of PVOH and various composites. The stiffness of the PVOH + no protein control film (< T_g) was

reduced by the addition of the insulin. The T_g of the PVOH + no protein control films did not change with the addition of insulin (Figure 4.22 b). The Tan δ of PVOH + no protein control film (>T_g) was reduced with the addition of insulin in Figure 4.22 (c). This suggested that the PVOH + insulin (control/fibril) films have a lower extent of molecular slippage within the films. Compared to the PVOH + insulin control film, the decrease in the mobility was more significant for PVOH + insulin fibril films.

4.11 Impact of Insulin on Hydrated PVOH Film Structure

Since film mechanical behaviour is related to its structure, the PVOH films with insulin were examined visually and by SEM to further understand the impact of addition of insulin to the films

4.11.1 Visual examination

The addition of insulin to PVOH caused a difference in the appearance of the PVOH control films (Table 4.3). Native insulin caused the films to be opaque. Insulin fibrils contributed to the rough top surface of the PVOH films, which suggests that the PVOH settled to the bottom of the tray and fibrils remained on the surface during the drying process. In addition, a close examination by a trained eye suggested the presence of voids in the PVOH + insulin fibril films (Staiger, per. comm.) Microscopy examination was therefore undertaken.

Film samples	**Visual**
PVOH + no insulin control	Clear, smooth surface
PVOH + 0.6% insulin control	Opaque film, smooth surface
PVOH + 0.6% insulin fibrils	Roughness on top with white aggregates, smooth bottom surface

Table 4.3 *Comparing the impact of buffers and proteins on PVOH film: qualitative attributes.*

(a)

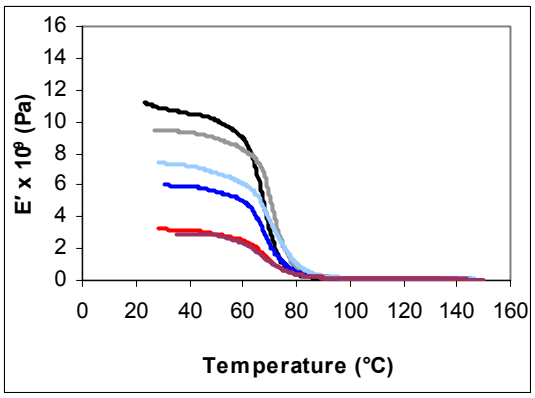

Sample	E′ at 36°C (x10^9) Pa
PVOH + no insulin control	9.9 ± 1
PVOH + 0.6% insulin control	6.7 ± 1
PVOH + 0.6% insulin fibrils	3.0 ± 0.2

(b)

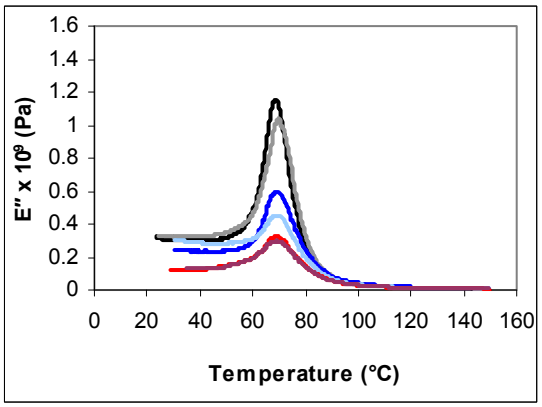

Sample	T_g (°C)
PVOH + no insulin control	70 ± 0.1
PVOH + 0.6% insulin control	70 ± 0.1
PVOH + 0.6% insulin fibrils	70 ± 0.1

(c)

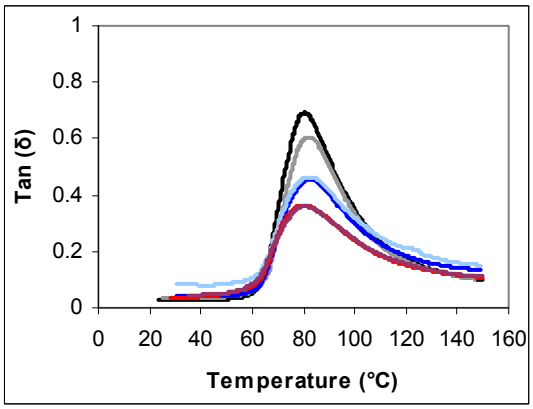

Sample	Tan δ at 80°C
PVOH + no insulin control	0.65 ± 0.05
PVOH + 0.6% insulin control	0.46 ± 0.01
PVOH + 0.6% insulin fibrils	0.36 ± 0.01

Figure 4.22 *E' curve (a), E" curve (b) and Tan δ curve (c) of 2.5% PVOH films with and without 0.6% insulin measured by DMA. Sample: PVOH + no insulin control replicate 1 (black), replicate 2 (grey), PVOH + insulin control replicate 1 (blue), replicate 2 (pale blue), PVOH + insulin fibrils replicate 1 (red), replicate 2 (plum). Samples had been dried at 60°C in vacuum oven for 24 hr. The E' values at 36°C (a), T_g values from E" peak (b) and the Tan δ intensities (c) are tabulated for each profile.*

4.11.2 Examination of film microstructure by SEM

Film microstructural characteristics are closely related to the mechanical properties of the films (Hernandez-Izquierdo and Krochta 2008, Roohani *et al.* 2008). Thus the morphology of the PVOH + insulin films was examined by surface examination of cast films (Figure 4.23) and freeze-fractured films (Figure 4.24) using scanning electron microscopy (SEM). The surface of the pure PVOH film appeared smooth and uniform at both magnifications (Figure 4.23 a and b). The PVOH + insulin control film showed some unevenness on its surface (Figure 4.23 c), which at a higher magnification revealed the presence of grainy-like structures (Figure 4.23 d). It was found that these structures were evenly distributed on the surface of the PVOH + insulin control films. The PVOH + insulin fibril films (Figure 4.23 e and f) showed a rough and uneven surface with voids in some places. The roughness was uniformly distributed but the voids (< 10 μm) were found to be present in some places on the surface.

The grainy-like structures present in the PVOH + insulin control films may be aggregated insulin formed as water evaporated during the film formation. Since insulin dissolved at low pHs only (pH 2) and the casting solution is at pH 4, insulin may have formed precipitates.

Further characterisation of the interior of the films involved field emission (FE)-SEM examination of their fractured surfaces. Figure 4.24 shows the full fractured surface of the films, with the arrow indicating the direction in which the fracture took place. The PVOH + no protein control films have a smooth glassy morphology. Films containing native insulin show some slight roughness, maybe due to the grainy-like structures. Films with insulin fibrils in them show ridges and roughness in their fractured surface.

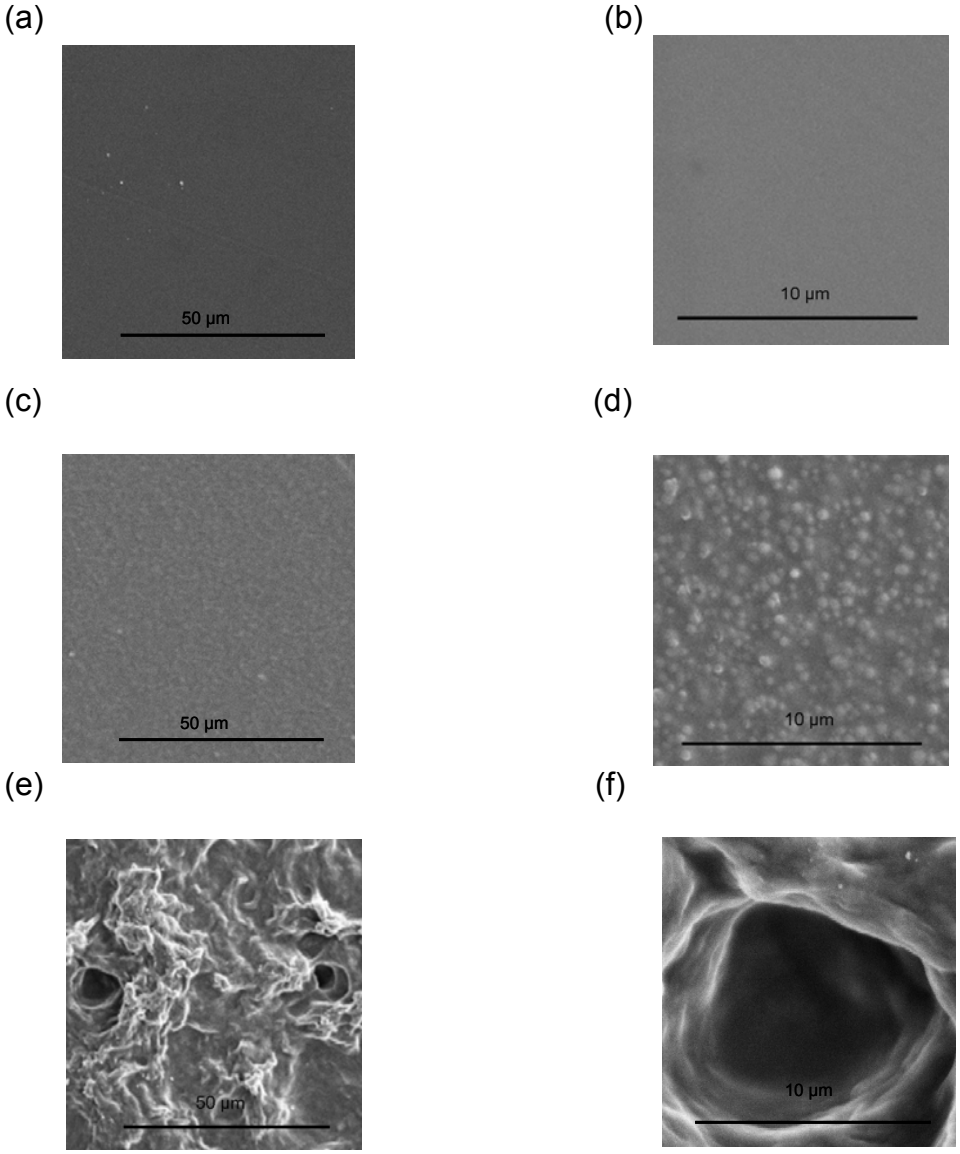

Figure 4.23 *SEM images of the surface of cast PVOH film samples: (a and b) PVOH + no protein control, (c and d) PVOH + insulin control, (e and f) PVOH + insulin fibrils.*

A composite material is expected to show a smooth fractured surface if its components are adhered well (Staiger, pers. comm.). Figure 4.24 (a), (b) and (c) illustrate that greater unevenness is conferred by the slow initiation of the fracture (Staiger, pers. comm.), indicated by the arrow. The greatest level of unevenness is present in Figure 4.24 (c) suggesting that the presence of insulin fibrils posed hindrance to the fracture.

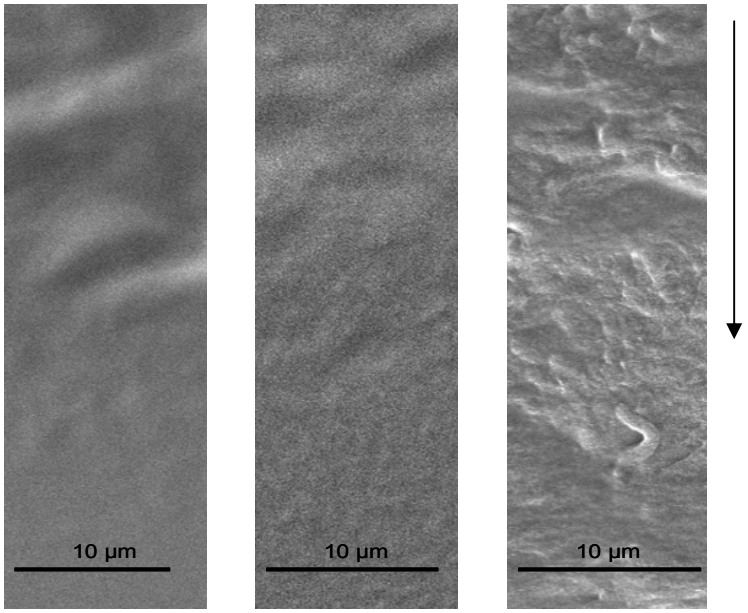

Figure 4.24 *FE-SEM images of fractured surfaces, of a) PVOH + no insulin control, b) PVOH + insulin control and c) PVOH + insulin fibril films. Images reveal that the fracture was initiated from top end (Staiger, pers. comm.). Arrow indicates direction of fracture.*

Further examination of the fractured surface of the films at a much higher magnification revealed more structural detail (Figure 4.25 a, b and c). Interestingly, the interior of the PVOH + insulin control film also showed that grains were present, similar to the film surface in Figure 4.23 (b). This observation confirmed that the insulin is distributed evenly in the film.

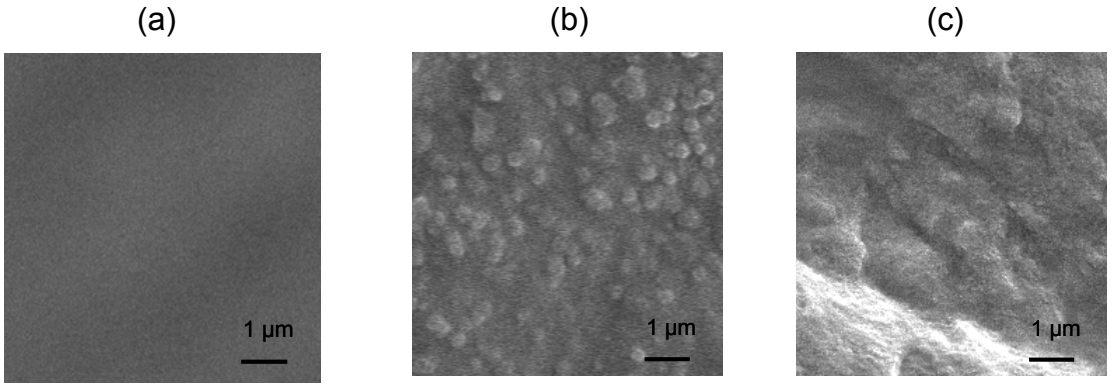

Figure 4.25 *FE-SEM images of freeze fractured surfaces of (a) PVOH + no insulin control, (b) PVOH + insulin control and (c) PVOH + insulin fibrils, films.*

The SEM examinations suggested that in PVOH + insulin control films, there is poor bonding between the insulin and the PVOH. This structural information correlates to the DMA findings in section 4.10.2.2, since poor interfacial bonding leads to a reduction in the stiffness which is manifested in reduced storage modulus (decreased E′ of the PVOH + insulin control/fibril film at < T_g in Figure 4.22 a).

The presence of voids in the PVOH + insulin fibril films were only visible in some places on the film surface and not in the interior (Figure 4.25 c). The SEM studies suggested that the PVOH + insulin fibril film mechanical behaviour was affected by the presence of some porosity and possible voids. Hence, PVOH + insulin fibrils films were treated with a hot pressing technique (section 5.1) to minimise the contributions of voids on the mechanical behaviour of the films.

4.11.3 Film crystallinity

Measurement of the degree crystallinity is important since crystallinity affects the physical properties of polymers (Sakurada 1985). An increase in polymer crystallinity may lead to a reduction in its damping peak intensity (Nielsen 1974) which was found in the PVOH + insulin (control/fibril) films. X-ray diffraction was undertaken to determine in the crystallinity in PVOH films as a function of added insulin, both control and after fibrillisation.

An X-ray diffraction equatorial scan of the PVOH films is shown in Figure 4.26. A quantitative evaluation was undertaken since the breadth of the peak can be related to the crystallization of the material by the Scherrer equation, where the peak width is inversely proportional to crystal size. In 1918, Scherrer first observed that small crystallite size could give rise to line broadening (Patterson 1939). A well known equation (Hammond 1997) for relating the crystallite size to the peak broadening is called the Scherrer formula, $t = K\lambda/(\beta \cos \theta)$ where:

t = crystal depth/thickness (Å)

K = Scherrer consTant, arbitrary factor related to crystal size and value that falls constant in the range 0.87-1.0, in this case assumed as K = 0.9

λ = 1.54 Å, the wavelength of the radiation

β = The integral breadth of a reflection (in radians 2θ) located at 2θ, calculated as FWHM (full width at half maximum height)

θ = scattering angle

The Scherrer formula was used to calculate crystal size of PVOH films in this experiment.

The diffraction patterns of the films were overlapped as shown in Figure 4.26. Peaks were observed at 2θ=19.6° for PVOH, 19.7° for PVOH with native insulin and 19.4° for PVOH with insulin fibrils. The data correlate to the literature, where the PVOH XRD peak was found at 19.4° (Yu *et al.* 2003). Peak positions are sensitive to the intermolecular bonding which draws the molecules together. The intensity of the peaks can be arranged in a decreasing order as such; PVOH + insulin fibril > PVOH + insulin control > PVOH + no insulin control, which suggests that the protein addition may have led to a small increase in the average crystallinity of the films.

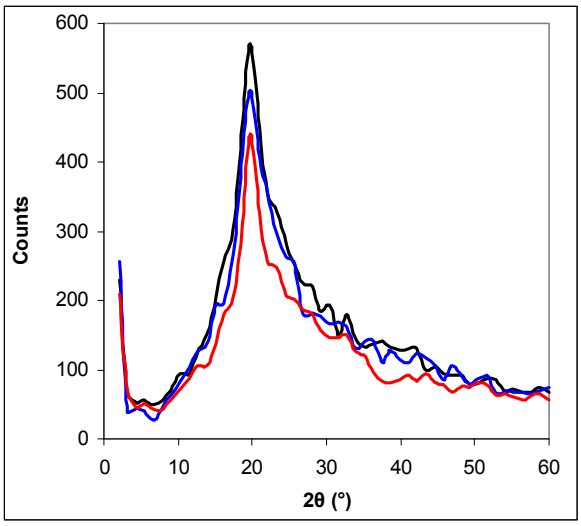

Figure 4.26 *X-ray diffractometer scan of PVOH films with and without protein fibrils. Graph represent PVOH + no insulin control (red), PVOH with 0.6% insulin control (blue) and PVOH with 0.6% insulin fibrils (black).These were not replicated.*

The calculated crystal size of the films is shown in Table 4.4. The data suggest that insulin control and insulin fibril addition may have had a small effect on the crystal size in the films.

Sample	PVOH + no insulin control	PVOH + insulin control	PVOH + insulin fibrils
Crystal size (nm)	7.3	7.1	7.0

Table 4.4 *Effect of insulin addition on crystal size of PVOH films.*

4.12 Summary

A reliable film manufacture method has been developed. The impact of the film manufacturing method on native protein and protein fibrils was determined to ensure that both control and fibrillated proteins were stable to the procedures involved. The results suggest that the solution casting method for small scale manufacture of films with fibrils was successfully accomplished. However, films prepared with insulin fibrils required an additional hot pressing step to process the films to minimise defects from voids in the films.

Film mechanical properties were obtained from UTM and DMA analysis. The effect of the solution components on mechanical properties was minimised by dialysing the proteins. The impact of water as a plasticiser was found to affect the viscoelastic behaviour of the films, including the T_g. The impact of water was minimised by vaccum drying the films.

The method developed with the model protein, bovine insulin, was applied on proteins from crystallins which is discussed in chapter 5. The thermomechanical impact of fibrils on PVOH films using the optimised film manufacture method developed in this chapter will be assessed in chapter 5.

4.13 References

Adam, S. Z., and J. L. Alan. 2001. Intercalated clay nanocomposites: Morphology, mechanics, and fracture behavior. *Journal of Polymer Science Part B: Polymer Physics* 39: 1137-1146.

Aoi, K., R. Nakamura, and M. Okada. 2000a. Polypeptide-synthetic polymer hybrids, miscibility of poly(vinyl alcohol) with polysarcosine. *Macromolecular Chemistry and Physics* 201: 1059-1066.

Aoi, K., A. Takasu, and M. Okada. 2000b. DNA-based polymer hybrids Part 1. Compatibility and physical properties of poly(vinyl alcohol)/DNA sodium salt blend. *Polymer* 41: 2847-2853.

Bhattacharyya, S., J.-P. Salvetat, and M.-L. Saboungi. 2006. Reinforcement of semicrystalline polymers with collagen-modified single walled carbon nanotubes. *Applied Physics Letters* 88: 233119-3.

Bhattacharyya, S., C. Sinturel, J. P. Salvetat, and M.-L. Saboungi. 2005. Protein-functionalised carbon nanotube-polymer composites. *Applied Physics Letters* 86: 113104-113107.

Cadek, M., J. N. Coleman, V. Barron, K. Hedicke, and W. J. Blau. 2002. Morphological and mechanical properties of carbon-nanotube-reinforced semicrystalline and amorphous polymer composites. *Applied Physics Letters* 81: 5123-5125.

Cadek, M., J. N. Coleman, K. P. Ryan, V. Nicolosi, G. Bister, A. Fonseca, J. B. Nagy, K. Szostak, F. Beguin, and W. J. Blau. 2004. Reinforcement of polymers with carbon nanotubes: The role of nanotube surface area. *Nano Letters* 4: 353-356.

Calvert, P. 1999. Nanotube composites: A recipe for strength. *Nature* 399: 210-211.

Cassu, S. N., and M. I. Felisberti. 1999. Poly(vinyl alcohol) and poly(vinylpyrrolidone) blends: 2. Study of relaxations by dynamic mechanical analysis. *Polymer* 40: 4845-4851.

Chang, M.-H., and B. C. Kim. 2007. Rheological investigation of the effects of introducing diethylene glycol on the physical properties of PVA solutions and PVA films. *Macromolecular Symposia* 249-250: 591-600.

Cherny, I., and E. Gazit. 2008. Amyloids: Not only pathological agents but also ordered nanomaterials. *Angewandte Chemie International Edition* 47: 4062-4069.

Coleman, J. N., Khan, U., Gun'ko, Y. K. 2006. Mechanical reinforcement of polymers using carbon nanotubes. *Advanced Materials* 18: 689-706.

Dobson, C. M. 2004. Experimental investigation of protein folding and misfolding. *Methods Investigating Protein Folding, Misfolding and Nonnative States: Experimental and Theoretical Methods* 34: 4-14.

Ehrenstein, G. W., G. Riedel, and P. Trawiel. 2004. *Thermal analysis of plastics*. Hanser Publishers, Munich, pg 139-171, 236-299.

Garvey, M., S. L. Gras, S. Meehan, S. J. Meade, J. A. Carver, and J. A. Gerrard. 2008. Protein nanofibres of defined morphology prepared from mixtures of crude crystallins. *International Journal of Nanotechnology* Submitted.

Gras, S. L. 2007. Protein misfolding: A route to new nanomaterials. *Advanced Powder Technology* 18: 699-705.

Guo, P., X. Chen, X. Gao, H. Song, and H. Shen. 2007. Fabrication and mechanical properties of well-dispersed multiwalled carbon nanotubes/epoxy composites. *Composites Science and Technology* 67: 3331-3337.

Hammond, C. 1997. *The basics of crystallography and diffraction*. Oxford University Press, New York.

Hernandez-Izquierdo, V. M., and J. M. Krochta. 2008. Thermoplastic processing of proteins for film formation:a review. *Journal of Food Science* 73: R30-R39.

Jahn, T. R., and S. E. Radford. 2008. Folding versus aggregation: Polypeptide conformations on competing pathways. *Archives of Biochemistry and Biophysics* 469: 100-117.

Jansson, A., and F. Thuvander. 2004. Influence of thickness on the mechanical properties for starch films. *Carbohydrate Polymers* 56: 499-503.

Kapphahn, R. J., C. M. Ethen, E. A. Peters, L. Higgins, and D. A. Ferrington. 2003. Modified αA crystallin in the retina: Altered expression and truncation with aging. *Biochemistry* 42: 15310-15325.

Kim, E. M., M. H. Han, Y. J. Lee, D. H. Song, H. K. Lee, O. W. Kwon, D. S. Shin, S. S. Han, S. K. Noh, J. K. Shin, Y.-S. Gal, and W. S. Lyoo. 2007. Characterization of poly(vinyl alcohol) films with various molecular parameters. *Journal of Applied Polymer Science* 106: 3259-3267.

Lau, K.-t., M. Lu, and K. Liao. 2006. Improved mechanical properties of coiled carbon nanotubes reinforced epoxy nanocomposites. *Composites Part A: Applied Science and Manufacturing* 37: 1837-1840.

Longares, A., F. J. Monahan, E. D. O'Riordan, and M. O'Sullivan. 2004. Physical properties and sensory evaluation of WPI films of varying thickness. *Lebensmittel-Wissenschaft und-Technologie* 37: 545-550.

Manocha, L. M. 2006. Composites with nanomaterials in K. E. Geckeler and E. Rosenberg, eds. *Functional Nanomaterials*. American Scientific Publishers, Stevensen Ranch, pg 275-286.

McCaig, M. S., and D. R. Paul. 2000. Effect of film thickness on the changes in gas permeability of a glassy polyarylate due to physical agingPart I. Experimental observations. *Polymer* 41: 629-637.

Meehan, S., Y. Berry, B. Luisi, C. M. Dobson, J. A. Carver, and C. E. MacPhee. 2004. Amyloid fibril formation by lens crystallin proteins and its implications for cataract formation. *Journal of Biological Chemistry* 279: 3413-3419.

Mi, Y., X. Zhang, S. Zhou, J. Cheng, F. Liu, H. Zhu, X. Dong, and Z. Jiao. 2007. Morphological and mechanical properties of bile salt modified multi-walled carbon nanotube/poly(vinyl alcohol) nanocomposites. *Composites Part A: Applied Science and Manufacturing* 38: 2041-2046.

Nielsen, L., R. Khurana, A. Coats, S. Frokjaer, J. Brange, S. Vyas, V. N. Uversky, and A. L. Fink. 2001. Effect of environmental factors on the kinetics of insulin fibril formation: Elucidation of the molecular mechanism. *Biochemistry* 40: 6036-6046.

Nielsen, L. E. 1974. *Mechanical properties of polymers and composites*. Marcel Dekker, Inc., New York, pg 2-18, 139-205.

Park, J.-S., J.-W. Park, and E. Ruckenstein. 2001. Thermal and dynamic mechanical analysis of PVA/MC blend hydrogels. *Polymer* 42: 4271-4280.

Park, Z.-Y., and D. H. Russell. 2001. Indentification of individual proteins in complex protein mixtures by high-resolution, high-mass-accuracy MALDI TOF-Mass spectrometry analysis of in-solution thermal denaturation/enzymatic digestion. *Analytical Chemistry* 73: 2558-2564.

Patterson, A. L. 1939. The Scherrer formula for x-ray particle size determination. *Physical Review* 56: 978-982.

Peng, F., C. Hu, and Z. Jiang. 2007. Novel poly(vinyl alcohol)/carbon nanotube hybrid membranes for pervaporation separation of benzene/cyclohexane mixtures. *Journal of Membrane Science* 297: 236-242.

Petersson, L., and K. Oksman. 2006. Preparation and properties of biopolymer-based nanocomposite films using microcrystalline cellulose in K. Oksman and M. Sain, eds. *Cellulose nanocomposites: processing, characteisation and properties*. American Chemical Society, Washington, DC, pg 135.

Pongjanyakul, T., and S. Puttipipatkhachorn. 2008. Alginate-magnesium aluminum silicate composite films: Effect of film thickness on physical characteristics and permeability. *International Journal of Pharmaceutics* 346: 1-9.

Puchtler, H., and F. Sweat. 1965. Congo red as a stain for fluorescence microscopy of amyloid. *The Journal of Histochemistry and Cytochemistry: Official Journal of the Histochemistry Society* 13: 693-694.

Puchtler, H., F. Sweat, and M. Levine. 1962. On the binding of Congo red by amyloid. *The Journal of Histochemistry and Cytochemistry: Official Journal of the Histochemistry Society* 10: 355-364.

Radford, S. E. 2000. Protein folding: progress made and promises ahead. *Trends in Biochemical Sciences* 25: 611-618.

Roohani, M., Y. Habibi, N. M. Belgacem, G. Ebrahim, A. N. Karimi, and A. Dufresne. 2008. Cellulose whiskers reinforced polyvinyl alcohol copolymers nanocomposites. *European Polymer Journal* 44: 2489-2498.

Roos, Y., and M. Karel. 1991. Water and molecular weight effects on glass transitions in amorphous carbohydrates and carbohydrate solutions. *Journal of Food Science* 56: 1676-1681.

Rosenthal, A. J. 1999. *Food texture: measurement and perception*. Aspen Publishers, Inc., Gaithersburg, pg 131-132.

Ryan, K. P., M. Cadek, V. Nicolosi, S. Walker, M. Ruether, A. Fonseca, J. B. Nagy, W. J. Blau, and J. N. Coleman. 2006. Multiwalled carbon nanotube nucleated crystallization and reinforcement in poly (vinyl alcohol) composites. *Synthetic Metals* 156: 332-335.

Safadi, B., R. Andrews, and E. A. Grulke. 2002. Multiwalled carbon nanotube polymer composites: Synthesis and characterization of thin films. *Journal of Applied Polymer Science* 84: 2660-2669.

Sakurada, I. 1985. *Polyvinyl Alcohol Fibres*. Marcel Dekker, Inc., New York, pg 83-123.

Schadler, L. S., S. C. Giannaris, and P. M. Ajayan. 1998. Load transfer in carbon nanotube epoxy composites. *Applied Physics Letters* 73: 3842-3844.

Sionkowska, A. 2005. *New materials based on the blends of collagen and other polymers*. Nova Science Publishers Inc., New York, pg 133.

Tycko, R. 2004. Progress towards a molecular-level structural understanding of amyloid fibrils. *Current Opinion in Structural Biology* 14: 96-103.

Waterhouse, S. H., and J. A. Gerrard. 2004. Amyloid fibrils in bionanotechnology. *Australian Journal of Chemistry* 57: 519-523.

Waterhouse, S. H., J. A. Gerrard, K. H. Sutton, and N. G. Larsen. 2003. Amyloid formation, NZ Patent.

Westermark, G. T., K. H. Johnson, and P. Westermark. 1999. Staining methods for identification of amyloid in tissue. *Methods in Enzymology* 309: 3-25.

Yang, J. M., W. Y. Su, T. L. Leu, and M. C. Yang. 2004. Evaluation of chitosan/PVA blended hydrogel membranes. *Journal of Membrane Science* 236: 39-51.

Yu, Y.-H., C.-Y. Lin, J.-M. Yeh, and W.-H. Lin. 2003. Preparation and properties of poly(vinyl alcohol)-clay nanocomposite materials. *Polymer* 44: 3553-3560.

Zhang, X., T. Liu, T. V. Sreekumar, S. Kumar, V. C. Moore, R. H. Hauge, and R. E. Smalley. 2003. Poly(vinyl alcohol)/SWNT composite film. *Nano Letters* 3: 1285-1288.

Fibrils in Films

Chapter 4 established a method for the manufacture of PVOH + protein fibril films and provided preliminary evidence that adding fibrils from two different proteins: insulin and bovine crystallins into PVOH films had different impacts on their properties. In this chapter, a rigorous characterisation of films containing the two proteins was carried out. Characterisation of both the PVOH + insulin and PVOH + crystallin films were carried out using DMA, DSC-TGA, SEM and TEM to compare the impact of the 2 proteins on the PVOH films manufactured using the method developed in chapter 4.

5.1 The Impact of Hot Pressing on PVOH Film Viscoelastic Behaviour

In chapter 4 (section 4.11), it was observed that PVOH + insulin fibril films contained some voids. It was thought that voids may affect the mechanical properties of the films. To minimise the impact of voids on the viscoelastic properties of the films, the PVOH + no insulin control, PVOH + insulin control and PVOH + insulin fibril films were hot pressed (Watts *et al.* 2002). Films were cut into rectangular sizes of 60 mm x 7 mm and dried at 60°C for 24 hr. The dried films were hot pressed at 180°C, for 20 min. The selection of the hot press temperature required the PVOH to melt without any degradation effects. A DSC-TGA test was done, which provided a simultaneous measure of sample weight loss/heat flow over increasing temperature. The weight loss vs temperature, as described in section 4.8.3, provided the degradation temperature of samples. The heat flow *vs* temperature profiles can be used to obtain the melting points and it was found that the PVOH had a melting point of

194°C (Figure 5.1). The graph shows that PVOH started to melt at 174°C, thus a temperature higher than 174°C and lower than 194°C was used to hot press the PVOH composite films.

According to the standard practice of treating plastics, they should be conditioned under an appropriate relative humidity (RH) and temperature (Staiger, pers. comm.) In attempts to apply the standard practice on PVOH films, the hot pressed films were conditioned at 50% relative humidity (RH) under ambient temperature for 72 hr in accordance with the ASTM standard (ASTM Standard, 2005) prior to DMA testing.

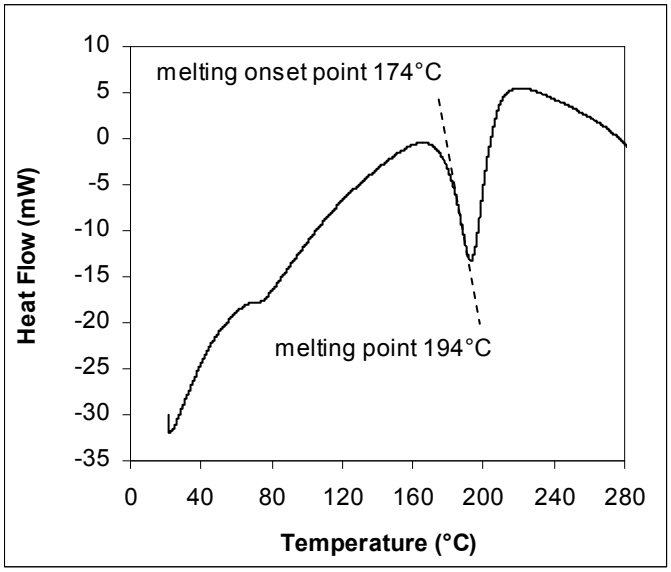

Figure 5.1 *Profile showing the onset and the end, of PVOH melting. Samples were analysed in duplicates by the DSC-TGA, SDT Q600, which simultaneously provides heat flow measurement and weight change.*

The PVOH + insulin fibril films in Figure 5.2 (a and b) show that a smoother less flaky appearance of the hot pressed films compared to the pre-hot pressed films. However, some voids were still present in some areas of the film. The hot pressed PVOH + insulin control films did not have the grainy structures which were visible prior to hot pressing the films (image not shown).

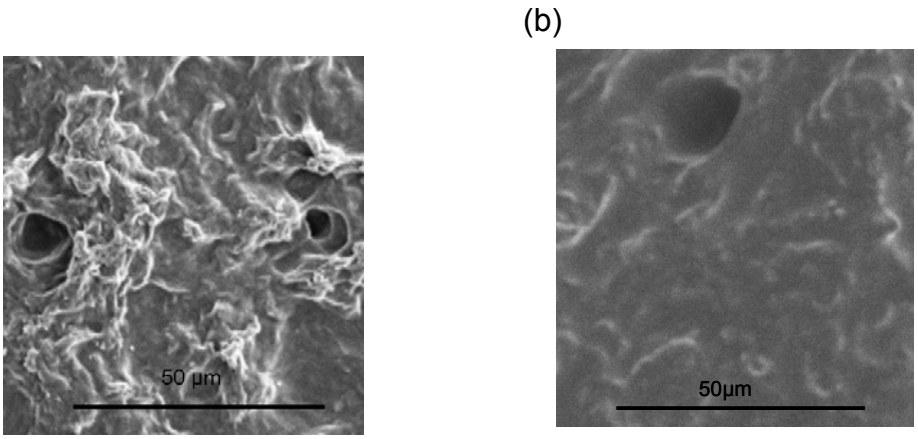

Figure 5.2 *SEM images of the surface of cast 2.5% PVOH + 0.6% insulin fibrils films: (a) before hot pressing and (b) after hot pressing. The PVOH + no insulin control film and PVOH + insulin control film showed an even surface (image not shown).*

After hot pressing and standard conditioning of the PVOH films with insulin, the DMA tests were carried out. Figure 5.3 (a) shows that there was no observable change in the stiffness (E′) of the PVOH with the addition of insulin fibrils. However, a decrease in the T_g of the films was observed with the addition of insulin (Figure 5.3 b). This means that the PVOH transformed from the glassy to rubbery state at a lower temperature when insulin was present, suggesting that insulin reduced the thermomechanical properties of PVOH. At temperatures above T_g, Figure 5.3 (c) demonstrates that shows a decrease in Tan δ with the addition of insulin, which provides evidence that there is a lesser extent of molecular slippage in the insulin containing films (Menard 1999, Nielsen 1974). The results obtained in Figure 5.3 were not directly compared to the pre-hot pressed films (section 4.10), since they differ in the standard conditioning step. However, the result obtained in Figure 5.3 (c) is consistent with the pre-hot pressed data (chapter 4, Figure 4.22 c).

(a)

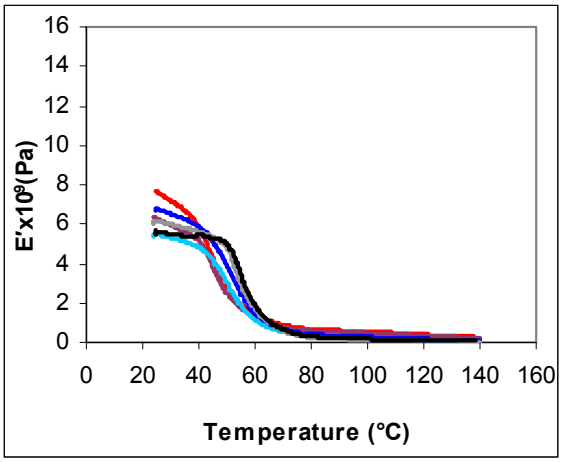

Sample	E′ at 30°C, x10^9 Pa
PVOH + no insulin control	5.5 ± 0.4
PVOH + 0.6% insulin control	6.3 ± 0.5
PVOH + 0.6% insulin fibrils	6.5 ± 0.5

(b)

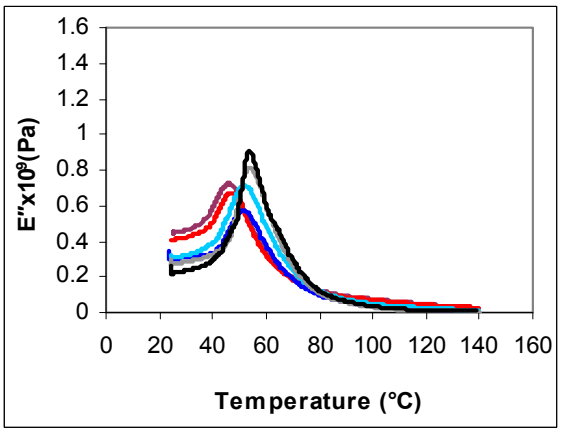

Sample	T_g (°C)
PVOH + no insulin control	74 ± 0.1
PVOH + 0.6% insulin control	70 ± 0.1
PVOH + 0.6% insulin fibrils	52 ± 0.1

(c)

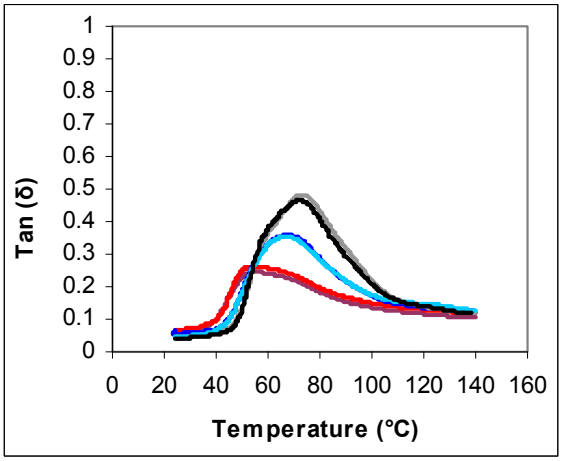

Sample	Tan (δ)
PVOH + no insulin control	0.47 ± 0.01
PVOH + 0.6% insulin control	0.35 ± 0.01
PVOH + 0.6% insulin fibrils	0.27 ± 0.01

Figure 5.3 *E' curve (a), E" curve (b) and Tan δ curve (c) of 2.5% PVOH films with and without 0.6% insulin measured by DMA. Sample are: PVOH + no insulin control replicate 1 (black) and replicate 2 (grey), PVOH + with 0.6% insulin control replicate 1 (blue), replicate 2 (pale blue), PVOH + insulin fibrils replicate 1 (red), replicate 2 (plum). Samples had been hot pressed at 180°C and conditioned at 50% (RH), at 23°C for 72 hr. The E' values at 30°C (a),* T_g *values from E" peak (b) and the Tan δ intensities (c) are tabulated for each profile. Errors represent standard deviation of the mean.*

5.2 The Potential of Crystallins in PVOH Films

In this section, addition of fibrils from crystallin proteins on the viscoelastic properties of PVOH films will be discussed. Section 4.9 showed some preliminary data on the increase in the tensile strength of PVOH films with added crystallins. Having optimised the methods for testing film viscoelastic properties with insulin in the previous sections, the methods were applied to crystallin proteins.

5.2.1 Visual and microstructural examination

Table 5.1 provides a comparison of the impact of crystallin addition on PVOH film visual attributes after vacuum drying. The PVOH films with crystallin protein were smooth, similar to the PVOH control. However, the addition of crystallin fibrils caused films to become opaque. Although the films with crystallin controls had small aggregate particles distributed in them, the particles did not affect the smoothness of the films.

The SEM examination of the surface of the films, showed no voids in the films with crystallins (Figure 5.4). PVOH + no crystallin control images were the same as previously reported with no unevenness observed (picture not shown). The films remained smooth with the crystallin fibril addition, unlike PVOH + insulin fibril films (chapter 4, Figure 4.23 e), there was no flakiness observed.

Film samples	Visual
PVOH + no crystallin control	Clear, smooth surface
PVOH + 0.6% crystallin control	White aggregates visible within the film otherwise clear film, smooth surface
PVOH + 0.6% crystallin fibrils	Opaque, smooth surface

Table 5.1 *Comparing the impact of crystallin proteins on PVOH film qualitative attributes.*

The SEM examination of PVOH with crystallins, confirmed that these films did not require the added step of hot pressing. Thus the dry films with crystallins were tested on the DMA without any additional processing.

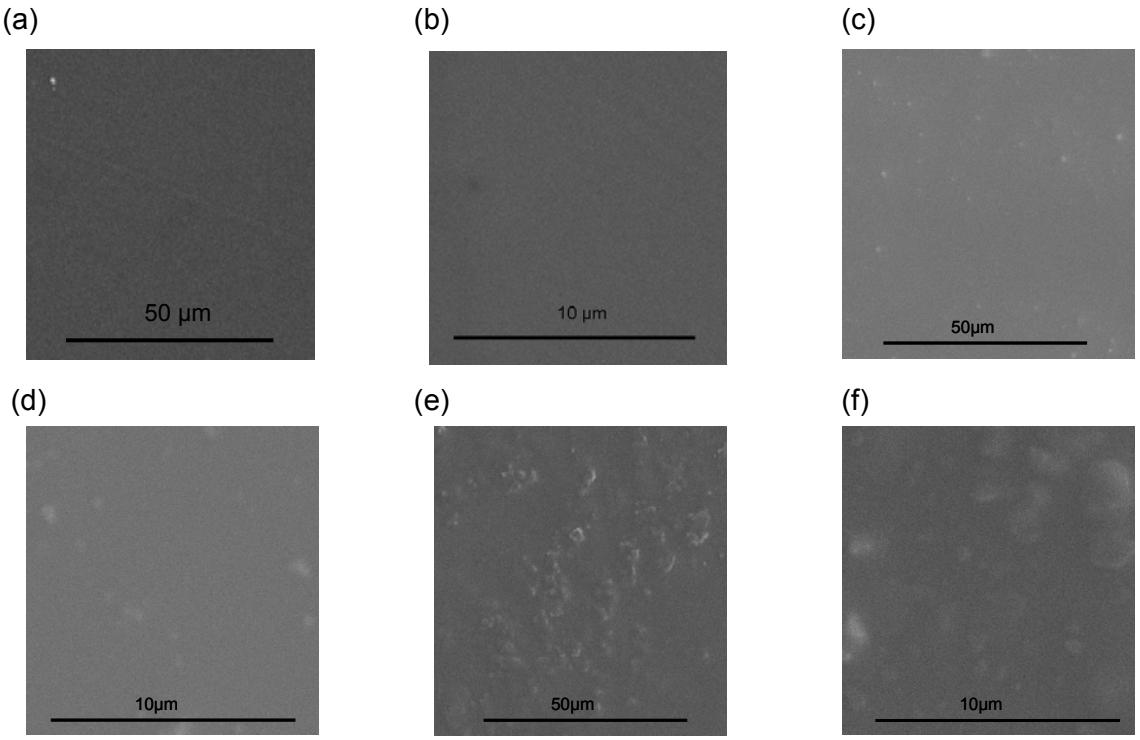

Figure 5.4 *SEM images of the surface of cast PVOH film samples: (a and b) PVOH + no crystallin control, (c and d) PVOH + crystallin control, (e and f) PVOH + crystallin fibrils.*

5.2.2 The Impact of crystallins on the viscoelastic properties of dry PVOH film

Crystallins were incorporated into PVOH films and dried for 24 hr in a vacuum oven at 60°C before testing on the DMA. This experiment is analogous to the PVOH with insulin films in section 4.10.2.2. The addition of crystallin fibrils caused an increase in the stiffness (E′) of the PVOH films, at temperatures below the below the T_g (Figure 5.5 a). The T_g of PVOH films remained unchanged with the addition of the crystallin control but there was small reduction with the addition of the crystallin fibrils. At temperatures above T_g, there was a decrease in Tan δ with the addition of the crystallins (control/ fibrils) (Figure 5.5 c). This is consistent with the results obtained for PVOH + insulin (control/fibrils) films (Figure 4.22 c) and further suggested that the molecular slippage was reduced by the addition of the proteins (control/ fibrils) to the PVOH films. Literature confirms that reduction in Tan δ (less damping) occurs when the polymer chain mobility is decreased in the nanocomposites (Nielsen 1974, Suhr *et al.* 2005).

(a)

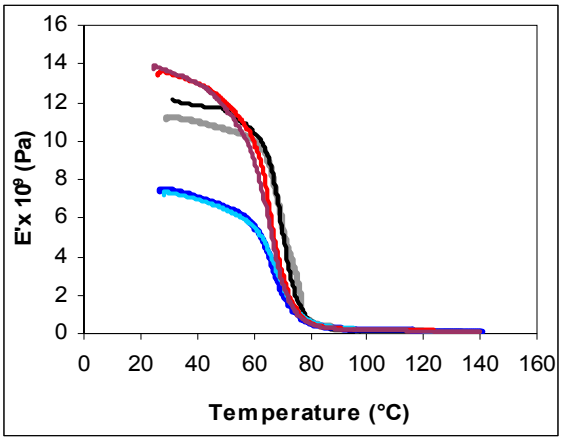

Sample	E′ at 30°C (x10^9) Pa
PVOH + no crystallin control	11.2 ± 0.5
PVOH + 0.6% crystallin control	7.3 ± 0.1
PVOH + 0.6% crystallin fibrils	13.6 ± 0.1

(b)

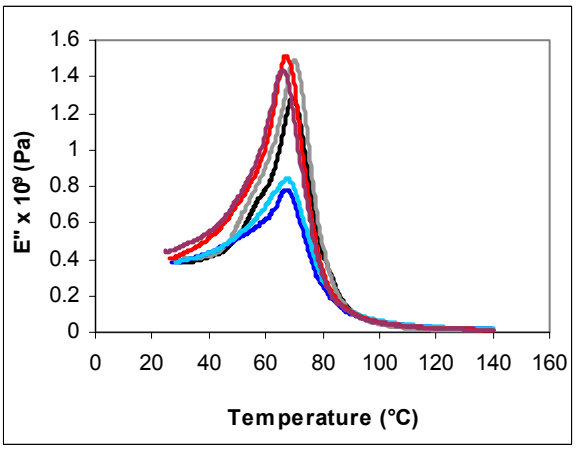

Sample	T_g (°C)
PVOH + no crystallin control	70 ± 0.2
PVOH + 0.6% crystallin control	70 ± 0.2
PVOH + 0.6% crystallin fibrils	69 ± 0.3

(c)

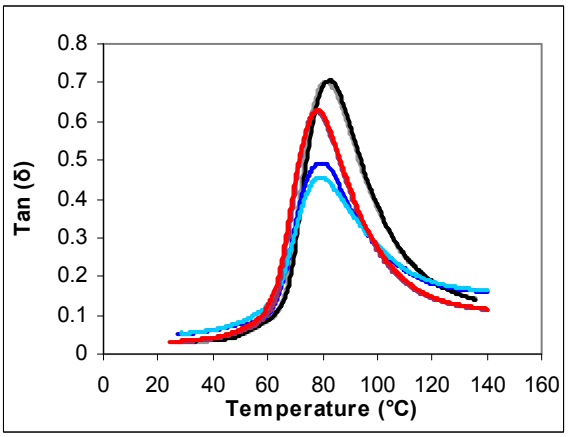

Sample	Tan δ at 80°C
PVOH + no crystallin control	0.70 ± 0.01
PVOH + 0.6% crystallin control	0.47 ± 0.04
PVOH + 0.6% crystallin fibrils	0.62 ± 0.01

Figure 5.5 *E' curve (a), E" curve (b) and Tan δ curve (c) of 2.5% PVOH films with and without 0.6% crystallin measured on the DMA. Sample are: PVOH + no crystallin control replicate 1 (black) and replicate 2 (grey), PVOH + crystallin control replicate 1 (blue) and replicate 2 (pale blue), PVOH + crystallin fibrils replicate 1 (red) and replicate 2 (plum). Samples had been dried at 60°C for 24 hr.*

5.3 Comparison of Protein Properties

Table 5.2 compares various characteristics of insulin and the crystallins in their native state. There are differences between the two in terms of size, since insulin is about 5 times smaller than the crystallins and their solubility profile, reflecting differing isoelectric points (insulin = 5.3, crystallins = 5.8-7.0) (Bours 1973, Conway-Jacobs and Lewin 1971, Spector *et al.* 1985). Crystallins have a lower degradation temperature in comparison to insulin. Microstructural study was carried out by TEM to further probe these differences in film properties.

Property	PVOH (86.5-89 % hydrolysed)	Bovine insulin	Bovine crystallins
MW (kDa)	115	~5.7	~20-28
Solubilising conditions	80°C (50 mg/ml))	pH 2 (11.4 mg/ml)	pH 7 (11.4 mg/ml)
Source	commercial	commercial	waste protein
Degradability	biodegradable	biodegradable	biodegradable
Purity, Cost	pure, reasonable	pure, expensive	crude, cheap,
Degradation temperature (°C)	290 ± 1	268 ± 3	256 ± 3

Table 5.2 *Comparison of properties of proteins and the PVOH.*

5.4 Film Microstructure Examination by TEM

TEM images were collected for microtomed transverse cross-sections of the PVOH composites, containing insulin and crystallins, (control/fibrils). TEM samples for PVOH + no protein control film could not be examined by this method since the film disintegrated in the preparation media.

Examination by TEM of the insulin control (Figure 5.6 a) shows an amorphous matrix indicative of insulin control scattered throughout the film. Figure 5.6 (b) illustrates that the PVOH + insulin fibril film had a network of nanofibres which were entangled with each other.

The crystallin control yielded a network-like structure, which may have formed amongst the native crystallin proteins (Figure 5.6 c). Interestingly, their distribution is similar to insulin fibrils and not to the native insulin structure. The PVOH + crystallin fibril films revealed large clusters of nanofibres which were not entangled, in contrast to the insulin fibril film (Figure 5.6 d). The image observed in Figure 5.6 (d) also shows that the PVOH + crystallin fibril films had structures which were larger in size than the PVOH + insulin fibrils films.

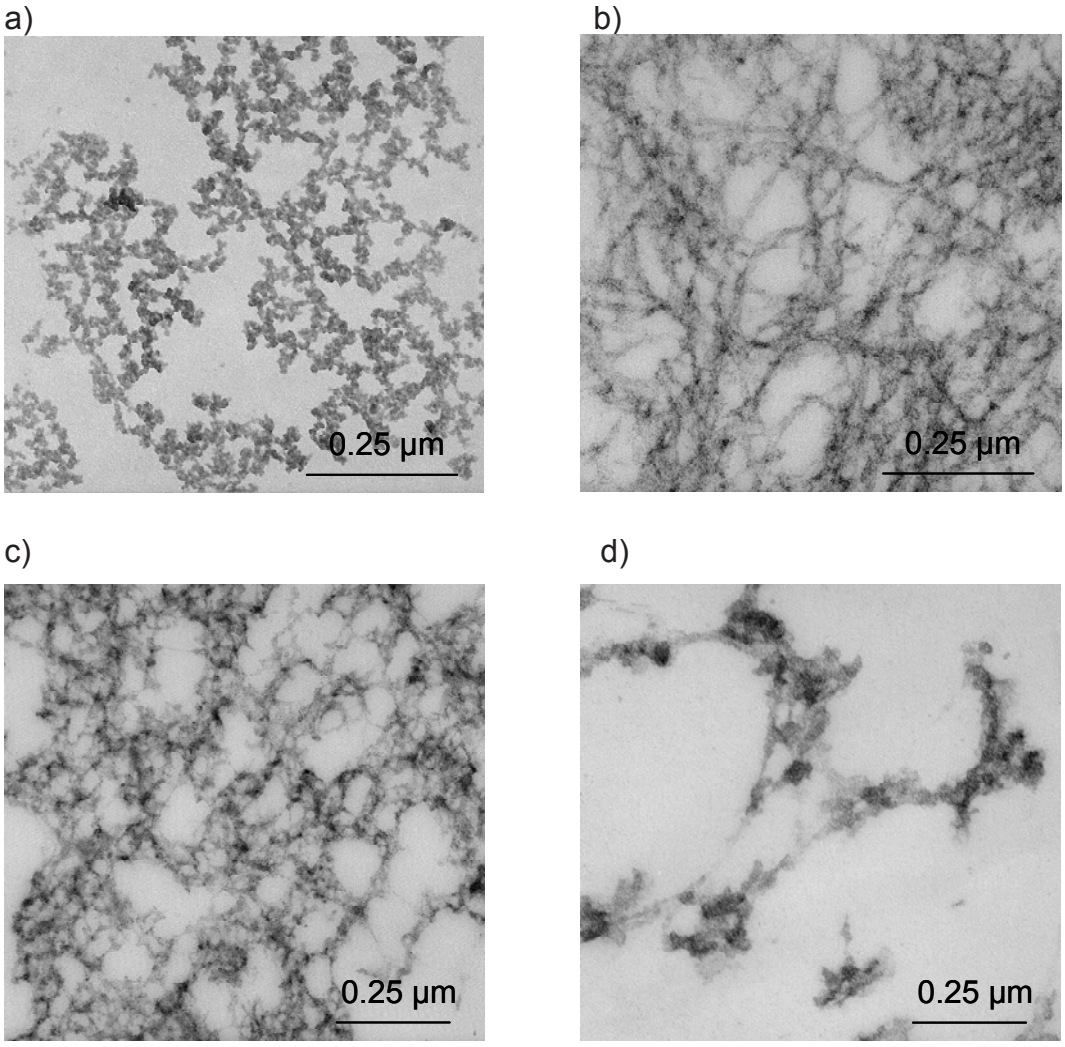

Figure 5.6 *TEM images of the cross-sections of PVOH cast films with and without proteins, A) PVOH + insulin control, B) PVOH + insulin fibrils, C) PVOH + crystallin control, D) PVOH + crystallin fibrils. Images are representative of more than five images.*

The images obtained in Figure 5.6, suggested that there is a difference in the way in which the insulin and the crystallin fibrils exist in the PVOH matrix. This may suggest that is also a difference in the interaction of the fibrils between themselves when mixed with PVOH. However, both protein fibrils have been shown to decrease the interfacial slip between nanofibres and PVOH.

The structural findings in this section provide evidence that fibrils entangle to form networks with potential applications as reinforcing agents for multicomponent mixtures and templates for functional nanostructures. However, future work should investigate methods to improve interaction between the fibrils and the matrix, for example by the use of compatibilisers (Chapleau *et al.* 1998, Xie *et al.* 2005).

5.5 Thermal Stability of Films

DSC-TGA analysis (Tang *et al.* 2005) of PVOH film nanocomposites was performed to gain a more detailed information about the impact of the protein nanofibres on the thermal stability of the PVOH. The real time characteristic TGA curves were generated using the Universal Analysis Data Acquisition System. The representative TGA curves for the PVOH (powder) control, insulin (powder) control and the crystallin (extract) control as well as the PVOH + insulin (control/fibril) and PVOH + crystallin (control/fibril) films are shown in Figure 5.7. The initial drop in weight is the loss of moisture from the samples. The graph shows that the thermal stability of pure PVOH is higher than the proteins. The introduction of proteins lowered the onset of the degradation temperature for PVOH.

Data from a typical TGA of the PVOH control and the nanocomposites are shown in Table 5.3. Bovine insulin had a higher degradation temperature compared to the crystallins. Both proteins indicated a slightly elevated thermal stability after fibrillisation. Table 5.3 also shows that the thermal stability of PVOH composites decreased with protein addition, and this may be due to the effect of the low thermal stability of the protein controls compared to its polymer

counterpart, PVOH. The extent of interaction between the protein and the PVOH may also contribute to the lowering of the thermal stability, since immiscibility between additives have shown to lower the thermal stability of composites (Aoi *et al.* 2000).

At temperatures higher than 500°C, the TGA curves level off. The weight % loss was the highest for composites with insulin fibrils compared to the PVOH without insulin fibrils. The weight % loss was lowest for the insulin powder.

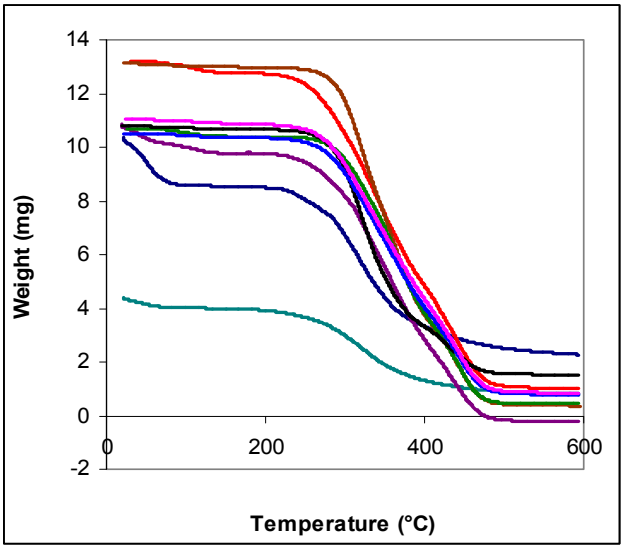

Figure 5.7 *TGA profiles for PVOH, proteins and PVOH-protein composites. Graph represents curves for: bovine insulin from the jar (dark blue), PVOH from the jar (brown), PVOH + no insulin control (green), PVOH + insulin control film (red), PVOH + insulin fibrils film (purple), PVOH + no crystallin control (black), PVOH + crystallin control film (blue), PVOH + crystallin fibrils film (pink), crystallin extract (teal). Samples were tested in duplicates. Graph shows one profile representative of each sample. Note: native crystallin testing was limited to about 4.5 mg since the protein has a large volume to weight ratio and the size of testing pans restricted the amount protein.*

Interestingly, in this section, it was found that although the thermal stability of the crystallins is lower than the insulin, its thermal stability rises much more prominently than insulin, when incorporated in the PVOH. This finding suggests that the PVOH is more compatible with the crystallins than the insulin and the strong interaction with PVOH is responsible for the increase in the thermal stability of the PVOH + crystallin (control/fibrils) nanocomposites.

Samples	Degradation Temperature (°C)
PVOH from the jar	293 ± 2
Insulin from the jar	265 ± 1
Insulin fibrils	268 ± 3
Crystallin extract	256 ± 3
Crystallin fibrils	252 ± 4
PVOH + 0.6% insulin control film	261 ± 3
PVOH + 0.6% insulin fibril film	262 ± 3
PVOH + 0.6% crystallin control film	280 ± 3
PVOH + 0.6% crystallin fibril film	278 ± 3

Table 5.3 *Shows the degradation temperature of the proteins before and after fibrillation and PVOH composites which were tested for their mechanical properties. The data represents an average of the duplicates analysis. Errors represent standard deviation of the mean.*

Although nanostructures have been thought to increase the thermal stability of polymers, some have reduced the thermal stability of polymers (Naebe *et al.* 2007) which is consistent with the findings in this section.

5.6 Summary

In this chapter, a TEM study of PVOH composites with insulin fibrils and crystallin fibrils showed that the manner in which the fibrils are distributed within the composites vary. Insulin fibrils had a network-like structure composed of narrow strands compared to crystallin fibrils which had larger aggregates in its structure. It was found that the bovine insulin fibril was distributed in a similar manner to the crude crystallin control.

The structural characterisation can be related to the mechanical behaviour of the films, since crystallin fibrils behaved in a different manner to insulin fibrils

and below the T_g the stiffness of the dry PVOH composite film containing 0.6% of crystallin fibrils increased in comparison PVOH + insulin fibril films.

The structural information was supplemented by the analysis of the thermal stability, which revealed a reduction in the degradation conferred by the proteins. However, the addition of crystallins reduced the degradation temperature for PVOH but the PVOH in turn stabilised the thermal degradation of the crystallins protein, which was not found with insulin.

The findings in this chapter also suggest that for PVOH + protein bionanomaterials, crystallins were more compatible than insulin. Thus fibrils formed from different source materials may be compatible with different polymers and optimisation will be required in each case. PVOH films with varying properties can be obtained by incorporation of fibrils from different protein sources. These results suggest that the protein source provides new options for processing and control. For example, the crystallins contain a mixture of proteins which form straight and curly fibrils in a heterogeneous mixture (section 4.1.2), and opens up the possibility of their multifunctional role in the bionanomaterial. Such an approach may consequently lead to the fabrication of cheap and readily available protein based nanostructures.

This chapter has demonstrated that a relatively small quantity of protein fibrils (0.6%) in a PVOH matrix is capable of changing its visual, microstructural and mechanical properties. Both the protein fibrils were found to reduce the molecular slipping within the PVOH films, which may be of interest to some applications. Although considerable development work will be required prior to commercial application, this work provides proof of principle that amyloid fibrils can be incorporated into a nanocomposite material and change its mechanical properties.

5.7 References

Aoi, K., R. Nakamura, and M. Okada. 2000. Polypeptide-synthetic polymer hybrids, miscibility of poly(vinyl alcohol) with polysarcosine. *Macromolecular Chemistry and Physics* 201: 1059-1066.

ASTM. Standard, 2005. D618-05 Standard practice for conditioning plastics for testing. *ASTM International*, West Conshohocken, PA, www.astm.org.

Bours, J. 1973. Free isoelectric focusing of bovine lens γ-crystallins. *Experimental Eye Research* 16: 501-515.

Chapleau, N., B. D. Favis, and P. J. Carreau. 1998. Measuring the interfacial tension of polymers in the presence of an interfacial modifier: Migrating the modifier to the interface. *Journal of Polymer Science Part B: Polymer Physics* 36: 1947-1958.

Conway-Jacobs, A., and L. M. Lewin. 1971. Isoelectric focusing in acrylamide gels: Use of amphoteric dyes as internal markers for determination of isoelectric points. *Analytical Biochemistry* 43: 394-400.

Menard, K. P. 1999. *Dynamic Mechanical Analysis: A Practical Introduction*. CRC Press, Boca Raton, pg 14-77.

Naebe, M., T. Lin, W. Tian, L. Dai, and X. Wang. 2007. Effects of MWNT nanofillers on structures and properties of PVA electrospun nanofibres. *Nanotechnology* 18: 225605.

Nielsen, L. E. 1974. *Mechanical properties of polymers and composites*. Marcel Dekker, Inc., New York, pg 2-18, 139-205.

Spector, A., R. Chiesa, J. Sredy, and W. Garner. 1985. cAMP-dependent phosphorylation of bovine lens alpha-crystallin. *Proceedings of the National Academy of Sciences of the United States of America* 82: 4712-4716.

Suhr, J., N. Koratkar, P. Keblinski, and P. Ajayan. 2005. Viscoelasticity in carbon nanotube composites. *Nature Materials* 4: 134-137.

Tang, C.-H., Y. Jiang, Q.-B. Wen, and X.-Q. Yang. 2005. Effect of transglutaminase treatment on the properties of cast films of soy protein isolates. *Journal of Biotechnology* 120: 296-307.

Watts, P. C. P., W. K. Hsu, D. P. Randall, H. W. Krotoa, and D. R. M. Waltona. 2002. Non-linear current–voltage characteristics of electrically conducting carbon nanotube–polystyrene composites. *Physical Chemistry Chemical Physics* 4: 5655–5662.

Xie, X.-L., Y.-W. Mai, and X.-P. Zhou. 2005. Dispersion and alignment of carbon nanotubes in polymer matrix: A review. *Materials Science and Engineering: R: Reports* 49: 89-112.

Summary and Conclusions

Amyloid fibrils have considerable potential as bionanomaterials. If they are to be employed as such on a commercial scale then a means of manufacturing them from crude sources of readily available materials is required. This thesis aimed to explore whether amyloid fibrils could be prepared from crude mixtures and whether chemical modification influenced the rate of fibril formation. It also explored the use of amyloid fibrils as components of a model nanocomposite material. Using PVOH as a model polymer, the mechanical and thermal impacts of these nanofibres produced from both, insulin and an industrial waste material, bovine eye lenses as novel additives in PVOH films were evaluated.

Initially, the impact of chemical modification on the propensity of a model protein, bovine insulin, to form amyloid fibrils was investigated. It was demonstrated that insulin can be modified *via* acetylation, reduction carboxymethylation, reduction pyridylethylation, trypsin cleavage and chymotrypsin cleavage to obtain crude mixtures of modified insulin. The crude modified insulin mixtures were assessed for their propensity to form fibrils at a range of temperatures; fibril formation was confirmed by the ThT assay and TEM.

Most of the modifications led to a decrease in the rate of formation and yield of amyloid fibrils. However, certain modifications increased the rate of formation and led to distinct changes in morphology when compared to fibrils formed from unmodified insulin. For example, reduction carboxymethylation of insulin resulted in the formation of straight, twisted fibrils compared to the straight and narrow fibrils formed in the insulin standard at pH 7.4. In contrast, the crude reduced pyridylethylated insulin formed wavy fibrils at pH 1.6, a very different morphology to the standard insulin fibrils.

Exposure to neutral and slightly alkaline buffer reduced the rate of insulin fibril formation even in the absence of chemical modification. This perhaps reflects that the oligomeric state can slow down amyloid formation under certain conditions.

The effect of enzymatic digestion on fibril formation of insulin was investigated by treatment of trypsin and chymotrypsin. It was found that the intact insulin in the partially trypsin digested insulin mixture formed long narrow and unbranched fibrils, which were similar to the insulin control at pH 1.6. However, the fully digested insulin peptides did not form any fibrils, under the same conditions. Chymotryptic digest of insulin formed a heterogeneous mixture of fibril structures, ranging from long, thin, and straight, as well as short and thick fibrils, at pH 1.6.

The successful formation of protein nanofibres from unpurified mixtures of modified insulin indicates that bovine insulin has the ability to form into nanofibres while still in the presence of other, derivatised polypeptides and peptides. Chemical modification of insulin showed that varying morphologies of fibrils can be prepared and the fibril structure was specific to the modification. These findings add to the enormous interest in the potential utility of amyloid fibrils as structural templates in nanomaterials science (Cherny and Gazit 2008, Gras 2007a, Gras 2007b, Gras *et al.* 2006) which requires the capacity to manipulate the fibril structure for such applications. Studies continue to determine ways of controlling peptide and proteins self-assembly to obtain amyloid fibrils (Griffin *et al.* 2008, Hong and Fink 2005, Hong *et al.* 2003) and these results suggest that simple chemical modifications can provide considerable control over higher order assembly processes.

Insulin fibrils have an “elastic modulus of 3.3 ± 0.4 GPa which ranks fibrils amongst the stiff polymers such as nylon” (Welland 2007). Insulin and crystallin amyloid fibrils were therefore trialled in a polymer model system of PVOH. PVOH nanocomposite films were manufactured with the addition of insulin fibrils or crude crystallin fibrils using a solution casting method. TEM studies showed that the solution casting method achieved fibrils dispersion. Congo red was

added to the casting solutions to confirm the presence of fibrils in the films, as well as to ensure the absence of fibrils in protein control films with added native protein. PVOH + insulin fibrils showed yellow-green birefringence in the films which was consistent with amyloid fibrils being present, while there was no yellow-green birefringence detected in the PVOH + insulin control films, confirming that the film manufacture method did not induce fibrillation in the native proteins.

Insulin fibril addition produced a rough film, in contrast to crystallin fibrils which led to the production of a smooth film. The film manufacture method was optimised for insulin fibril added composites to minimise voids in the PVOH + insulin (fibril/control) films *via* hot pressing. This step was not required for the crystallin fibril containing films, which did not contain voids.

Preliminary studies on hydrated films showed that insulin did not change the strength of the PVOH films, but increased their elongation. However, crystallin fibrils caused an increase in the tensile strength of the PVOH films, which was 20% higher than the crystallin control. DMA showed that both insulin and crystallin fibrils altered the mechanical properties of the polymer in a manner consistent with a decrease in molecular slippage within the polymer (Nielsen 1974). These changes suggested better compatibility of the crude crystallin fibrils with the PVOH than the insulin fibrils.

It has thus been shown that PVOH nanocomposite films with improved reinforcement of the PVOH matrix can be prepared using protein nanofibres assembled from a crude source. An enhancement of the tensile strength and elastic modulus of the PVOH films was obtained at low nanofibre loading (0.6%), which indicates efficient load transfer between the fibrils and the matrix. As a representative example, a 21% improvement of the stiffness was achieved by the additions of 0.6% crude crystallin fibrils, in the glassy region ($<T_g$) of the PVOH system. The potential for interfacial bond tailoring by the side chain amino acid of protein nanofibres makes protein nanofibres attractive as effective reinforcing agents of bionanocomposites.

Results show that nanofibres assembled from proteins affected the mechanical behaviour of the PVOH films to some extent. The pure insulin fibrils are morphologically long, straight and unbranching compared to the crude mixture of short, curly and long straight fibrils assembled from crude crystallins. Insulin and crystallins differed in their mechanical behaviour. It has thus been demonstrated that protein nanofibres affected the PVOH thermo-mechanical properties in a protein dependent manner.

With proof of concept now established, future work on the addition of protein nanofibres in PVOH should include the addition of crosslinkers such as glutaraldehyde and transglutaminase to act as a binder between the nanofibres. Moreover, compatibilisers can be added to enhance the interfacial bonding between nanostructures and polymers (Xie *et al.* 2005). Other polymers, such as epoxy resins, can also be used as a matrix to assess the effect of protein fibres on their mechanical properties.

The partial biodegradability of the amyloid fibrils is increasingly recognised in recently published work on composites of amyloid and commercial plastics (Arnold 2008). Protein nanofibre composites may have potential in products like food packaging or wrapping, filter membranes with selective adsorption properties conferred by functionalised nanofibres. Since protein nanofibres have been shown to confer changes in polymer strength, the availability of side chain amino acids in protein nanofibres offer better scope for their functionalisation than carbon nanotubes. Thus amyloid fibrils offer a complementary technology to carbon nanotubes for a wide range of potential applications.

6.1 References

Arnold, C. 2008. From diseases to devices. *Chemical and Engineering New: Science/Technology* 86: 48-50.

Cherny, I., and E. Gazit. 2008. Amyloids: Not only pathological agents but also ordered nanomaterials. *Angewandte Chemie International Edition* 47: 4062-4069.

Gras, S. L. 2007a. Amyloid fibrils: From disease to design. New biomaterial applications for self-assembling cross-beta fibrils. *Australian Journal of Chemistry* 60: 333-342.

—. 2007b. Protein misfolding: A route to new nanomaterials. *Advanced Powder Technology* 18: 699-705.

Gras, S. L., A. M. Squires, C. M. Dobson, and C. E. MacPhee. 2006. Functionalised fibrils for bio-nanotechnology. *International Conference On Nanoscience and Nanotechnology*, Brisbane, Qld.

Griffin, M. D. W., M. L. Y. Mok, L. M. Wilson, C. L. L. Pham, L. J. Waddington, M. A. Perugini, and G. J. Howlett. 2008. Phospholipid Interaction Induces molecular-level polymorphism in apolipoprotein C-II amyloid fibrils *via* alternative assembly pathways. *Journal of Molecular Biology* 375: 240-256.

Hong, D.-P., and A. L. Fink. 2005. Independent heterologous fibrillation of insulin and its β-chain peptide. *Biochemistry* 44: 16701-16709.

Hong, Y., R. L. Legge, S. Zhang, and P. Chen. 2003. Effect of amino acid sequence and pH on nanofiber formation of self-assembling peptides EAK16-II and EAK16-IV. *Biomacromolecules* 4: 1433-1442.

Nielsen, L. E. 1974. *Mechanical properties of polymers and composites*. Marcel Dekker, Inc., New York, pg 2-18, 139-205.

Welland, M. E. 2007. Insights into amyloid diseases. *Nano Today* 2: 56.

Xie, X.-L., Y.-W. Mai, and X.-P. Zhou. 2005. Dispersion and alignment of carbon nanotubes in polymer matrix: A review. *Materials Science and Engineering: R: Reports* 49: 89-112.

Summary and Conclusions

Amyloid fibrils have considerable potential as bionanomaterials. If they are to be employed as such on a commercial scale then a means of manufacturing them from crude sources of readily available materials is required. This thesis aimed to explore whether amyloid fibrils could be prepared from crude mixtures and whether chemical modification influenced the rate of fibril formation. It also explored the use of amyloid fibrils as components of a model nanocomposite material. Using PVOH as a model polymer, the mechanical and thermal impacts of these nanofibres produced from both, insulin and an industrial waste material, bovine eye lenses as novel additives in PVOH films were evaluated.

Initially, the impact of chemical modification on the propensity of a model protein, bovine insulin, to form amyloid fibrils was investigated. It was demonstrated that insulin can be modified *via* acetylation, reduction carboxymethylation, reduction pyridylethylation, trypsin cleavage and chymotrypsin cleavage to obtain crude mixtures of modified insulin. The crude modified insulin mixtures were assessed for their propensity to form fibrils at a range of temperatures; fibril formation was confirmed by the ThT assay and TEM.

Most of the modifications led to a decrease in the rate of formation and yield of amyloid fibrils. However, certain modifications increased the rate of formation and led to distinct changes in morphology when compared to fibrils formed from unmodified insulin. For example, reduction carboxymethylation of insulin resulted in the formation of straight, twisted fibrils compared to the straight and narrow fibrils formed in the insulin standard at pH 7.4. In contrast, the crude reduced pyridylethylated insulin formed wavy fibrils at pH 1.6, a very different morphology to the standard insulin fibrils.

Exposure to neutral and slightly alkaline buffer reduced the rate of insulin fibril formation even in the absence of chemical modification. This perhaps reflects that the oligomeric state can slow down amyloid formation under certain conditions.

The effect of enzymatic digestion on fibril formation of insulin was investigated by treatment of trypsin and chymotrypsin. It was found that the intact insulin in the partially trypsin digested insulin mixture formed long narrow and unbranched fibrils, which were similar to the insulin control at pH 1.6. However, the fully digested insulin peptides did not form any fibrils, under the same conditions. Chymotryptic digest of insulin formed a heterogeneous mixture of fibril structures, ranging from long, thin, and straight, as well as short and thick fibrils, at pH 1.6.

The successful formation of protein nanofibres from unpurified mixtures of modified insulin indicates that bovine insulin has the ability to form into nanofibres while still in the presence of other, derivatised polypeptides and peptides. Chemical modification of insulin showed that varying morphologies of fibrils can be prepared and the fibril structure was specific to the modification. These findings add to the enormous interest in the potential utility of amyloid fibrils as structural templates in nanomaterials science (Cherny and Gazit 2008, Gras 2007a, Gras 2007b, Gras *et al.* 2006) which requires the capacity to manipulate the fibril structure for such applications. Studies continue to determine ways of controlling peptide and proteins self-assembly to obtain amyloid fibrils (Griffin *et al.* 2008, Hong and Fink 2005, Hong *et al.* 2003) and these results suggest that simple chemical modifications can provide considerable control over higher order assembly processes.

Insulin fibrils have an “elastic modulus of 3.3 ± 0.4 GPa which ranks fibrils amongst the stiff polymers such as nylon” (Welland 2007). Insulin and crystallin amyloid fibrils were therefore trialled in a polymer model system of PVOH. PVOH nanocomposite films were manufactured with the addition of insulin fibrils or crude crystallin fibrils using a solution casting method. TEM studies showed that the solution casting method achieved fibrils dispersion. Congo red was

added to the casting solutions to confirm the presence of fibrils in the films, as well as to ensure the absence of fibrils in protein control films with added native protein. PVOH + insulin fibrils showed yellow-green birefringence in the films which was consistent with amyloid fibrils being present, while there was no yellow-green birefringence detected in the PVOH + insulin control films, confirming that the film manufacture method did not induce fibrillation in the native proteins.

Insulin fibril addition produced a rough film, in contrast to crystallin fibrils which led to the production of a smooth film. The film manufacture method was optimised for insulin fibril added composites to minimise voids in the PVOH + insulin (fibril/control) films *via* hot pressing. This step was not required for the crystallin fibril containing films, which did not contain voids.

Preliminary studies on hydrated films showed that insulin did not change the strength of the PVOH films, but increased their elongation. However, crystallin fibrils caused an increase in the tensile strength of the PVOH films, which was 20% higher than the crystallin control. DMA showed that both insulin and crystallin fibrils altered the mechanical properties of the polymer in a manner consistent with a decrease in molecular slippage within the polymer (Nielsen 1974). These changes suggested better compatibility of the crude crystallin fibrils with the PVOH than the insulin fibrils.

It has thus been shown that PVOH nanocomposite films with improved reinforcement of the PVOH matrix can be prepared using protein nanofibres assembled from a crude source. An enhancement of the tensile strength and elastic modulus of the PVOH films was obtained at low nanofibre loading (0.6%), which indicates efficient load transfer between the fibrils and the matrix. As a representative example, a 21% improvement of the stiffness was achieved by the additions of 0.6% crude crystallin fibrils, in the glassy region ($<T_g$) of the PVOH system. The potential for interfacial bond tailoring by the side chain amino acid of protein nanofibres makes protein nanofibres attractive as effective reinforcing agents of bionanocomposites.

Results show that nanofibres assembled from proteins affected the mechanical behaviour of the PVOH films to some extent. The pure insulin fibrils are morphologically long, straight and unbranching compared to the crude mixture of short, curly and long straight fibrils assembled from crude crystallins. Insulin and crystallins differed in their mechanical behaviour. It has thus been demonstrated that protein nanofibres affected the PVOH thermo-mechanical properties in a protein dependent manner.

With proof of concept now established, future work on the addition of protein nanofibres in PVOH should include the addition of crosslinkers such as glutaraldehyde and transglutaminase to act as a binder between the nanofibres. Moreover, compatibilisers can be added to enhance the interfacial bonding between nanostructures and polymers (Xie *et al.* 2005). Other polymers, such as epoxy resins, can also be used as a matrix to assess the effect of protein fibres on their mechanical properties.

The partial biodegradability of the amyloid fibrils is increasingly recognised in recently published work on composites of amyloid and commercial plastics (Arnold 2008). Protein nanofibre composites may have potential in products like food packaging or wrapping, filter membranes with selective adsorption properties conferred by functionalised nanofibres. Since protein nanofibres have been shown to confer changes in polymer strength, the availability of side chain amino acids in protein nanofibres offer better scope for their functionalisation than carbon nanotubes. Thus amyloid fibrils offer a complementary technology to carbon nanotubes for a wide range of potential applications.

6.1 References

Arnold, C. 2008. From diseases to devices. *Chemical and Engineering New: Science/Technology* 86: 48-50.

Cherny, I., and E. Gazit. 2008. Amyloids: Not only pathological agents but also ordered nanomaterials. *Angewandte Chemie International Edition* 47: 4062-4069.

Gras, S. L. 2007a. Amyloid fibrils: From disease to design. New biomaterial applications for self-assembling cross-beta fibrils. *Australian Journal of Chemistry* 60: 333-342.

—. 2007b. Protein misfolding: A route to new nanomaterials. *Advanced Powder Technology* 18: 699-705.

Gras, S. L., A. M. Squires, C. M. Dobson, and C. E. MacPhee. 2006. Functionalised fibrils for bio-nanotechnology. *International Conference On Nanoscience and Nanotechnology*, Brisbane, Qld.

Griffin, M. D. W., M. L. Y. Mok, L. M. Wilson, C. L. L. Pham, L. J. Waddington, M. A. Perugini, and G. J. Howlett. 2008. Phospholipid Interaction Induces molecular-level polymorphism in apolipoprotein C-II amyloid fibrils *via* alternative assembly pathways. *Journal of Molecular Biology* 375: 240-256.

Hong, D.-P., and A. L. Fink. 2005. Independent heterologous fibrillation of insulin and its β-chain peptide. *Biochemistry* 44: 16701-16709.

Hong, Y., R. L. Legge, S. Zhang, and P. Chen. 2003. Effect of amino acid sequence and pH on nanofiber formation of self-assembling peptides EAK16-II and EAK16-IV. *Biomacromolecules* 4: 1433-1442.

Nielsen, L. E. 1974. *Mechanical properties of polymers and composites*. Marcel Dekker, Inc., New York, pg 2-18, 139-205.

Welland, M. E. 2007. Insights into amyloid diseases. *Nano Today* 2: 56.

Xie, X.-L., Y.-W. Mai, and X.-P. Zhou. 2005. Dispersion and alignment of carbon nanotubes in polymer matrix: A review. *Materials Science and Engineering: R: Reports* 49: 89-112.

Experimental

7.1 General Methods and Materials

Unless otherwise stated, all chemicals, reagents and solvents were purchased from Sigma-Aldrich New Zealand Ltd., or BDH Laboratory Supplies, and were of analytical grade.

Bovine eye lenses were supplied by local abattoirs (CMP Canterbury Ltd, Seafield Road, Ashburton, New Zealand).

pH measurements were obtained using an UltraBasic UB10 pH meter purchased from Denver Instrument Co. and fitted with a high-performance glass body pH/Tris electrode. The electrode was calibrated against standard buffers at pH 4.0, 7.0 and 9.0, purchased from BDH Laboratory Supplies.

Dialysis was undertaken using Thermo Scientific SnakeSkin pleated dialysis tubing, 3.5 kDa molecular weight cut off (MWCO) or Pierce Slide-A-Lyzer MINI dialysis unit, 3.5 kDa MWCO, prepared as per instructions on packaging.

Polyacrylamide gel electrophoresis was routinely run using a NuPAGE system from Invitrogen with pre-cast NuPAGE Novex 4-12% Bis-Tris gels 1.0 mm (Invitrogen New Zealand Limited, Auckland, New Zealand). The gel images were captured using a BioImaging System, Syngene, A Division of the Synoptics Group equipped with Gene Snap from Gene Snap software.

Citraconylation and acetylation was carried out using the pH stat, 718 Stat Titrino, Metrohm Swiss Made, John Morris Scientific Pty Ltd. with 728 Stirrer-Metrohm.

For the measurement of protein concentrations, the Thermo Scientific NanoDrop 1000 Spectrophotometer was used (Thermo Fischer Scientific, Nanodrop Technologies Inc., Wilmington, Delaware, USA).

Freeze drying of samples was performed in an Edwards “Speedivac” Model 30P2 Centrifugal freeze drier.

Fluorescence spectroscopy assays were carried out using:
(1) Cary Eclipse Varian Fluorescence Spectrophotometer interfaced with Cary Eclipse version 2 operating software. It was equipped with a 450-5 nm excitation filter and emission spectra were recorded over a range from 460-560 nm. All cuvettes used with the Cary Eclipse Varian fluorescence spectrophotometer were 1 cm path length quartz cuvettes.
(2) Plate reader, Fluostar Optima, BMG Labtech (Alphatech Systems Limited, Auckland, New Zealand) with a set of 520-10/450-10 nm emission/excitation filters and gain set at 1444. For fluorometric measurements, on the plate reader, Nunc^{TM} 96 well optical bottom plates were used with Nunc^{TM} 236707 sealing tape, 130 x 78.32 mm. Nunc^{TM} products were supplied by In Vitro Technologies, Auckland, New Zealand.

For the ThT assays, fresh solutions of ThT were filtered through a 0.2 μm filter immediately before use. The filter cartridge was a Millex GP filter unit 0.2 μm, supplied by Millipore, and the 10 ml syringe was supplied by Bectn Dickinson.
The LC-MS system utilised in this thesis consisted of a Thermo Electron Corporation (San Jose, CA, USA) Finnigan Surveyor MS pump, Finnigan MicroAS auto-sampler, Finnigan Surveyor PDA detector and a ThermaSphere TS-130 column heater (Phenomenex, Torrance, CA, USA). A PDA detector was used which scanned from 190-350 nm and spectral anaysis was performed at 276-280 nm.

Microscopy: Optical microscopy imaging was carried out using a J Swift & Son optical microscope fitted with a cross-polarising lens. Electron micrographs were obtained using Hitachi H600 TEM operating at 80 kV. SEMs were carried out on a JEOL JSM 6100 SEM and a JEOL JSM-7000F FE-SEM.

Centrifugations were carried out on the Eppendorf Centrifuge 5810R (maximum speed 12 000 rpm) with fixed-angle rotor: F-34-6-38 (>1.5 ml) and F45-30-11 (<1.5 ml) with adapters in the fixed-angle rotor.

PVOH was supplied by BDH Laboratory Supplies (MW= 115 kDa, degree of hydrolysis= 86.5-89.0%).

Falcon tubes (50 ml) and Eppendorfs (1.5 ml) were utilised for reactions, storage of insulin derivatives and for making polymer solution for film manufacture.

The mechanical properties of the films were measured on:
(1) UTM, Model 1011 with an installed computer programme at New Zealand Institute of Crop and Food Research.
(2) DMA (Perkin Elmer, Diamond DMA, Distributed by New Zealand Scientific).
(3) DSC-TGA, SDT Q600 V20.5 Build 15, TA Universal Analysis, (Alphatech Systems Ltd., Auckland, New Zealand).

Hot pressing of films was carried out on a laboratory press, with an automatic press control (from Gibitre Instruments).

7.2 Protein Analysis

7.2.1 Protein concentration

The protein concentration of unknown solutions were determined on the Thermo Scientific NanoDrop 1000 Spectrophotometer using the nanodrop 1000 protein A_{280} application. Analyses of 1-3 µl samples were carried out in triplicates against a blank of distilled water (dH_2O) or the respective buffer.

7.2.2 Characterisation of proteins by NuPAGE

The procedure was adapted from Invitrogen supplies (Invitrogen 2003, Invitrogen 2007). Samples were prepared by mixing with NuPAGE lithium salt of dodecyl sulphate (LDS) sample buffer (4x) and sample reducing agent

(10x). The samples were placed in a water bath set at 70°C for 10 min to aid the reduction of disulfide bonds. Protein samples were run against wide range molecular weight marker Mark12™ (stained with Coomassie® R-250) purchased from Invitrogen (3.5-200 kDa). Each of the heated protein samples and the marker were loaded into separate wells in the polyacrylamide gel (NuPAGE Novex 4-12% Bis-Tris Gel 1.0 mm, 10 well). Samples were electrophoresed at a constant voltage of 200 V in running buffer (NuPAGE 2-(N-morpholino)ethanesulfonic acid (MES) –sodium dodecyl sulphate (SDS) at room temperature for 35 min. The MES-SDS running buffer was made up of 50 mM MES, 50 mM Tris base, 0.1% SDS, 1 mM ethylenediaminetetraacetic acid (EDTA) at pH 7.4. The proteins in the resultant polyacrylamide gel were stained in a solution of Coomassie brilliant blue stain (0.1% Coomassie brilliant blue (10% v/v), glacial acetic acid (50% v/v), methanol, dH_2O (40% v/v), pre-filtered at room temperature). After two hours of staining the gel was transferred into a destaining solution (glacial acetic acid (10% v/v), methanol (5% v/v), dH_2O (85% v/v)) at room temperature.

7.3 Insulin Acetylation Procedure

The procedures for insulin citraconylation and acetylation was modified from the literature (Blundell *et al.* 1972).

7.3.1 N-Terminal group protection

Bovine insulin solution was prepared at a concentration of 1 mg/ml in potassium phosphate buffer (50 mM, pH 8). Insulin was dissolved in a minimum volume of 12 mM HCl solution (pH 2) and then made up to the required concentration with the phosphate buffer. The pH of the protein solution was monitored after dilution using the pH meter and adjusted to pH 8 with dilute NaOH.

The insulin solution (1mg/ml, 20 ml) was placed in the pH stat vessel and the pH stat was started with a runtime of 1800 min containing 0.5 M NaOH and set to maintain a pH of 8. At 100 sec on the pH stat, a 25 times excess of citraconic acid anhydride (to all amino groups except lysine) was added to the protein

solution. Citraconic anhydride was added slowly ensuring that pH did not drop below 7.5. The solution was left to react while stirring for 30 min at pH 8.

To determine the impact of pH, the above reaction was carried out at pH 7 as well. Both the samples (pH 7 and pH 8) were analysed on ESI-MS. Insulin controls were reacted under the same buffer conditions as the citraconylated insulin, without any reagents and analysed.

One half of the citraconylated insulin (pH 8) was acetylated as described in the next section.

7.3.2 Acetylation

Citraconylation was followed by acetylation of the insulin amino group as previously described. The citraconylated insulin (1 mg/ml) was acetylated with the addition of 10-fold molar excess of acetic anhydride per lysine group. The reaction was carried out for 1 hr at 4°C at pH 8.0, maintained by the addition of 0.5 M NaOH on a pH stat that was utilised in section 7.3.1. The insulin standard was treated under the conditions above without the reagents and provided the controls for this experiment.

All samples were dialysed (3.5 kDa MWCO) at 4°C in 50 mM ammonium bicarbonate buffer and lyophilised. The samples were stored at -80°C and the reaction was subsequently analysed by LC-MS.

7.4 Reduction Carboxymethylation of Insulin

The reduction alkylation procedure used in this study was adapted from the literature (Shechter *et al.* 1973) and is described below.

7.4.1 Reduction

Bovine insulin (50 mg) was dissolved in 5 ml of 1 M Tris-hydrochloride buffer, 8 M urea (pH 8.0) containing 0.01% EDTA. DTE (30 mg) was added and the reduction proceeded for 1 hr at room temperature. An insulin control was also

treated with the same buffer, without the reducing agent. The reduced insulin was subsequently carboxymethylated and pyridylethylated separately.

7.4.2 Carboxymethylation

IAA (150 mg) was added to the reduced insulin reaction mixture and the reaction further proceeded for 20 min at room temperature. The RCM insulin obtained was gel filtered as described below.

7.4.3 Pyridylethylation

4-VP (150 mg) was added to the reduced insulin mixture and was left to react for 20 min under nitrogen bubbling into the solution, at room temperature (in fumehood). The mixture obtained was centrifuged at 10000 rpm for 10 min at 4°C. The pellet and supernatant obtained were subjected to gel filtration as described below.

7.4.4 Gel filtration chromatography

RCM and RPE insulin samples were subjected to gel filtration (Shechter *et al.* 1973) using AKTA fast performance liquid chromatography (FPLC), from Amersham Biosciences in conjunction with a pump (UPC-900), detector (P-920) and a fraction collector (Frac-950). Sephadex G-25 resin was prepared for column chromatography as per the instruction of the supplier, Amersham Biosciences. The resin was filled into a column (100 cm x 2.5 cm) and equilibrated with 50 mM ammonium bicarbonate buffer (pH 7.85). The insulin sample were loaded at 2-10 mg/ml and eluted using 50 mM ammonium bicarbonate at a flow rate of 4 ml/min. Fractions were collected at 10 ml/per tube. The fractions corresponding to the protein peak as judged by UV absorbance at 280 nm were pooled and lyophilised.

7.5 Procedure for Enzymatic Cleavage of Insulin

7.5.1 Trypsin digestion of insulin

The trypsin utilised was from bovine pancreas (L-1-tosylamide-2-phenylethyl chloromethyl ketone (TPCK) treated, salt-free, lyophilised powder and obtained form Sigma-Aldrich). The Sigma technical bulletin for trypsin digestion of

peptides and proteins was used for insulin digestion (Sigma-Aldrich 2007). A ratio of 1:50 (w/w) of enzyme to substrate was used in this experiment. Insulin (5 mg/ml) was dissolved in 100 mM ammonium bicarbonate pH 8.5. The trypsin was dissolved in 1 mM HCl to a concentration of 1 mg/ml. Trypsin solution was added to the protein solution and incubated for 4 hr at 37°C in a water bath. This provided a partially digested insulin sample which was stored at -80°C.

Half of the partially digested insulin was treated further with trypsin to obtain total digestion of the insulin. An aliquot of trypsin was added to the insulin every 4 hr over a 12 hr period to adjust the final trypsin to insulin molar ratio to 1:6 (total trypsin to insulin). After the 12 hr sequential digestion, the sample was stored at -80°C.

An insulin standard was treated under the same buffer conditions, without the enzyme and was referred to as the insulin control. Samples were stored at -80°C and lyophilised.

7.5.2 Chymotrypsin digestion of Insulin

α-Chymotrypsin (Type II, lyophilised powder) from bovine pancreas was used to cleave insulin (Sigma-Aldrich 2007). Insulin (5 mg/ml) was digested with chymotrypsin at 1:50, enzyme to protein ratio, in 100 mM ammonium bicarbonate buffer at pH 8.5. Solutions were incubated in a water bath at 37°C for 4 hr. Samples were digested in 500 µl fractions, in Eppendorfs. An insulin standard was treated under the same buffer conditions, without the enzyme and was referred to as the insulin control.

The general strategy to analyse the chymotrypsin digested fragments of insulin *via* LC-ESI-MS/MS involved the following steps (Yen *et al.* 2002): (1) chymotrypsin digestion of insulin was carried out at pH 8.5 to obtain peptides; (2) complete reduction was carried out with DTE and carboxymethylation by IAA as detailed in section 7.4.1 and 7.4.2; (3) LC-ESI-MS/MS analysis of the resulting peptides was carried out as described in section 7.6.3 and section 7.6.4 to identify the fragments. Treatment with DTE and IAA was necessary

because it was difficult to analyse fragments for disulfide-bonded peptides than those completely reduced and alkylated.

7.6 Mass Spectrometry

Mass spectrometry conditions were selected with advice from Nigel Joyce, New Zealand Institute of Crop and Food Research. Insulin solutions from the respective experiments were retained and stored at -80°C for mass spectrometry. All MS methods were based on the Finnigan™ LTQ™ manual (Thermo Electron Corporation, 2003).

7.6.1 ESI-MS

Electrospray ionisation-mass spectrometry (ESI-MS) was used to screen the degree of insulin citraconylation at pH 7 and pH 8 (section 2.3.1). Insulin sample that had or had not been treated with citraconic acid at pH 7 and 8 were also analysed, for comparison.

Insulin samples at a concentration of 0.1 mg/ml were injected *via* an ESI source. The ionised peptides were scanned by API-MS (LTQ, 2D linear ion-trap, Thermo-Finnigan, San Jose, CA, USA) with ESI in the positive mode. Data were acquired for relevant parent masses up to 2000 amu. Spectral scans were obtained at normal (16700 amu/sec) resolution for full scan followed by zoom (1100 amu/sec) or ultra-zoom (27 amu/sec) for charge state calculation. Appropriate parent masses based on charge states were selected for MS^2 fragmentation with an applied collision energy of 35 arbitrary units. Data were processed with the aid of Xcalibur1.4 (Thermo Electron Corporation).

7.6.2 LC-ESI-MS of insulin and modified insulin

The following samples were anaylsed by liquid chromatography-electrospray ionisation-mass spectrometry (LC-ESI-MS): insulin standard (section 2.2.4), citraconylated acetylated insulin with unmodified insulin (section 2.3.2), acetylated insulin (section 2.3.4), reduced alkylated insulin (sections 2.4.4 and 2.4.5), trypsin treated insulin (section 2.5) and the supernatant of the

aggregated crude acetylated insulin (section 3.4.1). LC-ESI-MS analysis of 0.1 mg/ml insulin solutions was carried out by injecting 10 µl samples. Insulin was resolved on a Zorbex 2 column with mobile phase A and B (A: 0.2% formic acid in distilled H_2O, B: 0.2% formic acid in acetonitrile) and pumped *via* a Surveyor MS pump at a flow rate of 300 µl/min, the eluent was introduced to mass spectrometer *via* electrospray. Ions were scanned over a range of 800-2000 m/z $[M+H]^+$ at an orifice potential of 4.2 kV, with an activation time of 30 msec. The mass spectra corresponding to the insulin LC peak present in the TIC chromatogram were averaged in order to improve the ion statistics, leading to a better molecular weight determination. Data were collected in full scan with a secondary dependent scan event to select data for ultrazoom mapping. LC-ESI-MS data were analysed using Xcalibur software.

7.6.3 Identifcation of insulin site of acetylation, by LC-ESI-MS/MS

The acetylated insulin described in section 2.3.5 was analysed for the site of acetyl attachment on the insulin chain by mass sequencing as described below. The chymotrypsin treated insulin was also reduced and carboxymethylated before trypsin digestion and the fragments were identified by LC-ESI-MS/MS.

7.6.3.1 Reduction carboxymethylation

The crude acetylated insulin sample was denatured prior to any digestion with protease so that the protease will have as much access to the recognised amino acid sequence as possible. To help achieve this, the crude protein was reduced and carboxymethylated as per section 7.4.1 and 7.4.2, on a smaller scale volume of 200 µl, at 5 mg/ml. The insulin control was also reduced and carboxymethylated in a similar manner.

7.6.3.2 Protease digestion

The reduced carboxymethylated insulin sample was digested with trypsin as described in section 7.5.1. A 10 µl aliquot of the proteolytic digest was loaded onto the LC column and separation was performed on a Zorbax-300SB-C8, 5 µm, 150 x 4.6 mm column with a guard cartridge (Agilent, p/n883995-906) with a mobile flow rate of 300 µl/min at 25°C. The mobile phase consisted of dH_2O (A) and acetonitrile (B) both containing 0.2% formic acid. An elution gradient of

95% A held for 5 min then switched to 70% A with a linear gradient to 20% A over 45 min was applied. The column was then washed with 5% A for 5 min before being re-equilibrated with 95% (A). The eluent was dispersed with ESI in the positive mode to assist ionisation of the peptides into the ion-trap mass analyser scanning from 400-2000 m/z. Full scan normal/zoom data were automatically filtered to select M+2H and M+3H peptide states for MS^2 fragmentation to produce fragments expected.

7.6.3.3 MS/MS analysis of peptide ions

X-calibur software provided with the mass spectrometer enabled the acquisition of mass spectra in a non-redundant manner so that as many peptides as possible were surveyed from the complex mixture. During this process, an experimental method was set up in which one full range MS scan (400-2000 m/z) was acquired followed by the acquisition of MS/MS scans.

7.6.3.4 Peptide sequence identification using SEQUEST

SEQUEST compares experimental MS/MS spectra to theoretical MS/MS spectra from database proteins and calculates a correlation value, which can be examined in order to determine how well a particular experimental spectrum matches the corresponding theoretical spectrum (Eng *et al.* 1994). The acquired MS/MS spectra for each sample were searched using the SEQUEST algorithm (BioWorks 3.1 SR1, Thermo Electron) against the UniProt database (5.26.05 download; 125,244 entries). Searches were performed, with trypsin specified as the enzyme, with an allowance for up to two missed cleavage sites. Searches from multiple fractions or replicates within an experiment were combined in BioWorks using a MultiConsensus report to generate a comprehensive list of peptides and proteins identified in a particular experiment.

Data were filtered and scored against the database consisting of bovine insulin A and B chains and trypsin with the expected variable amino acid modifications of carboxymethylated (+58) on cysteine (C) and acetylation (+42) on N-terminal amines and lysine (K). In addition, a missed cleavage of one amino acid was allowed for potential steric hindrance to cleavage of the acetylated lysine B29. Possible peptide combinations were then filtered to show only matches with

greater than 30% Y and B ion confirmation and a preliminary score of greater than 200.

SEQUEST performs two types of scoring. After finding all peptides that match within your mass tolerance, SEQUEST does a preliminary scoring of these candidates to weed the list down to 500 for the final correlation analysis. The scoring is based on the number of ions in the MS/MS spectrum that match with the experimental data. Larger peptides will have bigger Sp values. A 20 residue peptide will usually have an Sp value of over 1000, while a 6 residue peptide will likely be below 500.

7.6.4 Identification of insulin chymotryptic digest, by LC-ESI-MS/MS

The chymotrypsin treated insulin and the untreated insulin (control) were reduced, alkylated and analysed by the liquid chromatography-electrospray ionization-mass spectrometry/mass spectrometry (LC-ESI-MS/MS) method described in section 7.6.3 except that the MS/MS data obtained with the insulin chymotryptic digest was searched against chymotrypsin specified as the enzyme on SEQUEST. Two missed cleavages were allowed for chymotrypsin during the search and several insulin fragments matching the expected fragments obtained theoretically was found (section 2.6).

7.7 Procedures for Insulin Amyloid Formation and ThT assay

Insulin fibrils were initially prepared by the small scale method and subsequently *in situ* on the plate reader with modifications from the literature (Nielsen *et al.* 2001). Fibrils were analysed by the ThT fluorescence assay (LeVine 1999).

7.7.1 Small scale fibrillation and ThT assay

Solutions of insulin were prepared in duplicate to the required concentration, ranging from 0.57 to 5.7 mg/ml in buffers with pHs ranging from 1.6 to 7.4, before and after the chemical modifications (listed in Table 7.1). These samples were aliquoted (50 µl) into sealed Eppendorf tubes and placed in an incubating

oven set at 60°C. The aliquoted samples were removed from the incubation ovens every 15 min or 30 min. The samples were frozen immediately (-80°C) until required for analysis. An insulin control (0 hr) was immediately stored at -80°C for each treatment condition for the duration of the experiment.

Derivatised insulin	pH	Buffer	(mg/ml)
Insulin standard	1.6	20% acetic acid, 100 mM NaCl	5.7
Insulin control Crude acetylated insulin	1.6	20% acetic acid, 100 mM NaCl	5.7
Insulin control Tryptic digest of insulin	1.6	20% acetic acid, 100 mM NaCl	5.7

Table 7.1 *The modified insulin samples used to assess the influence of chemical modification on the formation of insulin amyloid.*

For the ThT assay, the fibril solution was diluted in a Tris buffer (50 mM Tris, 100 mM NaCl, pH 7.5) containing ThT (5 to 10 μM) in a cuvette. The final concentration of protein in the cuvette was 20 μg/ml. The resulting, (protein + ThT + buffer) solution was mixed for 3 min to allow binding between the dye and protein to equilibrate, before the emission spectra were recorded from 450 to 560 nm. Optimum fluorescence at 482 nm was monitored for amyloid detection.

7.7.2 *In situ* fibrillation and ThT assay

In the subsequent part of this study, a plate reader was available for *in situ* insulin fibrillation. This procedure allowed a large number of samples to be assayed using small reaction volumes. Solutions of insulin were prepared in triplicate to the required concentration ranging from 0.57 to 5.7 mg/ml in buffers with pHs ranging from 1.6 to 7.4 (listed in Table 7.2). These samples were aliquoted (200 μl) into 96 well, clear bottomed Nunc^{TM} fluorescence well plates. ThT (1 mM) was added directly to the wells to give a final concentration of 5 μM. As controls, insulin samples without ThT were also incubated in the well plates.

Derivatised insulin	pH	Buffer	(mg/ml)
Crude acetylated insulin	1.6	20% acetic acid, 100 mM NaCl	2.9
Crude reduced carboxymethylated insulin	7.4	50 mM potassium phosphate buffer, 100 mM NaCl	0.1, 1
Crude reduced pyridylethylated insulin pellet	1.6	25 mM HCl buffer, 100 mM NaCl	2
Crude reduced pyridylethylated insulin supernatant	7.4	50 mM potassium phosphate buffer, 100 mM NaCl	5.7
Tryptic digest of insulin	1.6	20% acetic acid, 100 mM NaCl	5.7
Chymotryptic digest of insulin	1.6	20% acetic acid, 100 mM NaCl	5.7
	1.6	25 mM HCl buffer, 100 mM NaCl	5.7

Table 7.2 *The modified insulin samples used to assess the influence chemical modification on the formation of insulin amyloid.*

The well plates were sealed with Nunc^{TM} 236707 sealing tape, to minimise evaporation, and incubated at temperature of 60°C (except for trypsin digest which was analysed at 45°C). Fluorescence at 482 nm was recorded over time until maximum fluorescence of 65000 was reached.

7.7.3 Procedure for determining the impact of pH and insulin fibril concentration on ThT fluorescence

Insulin fibrils were formed by incubation of an insulin solution (5.8 mg/ml in 20% acetic acid buffer, 100 mM NaCl, pH 1.6) at 60°C in an oven for 4 hr, as discussed in section 3.2.5. The fibril solution was diluted separately in (1) 50 mM Tris, 100 mM NaCl, pH 7.5 and (2) 20% acetic acid. Fibrils were diluted at a range of 0 to 0.04 mg/ml at pH 7.5 and 0 to 2.9 mg/ml in 20% acetic acid. All dilutions were done in triplicate. The solutions were pipetted into 96 well plates. ThT was added directly to the wells to give a final concentration of 5 μM and fluorescence was read 482 nm. A fresh solution of insulin was prepared in acetic acid buffer and ThT was added to correct for any fluorescence from native insulin and ThT dye.

7.7.4 The impact of pH on insulin fibrils assessed by ThT

Insulin solution prepared in 25 mM HCl (100 mM NaCl, pH 1.6) at 11.4 mg/ml, was incubated at 60°C in an oven for 24 hr, to form fibrils. The fibrils mixtures (100 µl) were dialysed using the Slide-A-Lyzer MINI dialysis unit (MWCO 3.5 kDa) against 1 l of the different buffers (Table 7.3) for 3 hr. Insulin fibrils dialysed at pH 6.5, was redialysed at pH 2 (12 mM HCl) to determine the impact of acidification of the fibrils. The dialysed fibrils were frozen at -80°C and analysed by ThT assay and TEM. A fresh insulin control solution was prepared in HCl (12 mM, pH 2) and analysed.

Buffer	pH
12 mM HCl	pH 2.0
50 mM citrate buffer	pH 3.5
50 mM sodium acetate	pH 4.5
50 mM potassium phosphate	pH 6.5

Table 7.3 *Insulin fibrils dialysed in the different buffers and pHs.*

The ThT assay was carried out on the plate reader. Fibril solutions were defrosted at room temperature and diluted separately in 50 mM Tris buffer (pH 7.5, 100 mM NaCl) to obtain 5-20 µm protein solution in the wells of a 96 well plate reader. Fluorescence emission intensity of the samples was measured at 482 nm using the Fluostar Optima plate reader. Fluorescence was measured in triplicate and averaged.

TEM was carried out on the samples to determine the impact of pH on preformed insulin fibrils (section 3.2.6).

7.8 Extraction and Fibrillation of Crude Bovine Eye Lens Proteins

7.8.1 Extraction of crystallin proteins

The crystallin protein extraction method was adapted from (Garvey *et al.* 2008). Bovine lenses were homogenised in 50 mM Tris at pH 7.2 (1 mM DTE and 0.04% NaN_3, with 2 mM phenylmethylsulphonyl fluoride) using a magic bullet blender. The homogenate was centrifuged at 12,000 rpm for 60 min at 4°C. The supernatant was removed (centrifugation was repeated whenever a clear supernatant was not obtained) and analysed for protein concentration using the Nanodrop (A_{280}). The crystallin stock solution was freshly utilised for fibril studies and stored at -80°C for any other experiments.

7.8.2 Formation of fibrils from crystallins

Amyloid fibrils were formed directly from crude mixtures of bovine eye lens proteins using methods adapted from Garvey *et al.* (2008). The crude protein sample was diluted at 22 mg/ml into a solution 10% TFE v/v (pH 2). The pH of the protein solution was adjusted with dilute NaOH or HCl to pH 2 and samples were fibrillated by incubation at 60°C for 4 weeks.

7.8.3 ThT assay

Crystallin control and fibril solutions were assessed for ThT dye binding capacity, using a method adapted from (Thorn *et al.* 2005). Protein solutions were assayed at 50 µg/ml in 50 mM Tris buffer at pH 7.5, with 5µm ThT. Fluorescence emission intensity of the samples was measured at 482 nm using the Fluostar Optima plate reader. Fluorescence was measured in triplicate and averaged.

7.9 TEM Imaging of Amyloid

Insulin and crude bovine eye lens fibril formation and morphology were assessed by TEM, as described in the literature (Burke and Rougvie 1972, Whittingham *et al.* 2002), to confirm the presence of fibrils. TEM samples were

prepared by placing small aliquots (2 µl) of protein fibril samples (0.5-1.0 mg/ml) on carbon-coated copper grids covered with plastic films. The grid was then rinsed once with 3 µl of dH_2O, negatively stained with 2 µl of uranyl acetate (2% w/v) and dried with filter paper. Samples were analysed under magnifications of 60 000 to 100 000x, on a TEM.

7.10 Film Manufacture

7.10.1 PVOH solution

PVOH was prepared at a concentration of 5% w/v with dH_2O as the solvent. The PVOH powder was dispersed in dH_2O and full salvation was obtained by stirring with a glass rod with heating at 80°C in a water bath for 4 hr. The solution was left to settle for 24 hr to allow air bubbles to float out of the solution prior to casting.

7.10.2 Preparation of protein fibrils for films

Protein solutions were prepared as follows:
Insulin control solution was prepared by dissolving insulin in a small volume of 12 mM HCl (pH 2) and making up to volume with 12 mM HCl (pH 4). Insulin fibril solution was obtained by dissolving insulin in HCl (pH 1.6, 25 mM HCl, 100 mM NaCl) and incubating at 60°C for 24 hr.

Crystallin fibril solution was prepared by diluting the fresh protein extract in 10% TFE (pH 2) to 11.4 mg/ml and incubating at 60°C for 4 weeks. The crystallin control solution was prepared at pH 2 without TFE.

Both the protein fibril solutions were dialysed (SnakeSkin pleated dialysis tubing with a MWCO 3.5 kDa) in 12 mM HCl (pH 4) to remove salts. The presence of fibrils was detected by ThT and TEM. Fibrils were stored at -80°C and used for film casting the next day.

Both buffers used to make protein fibrils, HCl buffer (25 mM HCl, 100 mM NaCl) and 10% TFE were diluted separately in 12 mM HCl (pH 4), similar to the proteins.

All dialysis was carried out with a 3.5 kDa MWCO dialysis tubing in 2 l of 12 mM HCl (pH 4).

7.10.3 PVOH + protein (control/fibril) solution

Protein fibrils, as detailed in section 7.8.2, were prepared for addition to the PVOH solution. The desired volume of fibrils was added to the PVOH solution and gently swirled to obtain uniform fibril dispersion. The solutions were mixed and poured into casting trays for film formation. The preparation process was as follows:

A Schott bottle containing 1 l of 5% w/v PVOH in dH_2O was produced and utilised for the entire batch of films prepared for DMA, DSC-TGA, and microscopy work. 50 g PVOH powder was dissolved into 1 l of dH_2O and stored at room temperature as described in section 7.10.1.

A 24 ml of 0.6% w/v protein fibril + 2.5% PVOH film composite was produced by mixing 12 ml of 1.2% fibril solution with 12 ml of 5% w/v PVOH solution, without introducing bubbles. However, in the preliminary studies, 0.2% protein was utilised. Before casting, each solution was left standing for 30 min to displace any air trapped in the solution by giving time for the bubbles to rise to the surface.

PVOH + no protein control, PVOH + protein control and PVOH + protein fibrils composite solutions were prepared in triplicate to produce 3 films per sample.

7.10.4 Solution casting

Film casting method was adapted from the literature with some modifications (Aoi *et al.* 2000, Kim *et al.* 2007, Park *et al.* 2001, Wang and Sain 2007). Films were prepared by solution casting into a rectangular gel casting tray, with a length of 10 cm and a width of 7 cm and depth of 1.5 cm. The casting tray was,

HE 47-10 casting kit composed of a gel running tray inserted into a gel casting tray (generally used for Hoefer HE 33 Horizontal Agraose Unit), supplied by Amersham Biosciences (Figure 4.3). The solution was poured into the middle of the tray and allowed to spread out to cover the tray. Air bubbles were avoided but in some cases a thin glass pipette was gently used to remove any air bubble in the solution. A bubble level with dual axis (supplied by the workshop, School of Biological Sciences, University of Canterbury), was utilised to check the flatness of the trays on the bench.

Each film comprised of 24 ml of solution with solvent evaporation under ambient conditions for 5 days. The film was removed by carefully peeling from the trays. This was achieved by lifting the edge with thin tweezers and peeling the film by hand while wearing protective gloves. These steps produced a film of 9 cm in length and 6 cm in width, with an average thickness of 0.07 ± 0.02 μm, measured using an electronic digital caliper. The films were then cut into strips 7±1 mm wide using a razor blade and a steel chopping block scored with parallel lines, which acted as a template.

7.10.5 Determination of moisture content

The moisture content of films was determined by air oven drying at 60°C for 72 hr. The loss of film weight over time was monitored until there was no change in weight. Ten film samples were analysed and moisture was determined by the % weight loss.

7.11 Treatment of Films Prior to Mechanical Testing

All films were prepared by solvent evaporation for 5 days after casting and equilibration under ambient conditions for 48 hr (after peeling from the trays). These have been referred to as the hydrated films.

7.11.1 Vacuum drying

The hydrated films were initially dried in a vacuum oven (Vacuum drying oven, with an end vacuum of 10^{-2} mbar) at 60°C from 0 hr to 72 hr to determine the

length of time required to dry the films. Seven replicates of the films samples were analysed and the weight loss measured over the length of drying time.

The hydrated films were subsequently dried for 24 hr at 60°C in the vacuum oven for UTM and DMA testing of dry films. The dried films were cooled inside a desiccator (Secador auto-dessicator cabinet with 280 V automatic electronic dryer) for 2 hr before testing.

7.11.2 Hot pressing the PVOH + insulin composite

Dried films were cut into samples of 7 mm in width and 60 mm in length avoiding any edge effects. A sample was then wrapped in a smooth piece of Al foil that had been coated with a release wax (silicone FMG spray from ITW Polymers and Fluids, New Zealand). The foil wrapped film was then placed in a mould for hot pressing. The films were hot pressed at a temperature of 180°C, a pressure of 2.5-3 MPa using a processing time of 20 min. The hot pressed samples were then conditioned at 50% RH at 23°C. Samples were hot pressed in duplicate.

Conditioning at a equilibrium of 50% (RH) at 25°C, was obtained over saturated aqueous of the following alkalis: potassium carbonate 42.8%, calcium nitrate 50.0%, magnesium nitrate 52.9%, sodium bromide 57.7% (Staiger, pers. comm.) The humidity in the chamber was maintained by a Thermometer Hygrometer (Mason's wet and dry bulb hygrometer).

7.12 Procedure for Testing the Presence of Fibril in Films, using Congo Red

Samples were stained for amyloid following the procedure in literature with some modifications (Westermark *et al.* 1999). CR solution (1 mg/ml) was prepared in dH_2O and filtered using 0.2 µm filter cartridges. CR staining of the casting solution was done by adding CR to: the protein (control, fibril) solution and to the no insulin control solution at 0.08 mg/ml prior to mixing with PVOH solution. The solutions were allowed to stain for 30 min on a shaker. The

stained solution was dialysed in pH 4 (12 mM HCl) to remove excess dye and the salts.

After dialysis the dyed solutions were mixed with PVOH and films were cast. All films were cast at 2.5% PVOH. Insulin concentrations were 0.2, 0.4 and 0.6% in the PVOH + insulin (control/fibril) films. Crystallins were at 0.6% in the PVOH + crystallin films. Triplicate specimens from each film were examined under polarising light microscopy.

7.13 Characterisation of Nanocomposite Films

7.13.1 Tensile testing

Preliminary mechanical testing of the PVOH films with and without protein involved the tensile testing of films on the Instron UTM, Model 1011 with an installed computer programme. The procedure was based on the in house methods for testing films at NZ Institute for Crop and Food Research. A 100 N load cell with a crosshead speed of 50 mm/min was utilised. Tensile tests were performed on a hydrated PVOH + insulin (control/fibril) (0.2%) and PVOH + crystallin (control/fibril) films (0.2%), and dry PVOH + insulin (control/fibril) (0.6%) films only.

Strips were cut from the central region of the films to the dimensions 60 (± 1) mm x 7 (± 1) mm. Before testing, the sample dimensions were recorded using a digital caliper. The manner in which the films were attached to the Instron varied between the hydrated and the dry films described below.

7.13.1.1 Hydrated films

In the preliminary study, hydrated films were tested after 48 hr of equilibration at room temperature. Samples were stored in a desiccator during the testing period. Film strips were mounted using tapes and hooks as shown in the image in chapter 4, Figure 4.11. A straight hook was mounted into the Perspex base plate of the Instron and an extensigraph cradle was mounted into the cross-

head load cell. Film strips were taped on both ends and stuck to the hook at the base and the cradle hook on the crosshead, and the tensile test was activated.

7.13.1.2 Dried films

PVOH + insulin (control/fibril) films were dried for 24 hr at 60°C and subsequently stored in a desiccator in the laboratory until measurements commenced. Testing was performed by holding the test sample at each end with mechanical grips which were constructed (by Department of Mechanical Engineering, University of Canterbury) for the tensile testing. The screw wedged grips were attached to the base of the UTM and on the load cell. Each end of the film strip was inserted into the grips of the sample holder and screwed to avoid slippage.

7.13.1.3 Tensile testing on the UTM

Films were uniaxially stretched at 50 mm/min until they broke and a stress *vs* strain graph was recorded on the computer. The stress, strain data obtained from the tensile test were analysed (using the in house method for New Zealand Institute for Crop and Food Research) and the % elongation and stress (MPa) of the films were determined. Three films were prepared and 3 strips per film were tested and the data was averaged.

7.13.2 X-ray diffraction

XRD components utilised were: Philips PW1729 X-ray generator, Philips copper anode Long Fine Focus X-ray tube (wavelength 1.54 Å) operating at 50 kV/40 mA (primary beam filter was nickel), Philips PW1820 Goniometer (stepping motor assembly), Philips PW1752 Monochromator, Philips PW1711 X-ray Proportional Detector, Philips PW1710 diffractometer control linked to a PC running VisualXRD control software and Traces Version 4 Search/Match processing software. The scan speed was 0.02° 2θ/sec with a step size of 0.02° 2θ.

The PVOH + no insulin control, PVOH + insulin control, PVOH + insulin fibril films were analysed on the XRD with assistance from Stephen Brown, Department of Geology, University of Canterbury. A glass slide (3.5 cm x 2.5

cm) was placed in the XRD chamber to support the free-standing film. A small section of the film was laid on the glass slide which was clamped inside the chamber. The films were scanned through 2θ values ranging from 2 to 30°.

7.13.3 Microscopy

Polarising microscope, TEM and SEM were used to image the films:

7.13.3.1 Polarising microscopy

A Leica DMRE light microscope (Leica, Wetzlar, Germany), with a cross polarising lens, interfaced to a computer was used to detect the presence of amyloid in the PVOH + protein film. The protein control, fibrillised protein and the no protein control solutions were CR stained prior to film casting and pink coloured films were obtained.

A small specimen of the cast film was placed on a microscope glass slide and a drop of water was added to moisten the specimen. The sample was covered with a cover slip and examined under the microscope. Samples were initially examined with a non polarising lens followed by the polarising lens.

7.13.3.2 TEM of films

Film casting solution

TEM grids of the casting solutions composed of 2.5% PVOH + 0.6% insulin control and 2.5% PVOH + 0.6% insulin fibrils were prepared as per section 7.9, to assess insulin fibril morphology.

Film cross-section (microtomed)

The transverse section of films was studies using a Hitachi H600 transmission electron microscope. The PVOH + insulin composites (control and fibrils) and PVOH + crystallin composite (control and fibrils) were examined by TEM. Composites were fixed in 2.5% glutaraldehyde in 0.075% phosphate buffer for one hour. After three buffer washes, samples were post fixed in 1% osmium tetroxide in water for 30 min. Sample were washed in buffer again and dehydrated in a series of 60%, 80% (acetone in water) and then 2 changes of

100% acetone. Infiltration was carried out overnight with two changes of Spurr resin/acetone mixture, followed by embedding in Spurr resin at 65°C. PVOH control was difficult to handle due to its solubility and fragmentation in the solvent. It was not fixed and was placed directly in 60% acetone. Sections approximately 100 nm thick were cut on an LKB Ultrotome, and stained with uranyl acetate and lead citrate to distinguish the protein and the matrix.

7.13.3.3 SEM

PVOH + insulin films were studied using the SEM and FE-SEM (with assistance from Mike Flaws, Senior Technician, Department of Mechanical Engineering, University of Canterbury). Imaging was carried out at an accelerating voltage of 7 kV. The morphologies of freeze fractured surface (in liquid nitrogen) of PVOH + no insulin control, PVOH + insulin control, PVOH +insulin fibrils film were studied using a FE-SEM. The morphologies of the cast surface of PVOH + no insulin control, PVOH + insulin control, PVOH +insulin fibrils film, PVOH + no crystallin control, PVOH + crystallin control, PVOH + crystallin fibrils films were examined on an SEM. Specimens were prepared by sputter coating with gold for both SEM and FE-SEM.

7.13.4 DMA

The viscoelastic properties of the films were studied using a Perkin Elmer Instruments Inc Diamond DMA (with assistance from Dr. Mark Staiger, Department of Mechanical Engineering, University of Canterbury). The DMA was operated in tension mode with nitrogen as the furnace purge gas and liquid nitrogen for controlled cooling. Samples were dynamically tested in tension mode using a frequency of 1 Hz, amplitude of 10 μm and a minimum tension force 300 mN, and force amplitude initial value of 4000 mN. Samples of 0.05-0.08 mm in thickness were prepared with a gauge length of 60 mm and a width of 7-8 mm. The storage of modulus (E″), loss modulus (E') and tan δ (E"/E') were measured over the range of 0-150°C using a heating rate of 2°C/min.

7.13.5 DSC-TGA

DSC-TGA was performed on a SDT Q600 (from Alphatech Systems Ltd., Auckland, New Zealand) under flowing nitrogen (100 ml/min) atmosphere at

10°C/min (with assistance from Kelvin Walst, Department of Chemistry, University of Canterbury) to determine the melting point and decomposition temperature. Samples of more than 8 mg were placed into platinum pans except for crystallins, which was tested at less than 5 mg. The temperature was increased from ambient conditions to 600°C during the test.

For the films, disk shaped specimens which were 4-5 mm in diameter were cut with scissors from the central regions of the cast films. The integral balance on the DSC-TGA measured the exact sample mass. Samples were tested in duplicate: PVOH from the jar, bovine insulin from the jar, crystallin extract, and the PVOH + protein (control/fibril) films including PVOH + no protein control films. Data analysis was performed on the TA Universal Analysis software, available on the computer attached to the DSC-TGA.

7.14 References

Thermo Electron Corporation, 2003. *Finnigan LTQ Getting Started, 97055-97012 Revision A*. Technical Publications, Thermo Electron Corporation, California, USA, pg 45-112.

Aoi, K., A. Takasu, and M. Okada. 2000. DNA-based polymer hybrids Part 1. Compatibility and physical properties of poly(vinyl alcohol)/DNA sodium salt blend. *Polymer* 41: 2847-2853.

Blundell, T. L., G. G. Dodson, D. C. Hodgkin, and D. A. Mercola. 1972. Insulin: the structure in the crystal and its reflection in chemistry and biology. *Advances in Protein Chemistry* 26: 379-402.

Burke, M. J., and M. A. Rougvie. 1972. Cross-β protein structures. I. Insulin fibrils. *Biochemistry* 11: 2435-2439.

Eng, J. K., A. L. McCormack, and J. R. Yates III. 1994. An approach to correlate tandem mass spectral data of peptides with amino acid sequences in a protein database. *Journal of the American Society for Mass Spectrometry* 5: 976-989.

Garvey, M., S. L. Gras, S. Meehan, S. J. Meade, J. A. Carver, and J. A. Gerrard. 2008. Protein nanofibres of defined morphology prepared from mixtures of crude crystallins. *International Journal of Nanotechnology* Submitted.

Invitrogen. 2003. NuPAGE technical guide. *Instruction Manual, Version 3*: pg 7-47.

—. 2007. Nu-PAGE Novex, bis-tris mini gels. *Quick Reference Card IM-8042 Version G*.

Kim, E. M., M. H. Han, Y. J. Lee, D. H. Song, H. K. Lee, O. W. Kwon, D. S. Shin, S. S. Han, S. K. Noh, J. K. Shin, Y.-S. Gal, and W. S. Lyoo. 2007. Characterization of poly(vinyl alcohol) films with various molecular parameters. *Journal of Applied Polymer Science* 106: 3259-3267.

LeVine, H., III. 1999. Quantification of β-sheet amyloid fibril structures with thioflavin T. *Methods in Enzymology* 309: 274-284.

Nielsen, L., R. Khurana, A. Coats, S. Frokjaer, J. Brange, S. Vyas, V. N. Uversky, and A. L. Fink. 2001. Effect of environmental factors on the kinetics of insulin fibril formation: Elucidation of the molecular mechanism. *Biochemistry* 40: 6036-6046.

Park, J.-S., J.-W. Park, and E. Ruckenstein. 2001. Thermal and dynamic mechanical analysis of PVA/MC blend hydrogels. *Polymer* 42: 4271-4280.

Shechter, Y., A. Patchornik, and Y. Burstein. 1973. Selective reduction of cystine I-VI11 in α-lactalbumin of bovine milk. *Biochemistry* 12: 3407-3413.

Sigma-Aldrich. 2007. Trypsin, Proteomics Grade, Sigma: Product Code T 6567, 2007. *Technical Bulletin*.

Thorn, D. C., S. Meehan, M. Sunde, A. Rekas, S. L. Gras, C. E. MacPhee, C. M. Dobson, M. R. Wilson, and J. A. Carver. 2005. Amyloid fibril formation by bovine milk κ-casein and its inhibition by the molecular chaperones α_s- and β-casein. *Biochemistry* 44: 17027-17036.

Wang, B., and M. Sain. 2007. Isolation of nanofibers from soybean source and their reinforcing capability on synthetic polymers. *Composites Science and Technology* 67: 2521-2527.

Westermark, G. T., K. H. Johnson, and P. Westermark. 1999. Staining methods for identification of amyloid in tissue. *Methods in Enzymology* 309: 3-25.

Whittingham, J. L., D. J. Scott, K. Chance, A. Wilson, J. Finch, J. Brange, and G. G. Dodson. 2002. Insulin at pH 2: Structural analysis of the conditions promoting insulin fibre formation. *Journal of Molecular Biology* 318: 479-490.

Yen, T.-Y., H. Yan, and B. A. Macher. 2002. Characterizing closely spaced, complex disulfide bond patterns in peptides and proteins by liquid chromatography/electrospray ionization tandem mass spectrometry. *Journal of Mass Spectrometry* 37: 15-30.

Appendix

(A)

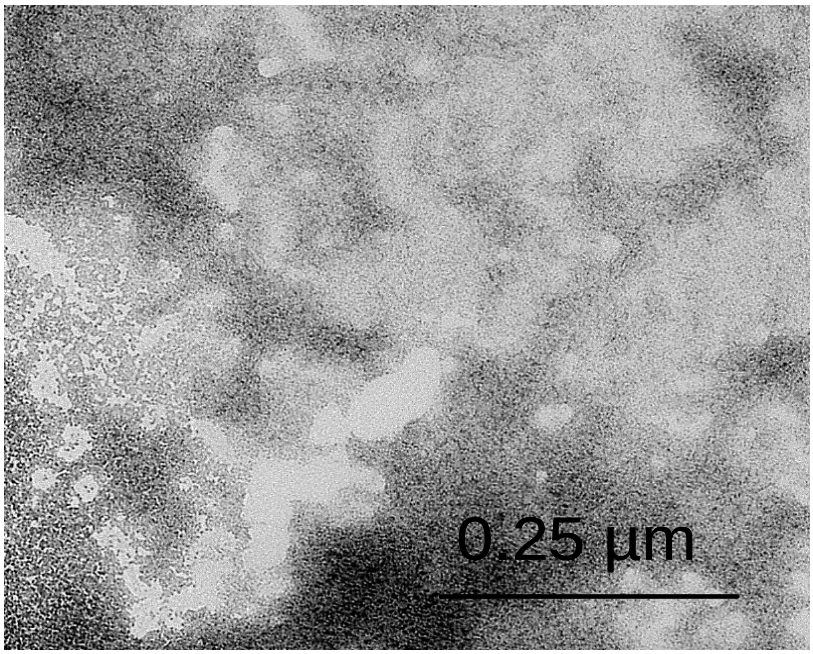

(B)

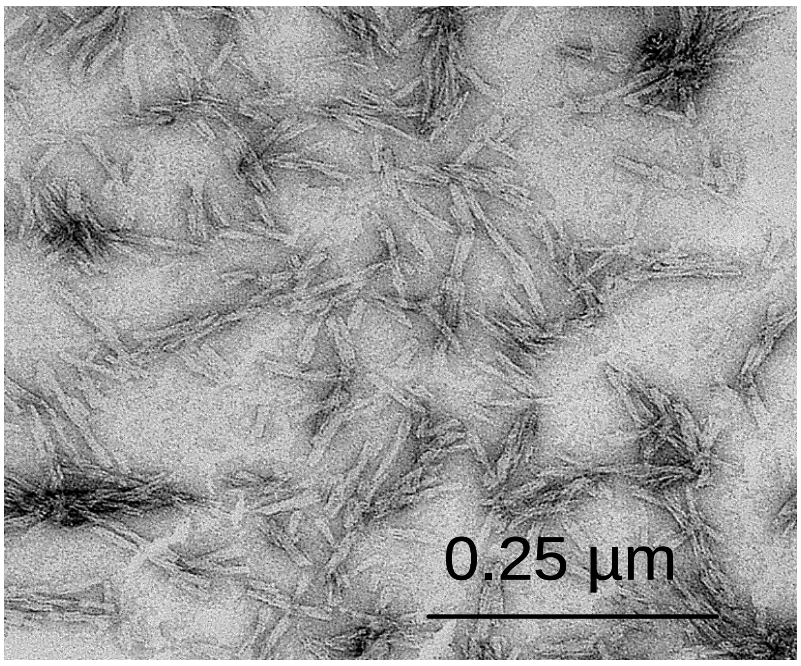

(C)

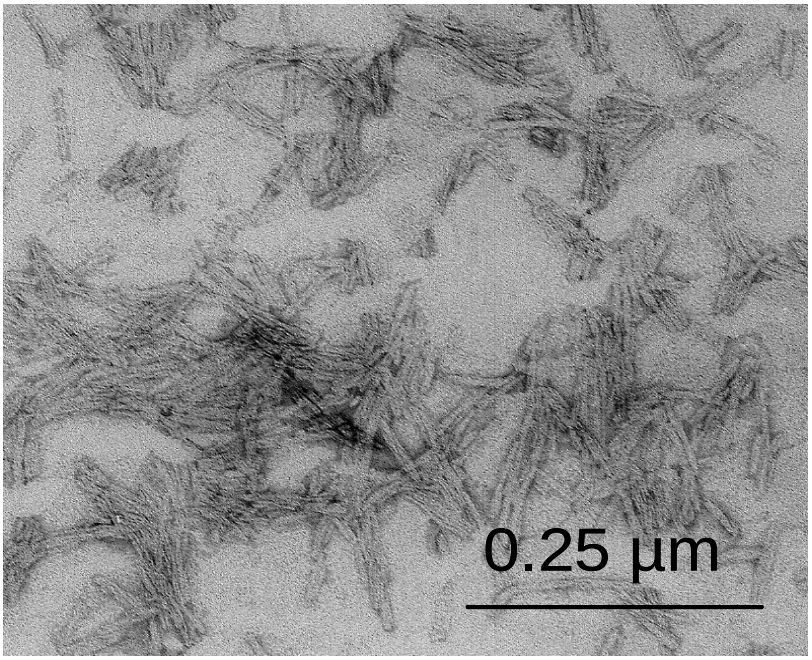

(D)

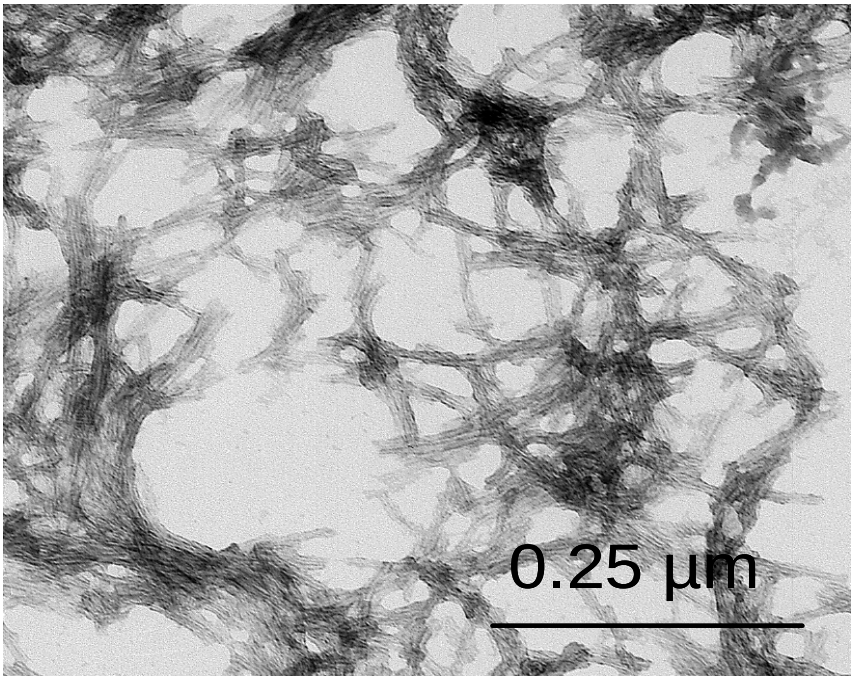

(E)

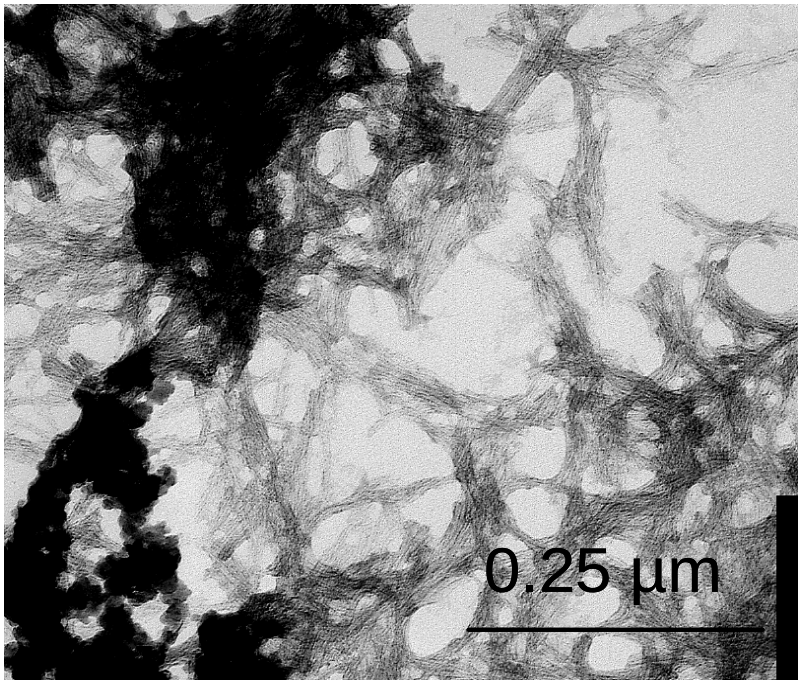

(F)

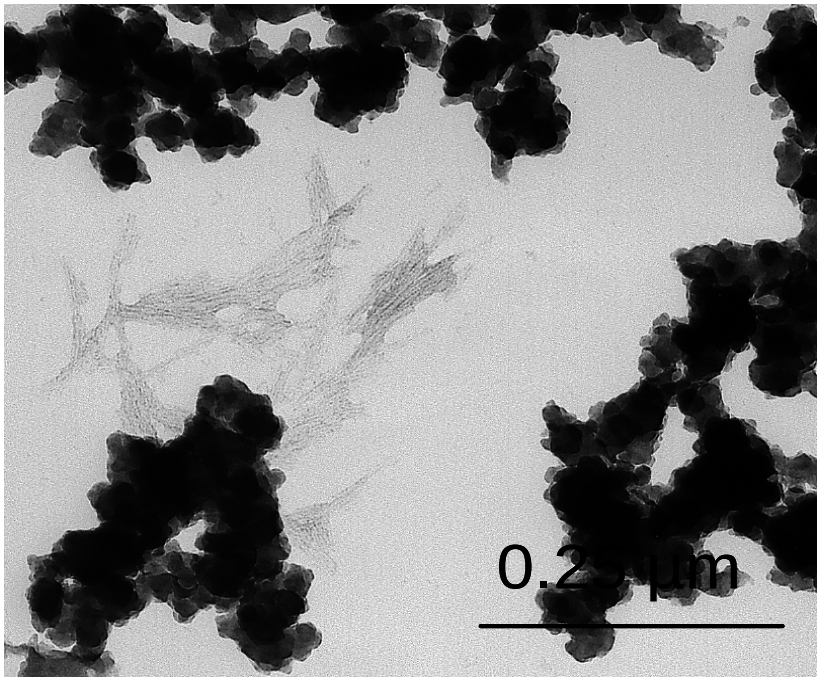

(G)

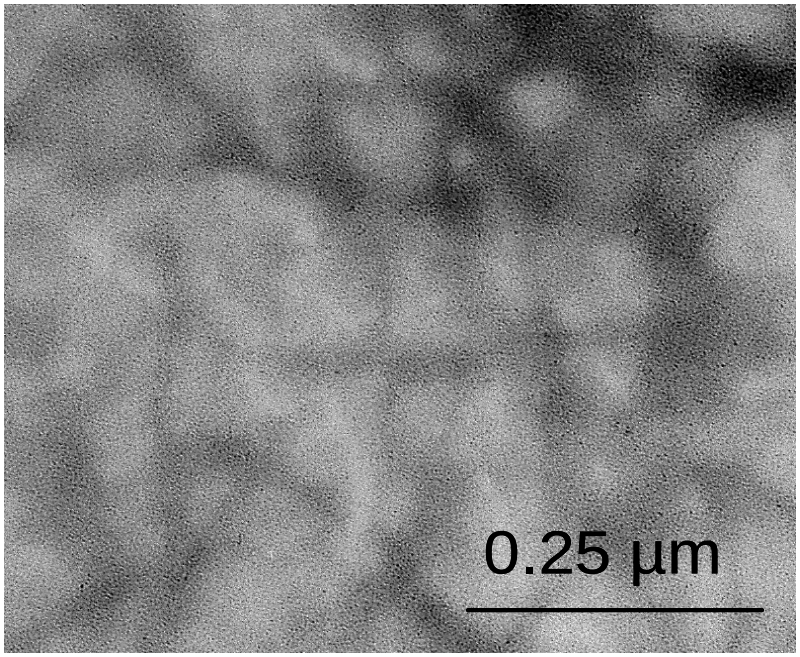

Figure 3.6 *Electron micrographs showing the impact of pH on insulin fibrils. Samples were at 11.4 mg/ml: (A) insulin control in 25 mM HCl (100 mM NaCl, pH 1.6) before fibrillation, (B) insulin fibrils in 25 mM HCl (100 mM NaCl, pH 1.6) at 60 ºC for 12 hr, (C) insulin fibrils after dialysis at pH 2, (D) pH 3.5, (E) pH 4.5, (F) pH 6.5 and (G) insulin fibrils after dialysis in pH 6.5, re-dialysed in pH 2. All samples had been frozen at -80°C for 24 hr before TEM examination. These images are a representation of triplicate samples.*